INVESTIGATION OF RCCI OPERATION WITH CUSTOMIZED PISTONS IN A LIGHT-DUTY MULTI-CYLINDER ENGINE USING DIESELINE

By

Christopher Wolfgang Gross

A dissertation submitted in partial fulfillment of
the requirements for the degree of

Doctor of Philosophy

(Mechanical Engineering)

at the

UNIVERSITY OF WISCONSIN – MADISON

2016

Date of Final Oral Examination: 6/22/2016

The dissertation is approved by the following members of the Final Oral Committee:

Rolf D. Reitz, Emeritus Professor, Mechanical Engineering
Jaal B. Ghandhi, Professor, Mechanical Engineering
David A. Rothamer, Associate Professor, Mechanical Engineering
Sage Kokjohn, Assistant Professor, Mechanical Engineering
James J. Schauer, Professor, Civil and Environmental Engineering

Abstract

In an attempt to increase efficiency and lower critical and highly regulated emissions (i.e., NOx, PM and CO2) many advanced combustion strategies have been investigated. Most of the current strategies fall into the category of low temperature combustion (LTC), which allow emissions mandates to be met in-cylinder along with anticipated reduction in cost and complexity. These strategies, such as homogeneous charge compression ignition (HCCI), premixed charge compression ignition (PCCI), partially premixed combustion (PPC) and reactivity controlled compression ignition (RCCI), use early injection timings, resulting in a highly lean charge with increased specific heat ratios to improve thermal efficiency and reduce PM emissions. Lower combustion temperatures also avoid the activation of NOx formation reactions. However, the lean air/fuel ratio decreases fuel oxidation rates of CO and HC and, due to longer ignition delays with high peak pressure rise rate (PPRR) and heat release rates (HRR), confines the engine's operating loads and speeds. A strategy to reduce these negative effects of LTC is RCCI, which generally uses two fuels with different reactivities in order to optimize ignitability and equivalence ratio stratification. It has demonstrated improvements in efficiency and low NO_x and PM emissions by utilizing in-cylinder fuel blending, while the simultaneous optimization of fuel reactivity results in increased engine operating space.

The current work investigates Reactivity Controlled Compression Ignition (RCCI) combustion in a light-duty multi-cylinder engine over steady-state and transient operating conditions using also fast exhaust sampling emissions equipment for UHC, NO and PM

measurements. A "single-fuel[1]" approach for RCCI combustion was studied using port-injected and direct-injected (DI) cetane improved gasoline with custom designed, 15.3:1 compression ratio, pistons. In addition, experiments were conducted using mixtures of gasoline and diesel, i.e., "dieseline", as the high reactivity fuel. The experiments were performed over a broad selection of "ad hoc" load and speed points in order to examine performance and emission effects of a less reactive DI fuel mixture to in turn reduce the need for a second fuel.

This work also helps to demonstrate the requirements for high levels of boost in a multi-cylinder engine during RCCI operation. Comparisons were also made to an HCCI/GCI like combustion strategy using similar gasoline/diesel fuel blends.

[1] *Single-fuel* means that one mixture of dieseline was used for the tests, and therefore can also be considered as partial fuel stratification (PFS).

Acknowledgements

Many individuals helped to realize this research with their support and guidance. Foremost I would like to thank Prof. Dr. Rolf Reitz for being my advisor and giving me the opportunity to work and be part of his laboratory and a student of his consortium. He has provided me with much insight and direction throughout the last four years in order to fulfill all the requirements for this degree. I would at this point also like to thank my committee members for their time and support.

The Engine Research Center and its graduate students and staff have been instrumental and supportive throughout this research, providing important help whenever needed. I want to specifically name Reed Hanson, Martin Wissink and Ryan Walker. All three have been a great resource of knowledge and gave a lot insight during my early days at the ERC.

I would like to acknowledge the Diesel Engine Research Consortium for their financial support in order to conduct this study. The reports, phone-conferences and annual meetings have provided a valuable experience and asset for my future.

My deepest gratitude goes out to my parents Monika and Werner who have been there for me every step of the way. They always have been a great support and source of motivation. And finally, I would like to thank my wife Michelle for her motivation and believe in me. She has been incredibly supportive from the very beginning of my work here at the ERC.

Table of Contents

List of Tables

List of Figures

Nomenclature

Abbreviations

AFR	Air Fuel Ratio
AHRR	Apparent Heat Release Rate
ATDC	After Top Dead Center
BMEP	Brake Mean Effective Pressure
BTDC	Before Top Dead Center
BTE	Brake Thermal Efficiency
BSFC	Brake Specific Fuel Consumption
CA50	Crank Angle at 50% Mass Fraction Burned
CAD	Crank Angle Degrees
CDC	Conventional Diesel Combustion
CFD	Computational Fluid Dynamics
CI	Compression Ignition
CL	Closed Loop
CN	Cetane Number
CO	Carbon Monoxide
CO_2	Carbon Dioxide
CR	Compression Ratio
CRI	Common Rail Injection/Injector
DAQ	Data Acquisition System
DI	Direct Injection
DOC	Diesel Oxidation Catalyst
DPF	Diesel Particulate Filter
Dxx	Diesel content of x-vol% mixed with Gasoline
ECT	Engine Coolant Temperature
ECU	Engine Control Unit
EGR	Exhaust Gas Recirculation
EHN	2-Ethylhexyl Nitrate
EIA	Energy Information Agency
EIHC	Emissions Index of HC
EINO	Emissions Index of NO
EPA	Environmental Protection Agency
EVC	Exhaust Valve Closing
EVO	Exhaust Valve Opening
FID	Flame Ionization Detector
FSN	Filter Smoke Number
FTIR	Fourier Transform Infrared

GCI	Gasoline Compression Ignition
GDI	Gasoline Direct Injection
GHG	Green House Gas
GM	General Motors
GMEP	Gross Mean Effective Pressure
GTE	Gross Thermal Efficiency
HC	Hydrocarbon
HCCI	Homogenous Charge Compression Ignition
HD	Heavy-Duty
HP	High Pressure
HPV	High Pressure Valve
HRR	Heat Release Rate
HTC	High Temperature Combustion
HTHR	High Temperature Heat Release
IC	Internal Combustion
ICE	Internal Combustion Engine
IMV	Inlet Metering Valve
ISFC	Indicated Specific Fuel Consumption
IMEP	Indicated Mean Effective Pressure
IVC	Intake Valve Closing
IVO	Intake Valve Opening
LD	Light-Duty
LFE	Laminar Flow Element
LHV	Lower Heating Value
LNT	Lean NOx Trap
LP	Low Pressure
LTC	Low Temperature Combustion
MAF	Mass Air Flow
MCE	Multi-Cylinder Engine
MON	Motor Octane Number
MPRR	Maximum Pressure Rise Rate
NC	Next Cycle
NI	National Instruments
NO_x	Oxides of Nitrogen
NMEP	Net Mean Effective Pressure
NTC	Negative Temperature Coefficient
NTE	Net Thermal Efficiency
NVO	Negative Valve Overlap
OEM	Original Equipment Manufacturer
OL	Open Loop
ON	Octane Number
ORNL	Oakridge National Laboratory

PCI	Premixed Compression Ignition
PCCI	Premixed Charge Compression Ignition
PFI	Port Fuel Injection/Injector
PID	Proportional Integral Differential
PM	Particulate Matter
PON	Pump Octane Number
PPCI	Partially Premixed Compression Ignition
PPRR	Peak Pressure Rise Rate
PRF	Primary Reference Fuel
RCCI	Reactivity Controlled Compression Ignition
RON	Research Octane Number
SAE	Society of Automotive Engineers
SCCI	Stratified Charge Compression Ignition
SCE	Single Cylinder Engine
SCR	Selective Catalyst Reduction
SI	Spark Ignition
SOI	Start of Injection
TDC	Top Dead Center
TWC	Three Way Catalyst
ULSD	Ultra Low Sulfur Diesel
UW	University of Wisconsin
VCT	Variable Cam Timing
VGT	Variable Geometry Turbo
VSA	Variable Swirl Actuator

Greek Symbols

Φ	Equivalence Ratio
Θ	Spray Plume Angle

Chapter 1 Introduction

1.1 Background and Motivation

Originally designed for stationary power applications by Nikolaus Otto and Rudolf Diesel, the internal combustion (IC) engine has come a long way to become the major source of mobile power all around the world. In 1888, Bertha Benz was the first to make a cross-country automobile journey with a two-stroke Benz Motorwagen and revolutionized people's mobility, but without concerns about the engine's inefficiency. Since then, advancements in materials, operating pressures, air and fuel systems, etc., have significantly increased the energy conversion efficiency and made IC engines the ideal mobile application due to their high power density.

However, IC engines still generate harmful combustion products, which can have adverse effects on the environment, climate and human health. With carbon-based fuels, such as gasoline or diesel being used for the majority of IC engine applications, combustion typically results in cylinder-out emissions species, such as unburned hydrocarbons (UHC), oxides of nitrogen (NO_x), carbon monoxide (CO), carbon dioxide (CO_2) and particulate matter (PM).

Despite those drawbacks, the IC engine remains the most feasible power source, especially for mobile applications, so that the main factors driving the development of the internal combustion engine today are efficiency improvements with considerations of emissions, energy reserves, and economics.

A reduction of dispersed emissions is crucial in order to lessen the impact on humans (e.g., ultrafine PM particles can cause asthma and cancer) and possible environmental effects (e.g., NO_x and CO_2 are known greenhouse gases responsible for climate changes around the world) [1]. While advancements in mining and exploration technologies for crude oil benefit the production of carbon-based fuels, energy reserves are expected to slowly be depleted due to the higher

consumption rate over the regeneration time of fossil oil. Economically speaking, modern IC engines have become progressively more complex, i.e., new materials and equipment costs for building a clean and efficient IC engine have become a stronger factor towards producing a cost-effective automobile.

In an effort to address these growing concerns about energy sources and their consumption as well as the emissions, diesel engines in general, and direct-injection diesel engines specifically, have received a considerable amount of interest. A diesel engine offers superior thermodynamic efficiency and reduced CO_2 emission advantages over spark-ignited gasoline engines by incorporating higher combustion efficiencies, more favorable specific heats in the charge and the ability to use high compression ratios. In a conventional direct-injected compression ignition (DICI) engine, the injected high pressure liquid fuel jet breaks up very rapidly into small droplets that begin to vaporize and mix with the surrounding hot air. Due to the high reactivity of diesel fuel the mixture auto-ignites readily without knocking. Following the pre-mixed combustion event, a diffusion flame is established in which the fuel burns at stoichiometric mixture conditions. Unfortunately, the diffusion-controlled combustion in diesel engines produces high PM and NO_x emissions due to hot fuel rich regions and high local temperatures, respectively. In addition, the lean nature of combustion complicates NO_x removal by catalytic exhaust after treatment. Figure 1-1, a local equivalence ratio – local temperature space diagram, illustrates the emission consequences stemming from the different combustion strategies [2].

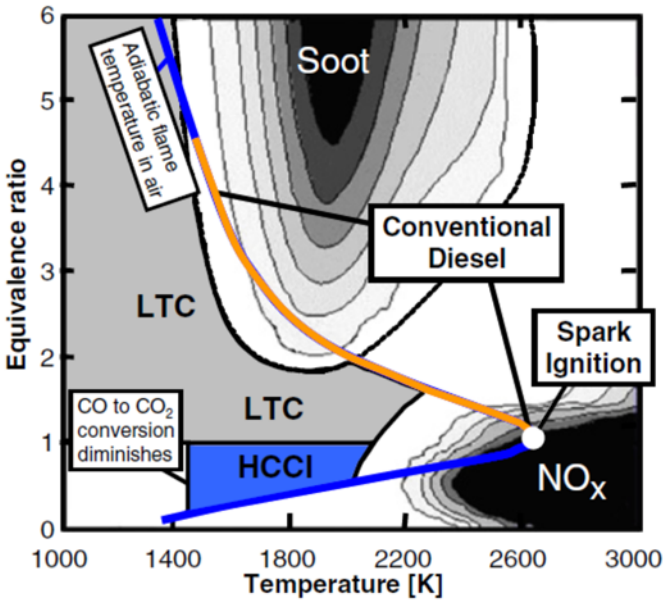

Figure 1-1 Diagram of local equivalence ratio vs. local temperature for NOx and soot formation for different combustion concepts [3]

There are options to reduce NO_x and PM emissions through exhaust after-treatment, but these generally come with trade-offs and penalties. Diesel Particulate Filters (DPF's), which reduce PM levels, are extremely effective. However, as the filter element fills up, the exhaust back pressure increases and thus thermal efficiency decreases. A regenerative cycle with a late fuel injection is required and implemented by the manufacturer in order to raise the exhaust temperature and burn soot off the filter walls, thus increasing the fuel consumption and reducing useful work output [4].

Commonly used after-treatment systems for NO_x reduction are Selective Catalytic Reduction (SCR) systems and Lean NO_x Traps (LNT). The effectiveness of a conventional three-way catalyst is prevented by the high exhaust oxygen concentration. A LNT, built-up from precious and expensive metals, allows storage of NO_x during lean operation, but requires periodic rich combustion to empty the trap and operates at an efficiency of only about 70% [5]. SCR systems have no need for rich operation as they use a separate Diesel Exhaust Fluid (DEF) to chemically reduce NO_x and are up to 95% effective. DEF also contributes to fuel consumption and

maintenance costs. In conclusion, after-treatment systems for NO_x and PM emissions are effective at reducing these emissions, but are extremely expensive and complex.

Combined with increasingly stringent regulations for PM and NO_x emissions and recently introduced CO_2 emission mandates for light- and heavy-duty IC engines, researchers have pursued the development of Low Temperature Combustion (LTC) concepts. Referred to as Premixed Charge Compression Ignition (PCCI), Premixed Compression Ignition (PCI) or Modulated Kinetics (MK), LTC concepts have the potential to reduce PM and NOx emissions while maintaining high thermal efficiency. Emissions are reduced in-cylinder, i.e., minimizing exhaust after-treatment costs and improving system efficiency and fuel consumption.

While a significant amount of research and development of LTC strategies has been conducted, the majority of the work has focused on steady-state operation. However, most engines in transportation applications require operation under transient conditions, and frequent or continuous changes in speed and load can negatively affect performance. Especially LTC concepts with their kinetically controlled combustion are more sensitive to changes in dilution and thermodynamic conditions. Therefore, it is important to investigate the transient behavior of LTC concepts and gather detailed information on their transient responses. This would allow minimizing the transient emission contribution and further close the gap between steady-state and transient operation in order to implement LTC strategies into mass production.

1.2 Research Objectives

The focus of this research is to investigate operation of Reactivity Controlled Compression Ignition (RCCI) combustion in a multi-cylinder engine using a "single-fuel" approach. The four primary objectives of this work are:

1.) Use a multi-cylinder light-duty engine in steady-state experiments to demonstrate and compare the performance of different reactivity dieseline mixtures for "single-fuel" RCCI combustion (Chapter 4). The work follows previous studies using gasoline blended with cetane improver additives, including EHN.

2.) Use a multi-cylinder light-duty engine in steady-state experiments to demonstrate the performance of boosted RCCI operation and discuss limitations of the production intake system (Chapter 5).

3.) Investigate and develop a comparison of HCCI-like combustion using dieseline to gasoline/dieseline RCCI operation (Chapter 6) within a multi-cylinder light-duty engine under steady-state operation

4.) Investigate and demonstrate performance of single-fuel RCCI operation using dieseline in a multi-cylinder light-duty engine under steady-state operation (Chapter 7)

5.) Use a multi-cylinder light-duty engine in transient experiments to demonstrate the performance of gasoline/dieseline RCCI operation versus gasoline/diesel RCCI fueling (Chapter 8).

1.3 Approach

In this study mainly metal engine experiments are used to address the objectives. For the first objective, steady-state multi-cylinder experiments are performed. Operating the engine under the

RCCI combustion strategy using a new piston design under similar conditions allows for an evaluation of fuel effects.

For the second objective, further steady-state multi-cylinder experiments are performed using the RCCI combustion strategy with a previously determined optimal dieseline (gasoline plus diesel) mixture in order to investigate limitations stemming from the intake system.

For the third objective, the main focus of the experiments is a comparison between two LTC strategies. First, HCCI (kinetics) simulations are performed to determine an optimum dieseline blend for the metal engine experiments that follow. Next the results are analyzed and compared to RCCI engine performance.

The fourth objective will be realized under the RCCI combustion strategy using once more an optimum dieseline blend to investigate and analyze performance of this single-fuel RCCI approach. A comparison is thereby made with typical gasoline/diesel and gasoline/dieseline operation.

The last objective involves transient multi-cylinder experiments using the RCCI combustion strategy to determine and explain the performance of gasoline/dieseline with the consideration of transient effects.

Chapter 2 Literature Review

2.1 Internal Combustion Engine

Converting chemical energy by burning fuel with air into mechanical work and thus generating motion power is the fundamental process of all internal combustion engines. Within this process, work is extracted from the use of hot gases that are produced following the compression and ignition of the fuel-air mixture inside the cylinder. Either an electric spark or compression induced auto-ignition thereby introduces ignition. Based on these methods of ignition engines and their combustion processes are typically categorized as spark ignition (SI) and compression ignition (CI), respectively.

2.1.1 Conventional Diesel Combustion

The modern compression ignition (CI) engine is the most fuel-efficient engine of our time and its fundamental process was first implemented by Rudolf Diesel in 1893. The Diesel cycle, as often referred to for ideal closed-loop thermodynamic cycles for CI combustion, has heat addition occurring at constant pressure [6]. With a higher load to peak pressure ratio, the Diesel cycle offers higher efficiency for a given peak pressure and is not limited to low compression ratios.

In this regard and with the increasing demand for improved fuel economy and growing concerns about the world's petroleum consumption has moved the industry's focus towards the CI engine and its advantages. It offers high thermal cycle efficiencies due to a lean fuel-air mixture combustion and high compression ratios. There is also no need to throttle the intake air, since the load is controlled by the amount of fuel injected directly into the cylinder, therefore reducing the pumping losses of the engine. And finally, the engine's calibration is not knocking limited, offering the capability of turbo/supercharging in order to increase its power output.

This Diesel combustion process, using high-reactivity fuel via direct-injection in a high-temperature mixing-controlled environment, is often also referred to as conventional diesel combustion (CDC). During CDC, with the absence of a spark plug to initiate combustion, higher charge gas temperatures auto-ignite the fuel. The ignition is facilitated by the fuel being injected near top dead center and under high pressures (1,000-3,000bar) in order to allow better atomization and thus better mixing with the air. Fuel penetration, i.e., liquid length, is a function of injector hole size, TDC temperatures and density. Ultimately a diffusion-limited burn of the diesel injection plumes is manifested. As can be seen in Figure 2-1, a high-temperature reaction zone surrounds a zone of rich fuel vapor. While the reacting fuel jets continue to further penetrate in to the center of the cylinder, rich partially broken down fuel fragments wait to be combusted at the outer flame surface.

Diesel combustion is typically associated with “knocking”, i.e., loud combustion noise. This phenomenon is a result of fast pressure rise rates during the ignition phase, also called the premixed burn phase. The premixed burn phase precedes the diffusion or non-premixed burn phase.

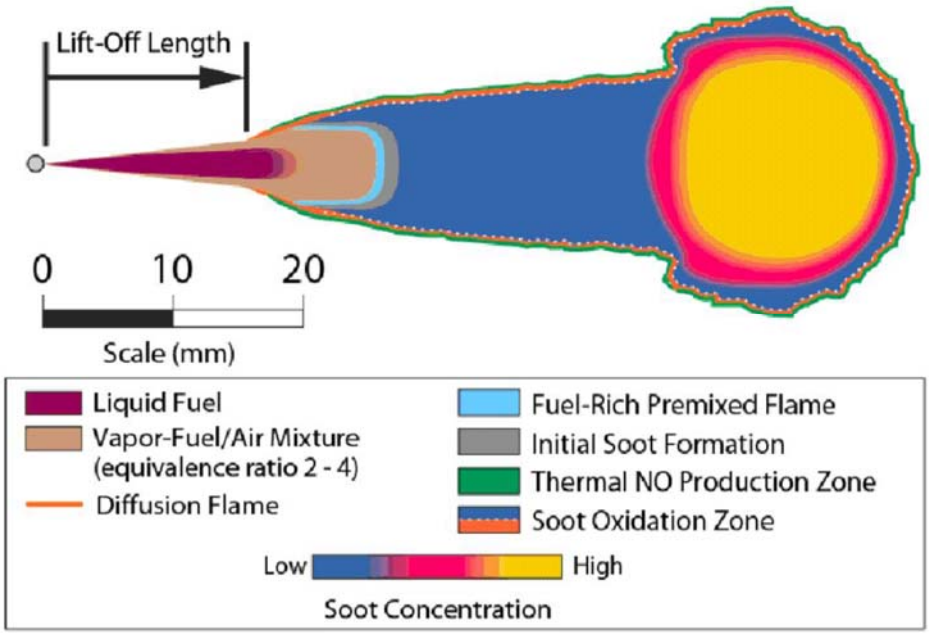

Figure 2-1 CDC Combustion regions and soot formation in diffusion flame [7]

2.1.2 Gasoline Combustion

When Nikolaus Otto designed the first of its kind Otto engine in 1876, the construction of the engine was far from today's SI engine design. The modern gasoline SI engine is a highly efficient internal combustion engine, where even direct-injected fuel delivery is playing an important and increasing part of its combustion process. The so-called Otto cycle can also be described as an ideal closed-loop thermodynamic cycle with isentropic compression and expansion. In contrast to the Diesel cycle however, heat addition occurs at constant volume, offering a higher maximum thermal efficiency for a given compression ratio [6].

The Otto combustion process uses less reactive fuel in order to prevent early auto-ignition of the mixture and thus in-efficiencies and damage to the piston and liner. Injection typically takes place in the intake system through a port injector, but gasoline direct-injection systems are also available, in which case fuel is injected into the cylinder early in the cycle. Both methods combust a slightly rich to slightly lean fuel-air ratio by using a spark plug as an ignition source at the appropriate timing. Depending on the requirements of the engine's power output, the equivalence ratio is adjusted, and while leaner combustion is desired for complete combustion, the limit for leaning out the mixture is typically at an equivalence ratio of ~ 0.76 due to the flammability limit of the fuel. The process is characterized as a flame-propagation dominated combustion.

The timing of the ignition in combination with the amount of fuel injected, (i.e., equivalence ratio) is crucial in order to optimize engine efficiency, fuel consumption and emissions. Unfortunately, these requests cannot be satisfied simultaneously.

Low Temperature Combustion Regimes

Due to more and more stringent emissions regulations and the consequent fuel efficiency penalties of current exhaust after-treatment systems, many advanced combustion strategies have

been the focus of recent engine research. By meeting emissions regulations in-cylinder, those strategies not only increase the engine's efficiency and lower its emissions, but also reduce the cost and complexity of next generation engine systems. Most of those combustion strategies fall into the category of low temperature combustion (LTC). A highly lean charge and low combustion temperatures help to largely avoid the NOx and PM islands [Figure 1-1], while, in addition, the specific heat ratios are increased, thus improving the thermal efficiency of the engine. However, where low combustion temperatures improve NOx emissions, they offset fuel oxidation rates of HC and CO. Furthermore, low combustion temperatures result in a low exhaust enthalpy, which leads to an insufficient amount of work available for extraction in the turbocharger. With several different LTC strategies commonly used and a general comparison being presented in Figure 2-1, more specific benefits and challenges for two such strategies are outlined in the following. As examples of the so-called premixed compression ignition (PCI) category they are: homogenous charge compression ignition (HCCI), and reactivity controlled compression ignition (RCCI).

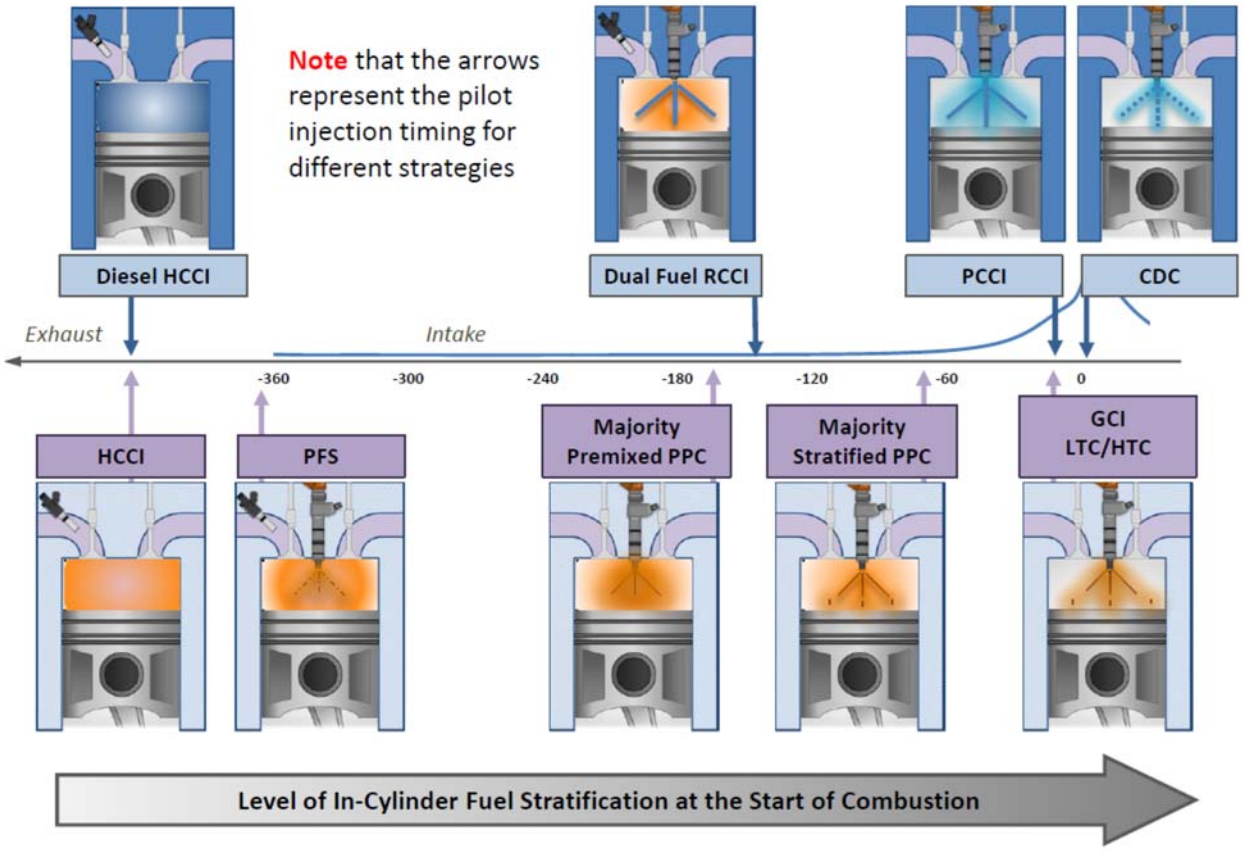

Figure 2-2 Various compression ignition strategies in terms of the level of stratification. Blue demonstrating Diesel/high-reactivity fuel and orange demonstrating Gasoline/low-reactivity fuel. Wagner et al.[8]

2.1.3 HCCI

Homogeneous Charge Compression Ignition (HCCI) is a hybrid of the well-researched Spark Ignition (SI) and Compression Ignition (CI) engine combustion concepts. It is an LTC strategy and therefore is used to provide both high thermal efficiency and low emissions, i.e., NOx and PM. In HCCI, as in an SI engine, a homogeneous fuel and air mixture is prepared in the inlet system, externally from the cylinder. Then, during the compression stroke, just as in a CI engine, the mixture burns without any ignition system due to an increase in temperature.

HCCI operation was first investigated in 1979 by Onishi et al. [9], originally termed Active Thermo-Atmosphere Combustion, as a method to improve low- and mid-load performance and a

reduction in HC emissions in a two-stroke engine. This was followed by other studies of this phenomenon [10]. Najt et al. [11] and later Thring [12] demonstrated that it is possible to achieve high efficiencies and low NOx emissions by using high compression ratios and lean mixtures for HCCI operation in 4-stroke engines. Based on these studies many researchers have investigated HCCI to further understand its operation and characteristics [13-15] .

During HCCI operation, the load of the un-throttled engine is controlled by the equivalence ratio of the charge (typically lean: 0.2-0.4) and the thermodynamic conditions (i.e., in-cylinder temperatures, composition and pressures). Combustion solely relies on chemistry and the process is therefore referred to as kinetically controlled. The well-mixed charge auto-ignites with almost simultaneous combustion across the entire cylinder. This leads to a fast release of heat and thus a rapid increase of cylinder pressure, that can not only cause noise vibrations and negative effects on heat loss but ultimately engine damage. On the other hand, too much leaning of the mixture will result in low combustion efficiencies or even misfire.

Recent research focuses on controlling combustion duration and phasing, along with techniques to slow down the rapid HRR and to broaden the operating range of HCCI. Work on boosted HCCI by Christensen et al. [16] and Olsson et al. [17] demonstrated extended high load up to 16bar IMEP by using intake pressures upwards of 3 bar (absolute). However, where boosting was able to significantly enhance IMEP, combustion phasing became too advanced, leading to engine knock. Christensen et al. [18] also showed that HCCI operation is possible over a wide variety of fuels, using several combination of iso-octane and n-heptane at an appropriate compression ratio and inlet air temperature.

Dec et al. [19, 20] made substantial efforts to allow control of the HRR by using high speed chemiluminescence along with investigation of using EGR in order to dilute the charge. Dec. et al. [21, 22], Sjoberg et al. [23, 24] and Manente et al. [25] demonstrated improved HCCI operation

by applying combinations of techniques, showing strong potential for achieving power levels and combustion stability close to that of turbo-charged diesel engines.

2.1.4 RCCI

Based on research by Bessonette et al. [26], Kokjohn et al. [27, 28] confirmed by initially employing computations that the ideal fuel blend for PCI strategies has auto-ignition qualities between gasoline and diesel and is dependent on engine load and operating conditions. By further addressing findings by Inagaki et al.[29], where stratification of fuel reactivity resulted in reduced heat release rates and combustion noise and showed high load capabilities and reduced EGR requirements for dual-fuel PCI strategies, Kokjohn et al. [30] and Hanson et al. [31] demonstrated a premixed dual-fuel strategy in a heavy-duty engine. The use of premixed port-injected gasoline and direct-injected diesel fuel reduced the peak pressure rise rate (PPRR) significantly and deployed the difference in reactivity between the two fuels by utilizing in-cylinder blending, allowing for efficient and clean combustion. This optimized strategy was called reactivity controlled compression ignition (RCCI) [32, 33].

RCCI is a chemically controlled combustion process similar to homogeneous charge compression ignition (HCCI) that provides control over the combustion phasing via the overall fuel reactivity (i.e., gasoline/diesel ratio) and control over the rate of heat release via the in-cylinder fuel reactivity stratification (i.e., injection strategy). Results of a sweep of gasoline fraction are shown in Figure 2-3. Experiments by Splitter et al. [34] revealed a staged combustion process wherein areas of high and low fuel reactivity result in a sequential auto-ignition process in order to extend the duration of the combustion process. The in-cylinder fuel reactivity gradients required for controlling combustion were established by a double injection strategy, which conditions the premixed fuel in the squish/near-liner region with the first injection (-80 to -50 deg ATDC) and

uses the second injection event (-45 to -30 deg ATDC) as an ignition source in the bowl of the piston.

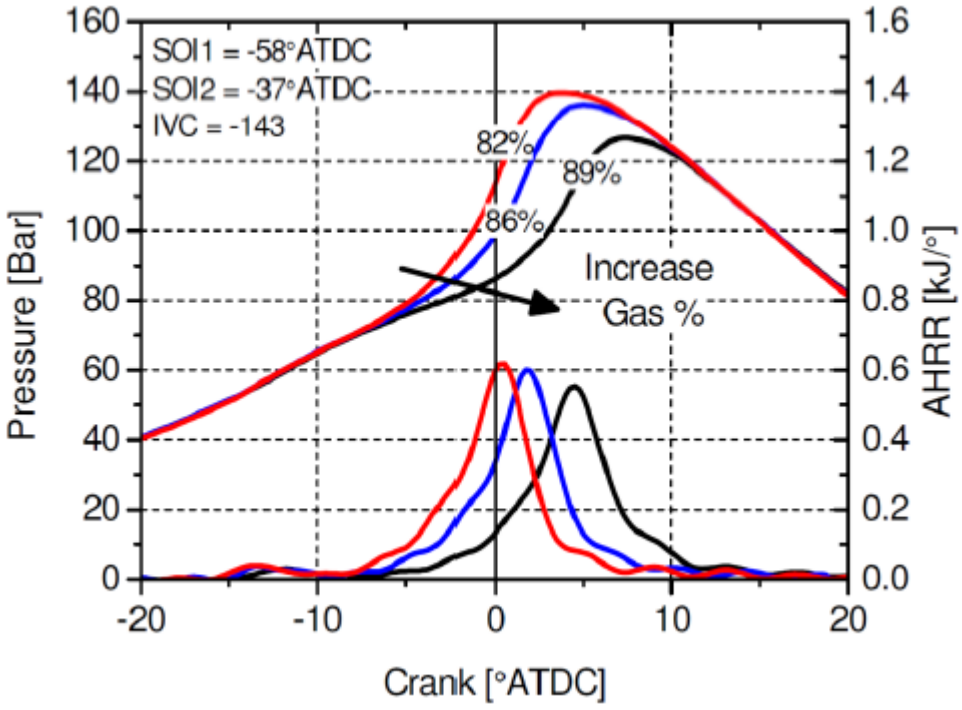

Figure 2-3 RCCI combustion for different gasoline-to-diesel ratios, Hanson et. al [31]

However, different levels of control are achieved not only by the use of two fuels with different reactivities, i.e., the ratio of non-reactive versus reactive fuel, but also by adjusting the intake temperature, rate of EGR, and duration and timings of the injection event(s). Figure 2-2 shows the level of combustion phasing control derived from changes in the percent gasoline amount:

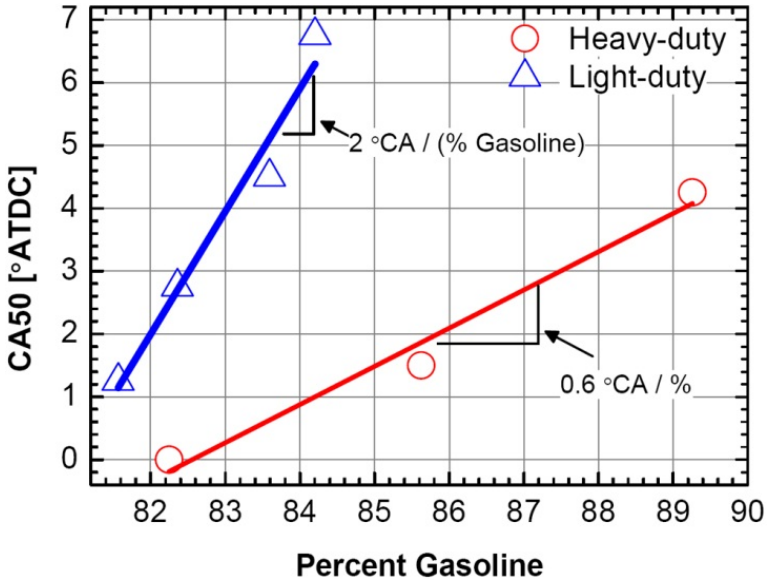

Figure 2-4 RCCI phasing change as a function of gasoline percent for LD and HD operation [32]

Further investigation of the characteristics of RCCI combustion have been of interest in recent engine research. The focus was put on efficiency and emission level improvements, as well as load extension and controllability of the RCCI concept. While work by Splitter et al. [35] reached gross indicated efficiencies of 60% and demonstrated clean and efficient RCCI engine operation from 4 bar brake mean effective pressure (BMEP) to 20 bar BMEP [36], with combustion efficiencies ranging from 97% at low loads to greater than 99% at high loads, work by Dempsey et al. [37] studied the controllability of dual-fuel RCCI in comparison with dual-fuel HCCI, and single-fuel partially premixed combustion (PPC). It was found that dual-fuel RCCI was able to recover changes in combustion phasing, imposed by changes in intake pressure and temperature, simply by modifying the global fuel reactivity.

A complete picture and summary of the recent development and progress in research for the RCCI combustion strategy has been published by Reitz et al. [38]. It highlights engine experiments and computational studies that were performed on light- and heavy-duty engines and draws a comparison to conventional and advanced combustion concepts using a wide range of fuels.

2.2 Emissions

2.2.1 Diesel Dilemma

Diesel engines have both benefits and problems with regards to their engine out emissions. They offer decreased partial combustion products like CO and HC, however they also produce high NOx and PM emissions. Diesel type combustion generates temperatures high enough to easily reach the activation levels of thermal NOx production. PM or soot emissions thereby stand in a trade-off with the NOx emission, but are as much of a concern as NOx due to the fact that it is a non-premixed system. Large gradients of air-fuel ratios present extremely rich areas, and cause fuel particles inside the injection plume to not be combusted before the flame is extinguished at the edge of the combustion chamber. With decreasing temperatures, late-cycle oxidation of the uncombusted fuel becomes very difficult and slow, and eventually the PM is exhausted as black soot.

This has led to a reliance on exhaust after-treatment systems in order to meet more and more stringent emissions mandates. While effective to meet emissions regulations, these exhaust after-treatment systems are less mature and add a significant increase in cost to the engine system due to their complex development and integration. Devices, such as Diesel Oxidation Catalysts (DOC), Diesel Particle Filters (DPF), Lean NOx Traps (LNT) and/or Selective Catalyst Reductant (SCR), also impact the engine efficiency negatively and increase fuel consumption [4].

Any left-over HC and CO emissions are easily removed by the use of a DOC system, however NOx and PM reduction systems typically require frequent combustion enrichment as part of their operating principles. A LNT system [5] or NOx absorber system mandates rich burn phases to burn off all the NOx collected over a certain time of operation and has yet to prove a very effective alternative. The SCR systems are a lower first-cost approach, nonetheless they require the use of a Diesel Exhaust Fluid (DEF), typically urea, as a dosing agent at significant levels. So, while there

are ways to control NOx emissions, the systems are negatively affected by adding costs through the need for precious metals and additional fuel.

The reduction of soot emissions faces the same challenges. A DPF system that reduces tailpipe soot emissions by collecting soot particles over a certain period of operation, must also be regenerated. This can be achieved in a passive or active way. The active way requires high temperatures to clean the filter, where either late in-cylinder post injections or fuel injections directly into the exhaust system are needed to light-off the close-coupled DOC system, thus increasing the DOC-out temperature, but also increasing the vehicles fuel consumption.

Note also that, while it already is a disadvantage for exhaust after-treatments economically, recently introduced CO2 emissions regulations are additionally creating problems from an emissions standpoint, i.e., vehicles using PM or NOx emissions after-treatment systems that ask for the use of additional fuel can fail to reduce and meet CO2 standards [39].

2.2.2 PCI

Two main advantages are offered by LTC concepts, and both are directly connected to the highly lean charge mixture. For one, the highly lean charge with its increased specific heat ratios improves the thermal efficiency, i.e., lowers fuel consumption and hence CO2 emissions, while simultaneously reducing PM emissions due to reduced rich regions [40]. This also causes the combustion temperatures to be reduced and thus avoids the activation of NOx formation reactions. The NOx is reduced due to volumetrically ignited overall lean air/fuel mixture without a flame front.

Even though NOx can still be problematic at high loads with high equivalence ratios or at conditions where mixture inhomogeneity is possible, EGR is a good measure to lower high combustion temperatures and to reduce the overall equivalence ratio by diluting the fresh air with combustion products and nitrogen.

PM emissions are not of any major concern, since a lean and well mixed charge combined with the absence of flame propagation helps to avoid the soot island seen in Figure 1-1.

On the other hand, HC and CO emissions are increased for PCI concepts. Due to the lower combustion temperatures, the fuel oxidation rates are decreased, hence creating high HC and CO engine-out levels [40]. Another source for HC emissions for PCI combustion is unburned fuel that is trapped in the ring crevice regions, along with combustion quenching. This phenomenon is prevalent in SI engines where a well-mixed air/fuel composition encounters the ring pack in the compression stroke and is trapped close to the cool cylinder walls.

After-treatment systems for PCI concepts entail a three-way catalyst (TWC) to reduce HC and CO and thus meet emission standards. However, due to low exhaust temperatures resulting from the low combustion temperatures of PCI, the conversion efficiency of a TWC is only about 90% effective. This leaves room for improvement of innovative after-treatment concepts or improved TWCs in order to meet future emissions standards.

2.3 Fuels, Additives & Cetane Improvers

While the majority of the research on RCCI combustion [27, 28, 30, 31, 34] has been done by using gasoline and diesel as the low and high reactivity fuels, respectively, the nature of RCCI and its strong dependence on a fuel reactivity stratification gradient to be present in the chamber in order to generate clean and efficient combustion opens the door to a broad range of fuels that may be used. Looking beyond the availability limits that some fuel alternatives might have in comparison to gasoline and diesel, which are widely available, alternative fuels can offer improvements in emissions and efficiency.

Splitter et al. [41] conducted heavy-duty engine experiments and simulations for E85 (85% ethanol/15% gasoline)-diesel RCCI combustion and observed chemistry and fuel property effects

that required higher quantities of diesel fuel. Similarly, Curran et al. [42] tested the effects of E85 as a low-reactivity component in a light-duty engine and found that besides its effect on emissions, E85 allowed for significant load expansion. Hanson investigated moderate fuel blends of E20 (20% ethanol/80% gasoline) and B20 (20% biodiesel/80% diesel) [43], as well as higher levels of ethanol and biodiesel [44], and also saw difficulties in controlling the combustion event due to differences in fuel properties. Dempsey et al. [45] also performed light-duty tests with a wide array of low- and high reactivity fuels.

There are, however, practical challenges to the use of two different base fuels (i.e., two fuel tanks). In order to avoid the need for two separate fuel tanks and other additional complications that may occur from the use of two fuels. Some work has been performed using a fuel additive (i.e., cetane improver) to be mixed with the same single main fuel that is used as the port-injected low reactivity fuel. By doing so the vehicle would only require one primary fuel tank along with an additive tank sized similar to a diesel exhaust fluid tank (DEF). For example, using an average of 60% port-injected fuel and 40% direct-injected fuel with a fixed rate of 5% cetane improver added to the direct-injected fuel, the consumption would be about 2% of the total fuel, which reduces the practical challenges for RCCI combustion.

Work by Splitter et al. [46] evaluated the use of gasoline/DTBP (di-tert-butyl peroxide) as the reactive fuel in a heavy-duty engine allowing for efficient RCCI combustion. Further work by Splitter et al. [35] combined an alternative low-reactivity fuel and the high reactive gasoline/DTBP fuel blend to achieve gross indicated thermal efficiencies approaching 60%. Hanson et al. [47] investigated the use of gasoline/EHN as the reactive fuel, achieving high peak efficiencies at 4.5 bar gross indicated mean effective pressure (IMEP) and highlighting differences in high temperature heat release (HTHR) as well as low temperature heat release (LTHR). In similar experiments in a light-duty engine, Kaddatz et al. [48] used E10 (10% ethanol/90% gasoline) as

the non-reactive fuel and E10/EHN as the reactive fuel. While NO_x levels were slightly higher due to the fuel-bound nitrogen at 9 bar gross IMEP, approximately 50% gross indicated[2] thermal efficiency was achieved. Dempsey et al. [49] recently continued the work on EHN by characterizing its behavior for different volume percentages. He observed a strong dependence of NO_x emissions on the global EHN concentration with a large increase in NO_x emissions over conventional dual-fuel RCCI combustion. Results by Gross et al. [50] showed similar trends for the use of EHN as a cetane improver during steady-state as well as transient RCCI operation. Attempts to match CA50 led to late main SOI timings and longer DI injection durations due to the increased amount of DI fuel, and therefore to distinct differences in the combustion characteristics between gasoline/diesel and gasoline/gasoline+EHN RCCI combustion. Thus, it was observed that the NO emissions were increased above the fuel bound threshold caused by the injection strategy adjustments.

2.4 Multi-Cylinder Engine

In general, multi-cylinder engines (MCE) have been uncommon for use in combustion research, and even more so for advanced combustion strategies. During MCE operation it is hard to control thermal- and volumetric cylinder-to-cylinder interferences, such as gas exchange, gas residual amounts, etc. Furthermore, multi-cylinder engines create an additional challenge in terms of instrumentation, i.e., multiplication of control variables, and require additional laboratory equipment and measurement systems. Despite all this, multi-cylinder testing is important to understand the performance of LTC combustion strategies, such as HCCI and RCCI, in order to be adopted in production engines.

[2] *Gross* refers to the compression and expansion strokes only (e.g. -180° aTDC to 180° aTDC). *Indicated* means the cycle work was calculated from the cylinder pressure, which does not account for engine friction and other losses.

Past work [51, 52] has shown the capability to operate advanced combustion strategies on the stock engine set-up, but also pointed out problems faced during operation, as stated above. Thus, modifications, such as variable cam timing (VCT) and turbocharger downsizing had to be made to allow operation. Curran et al. [53] applied the RCCI combustion strategy, highlighting the importance of cylinder-to-cylinder balancing by trimming combustion parameters for each cylinder.

Recently, researchers at the University of Wisconsin (UW) Madison Engine Research Center (ERC), Oakridge National Laboratory (ORNL) and Argonne National Laboratory (ANL) [42, 43, 48, 50, 54, 55] have investigated RCCI combustion with comparisons to conventional diesel combustion (CDC), determining fuel flexibility on a multi-cylinder engine. In order to obtain operation and maintain combustion with maximum efficiencies, cylinder balancing by adjusting control parameters was necessary. Accordingly, improvements in the air handling and charge air system need to be a priority to minimize differences between each cylinder. Building on their results, more work needs to be done that contributes to further exploration of RCCI combustion in a multi-cylinder engine and to experimental multi-cylinder research in general.

2.5 Transient Engine Operation

Historically, the majority of experimental engine research has been performed under steady-state conditions. This is due to the fact that testing is facilitated and no special fast response equipment is needed. However, most vehicles, on- and off-road, operate by constantly changing their engine speeds and load points, so that today's certification tests, such as the US FTP75, US06 and HWFET [56 pp.543-620 #65, 57] , are performed under transient conditions to simulate realistic engine operation. As a result, extrapolated steady-state data is often used out of convenience, but it has been shown repeatedly in the literature to be an unreliable indicator of

transient operation since it poorly matches realistic, in-use emissions [58-62]. For example, steady-state approximations do not catch the major portion of emissions that occur in the first short period of a fast speed and/or load change [63]. In a comparison between an ISO 8-mode duty-cycle and several transient test cycles [59], steady-state tests predicted NO_x within 10% of the transient cycle emissions, but a great disparity was seen for UHC and PM emissions. In addition, major variations were shown from test-to-test as well as engine-to-engine, highlighting the accuracy needed to match a test cycle with a realistic transient duty cycle. Swain et al.'s [58] approach of weighting the mode points still led to an under-prediction of the UHC and PM emissions by as much as 60%. Adding correction factors or applying parameters for quasi-steady approximations have been used to get a correlation between steady-state and transient results [60], but did not add predictive capability, which illustrates the difficulty to predetermine in-use test cycle emissions.

With these findings in mind, Glewen [64] was one of the first to investigate the performance of transient LTC in order to determine deviations from steady-state operation. Being developed from mostly steady-state data, new assumptions and experiments to verify transient LTC capability are very valuable. He found that changes in boundary conditions, especially intake O2 concentration, caused the highest variations for LTC transient emissions. Hence, limitations of the air system's response, i.e., slower EGR response rate, lead to an imbalance between the air and fuel systems, where adjustments would result in changes to load and drivability. Hanson et al. [65] and Gross et al. [50] saw similar results later during experiments for RCCI combustion. EGR lag and turbocharger lag were limiting factors, and resulted in deviation of the control variables. Both also found that the thermal inertia of the engine greatly affected the transient performance in LTC, where delays in temperature response further increased the differences in steady-state operation compared to CDC.

2.6 Turbo- and Supercharging

Previous studies have shown that boosted RCCI operation can be crucial to improve performance and maximize efficiencies [35]. As shown in this work and highlighted previously by Hanson [44] and Gross et al. [50] , the inappropriate turbocharger size of the stock engine causes poor transient response and low intake pressure levels. The present work will address limitations in boosting caused by the single-stage turbocharger by using instead building air. A variable pressure control valve that has been installed is able to boost intake pressures up to about 6.0 bar, thus significantly expanding the achievable range of intake manifold pressure.

Chapter 3 Laboratory Setup, Instrumentation and Experimental Conditions

This chapter presents details of the experimental light-duty MCE diesel engine laboratory and its instrumentation. It also highlights the data acquisition and post-processing that was used to carry out the present study. It introduces the RCCI piston design that was used instead of the stock original equipment manufacturer (OEM) design. The chapter further reports on the specifications of the fuels that were used in the experiments, and gives insights into the calibration and test procedures.

3.1 Light-Duty MCE Setup

3.1.1 Engine

The engine used for the experiments is a modified General Motors/Opel Z19DTH 1.9liter multi-cylinder diesel engine. This engine is certified to EURO IV specification and utilizes standard production hardware, such as a Bosch common rail injection (CRI) system, a variable geometry turbine (VGT), cooled high pressure (HP) EGR, and a variable swirl actuation (VSA) intake port geometry. Exhaust after-treatment consisted of a close-coupled diesel oxidation catalyst (DOC) – DPF unit. The engine was maintained in its factory configuration as much as possible to preserve the transient characteristics of the OEM engine. However, modifications to the engine had been made in order to allow port fuel injection into the intake manifold, as well as to add a low pressure (LP) EGR system. The LP EGR (not used in this study) was installed by modifying the pre-compressor inlet and repositioning the after treatment unit. In the present study, a variable air pressure regulator, capable of simulating a supercharger, was added to provide more flexibility and control of the air system.

In addition, the production air-to-air intercooler was replaced by an air-to-water intercooler, set to match the OEM cooling capacity. Table 3-1 describes the specifications of the engine and Figure 3-1 shows a schematic of the engine system.

Table 3-1 GM 1.9L Engine Specifications

Engine Type	EURO IV Diesel
Bore [mm]	82
Stroke [mm]	90.4
Displacement [L]	1.9
Cylinder Configuration	Inline 4; 4 valves per cylinder
Swirl Ratio [-]	Variable (2.2-5.6)
Compression Ratio [-]	16.7 (stock); 15.3 (custom Piston)
Turbocharger	Custom Garrett M53 VGT w/o compressor
EGR Systems	Hybrid High/Low Pressure, Cooled
ECU	Bosch EDC16 (OEM); Drivven (new)
Injection Pump	Bosch CP1H3
Common Rail Injectors	Bosch CRIP2-MI, 148° Included Angle 7 holes, 440 flow number
Port Fuel Injectors	Delphi, 2.27 g/s steady flow, 400 kPa fuel pressure

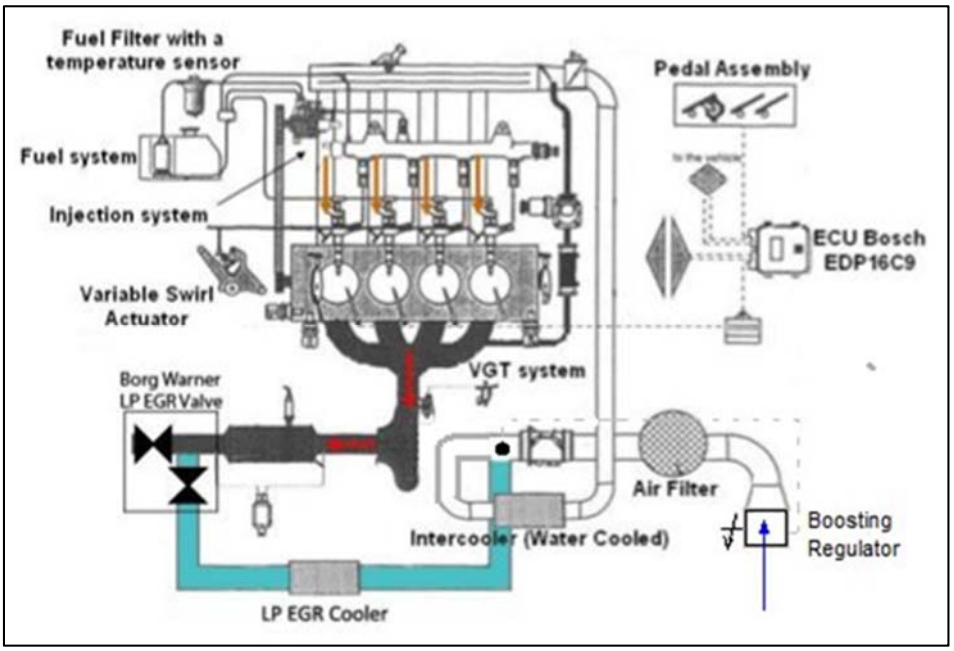

Figure 3-1 Schematic of the test engine laboratory

3.1.2 Hydrostatic Dynamometer

The engine was connected to a hydrostatic dynamometer developed at the UW Madison that is able to handle fast speed and load transients [66-68]. The system is capable of providing motoring and absorbing torque features with a low rotational inertia in order to replace a traditional electric dynamometer set-up. There are two pump/motor assemblies that work in conjunction, with one assembly being directly mounted to the engine's crankshaft. The engine-mounted pump/motor is forced to pump hydraulic fluid at high pressures in order to absorb the load. During motoring, the second assembly pumps fluid through the first pump/motor assembly. A high speed servo valve is ultimately used to control the load by varying the restriction. The closed-loop control of the servo valve, along with the control and monitoring of auxiliary pumps, motors, valves, pressures and temperatures, is provided by a NI cRIO-9102. A detailed documentation of the dynamometer control and implementation of the data acquisition system is discussed by Burton [69].

The crankshaft torque, used for the control of the dynamometer as well as for data processing and engine calibration, was measured using a HBM T-40 in-line torque transducer. It allows precise rotational speed measurements, thus to be converted to an accurate torque output of the engine. Overall laboratory set-up is highlighted in further detail by Glewen [64].

3.2 Instrumentation

3.2.1 Engine Controls

A Drivven engine controller [Figure 3-2] replaced the OEM engine control unit (ECU). It allows full access to all engine parameters and enables control of the additional port fuel injection (PFI) injectors in order to operate specifically, but not only in the RCCI combustion mode. The Drivven controller gives real-time access and modification possibilities to all engine maps and other control parameters via 2-D torque-based tables. All data is acquired using the data acquisition

(DAQ) software package DCAT, built into the Drivven controller, with a crank-angle (crankshaft encoder with 2048 pulses per revolution) and cycle-basis (once per cycle). This ensures alignment of all time-based signals. The Drivven controller also features a next-cycle controller that on a cycle-basis measures a given pressure metric and then uses a PID controller to manipulate a specific control parameter. For the current work, CA50 is measured on each cycle and the PID controller then adjusts the PFI ratio in order to match pre-determined CA50 targets.

Figure 3-2 Drivven hardware for real-time engine control system

3.2.2 Air Flow and Boosting

Intake air flow rate measurements are performed via an OEM mass airflow (MAF) sensor and a laminar flow element (LFE). A comparison between the two showed good agreement and thus the LFE was used in the post processing of the present work. Building air is used to provide airflow through a variable air pressure regulator and to eliminate humidity effects. The air was heated to the wanted intake air temperature via a heating element that is installed upstream of the LFE and MAF.

The pressure regulator, capable of simulating a supercharger, was added to provide more flexibility and control of the air system. This has become necessary to overcome the drawbacks of

the turbocharger when used in combination with low exhaust enthalpy due to low exhaust temperatures. In addition, the compressor side of the turbocharger setup was removed, allowing the elimination of effects seen in previous results and induced by the combination of VGT boost control and regulator control of the supply air. By taking off the compressor and stripping out the shaft and blades of the turbine side [Figure 3-3], the boost pressure can be controlled by a variable control valve only. Therefore, the regulator for the variable control valve was replaced in order to increase its range (now 0 to 100 psi; previously 0-20 psi) and thus is able to supply the required boost levels. While the blades and shaft have been removed, the VGT mechanisms and the control of the duty cycle of the turbocharger via Drivven was kept in place in order to have control over the backpressure, which was set to reach a turbocharger efficiency between 45-50%. This was considered an appropriate value, considering current research showing combined turbocharger efficiencies of up to 75% for optimized turbocharger setups.

Figure 3-3 Custom Garret M53 VGT w/o compressor

3.2.3 Fuel Flow & Delivery

The experimental set-up included two fuel systems. In addition to the common-rail DI system, an additional PFI system was constructed by Hanson [44]. The production common-rail system consists of a CP1H3 pump that is able to provide rail pressures up to 1600bar, and Bosch CRIP2-

MI injectors that allow up to 5 injections per cycle. Excess fuel from the pump, rail and injectors is re-circulated after running it through a heat-exchanger, and the supply pressure and temperature is kept constant. A schematic of the DI system is shown in Figure 3-4.

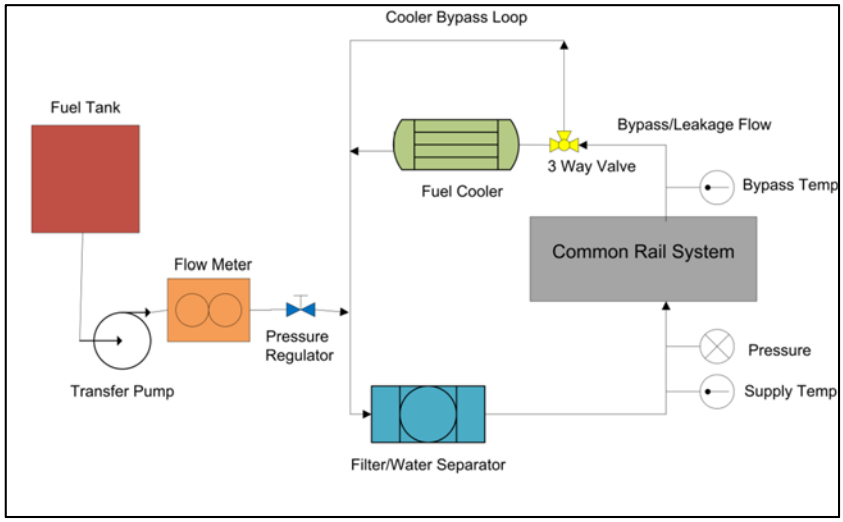

Figure 3-4 Diagram of the DI system set-up, Glewen [64]

The PFI system was installed in order to allow the injection of volatile, low reactivity fuel and thus to perform LTC and RCCI operation. As shown in Figure 3-5, fuel supply to the Delphi PFI injectors is achieved by the installation of the fuel system on the stock intake manifold. The overall schematic of the PFI system is provided in Figure 3-6.

Figure 3-5 Modified GM 1.9L intake manifold and port fuel injection system

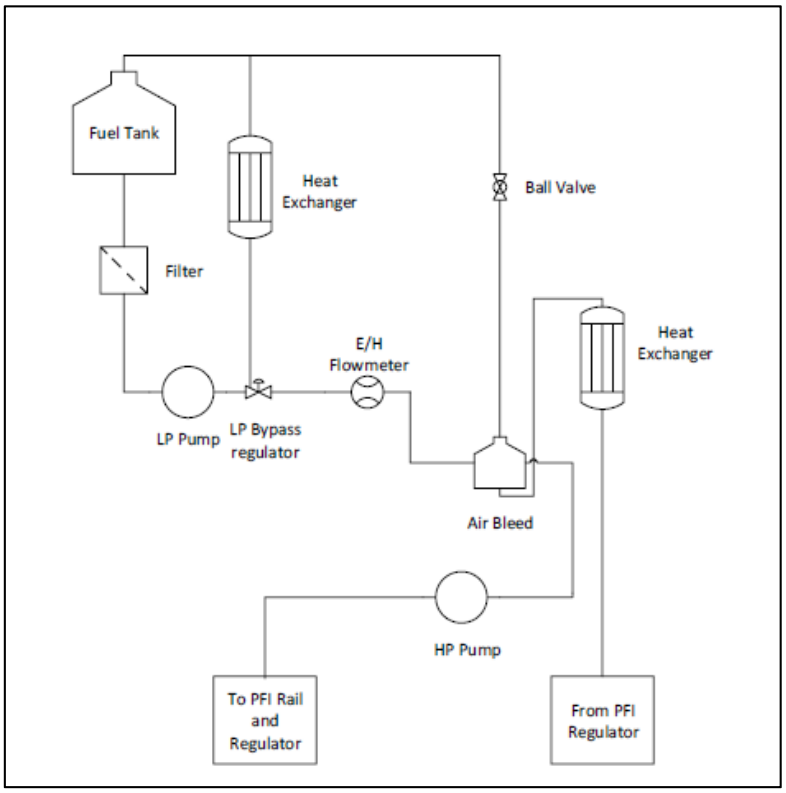

Figure 3-6 Diagram of PFI fuel system, Hanson [44]

3.2.4 Temperatures and Pressures

Pressure and temperature measurements are taken across the whole engine set up, including as intake and exhaust manifolds, EGR system, charge air cooler, and other auxiliary hardware, in order to draw a complete picture of the engine's performance and its operational state.

3.2.5 O2-Measurement and EGR

Commercially available Bosch oxygen wideband sensors were installed in the intake manifold near cylinder 2, in the intercooler, and in the exhaust manifold. The oxygen readings of the intake and exhaust were used to determine the EGR rate.

3.3 Engine Out Emissions

3.3.1 Gaseous Emissions

Gaseous emission measurements can be categorized in two ways. High speed measurements of NO and UHC were provided by a Cambustion CLD 400 [70] and a HFR 500 fast response system [71], respectively. This gave near crank-angle time resolution for transient operation capability. The setup allowed the measurement of NO at two locations in the exhaust manifold (near cylinder 2 and pre-turbine) and UHC emissions pre- as well as post-diesel oxidation catalyst (DOC). Note, that the Cambustion CLD 400 system only measures NO and not NO2 and NOx. The results over all crank angles were averaged to provide a single value for each cycle. In the slow speed category and thus under steady-state conditions, H_2O, CO and CO_2 along with NO, NO2 and UHC were acquired using a MKS 2030 HS Fourier transform infrared spectrometer (FTIR). Heated filters and lines, regulated at 190C, prevented particulate build-up and condensation from forming. The FTIR was not used for transient testing due to an inadequate emissions resolution, where a long sample line together with a low flow rate do not permit a cycle-resolved measurement.

3.3.2 Particulate Matter

An AVL 439 Opacity-meter provided steady-state and transient smoke opacity emissions, which can be converted to an approximated PM mass value [72, 73]. An overview of the all emissions equipment is given in Table 3-2.

Table 3-2 Emissions equipment and sensor specifications

Instrument	Species	Method of Measurement	Application
MKS 2030 HS FTIR	CO, CO2, UHC, NO, NO2	Fourier Transform Infrared Spectroscopy	Steady-State
Cambustion CLD 400	Nitric Oxide (NO)	Chemi-Luminescence Detection	Transient & Steady-State
Cambustion HFR 500	Unburned Hydro-Carbons (UHC)	Heated Flame Ionization Detection	Transient & Steady-State
AVL 439 Opacity-meter	Exhaust Smoke	Light Intensity Detector (Beer-Lambert-Law)	Transient & Steady-State
Bosch Wideband O2 Sensor (17014)	Intake and Exhaust O2	Nernst (2-state sensor) principle	Transient & Steady-State

3.4 Cylinder Pressures and Balancing

Cylinder pressure is measured in all 4 cylinders, with cylinders 1,3 and 4 using pressure sensing glow plugs from BERU and cylinder 2 is equipped with a Kistler 6058 piezoelectric pressure transducer in combination with a Kistler 510 charge amplifier. While the pressure traces for cylinders 1, 3 and 4 are utilized to indicate combustion and combustion phasing as well as cylinder-to-cylinder timing differences, the more accurate trace of cylinder 2 is used to calculate important combustion metrics. Cylinder 2 was found previously to be the best choice to approximate overall engine operation [53, 74]. The acquired cylinder pressure traces are averaged for 200 cycles, and a zero-phase, low-pass Butterworth filter with the cutoff frequency at 2200 Hz is applied to prepare the pressure trace for use in heat release calculations.

Adjustments were made to the BERU pressure glow plugs prior to this study to better match pressure traces and heat release rates between all 4 cylinders. These adjustments became necessary after the piston swap and follow similar investigations made for the hybrid car, where BERU plugs are used solely. In order to achieve better agreement, as can be seen in Figure 3-8 and 3-9, the BERU glow plug pressure transducers had to be through roughly cleaned and torqued down to a value of 11Nm. This ensures that the mechanical stresses acting on the plugs are equal [Figure 3-

7]. In addition, after a warm-up phase, gain values within Drivven were adjusted during motoring to fully match traces from the BERU plugs with the Kistler transducer trace acquired from cylinder 2.

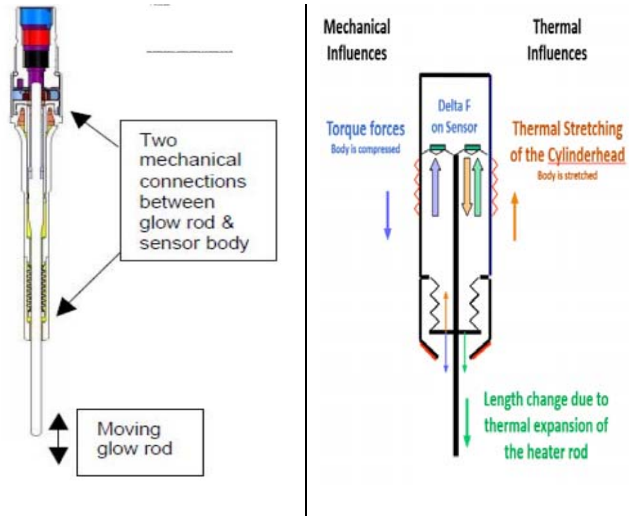

Figure 3-7 BERU glow plug working principle

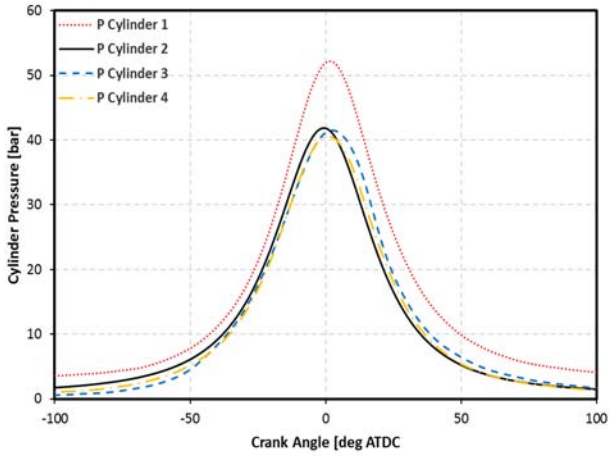

Figure 3-8 1,500 rev/min motoring trace before adjustment

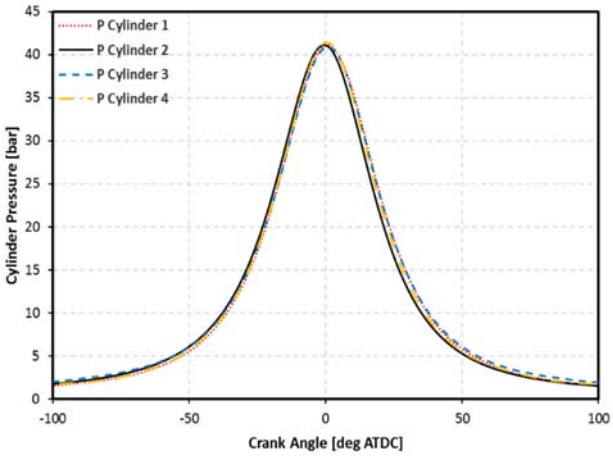

Figure 3-9 1,500 rev/min motoring trace after adjustment

During operation significant cylinder-to-cylinder variations, such as cylinder wall temperatures, intake manifold distribution, rail pressure, etc. affected the balancing of the cylinders. This can lead to substantial differences in combustion phasing between each of the cylinders, especially for a kinetically controlled combustion regime like RCCI. To counter and minimize these effects, the diesel injection duration and thus the diesel-to-gasoline ratio of each of the four cylinders was adjusted to match the IMEP and CA50 as close as possible. This was accomplished within the Drivven software, where in a first step the PFI and DI adjustment factors were tuned and kept constant for the rest of the testing, followed by an additional adjustment of the DI injection duration for each cylinder. Note, that cylinder 2 was kept constant at a factor of 1 and served as the target values for setting phasing and IMEP for cylinders 1, 3 and 4 due to the fact that previous tests had shown that cylinder 2 best reflects the overall performance of the engine [53, 74]. The adjustments were optimized for each speed and load case and over the PFI fuel sweep carried out in this study to assure the matching of IMEP over all four cylinders. Figure 3-10 shows an average of the required DI injection duration adjustments over all data collected for each of the DI fuels tested. Additional figures are presented in Appendix A. While the adjustment factors show variations of up to +/- 15%, the cylinder-to cylinder variations of the DI duration are as low as 2.3% for cylinder 1, and as high as 22% for cylinder 3. This makes sense, since the intake air with the premixed PFI fuel streams in from one side, more-or-less bypassing cylinders 3 and 4 and then dead-ending at cylinder 1. This is a good indication of the limitations this stock intake manifold also holds for optimal operation of the RCCI combustion regime or any premixed combustion regime for that matter. Additional variations stem from the DI SOI timing, the specific test point as well as the DI fuel reactivity, and therefore ultimately the PFI faction and stratification that is accomplished.

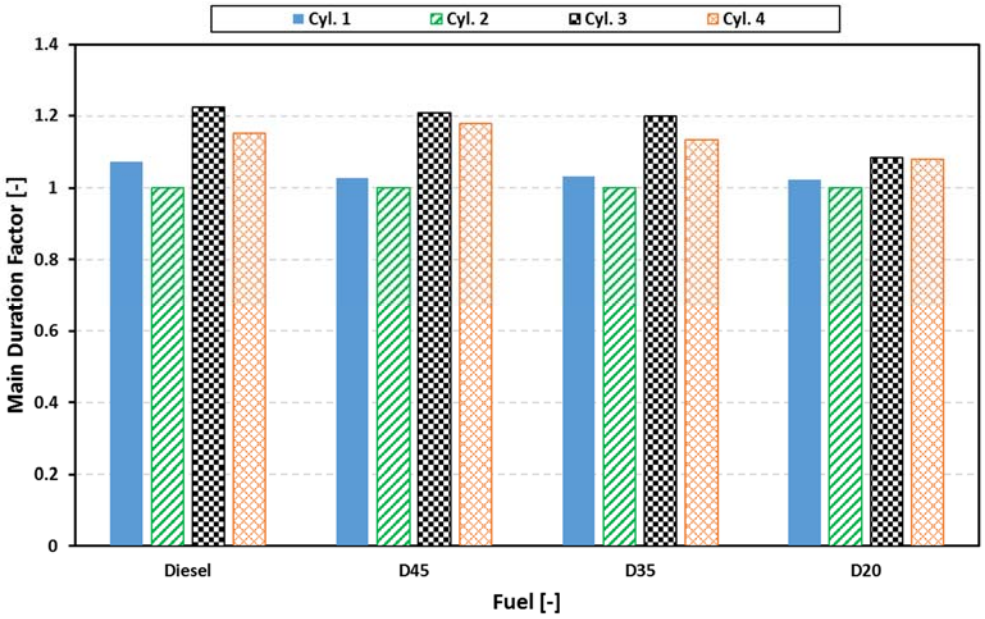

Figure 3-10 Cylinder Balancing for 4 different DI fuel types averaged over all speed and load cases

3.5 Data Analysis

3.5.1 Heat Release Rate

In order to allow for a complete analysis of combustion, heat release rate calculations are important to determine the phasing, shape and duration of the combustion process. In this study, the 1st law analysis is applied to give the relevant heat release equation. As mentioned in Section 3.4 the acquired pressure measurements are averaged for 200 cycles, and a zero-phase, low-pass Butterworth filter with the cutoff frequency at 2200 Hz is applied. The pressure derivative was then found using the coefficients of a Savitzky-Golay (SG) filter. The apparent heat release (AHRR) is based on derived ratio of specific heats (gamma) calculations via a linear regression curve fit of the compression and expansion strokes. Important combustion metrics, such as the crank angle at 50% of total heat release (CA50) and combustion duration (CA5-CA90), are then determined.

3.5.2 Uncertainty

Post processing of the acquired data is realized by a custom MATLAB code. The code has recently been updated, and now considers measurement uncertainty in order to statistically show data trends and thus differentiate between errors in the measurement. Applying Dempsey's approach [45] to determine accuracy and precision, measurement errors were propagated throughout the post processing code by applying the MATLAB Symbolic Math Toolbox to symbolically enter each equation. This allowed finding of partial derivatives for each independent variable at the variable values and for every sequential calculation and equation, thereby obtaining a 95% confidence intervals for all data. Those confidence intervals are included in the present results. The uncertainties of the instrumentation are shown in Table 3-3.

Table 3-3 Uncertainty values for laboratory instruments

Instrument	Species	Total [%]	Uncertainty for full Scale
MKS 2030 HS FTIR	CO, CO2, UHC, NO, NO2	2	-
Cambustion CLD 400	Nitric Oxide (NO)	1.41	2.81 ppm
Cambustion HFR 500	Unburned Hydro-Carbons (UHC)	1.41	42.5 ppm
AVL 439 Opacity-meter	Exhaust Smoke	0.1	0.1%
BEI H25 Series Optical Encoder	Speed [RPM]	3.5	0.5 bit
HBM T40 Torque Transducer	Crankshaft Torque	-	0.156 Nm
Pressure	Pressure [bar]	0.0025	0.005 bar
Type-K Thermocouple	Temperature [K]	-	1.5°C
Endress+Hausser Promass 80	DI & PFI fuel flow	0.01	0.02 g/s
Meriam Laminar Flow Element	Air Flow	0.03	0.8 g/s
Bosch Wideband O2 Sensor (17014)	Intake and Exhaust O2	1.75	-

3.5.3 Combustion Noise

While many different ways are readily available to measure combustion noise, in the present study combustion noise is also calculated within Drivven. The working principle of the Drivven method is proprietary, but has been proven in a previous investigation by Hanson [44] to almost identically match Shahlari's method, which, in turn, has shown good agreement with an AVL noise meter.

3.6 Simulation Models

3.6.1 Multi-Step Single-Zone RCCI

A multi-step single-zone Cantera model by Kokjohn [75] was used to determine IVC conditions and work cycle outputs for the reduced DOE test cases using D45. The model uses a basic chemical kinetics mechanism along with Wiebe heat release parameters. The fuel properties and kinetics for the chemistry calculations were represented by n-heptane and iso-octane in place of the ULSD and EEE. RCCI-type injection parameters matching the conditions during metal-engine experiments for the dieseline test cases were used for the calculations. Meanwhile, the specified PFI mass fraction included the EEE gasoline stemming from the PFI injection as well as the EEE content of the dieseline DI fraction, as a DI fuel mixture could not be represented.

The simulations were carried out using geometry data from the multi-cylinder engine, along with operating conditions from previously performed experiments, where BMEP and BTE were closely matched in order to obtain IVC and cycle work outputs.

3.6.2 Single-Zone HCCI

A simple single-zone Cantera model by DelVescovo [76] was used for simulations of the HCCI combustion regime. This was done in order to determine a fitting dieseline mixture to match CA50 values found throughout the prior dieseline investigations. Throughout the simulations, chemical

kinetics were described by a reduced primary reference fuel mechanism by Wang et. al. [77]. The mechanism consists of 73 species and 296 reactions, where major reaction pathways were mostly retained and the predictive capability was ensured. The fuel properties and kinetics for the chemistry calculations were again represented by n-heptane and iso-octane in place of the ULSD and EEE used to obtain mixtures of dieseline. Mass fractions of iso-octane and n-heptane were determined based on the different volumetric mixtures of EEE and ULSD, respectively. Test conditions and experimental performance results along with IVC conditions and cycle work results from the cycle simulation model, were used for the final HCCI simulations.

3.7 Experimental Conditions

3.7.1 Piston Design

Splitter et al. [78] was the first to investigate the effects of a custom piston design combined with a lower dynamic compression ratio (CR) of 14.88:1 for RCCI combustion in a heavy-duty engine, leading to light-duty engine tests performed by Hanson et al.[79] and Dempsey et al.[80] with a RCCI piston design featuring a dynamic compression ratio of 15.1:1. The results showed that the implementation of the so-called RCCI piston design improves overall performance and efficiency. The modifications to the light-duty piston design induce a low dynamic compression ratio of 15.3:1 and a further lowered ring land height of 4mm. The piston used for the present work is a second generation RCCI piston design [Figure 3-2]. It features a slightly higher compression ratio than the previously installed first generation pistons (CR: 13.75), which were designed in combination with most current developments for ultra-low CR [81, 82] . The pistons have a chamfer in order to maintain a low ring land height of 4mm while increasing the compression ratio as well as the bowl volume. The new design overcomes limitations in performance that were observed during tests with the previous design, especially during the evaluation of fuel additives that was a focus of this

study. The low compression ratio, compared to the stock design (CR:16.7:1) [Figure 3-3], primarily allows an increase of the engine's peak load without the use of EGR, while the lowered ring land height promotes reduced formation of hydrocarbons from the piston-liner crevice region [78]. In addition, heat transfer losses as well as friction losses are expected to be reduced with the shallow bowl geometry.

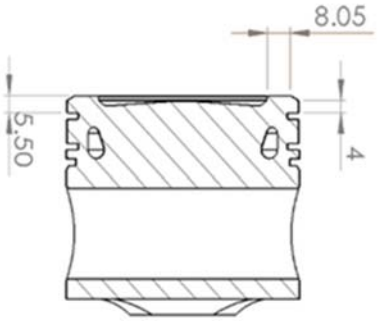

Figure 3-11 ERC RCCI.v2 Piston

Figure 3-12 Stock Piston

3.7.2 Fuels and Additives

To achieve RCCI combustion, a high reactivity and a low reactivity fuel are blended in cylinder. For the two studies presented, the low reactivity fuel used for the port-fuel injection was an EPA Tier II EEE gasoline with a 92 AKI (Anti Knock Index, also known as Pump Octane Number (PON)). For the high reactivity, direct injection of different fuels was used to assess their performance. A certification grade Ultra Low Sulfur Diesel (ULSD) [Table 3-4] was used to create a baseline. In the following the EEE gasoline [Table 3-5] was mixed with different amounts of the ULSD to create "dieseline". The custom nomenclature used represents the %-vol. content of the ULSD within the EEE gasoline, for example dieseline20 is a mixture of 20% ULSD and 80% EEE by volume. The properties for each of the dieseline mixtures can be found in Tables 3-6 through 3-10. Note, that for dieseline45, dieseline35 and dieseline20 fuel tests were performed to determine the AKI and cetane numbers while the PRF numbers for dieseline50 and dieseline60 were

determined based on their respective volumetric mixtures. Note also, that a small quantity of lubricity agent Infineum R655 was added to the DI fuel mixtures (10mL per 5 gallons of fuel) in order to provide adequate lubrication, similar to diesel fuel, and thus prevent damage to the common rail system.

It should also be pointed out the throughout the rest of this work the nomenclatures of dieseline45, dieseline35, etc. and D45, D35, etc. are interchangeable, with the short form mainly being used in figures, plots and captions.

Table 3-4 EEE Fuel Properties

Lower Heating Value [MJ/kg]	42.866
Ethanol [%]	0
Specific Gravity [@ 15.6 °C]	0.742
H/C [-]	1.92
RON [-]	96.4
MON [-]	88.5
AKI ((RON+MON)/2) [-]	92
Aromatics [vol%]	29
Olefins [vol%]	0
Saturates [vol%]	71

Table 3-5 ULSDiesel Fuel Properties

Lower Heating Value [MJ/kg]	41.28
Specific Gravity [@ 15.6 °C]	0.858
Cetane Number [-]	44.4
H/C [-]	1.702
Aromatics [vol%]	30
Olefins [vol%]	5
Saturates [vol%]	65
Sulfur [ppm]	9

Table 3-6 D60

Lower Heating Value [MJ/kg]	41.914
Ethanol [%]	0
Specific Gravity [@ 15.6 °C]	0.810
H/C [-]	1.825
PRF [-]	49.6

Table 3-7 D50

Lower Heating Value [MJ/kg]	42.073
Ethanol [%]	0
Specific Gravity [@ 15.6 °C]	0.798
H/C [-]	1.829
PRF [-]	56.8

Table 3-8 D45

Lower Heating Value [MJ/kg]	42.152
Ethanol [%]	0
Specific Gravity [@ 15.6 °C]	0.792
H/C [-]	1.830
RON [-]	75.4
MON [-]	66
AKI ((RON+MON)/2) [-]	70.7
Cetane Number [-]	30.4

Table 3-9 D35

Lower Heating Value [MJ/kg]	42.311
Ethanol [%]	0
Specific Gravity [@ 15.6 °C]	0.781
H/C [-]	1.834
RON [-]	79.3
MON [-]	70.4
AKI ((RON+MON)/2) [-]	74.9
Cetane Number [-]	27.2

Table 3-10 D20

Lower Heating Value [MJ/kg]	42.549
Ethanol [%]	0
Specific Gravity [@ 15.6 °C]	0.763
H/C [-]	1.840
RON [-]	86.8
MON [-]	79.6
AKI ((RON+MON)/2) [-]	83.2
Cetane Number [-]	21.8

3.7.3 Procedure

Engines operate over a wide speed/load range in vehicles. The test points for the study were chosen from the light-duty FTP-75 EPA test, where a large volume of data had been accumulated in the past to provide a baseline to compare RCCI with other combustion strategies [79, 83, 84] using so-called Ad-hoc points [84]. Two additional cases were added, a 4bar BMEP and a 2bar BMEP case both at 1,500 rev/min. The two additional test points were well defined and tested in previous tests at the ERC [44, 50]. The FTP modal points, shared by Argonne National Laboratory, are shown in Figure 3-12, which also highlights all 6 operating points for this study. A single-injection strategy and no EGR was used in all tests in order to simplify testing with the multi-cylinder engine, thus solely putting focus on combustion performance effects from varying the diesel amount in the direct-injected gasoline. For most tests an intake temperature between 55° and 60°C and an intake pressure of about 1.1bar was used to account for the lowered and different fuel reactivities. As mentioned before, the turbocharger efficiency was controlled to be at about 45% and rail pressure was kept constant at 500bar. Note, that adjustments had to be made to the common rail system for operation with gasoline/dieseline and in order to be able to pressurize the rail. The supply pressure was elevated from 30 psi (200kPa) to approximately 45 psi (300kPa) to prevent the fuel from cavitating. The increased supply pressure was also employed for the gasoline/diesel case for consistency purposes. The present steady-state tests were performed prior to the transient cases, and two different DI start of injection (SOI) timings were commanded. While sweeping over a range of several different PFI fractions in order to assess the combustion performance of the three previously mentioned DI fuel mixtures in comparison to diesel RCCI, the thermodynamically most efficient points could be determined. Meanwhile, a maximum pressure rise rate < 15bar/deg and noise level targets (<95 dB) for RCCI combustion were kept in place during testing.

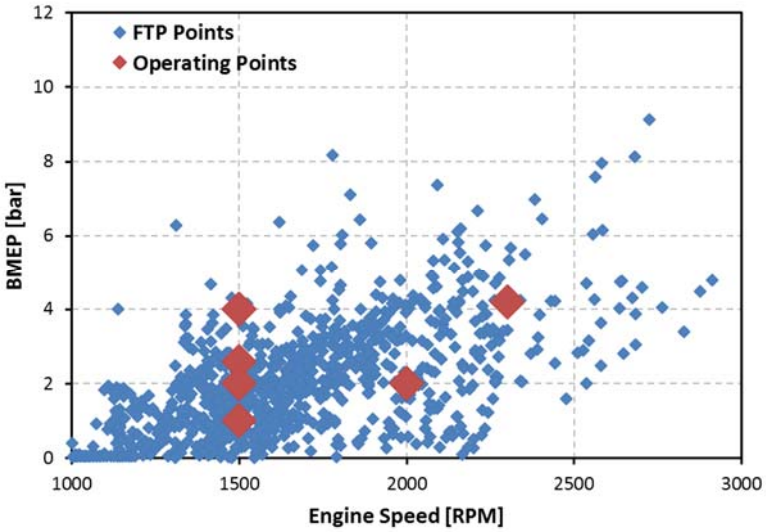

Figure 3-13 Engine operating points overlaid vs. FTP driving points for a light-duty diesel engine

The transient experiments were conducted by changing the accelerator pedal command. The pedal command is used as a desired torque output by the Drivven ECU and all relevant engine parameters are adjusted accordingly, based on 2D-tables (load and speed). For this study, load transients were performed at a constant engine speed of 1500 rev/min, i.e., a tip-in type transition. The previously performed steady-state at 2.6bar BMEP and 4bar BMEP served as the end points of load transients. Well established engine calibration at these two points, as well as interpolation of the intermediate points, allows for smooth operation during instantaneous step changes. Given that engine operation through these successive steady-state points in the table showed differences between the steady-state and transient results, this indicates the need for additional controls to minimize undesirable effects. Transient tests were performed for 3 different DI/PFI fuel species.

Note, that the closed-loop controller was disabled for all testing to prevent its intervention on the PFI ratio, while differences in regard to the commanded PFI ratio are considered to

accomplish cylinder balancing. In the following chapters the individual operating conditions will be highlighted again in more detail.

Table 3-11 gives an overview for the operating conditions for the investigation of dieseline as well as diesel RCCI operation.

Table 3-11 Engine Operating Conditions for steady-state evaluation of dieseline

Load (BMEP) [bar]	**4bar**
PFI Fuel Composition	EEE Gasoline
DI Fuel Composition (ULSD-in-Gasoline [Vol.%])	20%, 35%, 45%, 50%, 60%, 100%
Intake Pressure [bar]	~ 1.1
Exhaust Pressure [bar]	Backpressure set to simulate ~ 40-45% Turbocharger efficiency
Intake Temperature [°C]	55 to 60°
EGR [%]	0%
Air/Fuel Ratio [-]	~ 52
Global Equiv. Ratio [-]	~ 0.3 to ~ 0.4
PFI Gasoline Fueling [Mass %]	20 to 70
Main SOI timing [°ATDC]	-40° & -45°
DI Rail Pressure [bar]	500

Chapter 4 Performance and Emissions for Steady-State RCCI Combustion Using Dieseline

This chapter reports the experimental work to examine the performance of different dieseline mixtures as a high reactivity fuel for RCCI operation in a light-duty MCE diesel engine. In the first part, engine operating conditions are presented and further, performance results for all dieseline mixtures investigated are illustrated and a comparison to gasoline/diesel RCCI combustion is made. In the second part, the findings are further discussed and conclusions are drawn. The results shown thereby focus on a selection of the 6 operating points, while additional test material can be found in Appendix B. The selection consists of the 2.6 bar BMEP, 1,500 rev/min; the 4.0 bar BMEP, 1,500 rev/min and the 4.2 bar BMEP, 2,300 rev/min cases. The choice of selection was based on the fact that all three of conditions are well studied points overall and feature a distinguishable difference in load as well as two different engine speeds in order to present a comprehensive understanding of the performance of dieseline. Furthermore, this selection highlights two points for the later performed and presented transient testing between the 2.6 bar BMEP, 1,500 rev/min and the 4.0 bar BMEP, 1,500 rev/min.

As mentioned before, two different DI start of injection (SOI) timings were commanded while sweeping over a range of several different PFI fractions to assess the combustion performance. However, with all but one test point resulting in higher efficiencies for an SOI timing of -40 dATDC, the following figures and tables present the results for those cases solely.

4.1 Operating Conditions and Results

4.1.1 2.6 bar BMEP, 1,500 rev/min

In order to acquire comparable results between the tested DI fuel types, experimental operating conditions were intended to match as close to each other as possible. Figure 4-1, Figure

4-2 and Figure 4-3 highlight the run conditions for this first test case of 2.6 bar BMEP at 1,500 rev/min. It can be seen that the Brake Power output and BMEP were matched very closely for all DI fuels types. An intake pressure of 1.15 bar and an intake temperature of 54 °C [Figure 4-2] was maintained for all DI fuels to account for the lowered and different fuel reactivities. An exception had to be made for dieseline20, as the low reactivity at this load as well as at lower load points was not sufficient to achieve combustion. The intake temperature thus was raised to about 60 °C.

Meanwhile, turbo efficiencies were maintained constant at the targeted values over the whole CA50 range by employing the VGT mechanism. Equivalence ratios were fairly constant as well with only dieseline35 and dieseline20 resulting in slightly raised values over dieseline45 and diesel [Figure 4-3].

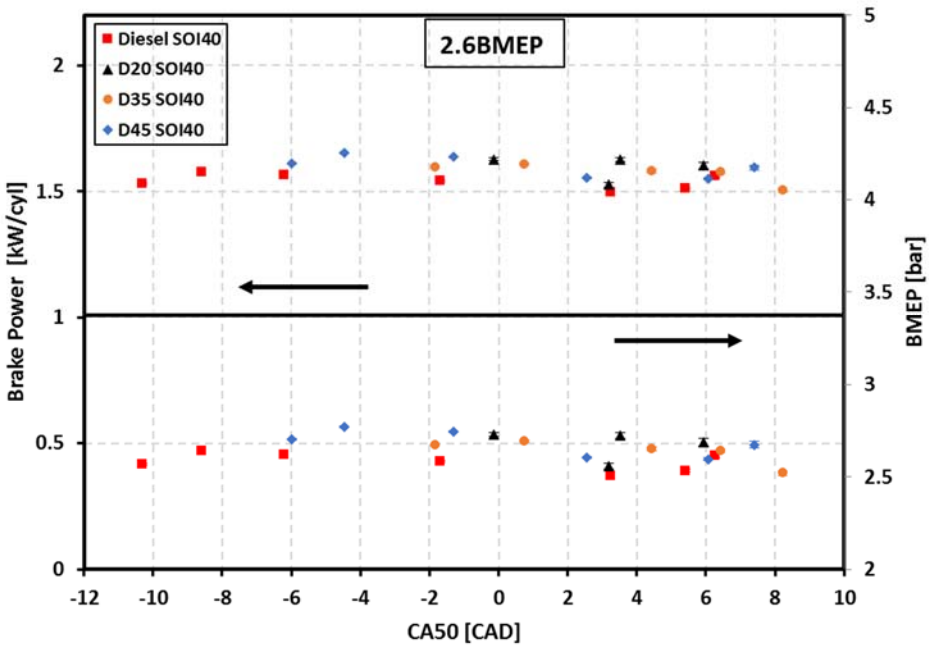

Figure 4-1 BMEP [bar] and Brake Power output [kW] as a function of combustion phasing (CA50) at the DI SOI timing of -40 dATDC

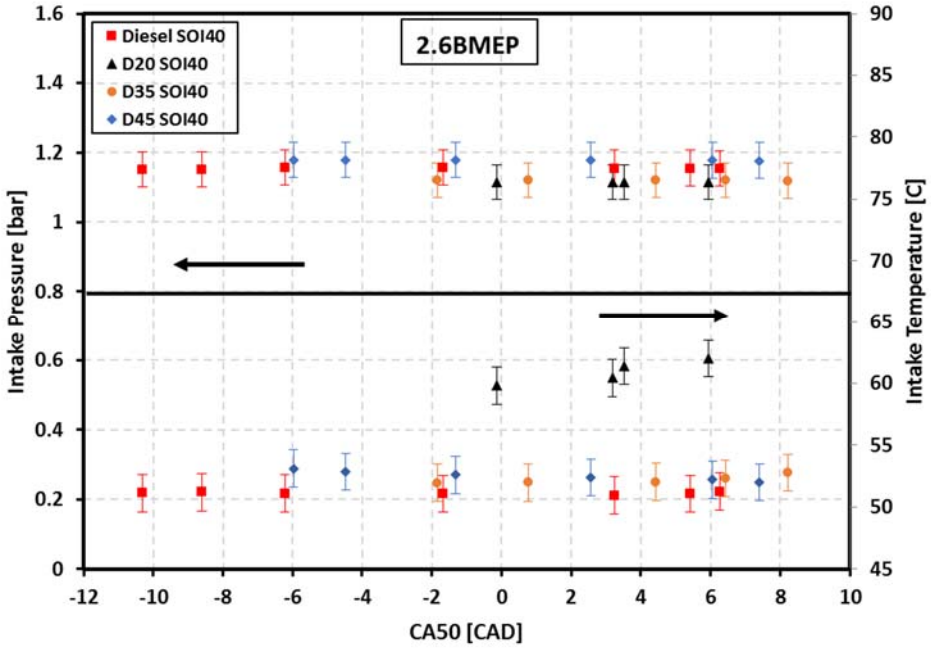

Figure 4-2 Intake Pressure [bar] and Intake Temperature [°C] as a function of the combustion phasing (CA50) at the DI SOI timing of -40 dATDC

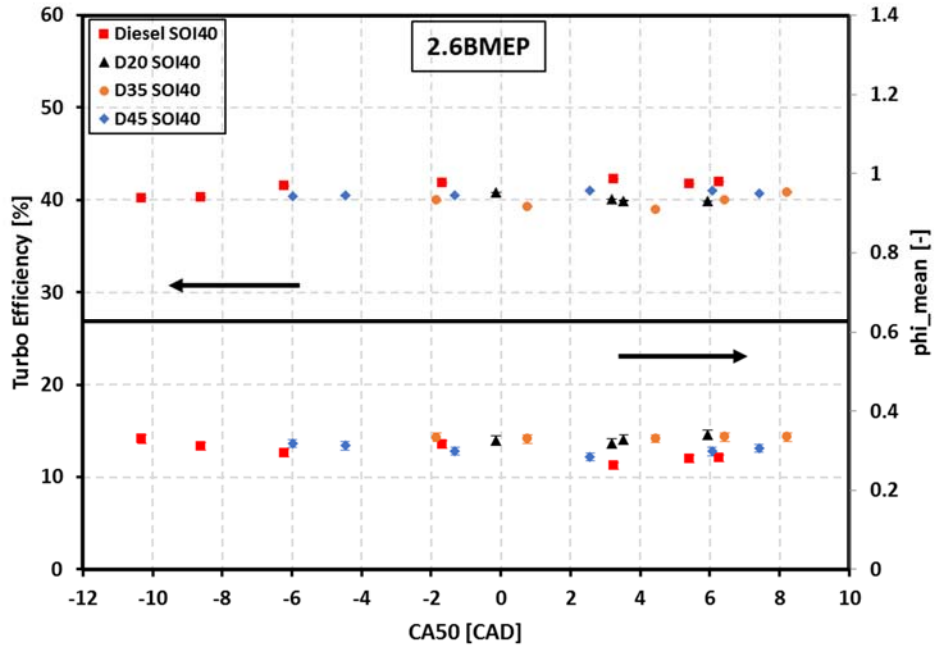

Figure 4-3 Turbo Efficiency [%] and global equivalence ratio [-] as a function of the combustion phasing (CA50) at the DI SOI timing of -40 dATDC

Based on these conditions, the following performance results were achieved. In Figure 4-4, the fuel energy and total fueling for the different DI fuels is shown. Thereby, a reduction in required fueling and energy leads to the increased levels of brake efficiency for the dieseline mixtures over diesel, while displaying identical combustion efficiencies [Figure 4-6]. Both efficiencies follow their expected trends, with a peak in brake efficiency shortly before TDC and a reduction in combustion efficiency at later CA50 timings. Brake efficiency gains are recorded for all dieseline cases and reach up to 1% for dieseline45 over the diesel baseline. Note that the combustion efficiency reaches adequate levels of 94% at the most thermodynamically efficient points.

The different amounts of ULSD within the DI fuel fraction is shown in Figure 4-5. Note, that these values reflect the amount of ULSD in comparison to the total fuel and not the fraction within the DI fuel. It should also be noted that while a single fuel approach is intended, the ULSD requirement reaches about 30% of the total fuel amount.

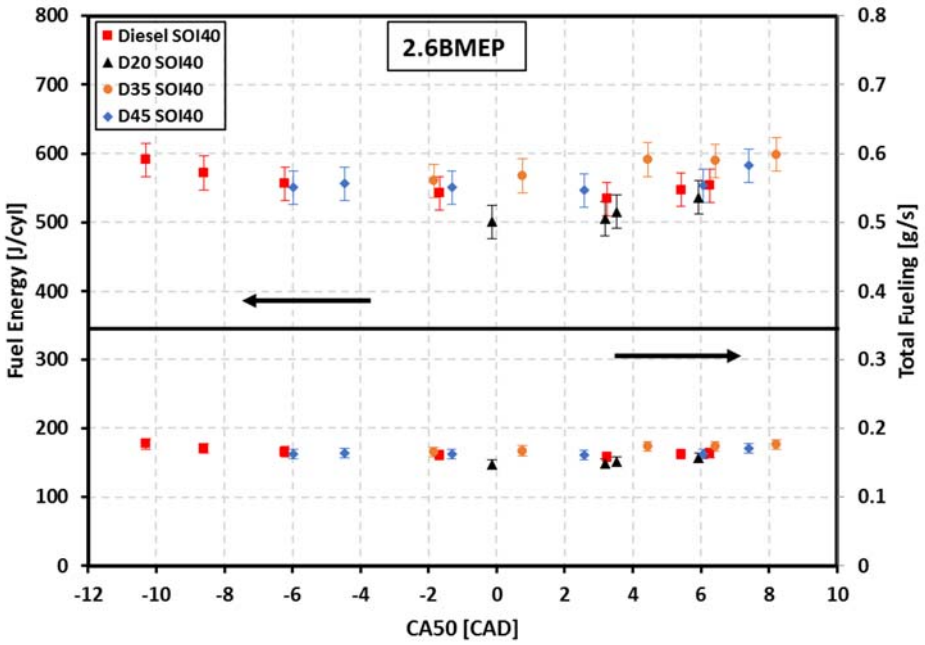

Figure 4-4 Fuel Energy [J/cyl] and Total Fueling [g/s] as a function of combustion phasing (CA50) at the DI SOI timing of -40 dATDC

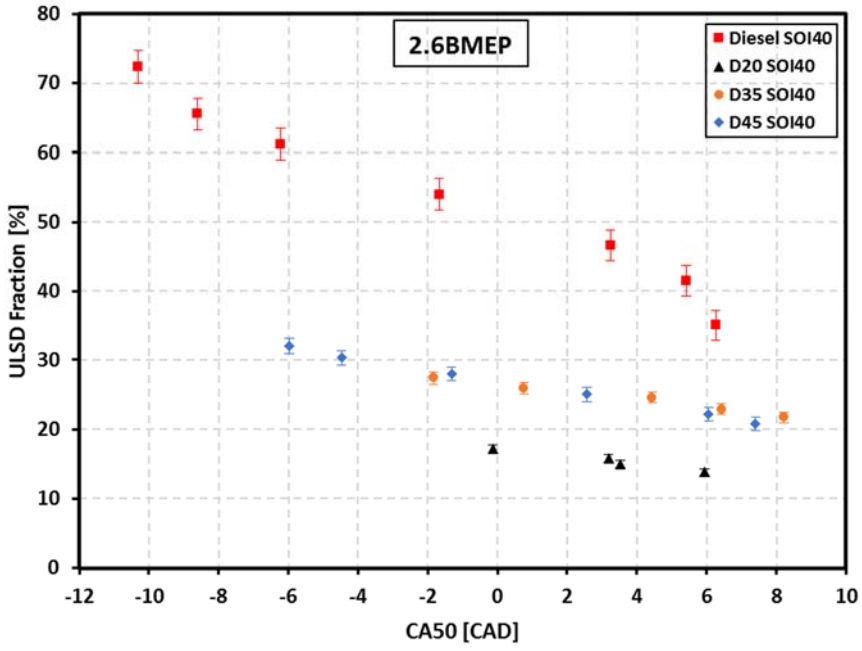

Figure 4-5 ULSD fraction within the total amount of fuel used [%]as a function of combustion phasing (CA50) at the DI SOI timing of -40 dATDC

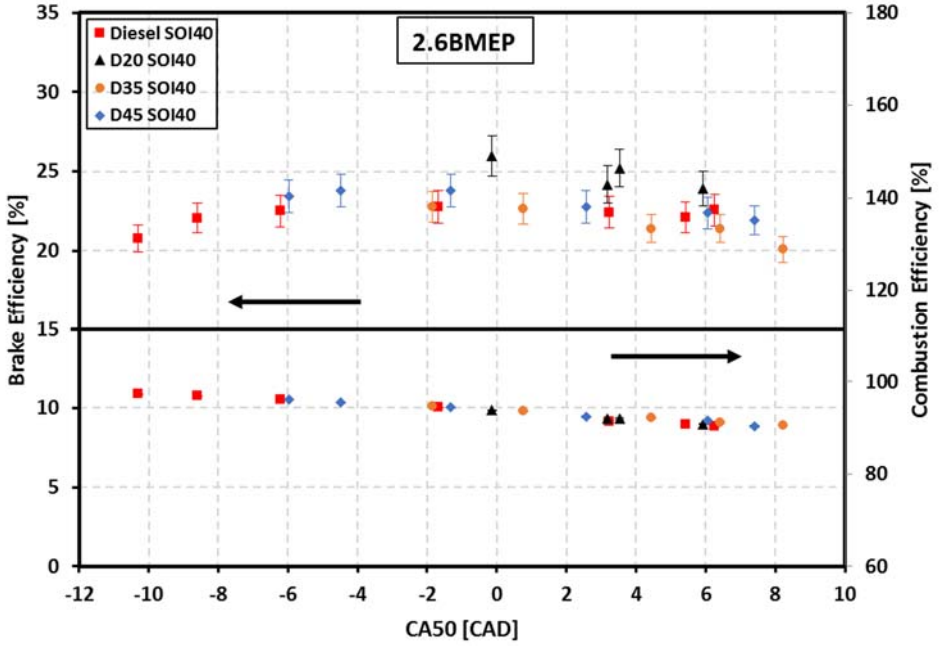

Figure 4-6 Brake efficiency [%] and combustion efficiency [%] as a function of the combustion phasing (CA50) at the DI SOI timing of -40 dATDC

Further comparison of the performance of the different DI fuel types is made in Figure 4-7 and Figure 4-8. Noise levels and maximum pressure rise rates (MPRR) for the dieseline DI fuels are only slightly increased especially for earlier CA50 values; still staying well under the self-imposed noise level target of 95 dB and 10 bar/CAD. Peak pressure and exhaust gas temperature follow expected trends and show more or less identical values for all DI fuels.

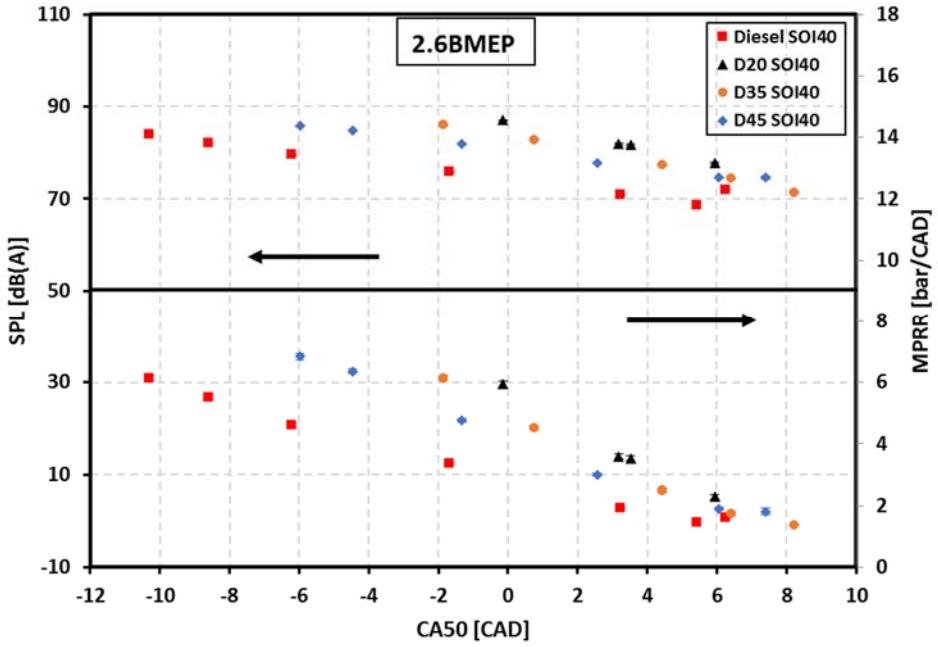

Figure 4-7 Sound pressure level [dB] and maximum pressure rise rate [bar/CAD] as a function of the combustion phasing (CA50) at the DI SOI timing of -40 dATDC

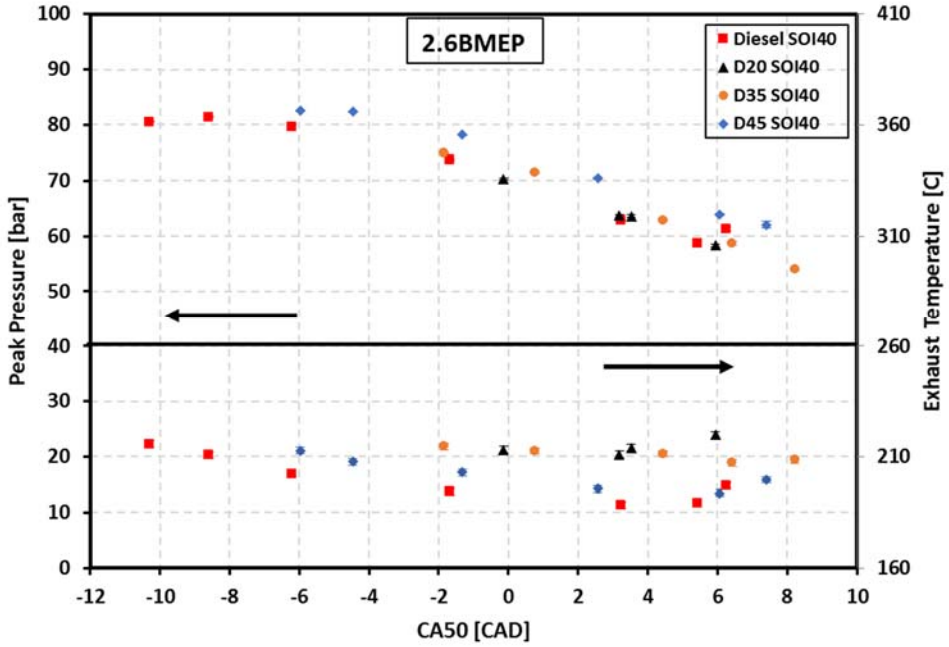

Figure 4-8 Peak cylinder pressure [bar] and exhaust temperature [°C] as a function of the combustion phasing (CA50) at the DI SOI timing of -40 dATDC

Table 4-1 highlights the run conditions for the cases of each fuel that resulted in the highest brake thermal efficiency. BTE numbers for dieseline20 thereby need to be taken out of consideration as alteration to the governed conditions were necessary to achieve combustion in the first place. Additionally, the CA50 variability of dieseline20 was very limited due to the low reactivity, leaving only a narrow range for proper operation.

Note, that for the other DI fuels a CA50 sweet spot can be determined at about – 1.5 dATDC for that load/speed condition. This agrees with CA50 values that had been found in previous investigations by Hanson [44] for optimal performance.

Table 4-1 2.6bar BMEP Operating Conditions for best brake efficiency cases of each DI fuel at SOI -40 ATDC

Fuel	**Diesel**	**D45**	**D35**	**D20**
Pedal Position [%]	16.5	17.4	18.7	19.3
DI Duration [ms]	0.473	0.533	0.640	0.683
PFI Duration [ms]	4.089	2.706	1.654	1.076
PFI Fraction [%]	46.0	37.9	21.9	14.5
Rail Pressure [bar]	505	495	490	500
Main SOI [deg. BTDC]	40	40	40	40
Intake Pressure [bar]	1.15	1.17	1.12	1.12
Intake Temp. [°C]	52	53	52	60
EGR [%]	0	0	0	0
MPRR [bar/deg.]	3.37	4.76	6.14	5.93
CA 50 [deg. ATDC]	-1.678	-1.317	-1.837	-0.139
Comb Noise [dba]	75.8	81.9	86.0	87.0
Phi [-]	0.316	0.298	0.334	0.325
BTE [%]	22.77	23.78	22.77	25.98
Comb. Eff. [%]	94.4	94.5	94.6	93.8

Pressure Traces

In order to draw a complete picture Figures 4-9, 4-10, 4-11 and 4-12 show the pressure traces and heat release rates for each of the DI fuels at the DI SOI timing of -40 dATDC including the low temperature heat release (LTHR). In the plots the respective case with the highest brake

thermal efficiency is highlighted. Note, the number of traces plotted gives good indication about the stability of the combustion and thus the achievable range of operation, i.e. with only 20% total ULSD (dieseline20), stable combustion was hard to achieve for a wide range of PFI fractions. dieseline35 and dieseline45 on the other hand allowed for smooth operation and an extended operating range almost to the point of pure Diesel. Furthermore, the tendency for later combustion phasing with a decrease in ULSD content becomes apparent with respect to the HRR trends, where the highest efficiency trace is advanced within the matrix. The decrease in ULSD content also diminishes the magnitude of the LTHR, while also delaying the onset of the intermediate temperature heat release rate (ITHR). Finally, the expected RCCI-like Gaussian distribution of the heat release rates is achieved for all DI fuels, including an increase in combustion duration for increasing PFI contributions.

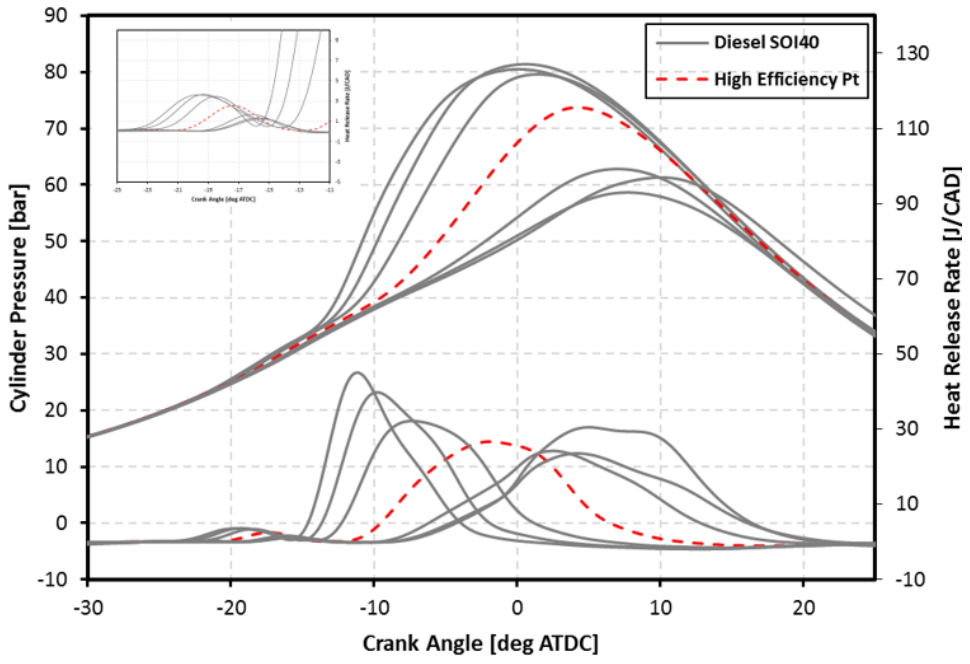

Figure 4-9 Cylinder Pressure [bar] and heat release rate [J/CAD] as a function of CAD for the Diesel RCCI case at the DI SOI timing of -40 dATDC

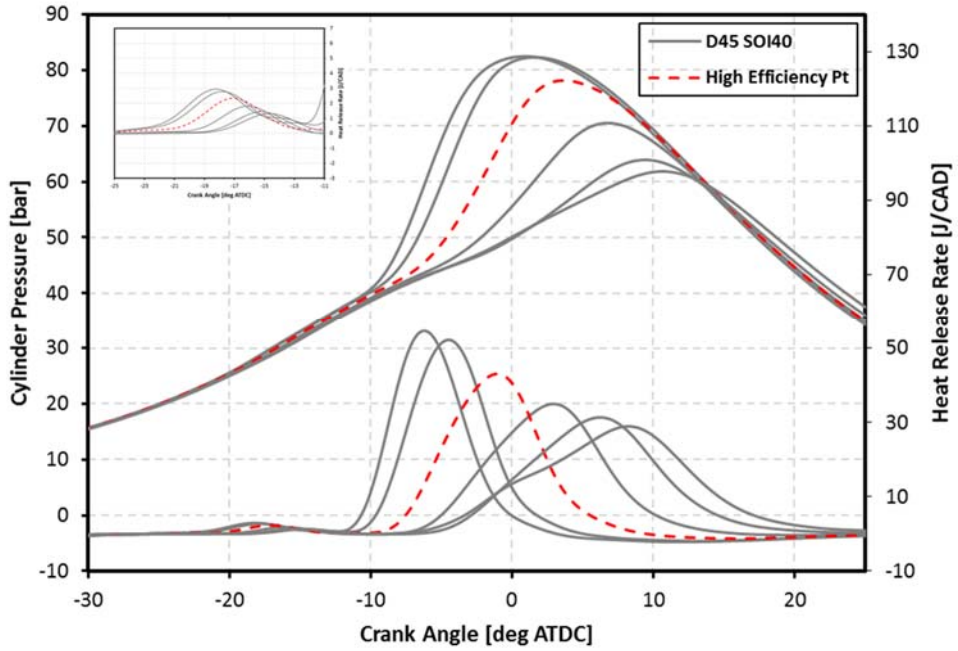

Figure 4-10 Cylinder Pressure [bar] and heat release rate [J/CAD] as a function of CAD for the dieseline45 RCCI case at the DI SOI timing of -40 dATDC

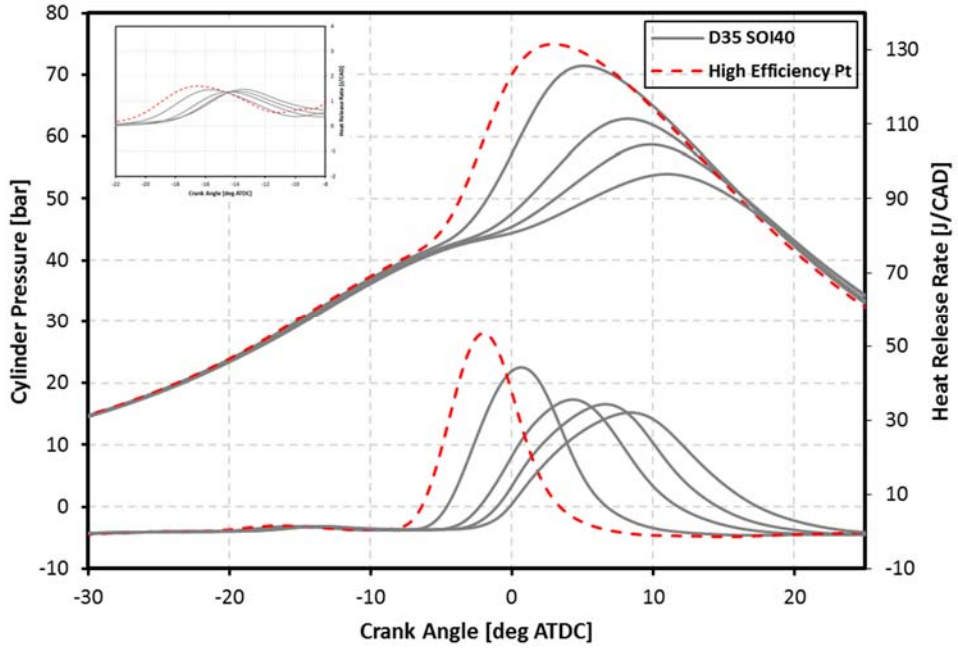

Figure 4-11 Cylinder Pressure [bar] and heat release rate [J/CAD] as a function of CAD for the dieseline35 RCCI case at the DI SOI timing of -40 dATDC

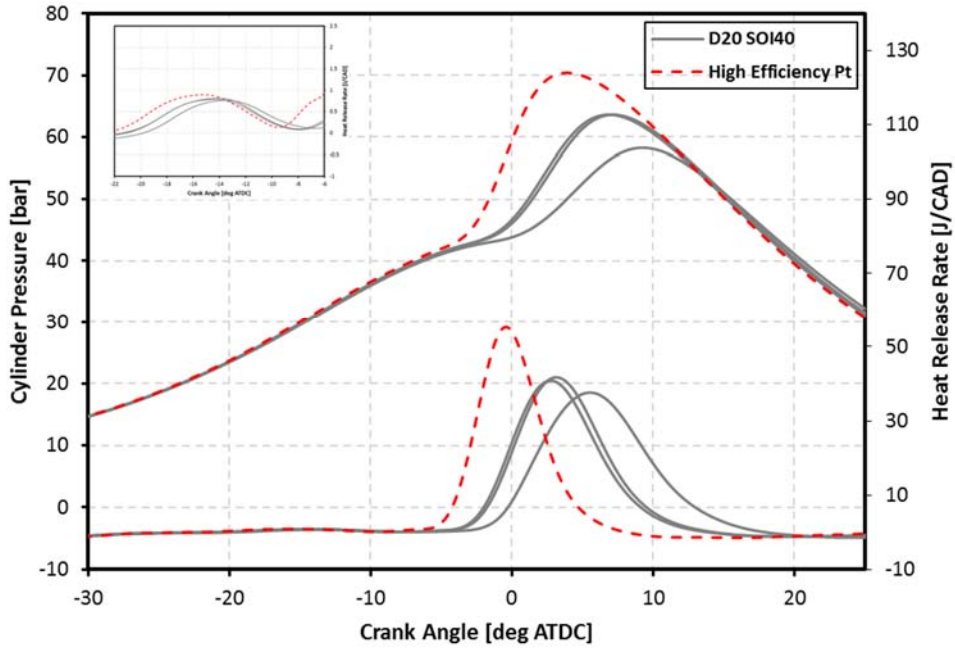

Figure 4-12 Cylinder Pressure [bar] and heat release rate [J/CAD] as a function of CAD for the dieseline20 RCCI case at the DI SOI timing of -40 dATDC

Emissions results

Engine-out emissions are plotted for all 4 DI fuels in Figures 4-13 and 4-14, which show the results for CO, unburned hydrocarbons (UHC) measured on a C_1 basis, NOx and opacity emissions with respect to the brake power output. As expected CO and HC emissions increase and NOx emissions are reduced with a retard in combustion phasing. Opacity is not of concern for the whole CA50 range. All DI fuels follow the same trend for all emission species and in the case of CO and UHC are basically identical with small reductions for the dieseline fuel. Some cases for CO and UHC are even becoming statistically significant with later timings. NOx results do the opposite. The difference between fuels is being decreased with later CA50 timings. Further note that, NOx emissions are increased with a reduction in ULSD content or overall ULSD fraction. With a small increase in combustion efficiency, and a subsequent increase in heat transfer for the dieseline cases, higher combustion temperatures can be expected leading to an increase in NOx

emissions. This is most likely caused by lengthened DI injection durations with a decrease in ULSD content in order to compensate for decreasing reactivity of the fuel, thus, leading to richer regions within the cylinder.

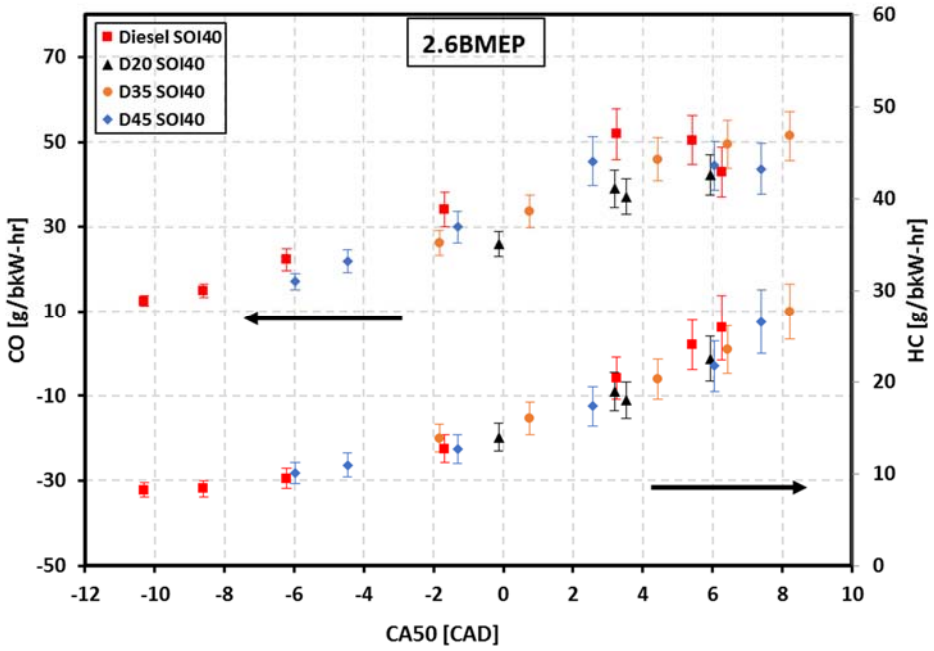

Figure 4-13 Engine-out CO and UHC_1 emissions [g/bkW-hr] as a function of the combustion phasing (CA50) at the DI SOI timing of -40 dATDC

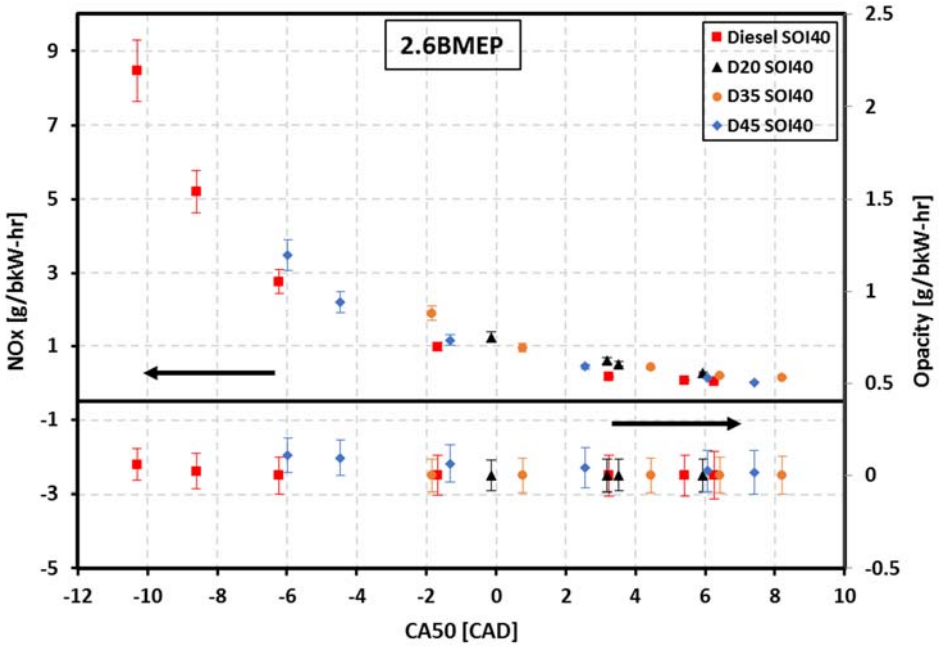

Figure 4-14 Engine-out NOx and Opacity emissions [g/kW-hr] as a function of the combustion phasing (CA50) at the DI SOI timing of -40 dATDC

4.1.2 4.0 bar BMEP, 1,500 rev/min

As stated earlier, this work highlights a selection of 3 test cases. The 4.0 bar BMEP, 1,500 rev/min case was again operated under steady state conditions in the RCCI combustion mode with a single DI injection and one injection for the PFI. Results for the different fuel mixtures at the earlier DI SOI timing of -40 dATDC are presented below.

The experimental operating conditions were intended to match as close to each other as possible. Figure 4-15, Figure 4-16 and Figure 4-17 highlight the run conditions for this test case. It can be seen that the Brake Power output and BMEP were matched very closely for all DI fuels types. An intake pressure of 1.15 bar and an intake temperature of 58 °C [Figure 4-16] was maintained for all DI fuels. Note that dieseline20 for this load point did not require adjustment to the operating conditions to achieve combustion. Turbo efficiencies were again maintained constant

at the targeted values over the whole CA50 range by employing the VGT mechanism. Values for equivalence ratios are basically identical for all cases.

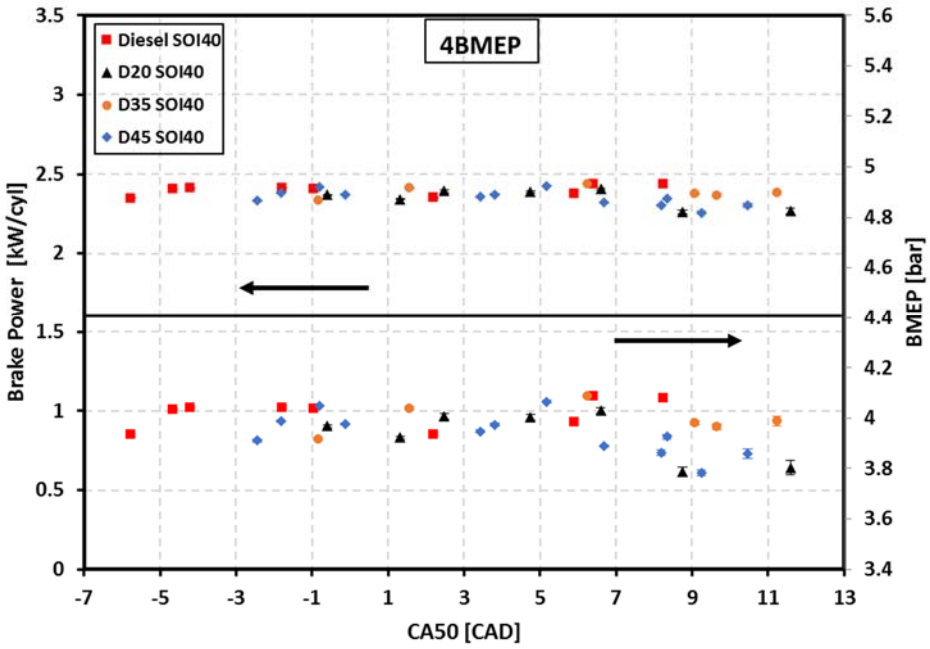

Figure 4-15 BMEP [bar] and Brake Power output [kW] as a function of combustion phasing (CA50) at the DI SOI timing of -40 dATDC

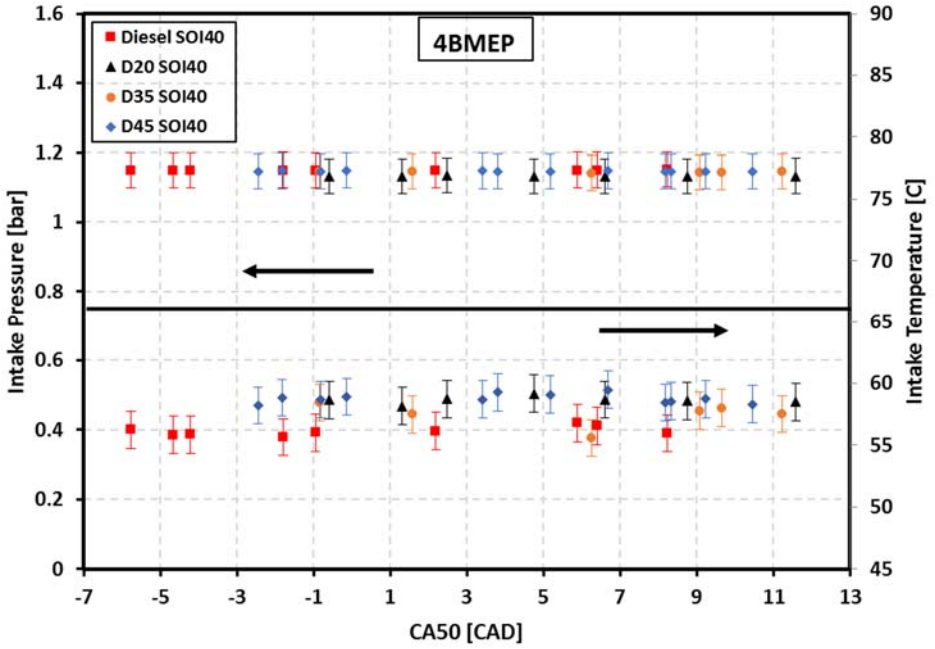

Figure 4-16 Intake Pressure [bar] and Intake Temperature [°C] as a function of the combustion phasing (CA50) at the DI SOI timing of -40 dATDC

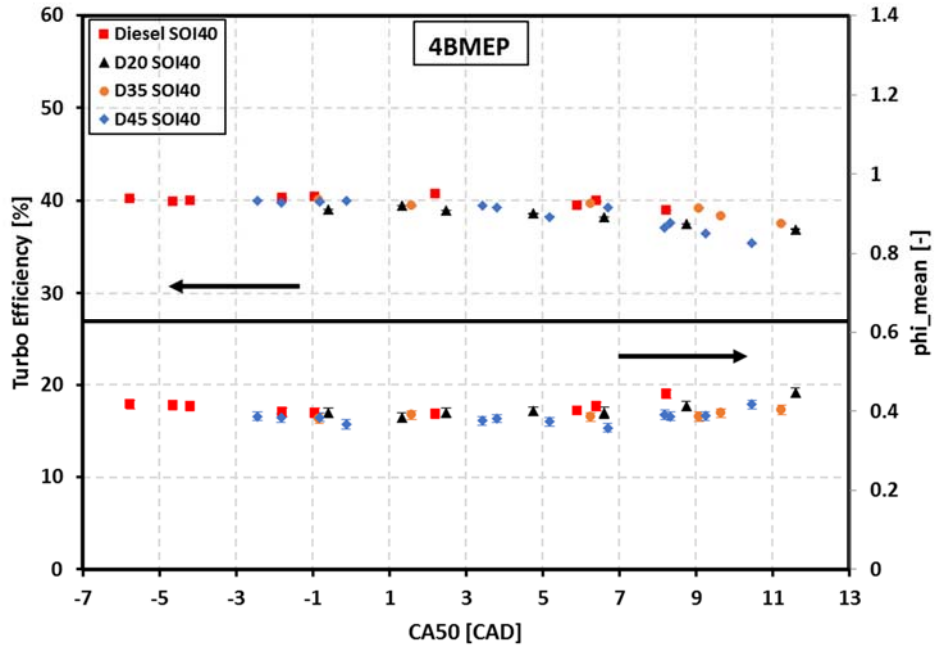

Figure 4-17 Turbo Efficiency [%] and global equivalence ratio [-] as a function of the combustion phasing (CA50) at the DI SOI timing of -40 dATDC

Figure 4-18 shows the fuel energy and total fueling for the different DI fuels. A small, at times statistically significant, reduction in required fueling and energy is achieved. This leads to the increased levels of brake efficiency for the dieseline mixtures over diesel, while again displaying identical combustion efficiencies [Figure 4-20]. Both efficiencies follow their expected trends. A peak in brake efficiency shortly after TDC for all DI fuels, and with that a sweet spot for combustion phasing, was found as a result of the CA50 sweep. Combustion efficiencies are reduced at later CA50 timings as expansion cooling is affecting complete combustion. Brake efficiency gains are recorded for all dieseline cases and reach up to about 2% for dieseline45 over the diesel baseline. Note that the combustion efficiency is kept high and reaches levels close to 95%.

The different amounts of ULSD within the DI fuel fraction can be seen in Figure 4-19. As expected, with an increase in load and therefore increased levels of PFI fuel, the ULSD content of the mixture is reduced, however, still reaching levels that are too high to qualify as a single-fuel RCCI approach.

Additional performance comparison between the different DI fuel types is made in Figure 4-21 and Figure 4-22. The noise levels are again very similar with small increases for dieseline. The MPRR for dieseline fuels are also increased for earlier CA50 values; both still maintaining the self-imposed targets. Peak pressure and exhaust gas temperature are identical in value and follow the expected trends with later CA50 timings. Note again that the increase in exhaust temperature directly affects the small drop in turbo efficiency as it was difficult to make the appropriate adjustments.

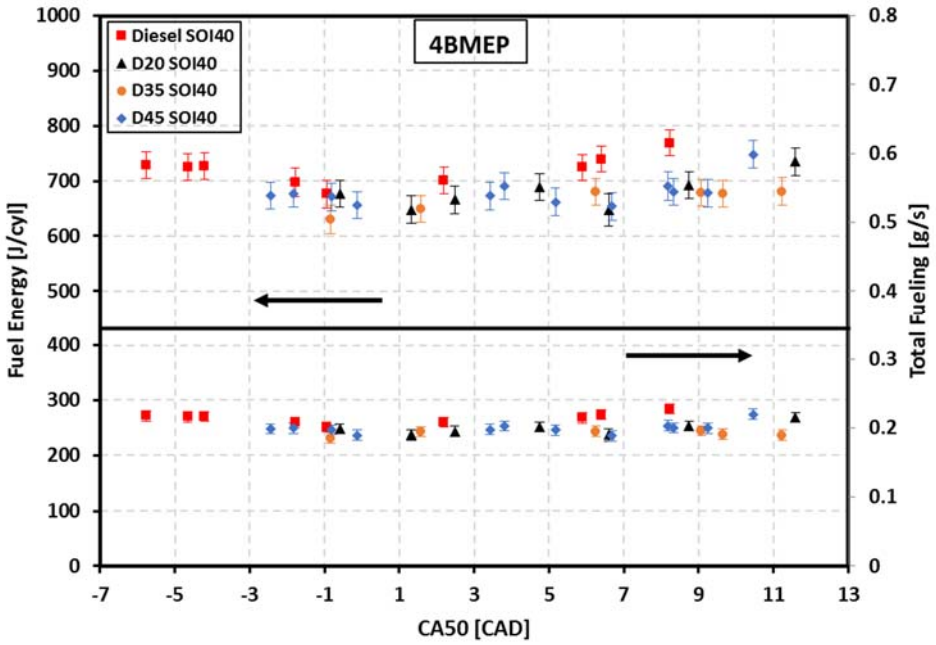

Figure 4-18 Fuel Energy [J/cyl] and Total Fueling [g/s] as a function of combustion phasing (CA50) at the DI SOI timing of -40 dATDC

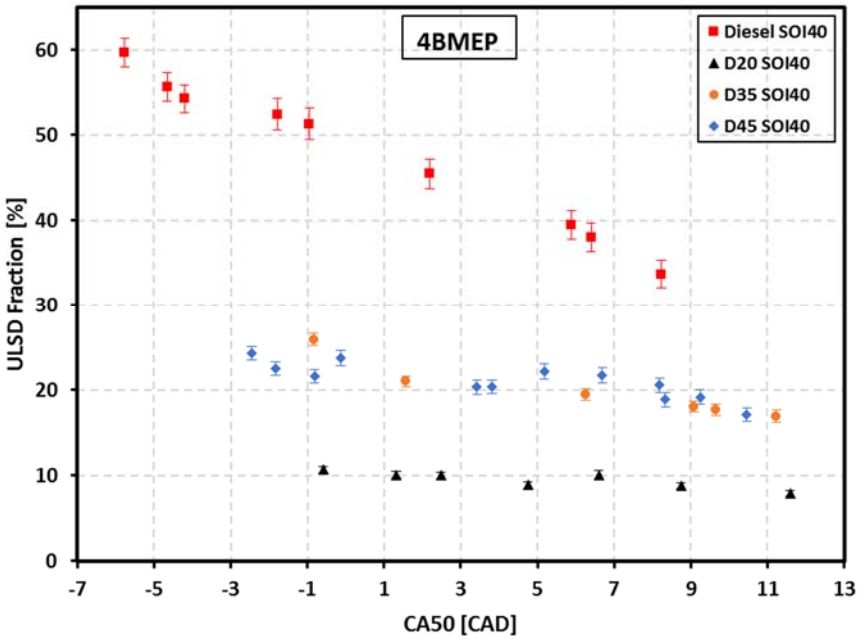

Figure 4-19 ULSD fraction within the total amount of fuel used [%] as a function of combustion phasing (CA50) at the DI SOI timing of -40 dATDC

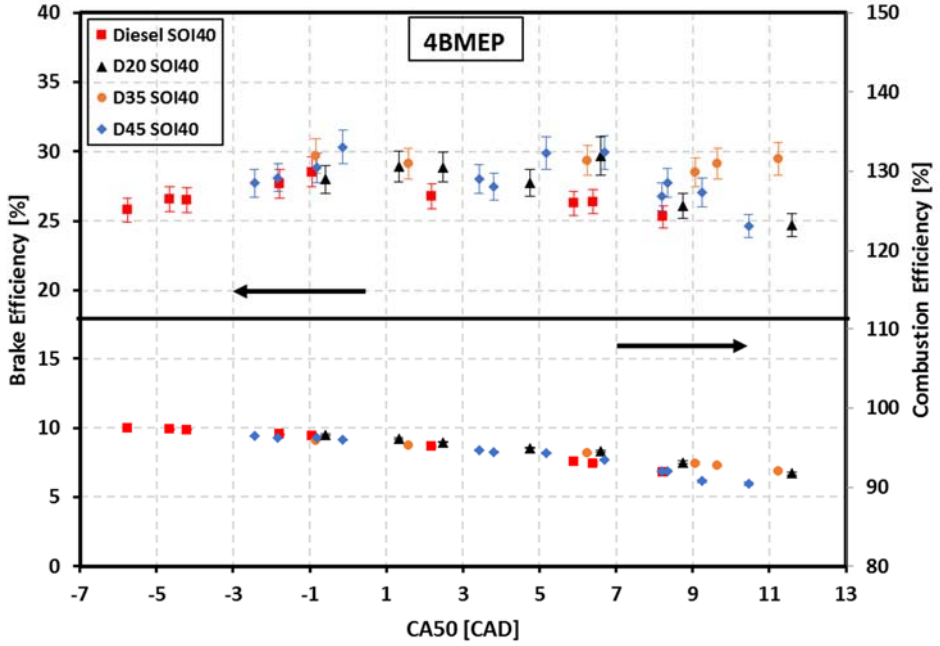

Figure 4-20 Brake efficiency [%] and combustion efficiency [%] as a function of the combustion phasing (CA50) at the DI SOI timing of -40 dATDC

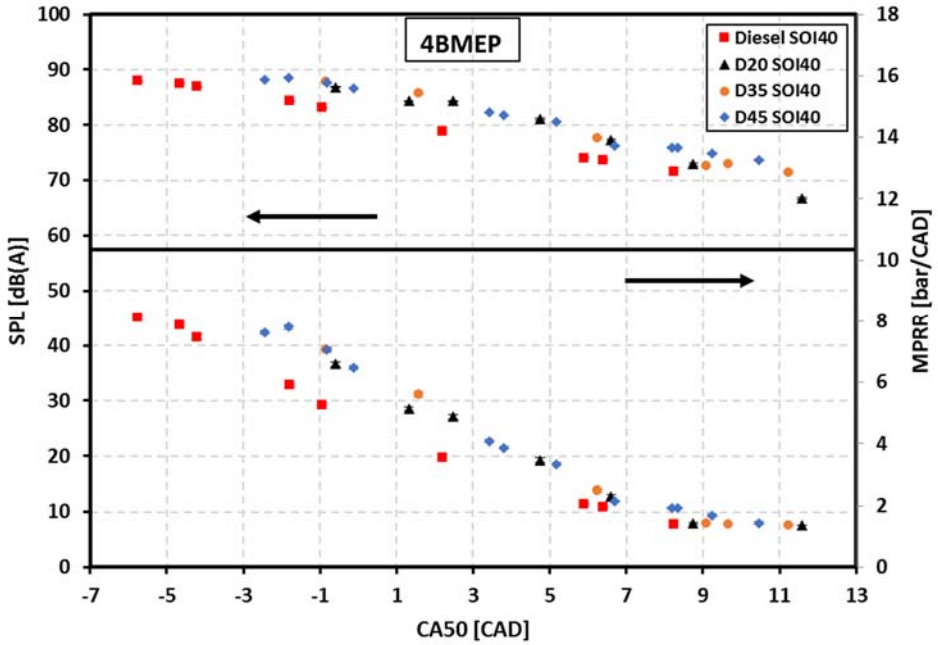

Figure 4-21 Sound pressure level [dB] and maximum pressure rise rate [bar/CAD] as a function of the combustion phasing (CA50) at the DI SOI timing of -40 dATDC

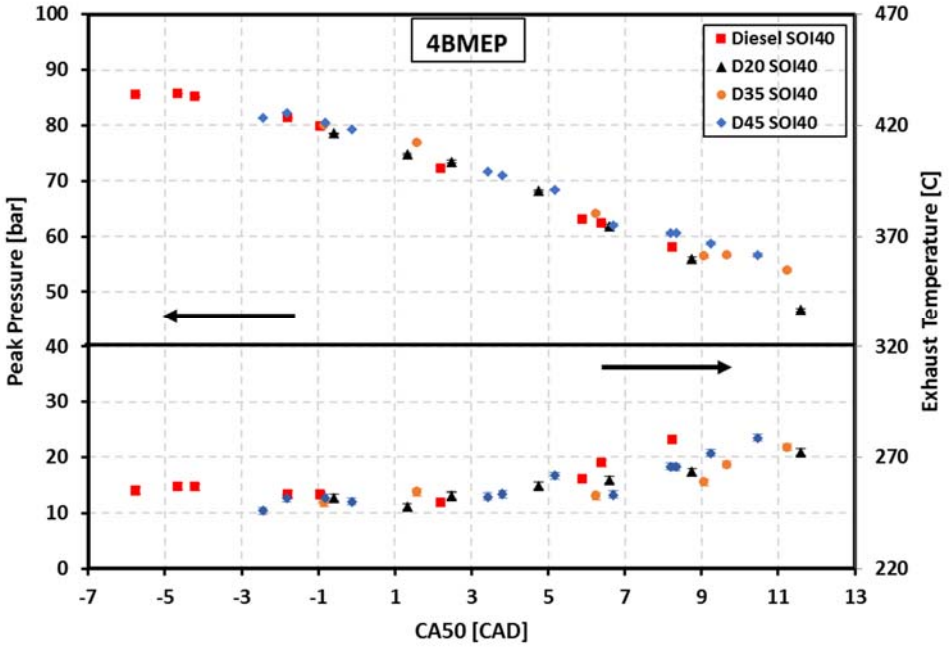

Figure 4-22 Peak cylinder pressure [bar] and exhaust temperature [°C] as a function of the combustion phasing (CA50) at the DI SOI timing of -40 dATDC

Table 4-2 presents the run conditions for the cases of each fuel that resulted in the highest brake thermal efficiency. Note that due to improvements in combustion stability at this higher load, the CA50 variability of dieseline20 was much improved. However, a late CA50 showed best performance results, and a CA50 sweet spot can again be determined at about – 0.6 dATDC for this load/speed condition for the other DI fuel mixtures.

Table 4-2 4bar BMEP Operating Conditions for best brake efficiency cases of each DI fuel at SOI -40 ATDC

Fuel	**Diesel**	**D45**	**D35**	**D20**
Pedal Position [%]	18.5	18	18	19.2
DI Duration [ms]	0.545	0.579	0.619	0.611
PFI Duration [ms]	4.273	3.738	3.219	3.636
PFI Fraction [%]	48.7	47.1	42.4	49.6
Rail Pressure [bar]	502	495	507	502
Main SOI [deg. BTDC]	40	40	40	40
Intake Pressure [bar]	1.15	1.15	1.14	1.14
Intake Temp. [°C]	56	58	58	59
EGR [%]	0	0	0	0
MPRR [bar/deg.]	5.27	6.46	7.06	2.30
CA 50 [deg. ATDC]	-0.945	-0.281	-0.841	6.599
Comb Noise [dba]	83.1	86.7	87.8	77.3
Phi [-]	0.395	0.367	0.382	0.395
BTE [%]	28.54	30.34	29.69	29.70
Comb. Eff. [%]	96.5	95.9	95.9	94.6

Pressure Traces

Pressure traces and heat release rates for each of the DI fuels at the DI SOI timing of -40 dATDC at the 4.0 bar BMEP, 1,500 rev/min load point are presented in Figure 4-23 through Figure 4-26. The plots again highlight the respective case with the highest brake thermal efficiency. Note, good indication on the stability of the combustion and thus the achievable range of operation can again be found in the number of traces plotted. This is true for most DI fuels at this operation condition. Only dieseline35 was difficult to control and against expectations did not allow for smooth operation at a full and extended operating range. Similar, diminishing LTHR trends can be observed at this load point as well. The heat release traces show again smooth Gaussian-like distributions combined with an increase in combustion duration for higher PFI ratios for each of the DI fuels.

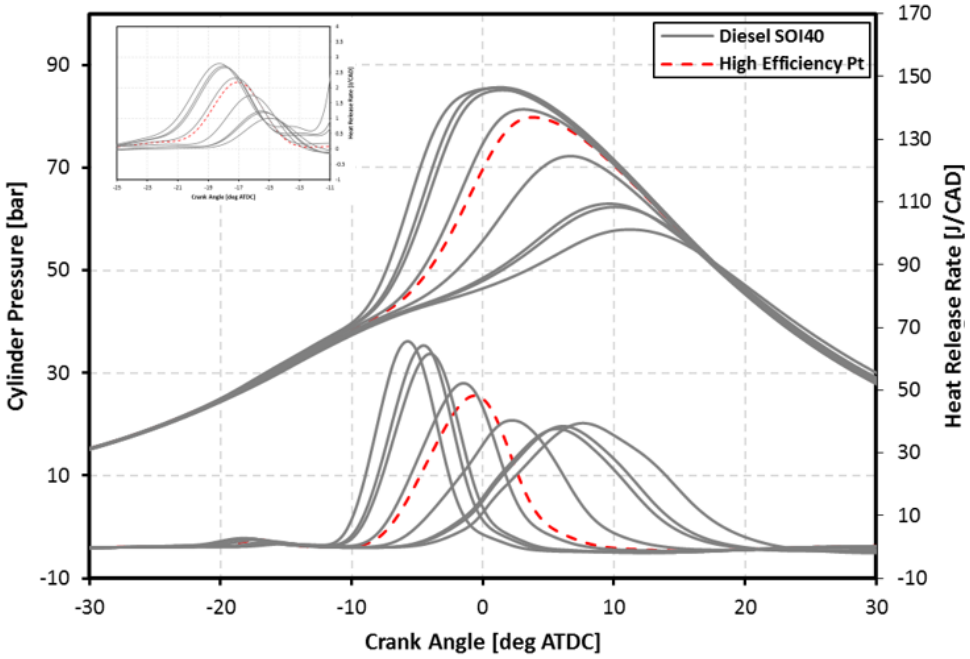

Figure 4-23 Cylinder Pressure [bar] and heat release rate [J/CAD] as a function of CAD for the Diesel RCCI case at the DI SOI timing of -40 dATDC

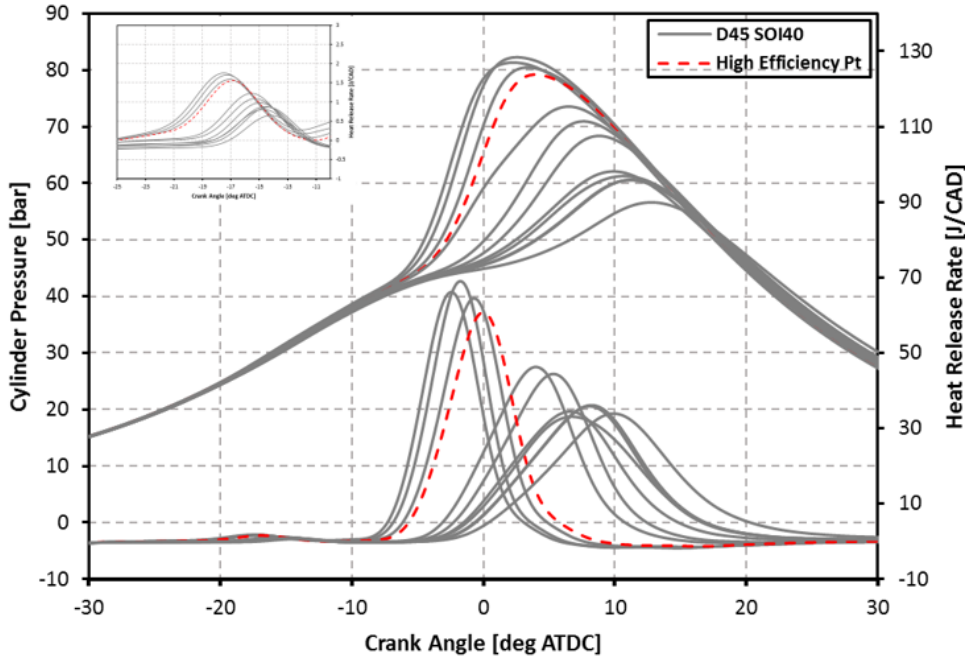

Figure 4-24 Cylinder Pressure [bar] and heat release rate [J/CAD] as a function of CAD for the dieseline45 RCCI case at the DI SOI timing of -40 dATDC

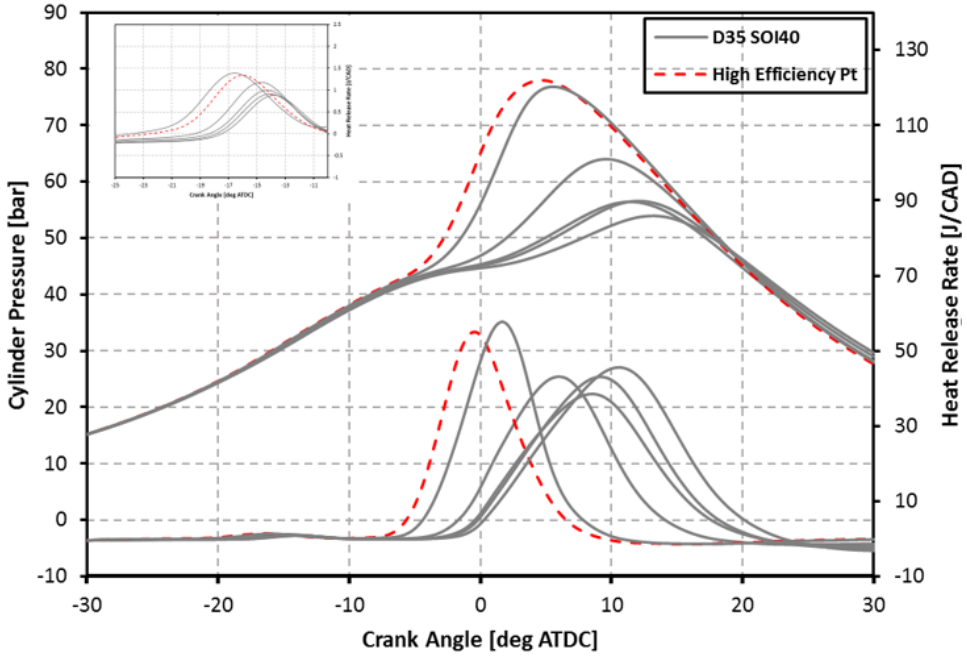

Figure 4-25 Cylinder Pressure [bar] and heat release rate [J/CAD] as a function of CAD for the Dieseline35 RCCI case at the DI SOI timing of -40 dATDC

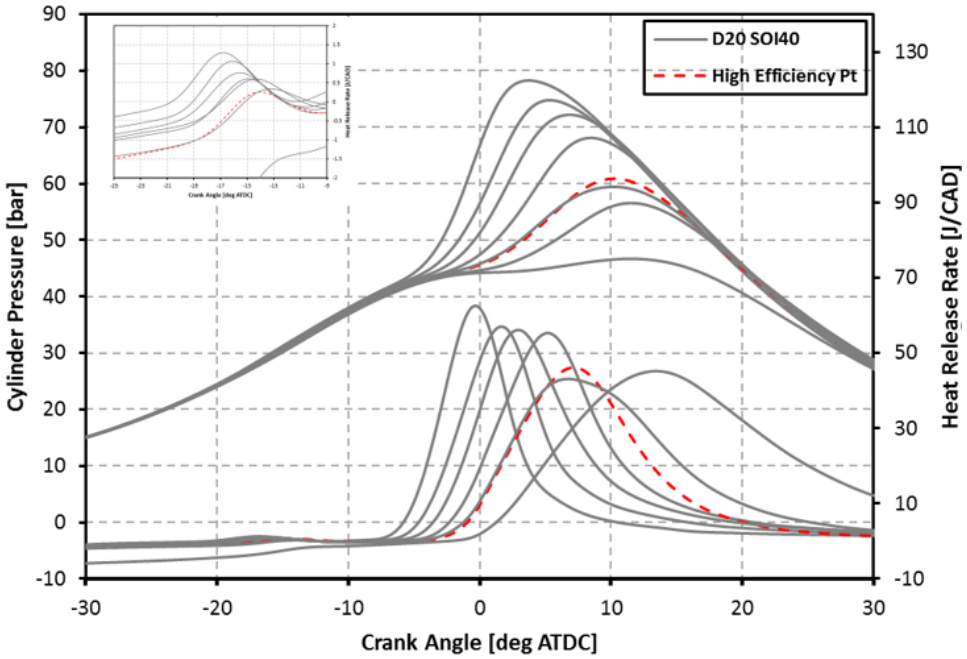

Figure 4-26 Cylinder Pressure [bar] and heat release rate [J/CAD] as a function of CAD for the dieseline20 RCCI case at the DI SOI timing of -40 dATDC

Emissions results

Figures 4-27 and 4-28 show the engine-out emissions for the 4.0 bar BMEP, 1,500 rev/min case. Results for CO, unburned hydrocarbons (measured on a C_1 basis), NOx and opacity emissions are plotted with respect to the brake power output. CO and HC emissions again increase and NOx emissions are reduced with a retard in combustion phasing. The overly lean charge prevents soot (opacity) from being an issue for the whole CA50 range. While all DI fuels follow the same trend for all emission species, HC and CO emission are slightly reduced for the dieseline fuels with respect to the diesel case at later timings. Especially the reduction in HC for the dieseline mixtures becomes statistically significant with later timings. The opposite is true for NOx emissions. The difference between the fuels is decreased with later CA50 timings. Note here that, while the ULSD content is further reduced from previous load points, NOx emissions still show an increase with a reduction in overall ULSD content.

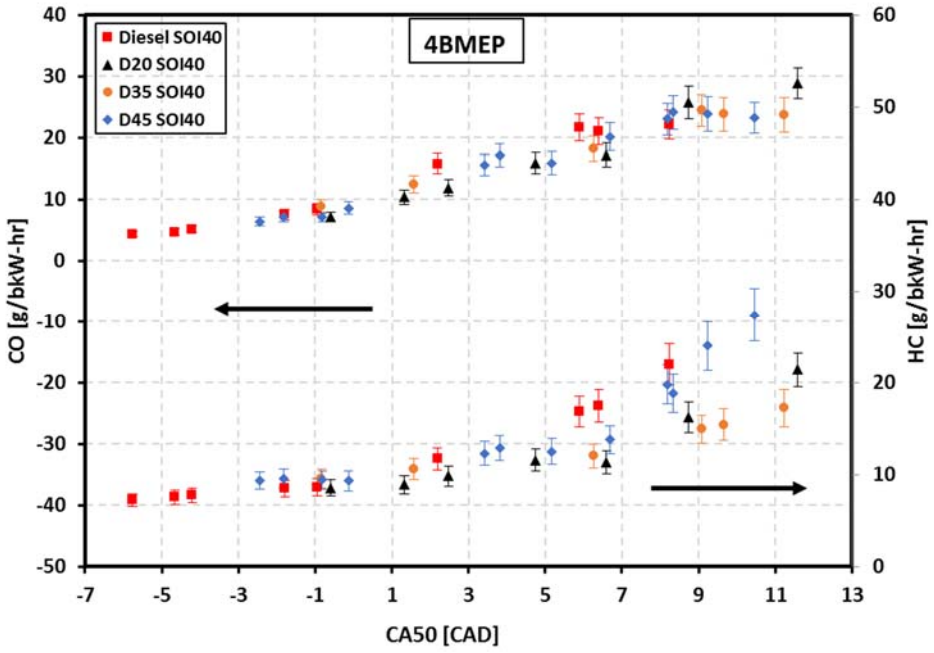

Figure 4-27 Engine-out CO and UHC_1 emissions [g/bkW-hr] as a function of the combustion phasing (CA50) at the DI SOI timing of -40 dATDC

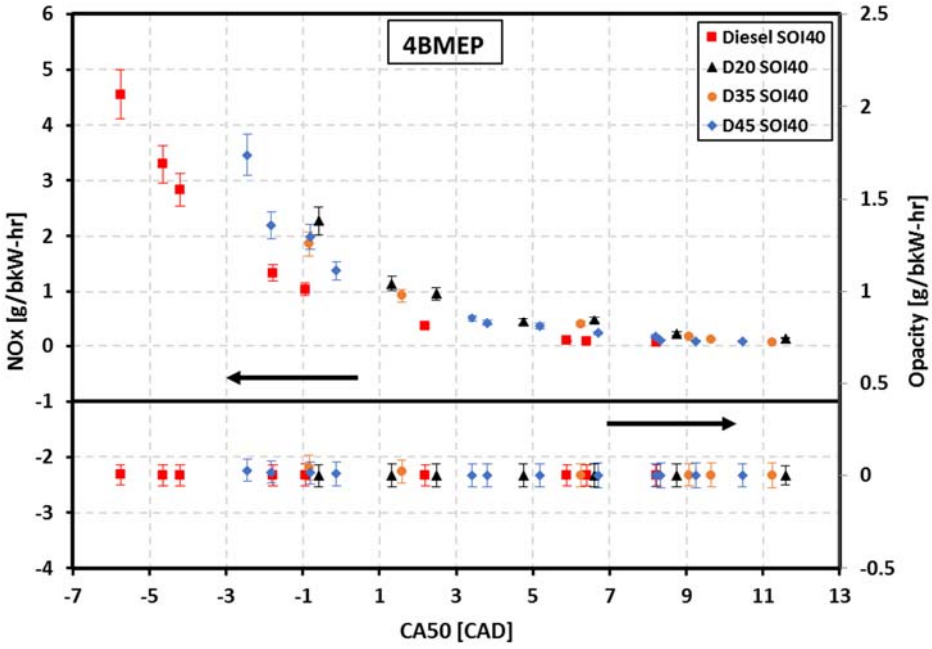

Figure 4-28 Engine-out NOx and Opacity emissions [g/bkW-hr] as a function of the combustion phasing (CA50) at the DI SOI timing of -40 dATDC

4.1.3 4.2bar BMEP, 2,300 rev/min

This final test point at 4.2bar BMEP, 2,300 rev/min was once more operated at steady state in the RCCI combustion mode with a single DI injection and one injection for the PFI. With regards to peak efficiency, the following results again feature the DI SOI timing of -40 dATDC.

Figure 4-29, Figure 4-30 and Figure 4-31 present the run conditions for this test case, where brake power output and BMEP were matched very closely for all DI fuels types. An intake pressure of 1.15bar and an intake temperature of 50 °C was maintained for the diesel and dieseline45 case. In terms of dieseline35 and dieseline20, intake temperatures (65 °C) had to be increased substantially along with an increase in intake pressure (~1.3 bar) in order to stabilize combustion and to reach appropriate CA50 levels [Figure 4-30]. Turbo efficiencies were again maintained fairly constant at the targeted values over the whole CA50 range by employing the VGT

mechanism. However, limits of adjustments were reached between the VGT mechanism and the response rate of the intake system at the increased engine speed, which ultimately led to marginally increased turbocharger efficiencies for dieseline35 and dieseline20 [Figure 4-31].

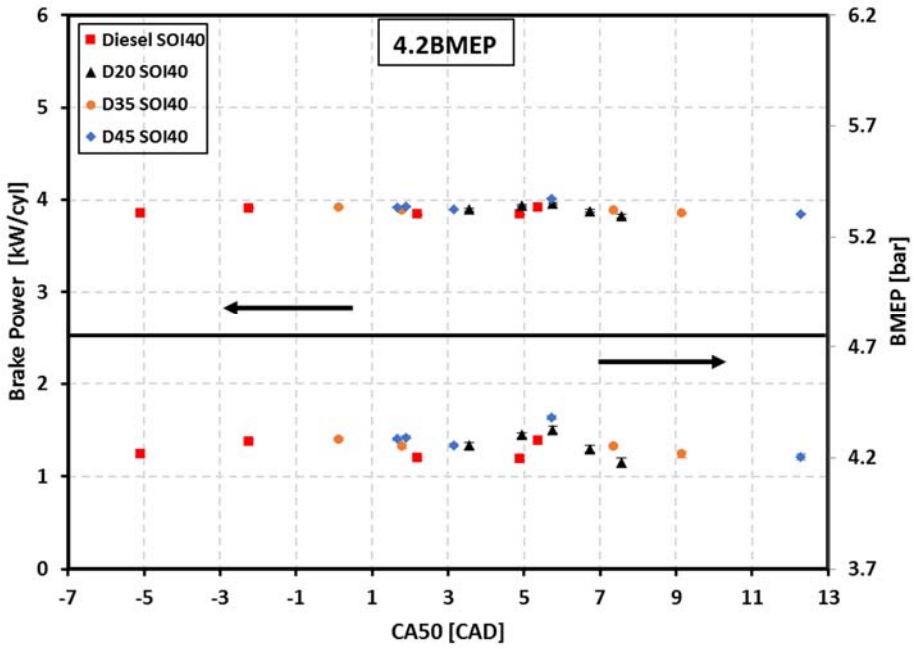

Figure 4-29 BMEP [bar] and Brake Power output [kW] as a function of combustion phasing (CA50) at the DI SOI timing of -40 dATDC

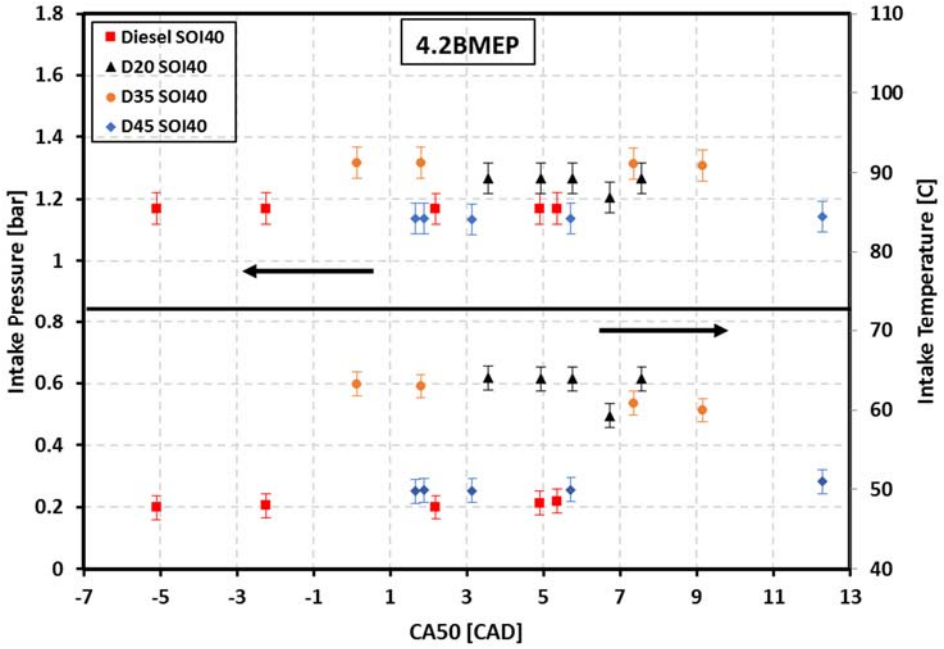

Figure 4-30 Intake Pressure [bar] and Intake Temperature [°C] as a function of the combustion phasing (CA50) at the DI SOI timing of -40 dATDC

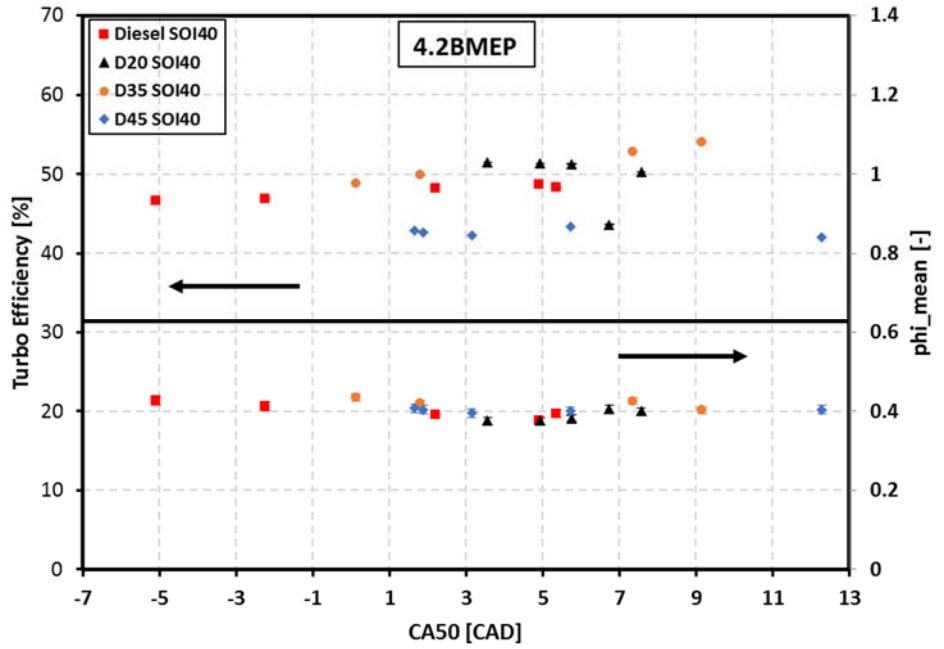

Figure 4-31 Turbo Efficiency [%] and global equivalence ratio [-] as a function of the combustion phasing (CA50) at the DI SOI timing of -40 dATDC

Similar to the previous two test points, a reduction in required fuel energy and total fueling for the dieseline cases over the diesel case was found [Figure 4-32], leading to increased levels of brake efficiency for dieseline45 and dieseline20. In the meantime, dieseline35 displays similar and even lower efficiencies than the diesel case despite the increased intake conditions, while all DI fuels again show identical combustion efficiencies with levels up to 96% complete combustion [Figure 4-34]. A brake efficiency peak is again pronounced, this time shortly after TDC, where efficiency gains for the dieseline cases over the diesel case are recorded with a maximum increase of about 1.5% for matching conditions. Note that dieseline20 and dieseline35 reach higher levels of brake efficiency, however, as mentioned before, do so at higher intake temperatures and pressures. The overall ULSD content is presented in Figure 4-33, showing further reduced levels at this increased load point, while still reaching values up to 24% of the total fuel. But, with regards to diesline35 and dieseline20, it is seen that an increase in temperature or pressure would assist in realizing levels of ULSD close to the additive percentages used in previous work [46, 49, 50].

Once more a complete performance comparison between the different DI fuel types is made in Figure 4-35 and Figure 4-36. While more distinct differences can be seen between the dieseline cases and the diesel case with increased values for dieseline, all DI fuels still meet the noise level and MPRR targets. The same is true for peak pressure and exhaust gas temperature levels.

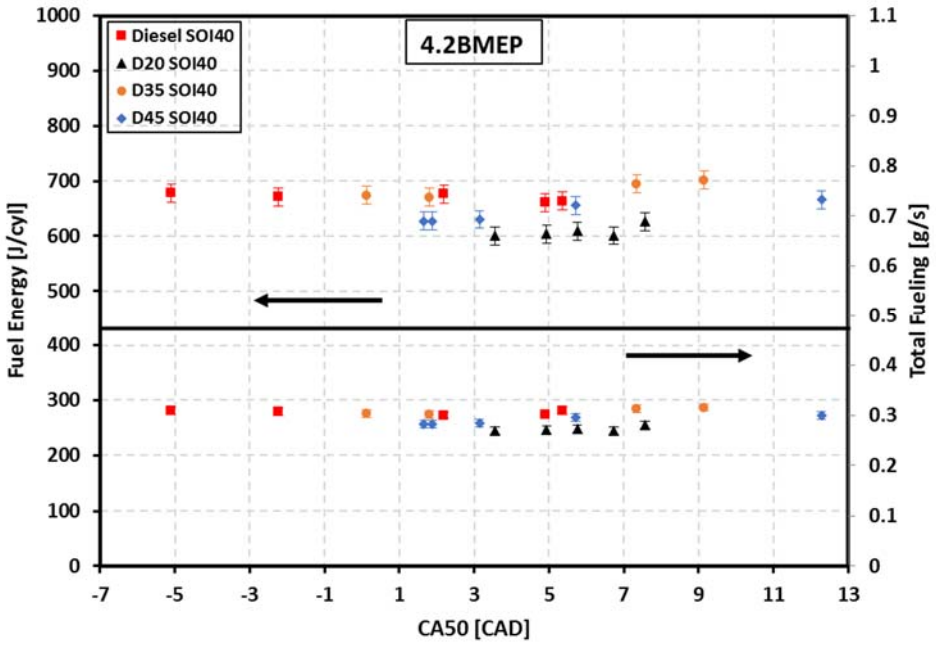

Figure 4-32 Fuel Energy [J/cyl] and Total Fueling [g/s] as a function of combustion phasing (CA50) at the DI SOI timing of -40 dATDC

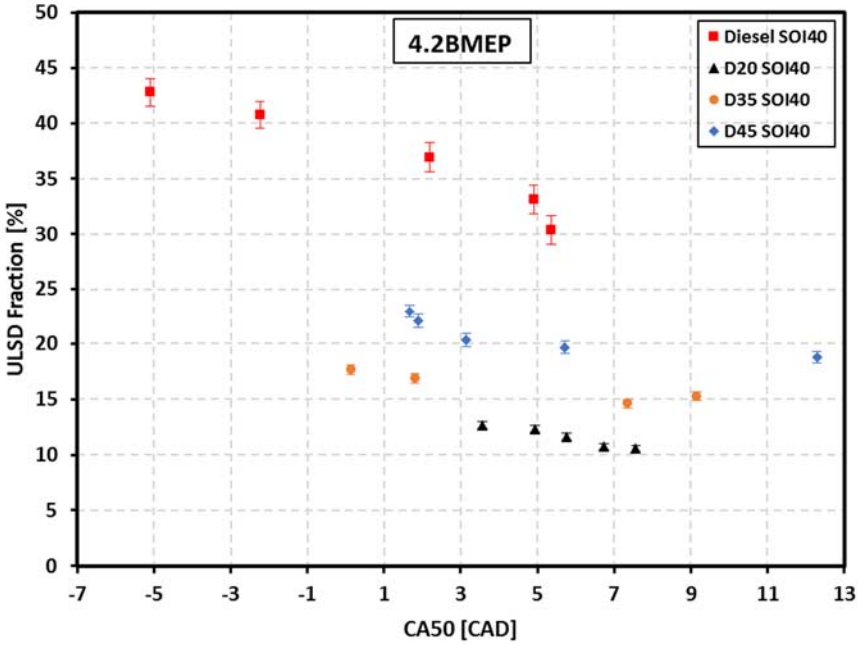

Figure 4-33 ULSD fraction within the total amount of fuel used [%] as a function of combustion phasing (CA50) at the DI SOI timing of -40 dATDC

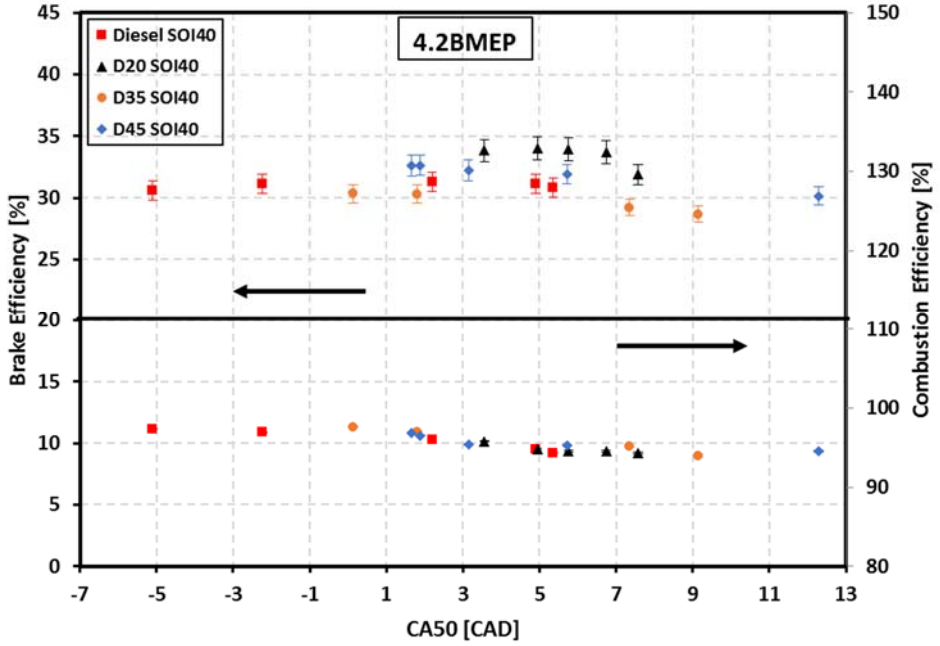

Figure 4-34 Brake efficiency [%] and combustion efficiency [%] as a function of the combustion phasing (CA50) at the DI SOI timing of -40 dATDC

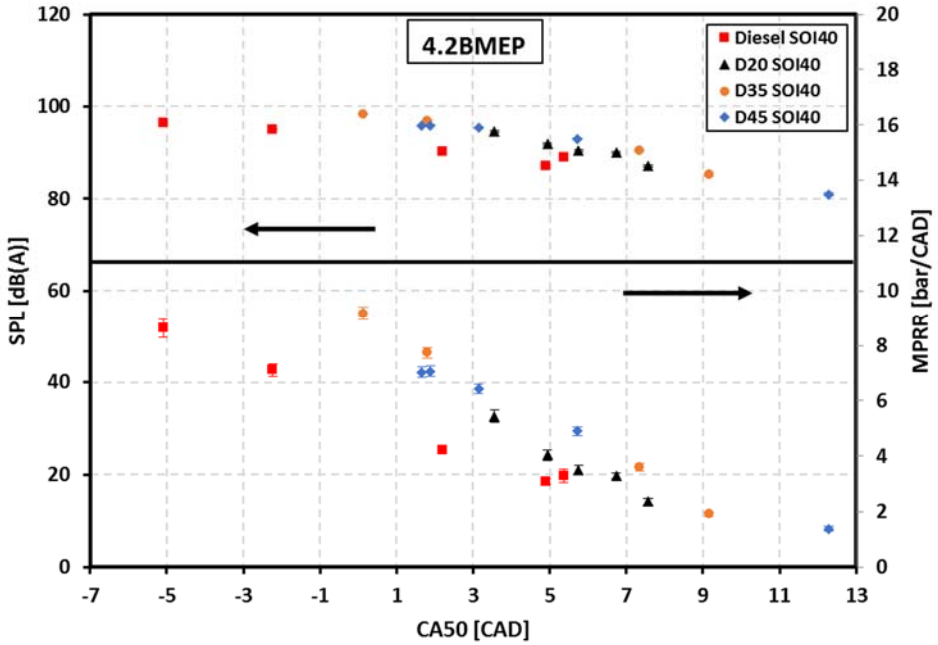

Figure 4-35 Sound pressure level [dB] and maximum pressure rise rate [bar/CAD] as a function of the combustion phasing (CA50) at the DI SOI timing of -40 dATDC

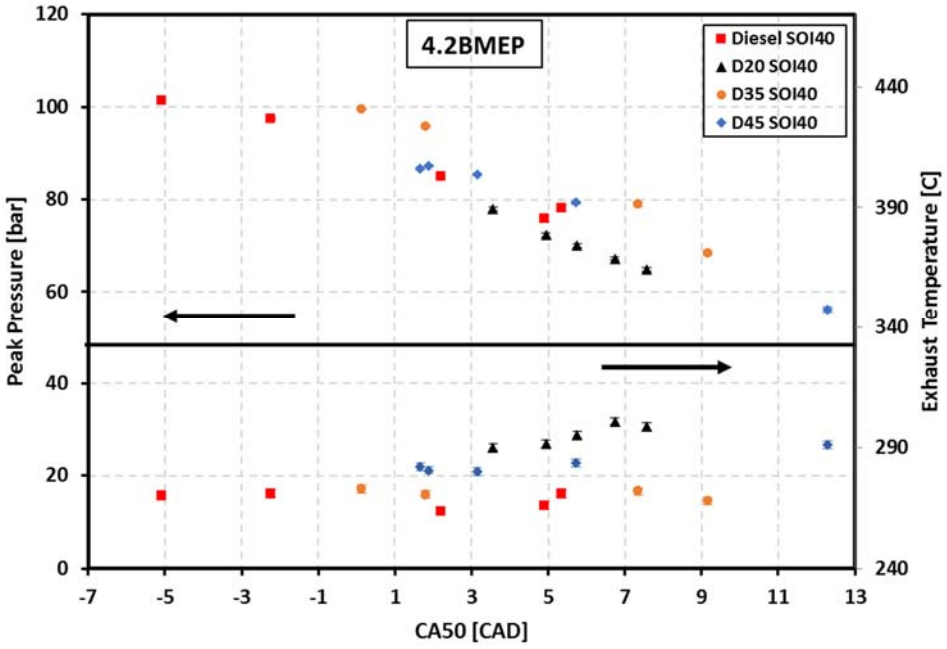

Figure 4-36 Peak cylinder pressure [bar] and exhaust temperature [°C] as a function of the combustion phasing (CA50) at the DI SOI timing of -40 dATDC

The points leading to highest brake thermal efficiency results are again summarized in Table 4-3. Note again that the intake manifold conditions for dieseline35 and dieseline20 were elevated to achieve stable combustion at this test point and while combustion was stable, the CA50 for peak efficiency performance is delayed over the diesel and dieseline45 cases. Regardless, an optimum can be determined for diesel and dieseline45 at about 2 dATDC for this load/speed condition. This will serve as a CA50 target for upcoming investigations.

Table 4-3 4.2bar BMEP Operating Conditions for best brake efficiency cases of each DI fuel at SOI -40 ATDC

Fuel	Diesel	D45	D35	D20
Pedal Position [%]	33.8	32.4	32.7	30.2
DI Duration [ms]	0.460	0.531	0.531	0.632
PFI Duration [ms]	4.834	4.028	3.963	2.863
PFI Fraction [%]	63.0	50.9	49.1	38.3
Rail Pressure [bar]	506	500	502	499
Main SOI [deg. BTDC]	40	40	45	40
Intake Pressure [bar]	1.17	1.14	1.32	1.27
Intake Temp. [°C]	48	50	64	64
EGR [%]	0	0	0	0
MPRR [bar/deg.]	4.22	7.06	6.09	4.03
CA 50 [deg. ATDC]	2.194	1.889	3.819	4.939
Comb Noise [dba]	90.3	95.9	95.0	91.8
Phi [-]	0.391	0.403	0.412	0.376
BTE [%]	31.29	32.65	32.08	34.04
Comb. Eff. [%]	95.9	96.5	96.9	94.8

Pressure Traces

Figure 4-37 through Figure 4-40 show the pressure traces and heat release rates for each of the DI fuels at the DI SOI timing of -40 dATDC. Once more the respective case reaching the highest brake thermal efficiency is highlighted. Note however, that for the dieseline35 case the highest efficiency point highlighted was reached at a DI SOI timing of -45 dATDC, and showed a retarded heat release rate distribution. A limited number of traces are shown here, but for dieseline20 the CA50 variability is much more restricted. This is due to the very narrow limits for stable combustion with this low reactive fuel blend. Similar to previously shown results, the heat release rates depict a typical Gaussian distribution for RCCI-type combustion with an increase in combustion duration with later CA50 timings. Interesting to note is the change in the LTHR at this engine speed with regards to the dieseline blends. The LTHR traces move very close to the ITHR and thus have an almost continuous rise into the high temperature heat release (HTHR) with decreasing diesel content.

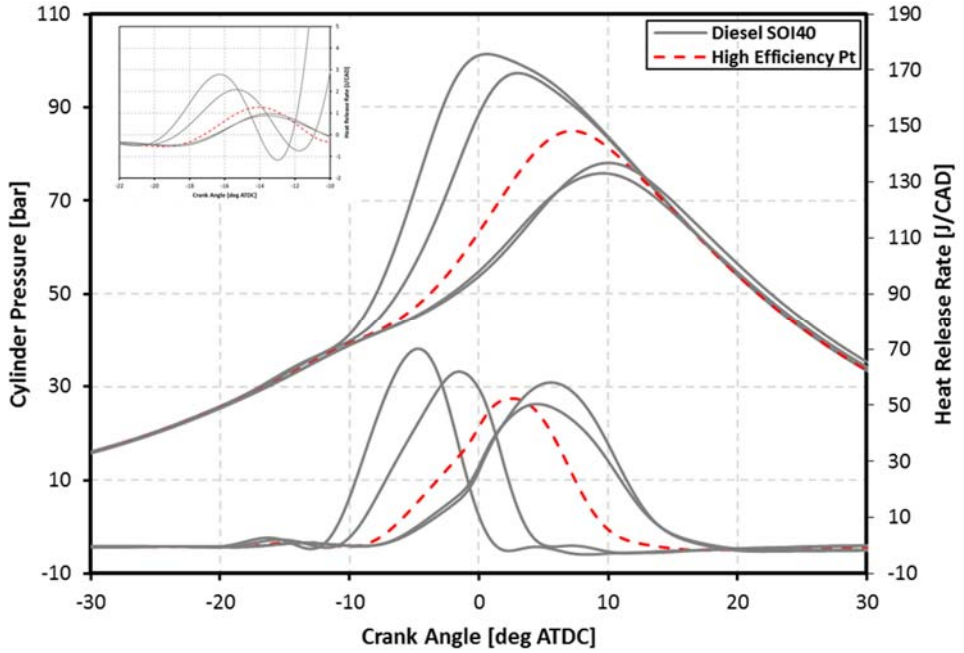

Figure 4-37 Cylinder Pressure [bar] and heat release rate [J/CAD] as a function of CAD for the Diesel RCCI case at the DI SOI timing of -40 dATDC

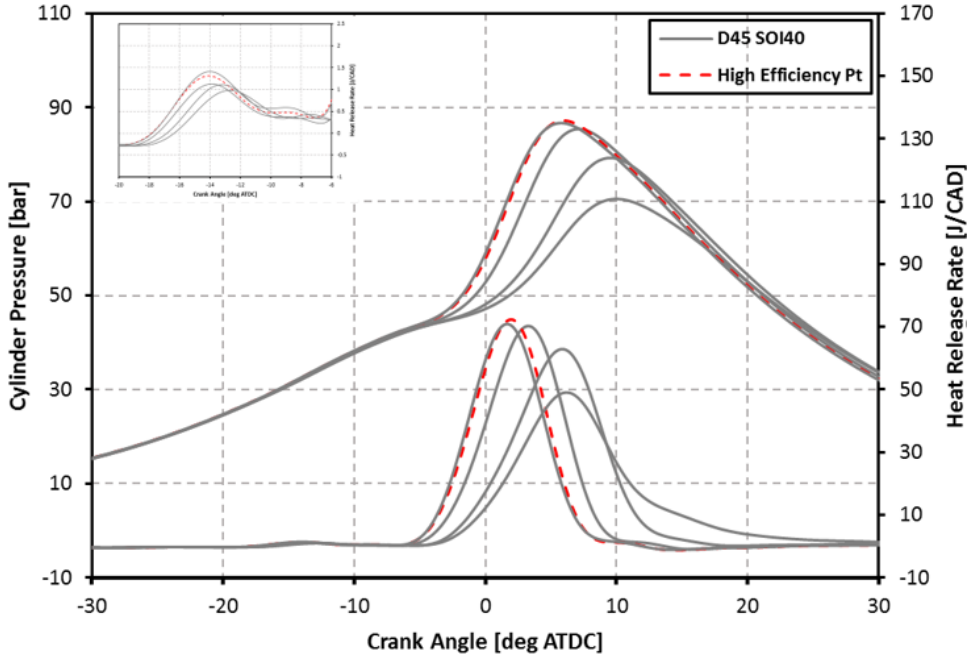

Figure 4-38 Cylinder Pressure [bar] and heat release rate [J/CAD] as a function of CAD for the dieseline45 RCCI case at the DI SOI timing of -40 dATDC

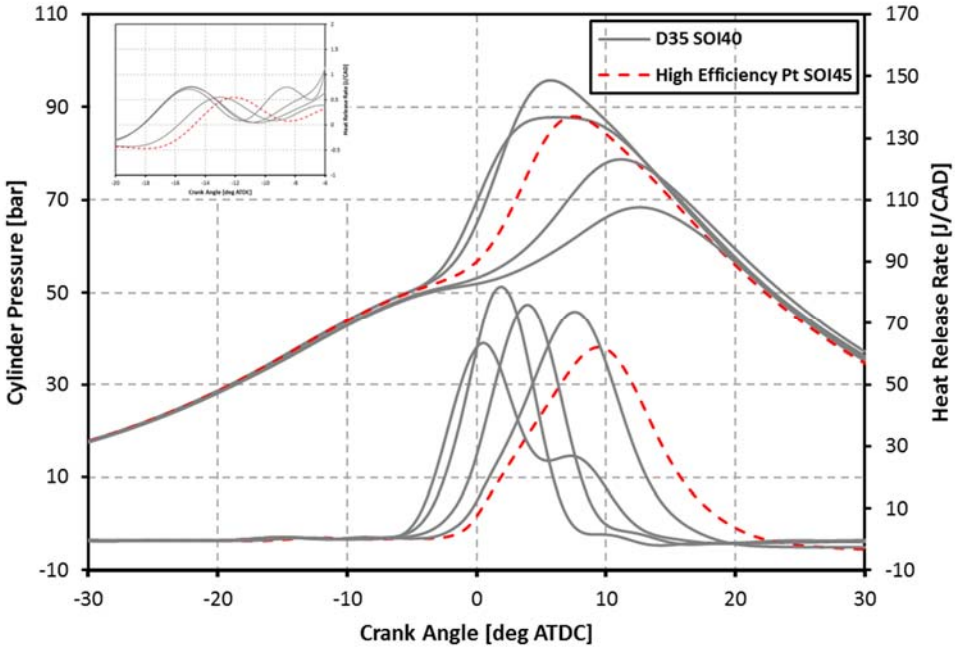

Figure 4-39 Cylinder Pressure [bar] and heat release rate [J/CAD] as a function of CAD for the dieseline35 RCCI case at the DI SOI timing of -40 dATDC

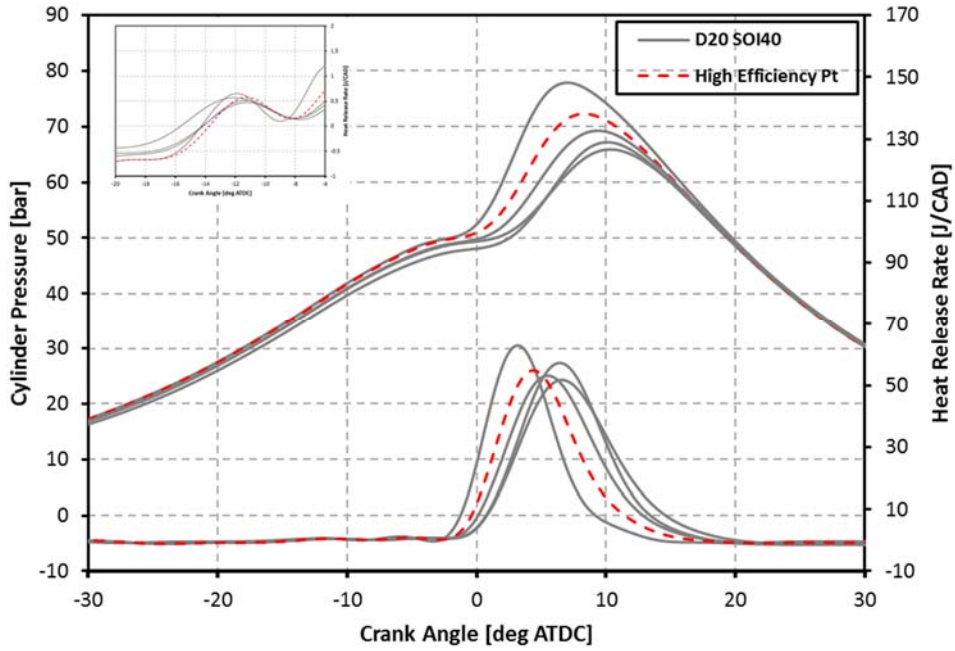

Figure 4-40 Cylinder Pressure [bar] and heat release rate [J/CAD] as a function of CAD for the dieseline20 RCCI case at the DI SOI timing of -40 dATDC

Emissions results

Engine-out emissions with respect to brake power output are plotted for all 4 DI fuels in Figures 4-41 and 4-42. CO and HC emissions for this 4.2 bar BMEP, 2,300 rev/min case show an expected increase with combustion retard and are slightly reduced for the dieseline blends over the diesel DI fuel. However, the overall levels for all DI fuels are significantly reduced over the 4.0 bar BMEP, 1,500 rev/min case. With an almost identical engine load, this can mostly be related to the difference in engine speed. Furthermore, the NOx emissions show identical and even slightly reduced values for the dieseline blends at this test point. Engine speed again plays an important factor in this observation, where less available time leads to an overall reduction in NOx. Opacity is again not of concern over the whole CA50 range.

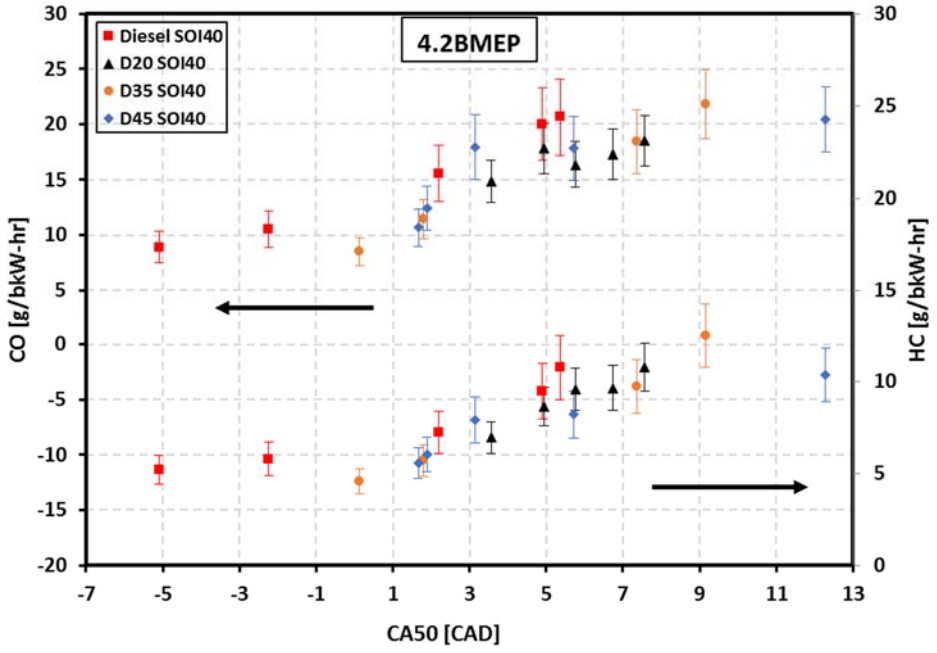

Figure 4-41 Engine-out CO and UHC_1 emissions [g/bkW-hr] as a function of the combustion phasing (CA50) at the DI SOI timing of -40 dATDC

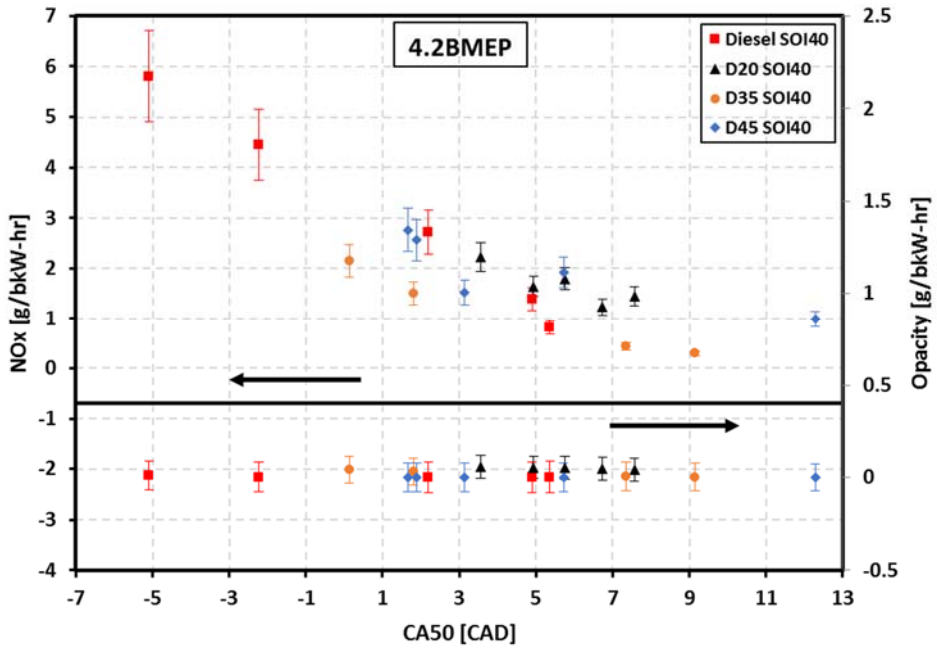

Figure 4-42 Engine-out NOx and Opacity emissions [g/bkW-hr] as a function of the combustion phasing (CA50) at the DI SOI timing of -40 dATDC

4.1.4 Investigation of higher-% Dieseline DI mixtures

As stated above the tests involved operating the engine at steady state in the RCCI combustion mode with a single DI injection and one injection for the port fuel injection. Results for all fuels and at all operating conditions concluded that the peak performances were found at a DI SOI timing of -40 dATDC for all but one case. Furthermore, the CA50 values at each operating point leading to peak efficiencies for all the fuels were found to be very similar. Under these conditions best thermal efficiencies were achieved for the 45%ULSD/EEE mixture [Figure 4-43 & Table 4-4].

Design of Experiments							
	DI Fuels	Cases (CA50 Sweep)					
		SOI 40 and SOI 45					
		1bar/1500	2bar/1500	2.6bar/1500	4bar/1500	2bar/2000	4.2bar/2300
Cases RUN (Best BTE)	Diesel	y	y	y	y	y	y
	D20	y	y	y	y	y	y
	D35	y	y	y	y	y	y
	D45	y	y	y	y	y	y

Figure 4-43 DOE for dieseline investigation to explore peak efficiencies

Table 4-4 Overview of performance and conditions for dieseline45 at all test points at the DI SOI timing of -40 dATDC

Dieseline45						
BMEP Load [bar]	1.0	2.0	2.6	4.0	2.0	4.2
Speed [RPM]	1500	1500	1500	1500	2000	2300
Pedal Position [%]	12.9	15.5	17.4	18	20.9	32.4
DI Duration [ms]	0.587	0.535	0.533	0.579	0.563	0.531
PFI Duration [ms]	1.192	1.968	2.706	3.738	1.056	4.028
PFI Fraction [%]	17.3	39.5	37.9	47.1	17.74	50.9
Rail Pressure [bar]	495	505	495	495	500	500
Main SOI [deg. BTDC]	40	40	40	40	40	40
Intake Pressure [bar]	1.17	1.17	1.17	1.15	1.17	1.14
Intake Temp. [°C]	52	53	53	58	50	50
EGR [%]	0	0	0	0	0	0
MPRR [bar/deg.]	2.72	3.18	4.76	6.46	4.22	7.06
CA 50 [deg. ATDC]	-1.963	-2.612	-1.317	-0.281	-1.514	1.889
Comb Noise [dba]	75.1	75.4	81.9	86.7	87.1	95.9
Phi [-]	0.188	0.223	0.298	0.367	0.251	0.403
BTE [%]	15.55	25.12	23.78	30.34	23.06	32.65
Comb. Eff. [%]	88.3	92.2	94.5	95.9	92.2	96.5

The results suggest that higher dieseline mixtures could possibly allow for gains in efficiency compared to dieseline45. Therefore, a smaller design of experiments, with only 3 operating points, including mixtures of 50%ULSD/EEE gasoline (D50) and 60%ULSD/EEE gasoline (D60), was conducted [Figure 4-44]. Dieseline20 and its low reactivity was not

considered anymore as it had significant drawbacks in terms of CA50 variability and unstable combustion, as was highlighted in the previous section.

Design of Experiments				
	DI Fuels	Cases (set CA50)		
		SOI 40		
		2.6bar/1500	4bar/1500	4.2bar/2300
Cases RUN	Diesel	y	y	y
	D35	y	y	y
	D45	y	y	y
	D50	y	y	y
	D60	y	y	y

Figure 4-44 Reduced DOE for additional dieseline mixtures to evaluate "preferred" fuels

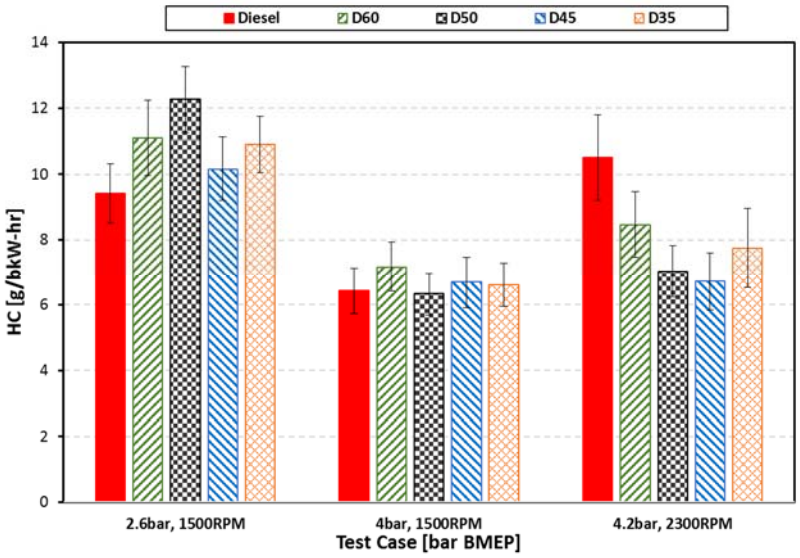

Figure 4-45 Hydrocarbon emissions [g/bkW-hr] for different DI fuels as a function of operating points at the DI SOI timing of -40 dATDC

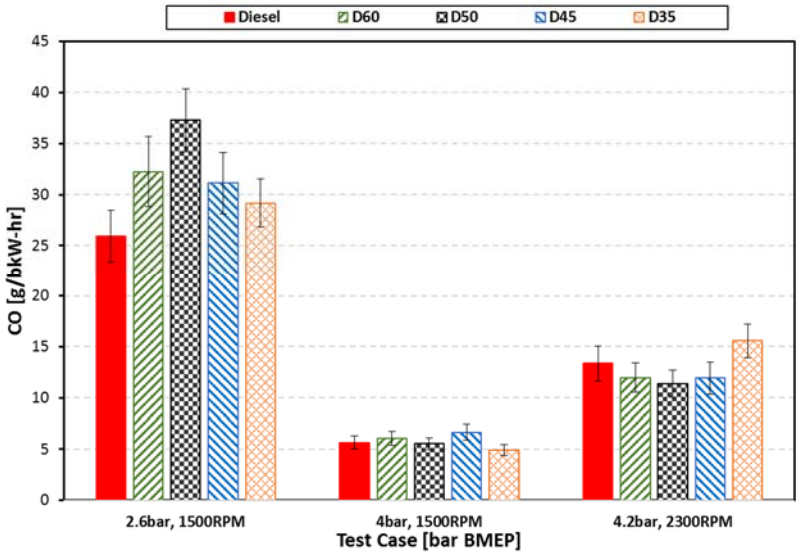

Figure 4-46 Carbon monoxide emissions [g/bkW-hr] for different DI fuels as a function of operating points at the DI SOI timing of -40 dATDC

In this reduced design of experiments (DOE), HC and CO emissions for dieseline are again more or less identical to Diesel RCCI operation, with even slight improvements at the high load conditions [Figure 4-45 and 4-46]. As shown previously, dieseline NOx emissions on the other hand are again raised above the levels of diesel RCCI due to the longer DI injection durations causing locally richer regions and thus an increase in NOx [Figure 4-47]. This reasoning was confirmed for dieseline50 and dieseline60, as they obey trend of the increasing NOx emissions for an increase in ULSD.

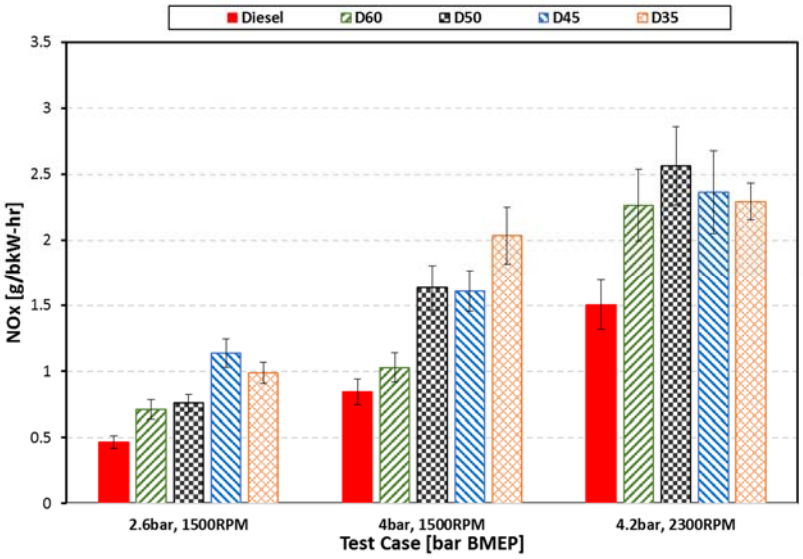

Figure 4-47 Nitric oxide emissions [g/bkW-hr] for different DI fuels as a function of operating points at the DI SOI timing of -40 dATDC

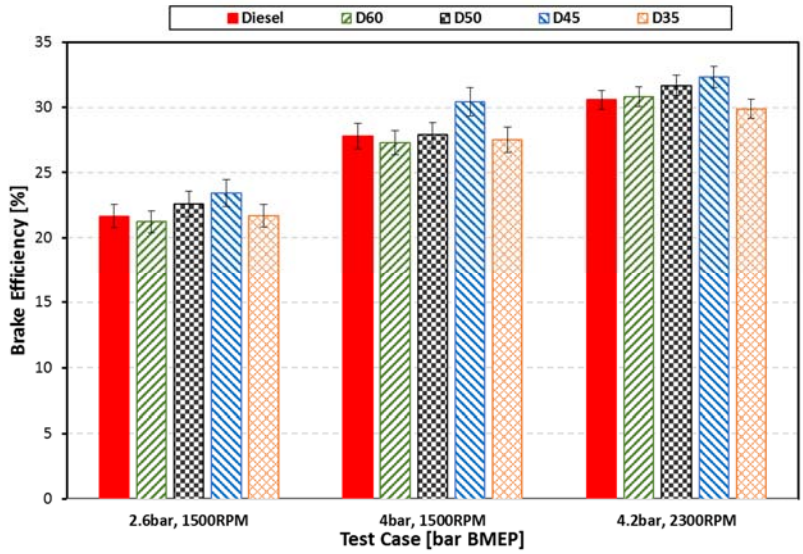

Figure 4-48 Brake efficiencies [%] for different DI fuels as a function of operating points at the DI SOI timing of -40 dATDC

In conclusion, the results indicate an optimum for RCCI operation with dieseline45, as can be seen in Figure 4-48. This allowed a further reduced DOE in upcoming investigation, where

dieseline45 served as the "preferred" fuel. An overview of the results for all 3 cases using dieseline45 is shown in Table 4-5.

Table 4-5 Overview of performance and conditions for dieseline45 at the DI SOI timing of -40 dATDC

Dieseline45			
BMEP Load [bar]	2.6	4.0	4.2
Speed [RPM]	1500	1500	2300
Pedal Position [%]	15.1	18.3	29.4
DI Duration [ms]	0.596	0.516	0.554
PFI Duration [ms]	1.733	3.983	3.655
PFI Fraction [%]	24.5	49.7	48.6
Rail Pressure [bar]	498	495	498
Main SOI [deg. BTDC]	40	40	40
Intake Pressure [bar]	1.12	1.12	1.12
Intake Temp. [°C]	55	55	55
EGR [%]	0	0	0
MPRR [bar/deg.]	3.86	6.09	4.69
CA 50 [deg. ATDC]	-1.471	-0.257	2.709
Comb Noise [dba]	79.9	85.9	91.8
Phi [-]	0.342	0.401	0.422
BTE [%]	23.42	29.41	32.34
Comb. Eff. [%]	95.2	97.1	96.4

4.2 Conclusions

The focus of this section of the study was to investigate the performance of different dieseline blends as the high reactivity fuel in a multi-cylinder light-duty engine during steady-state RCCI operation and to compare it with gasoline/diesel RCCI combustion under matching intake and operating conditions. The tests were performed for a total of 6 test points at two different DI SOI timings (-40 and -45 dATDC), and a selection of 3 points was highlighted.

The 6 cases investigated are:

- 1.0 bar BMEP, 1,500 rev/min
- 2.0 bar BMEP, 1,500 rev/min
- 2.0 bar BMEP, 2,000 rev/min

- 2.6 bar BMEP, 1,500 rev/min
- 4.0 bar BMEP, 1,500 rev/min
- 4.2 bar BMEP, 2,300 rev/min

All the DI fuels displayed emissions and combustion performance trends that are characteristic of RCCI combustion.

It was shown that it is possible to operate the MCE in RCCI mode using different dieseline blends at matching operating conditions over a wide range of CA50 values. Improvements of brake thermal efficiency (BTE) with small increases in heat transfer losses were seen from the performance results. BTE increased nominally by 3.25% at the 2.0 bar, 2,000 rev/min case up to 18.7% at the 1.0 bar, 1,500 rev/min case, resulting from improved fueling rates for the dieseline cases. Combustion efficiencies and thus emission results for CO and HC were found to be identical or even slightly improved for dieseline cases over the diesel RCCI case. NOx emissions were increased with a decrease in ULSD content, i.e., reduced reactivity of the DI fuel, due to longer DI injection durations in order to compensate for a reduction in reactivity.

It was also observed that MPRR and combustion noise were recorded under the self-imposed constraints of 10 bar/deg peak pressure rise rate and noise levels of 95 dB for all DI fuels with only a small increase for the dieseline cases. Furthermore, exhaust gas temperatures reached same levels for all fuel types. In the meantime, results revealed CA50 sweet spots for optimal and most efficient operation that also fall in line with former calibrations. Hence, subsequent investigations in this study targeted these CA50 values for best performance results. Finally, with regards to the DOE, investigations have shown that an optimum in performance is reached by using dieseline45 at an DI SOI timing of -40 dATDC, which as a result allowed the DOE to be reduced in following investigations using dieseline45 as the “preferred” fuel and only employing a SOI timing of -40 dATDC.

Chapter 5 Effects of Boost on Steady-State RCCI Combustion Using Dieseline45

This chapter presents experimental work to examine the performance of RCCI operation for different intake pressures. The load points used for the evaluation of increased boost pressure are consistent with the selection introduced and highlighted in the previous section. The tests were conducted in the light-duty MCE diesel engine employing the customized intake system. Besides the previously achievable RCCI boost pressure with the stock air handling system, pressures up to 2.1 bar were tested by using the supplied building air in combination with the VGT turbocharger. Utilizing the VGT mechanism allowed backpressures to be adjusted in order to reach appropriate combined turbocharger efficiencies. The tests were carried out using dieseline45 at a DI SOI timing of -40 dATDC, as this was found to provide best BTE levels overall (Chapter 4). In the second part, the findings are further discussed and conclusions are drawn, while supplemental material can be found in Appendix C.

5.1 Operating Conditions and Results

Figure 5-1 shows the brake efficiency results for an array of different intake pressures. It can be seen that besides the previously maintained intake pressures during RCCI operation using the stock turbocharger set-up, pressure up to 2.1 bar were tested by using the updated intake system. As expected the friction load is increased with increasing boost due to increased peak pressure levels along with the pumping work, reducing the brake efficiency for higher levels of intake pressure [Figure 5-2]. In order to keep the brake load constant to compensate for the increasing losses, fueling has to be increased, and this decreases brake thermal efficiencies. However, for a boost pressure of 1.1 bar, which is slightly higher than what was achievable during RCCI operation, slightly improved efficiencies were achieved for the 2.6 bar BMEP, 1,500 rev/min

and 4.0 bar BMEP, 1,500 rev/min cases. Note that for the 4.2 bar, 2,300 rev/min case, the achievable RCCI boost pressure is identical to the pressure setting of 1.1bar, which has been used throughout most of this study. Note also that the maximum boost pressure that could be reached at this point was only about 1.5 bar.

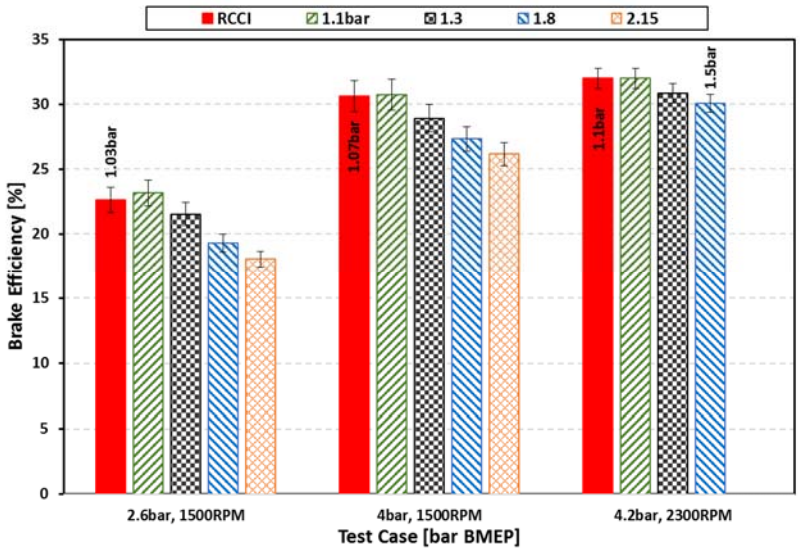

Figure 5-1 Brake efficiencies [%] for different intake pressures as a function of operating points at the DI SOI timing of -40 dATDC

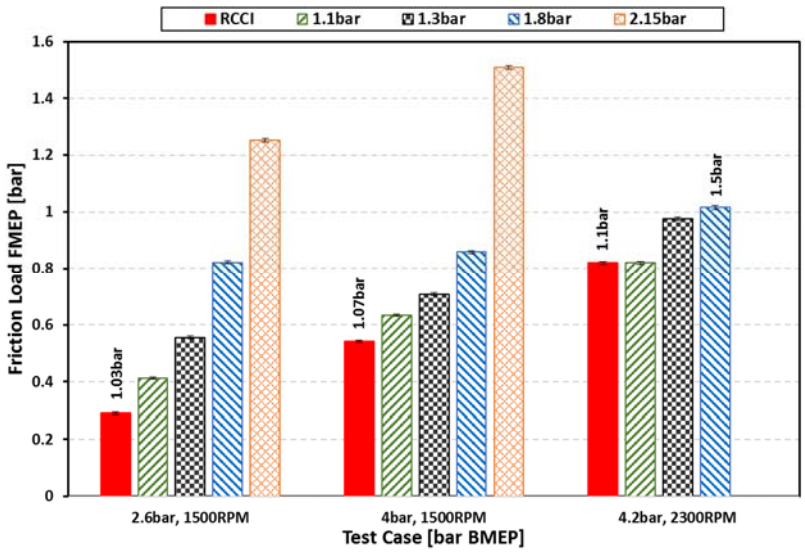

Figure 5-2 Friction load [bar] for different intake pressures as a function of operating points at the DI SOI timing of -40 dATDC

Regardless of the minor gains in efficiency at 1.1 bar boost pressure, the small increase in boost at these points is beneficial to the NOx numbers. They are decreased significantly [Figure 5-3] due reduced heat transfer losses, while only having small effects on HC and CO [Figure 5-4 and 5-5]. Higher boost levels, on the other hand, while only showing a substantial increase in HC at the high load/high speed case, display a significant increase in CO for all three test cases.

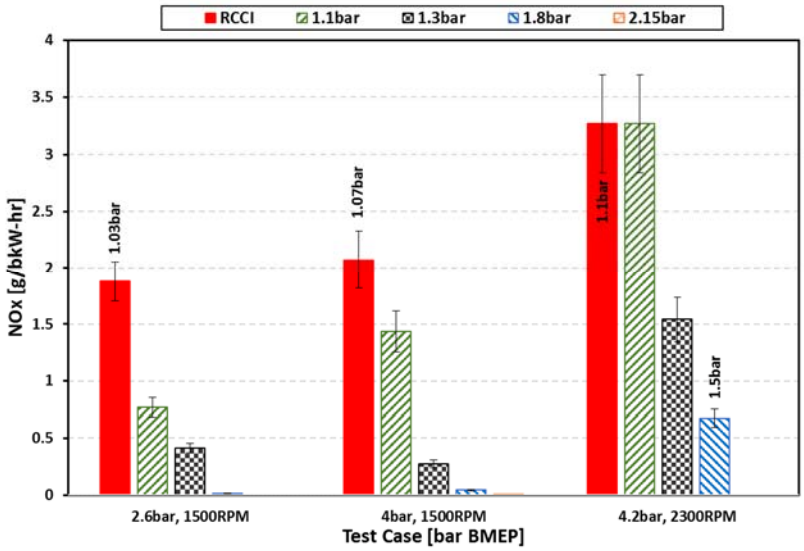

Figure 5-3 Nitric oxides emissions [g/bkW-hr] for different intake pressures as a function of operating points at the DI SOI timing of -40 dATDC

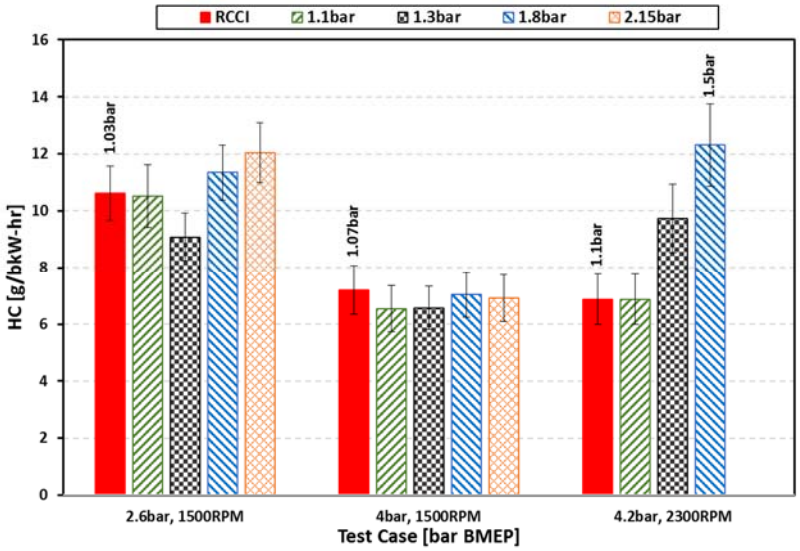

Figure 5-4 Hydrocarbon emissions [g/bkW-hr] for different intake pressures as a function of operating points at the DI SOI timing of -40 dATDC

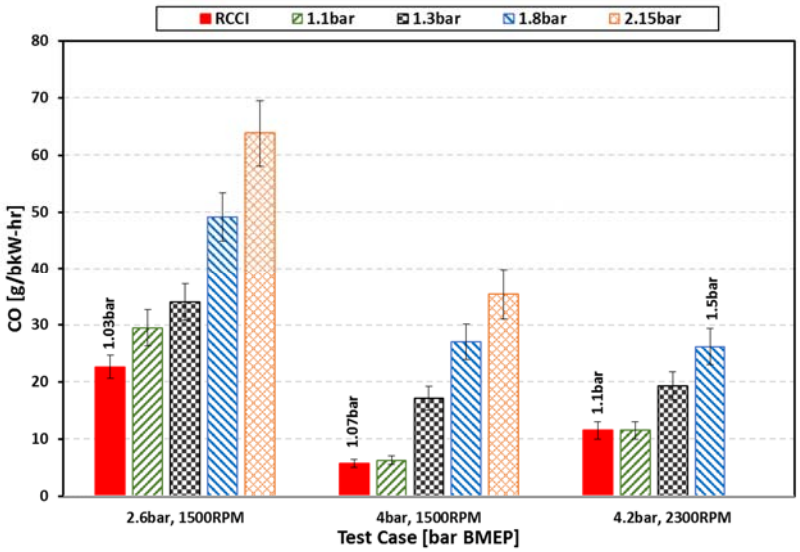

Figure 5-5 Carbon monoxide emissions [g/bkW-hr] for different intake pressures as a function of operating points at the DI SOI timing of -40 dATDC

Pressure Traces

In the following, the pressure traces and the heat release rates including the LTHR traces are presented for each of the three test cases, and a table, displaying the performance results for each of the intake pressure levels for each load point, is shown.

A first observation can be made when looking at the pressure traces for all cases, where the increase in boost leads to an increase in peak pressure levels. An increase in boost also increases the magnitude of LTHR and in addition the magnitude of the ITHR is also increased. Since CA50 was intended to be matched as close as possible for all boost levels, an increase in combustion duration and therefore also a reduction or flattening of the peak heat release levels [Figure 5-6, 5-7 and 5-8] can be observed. This is in direct correlation with the increase in PFI fraction [Table 5-1, 5-2 and 5-3], which was necessary to counteract the ignition advancement linked with an increase in boost.

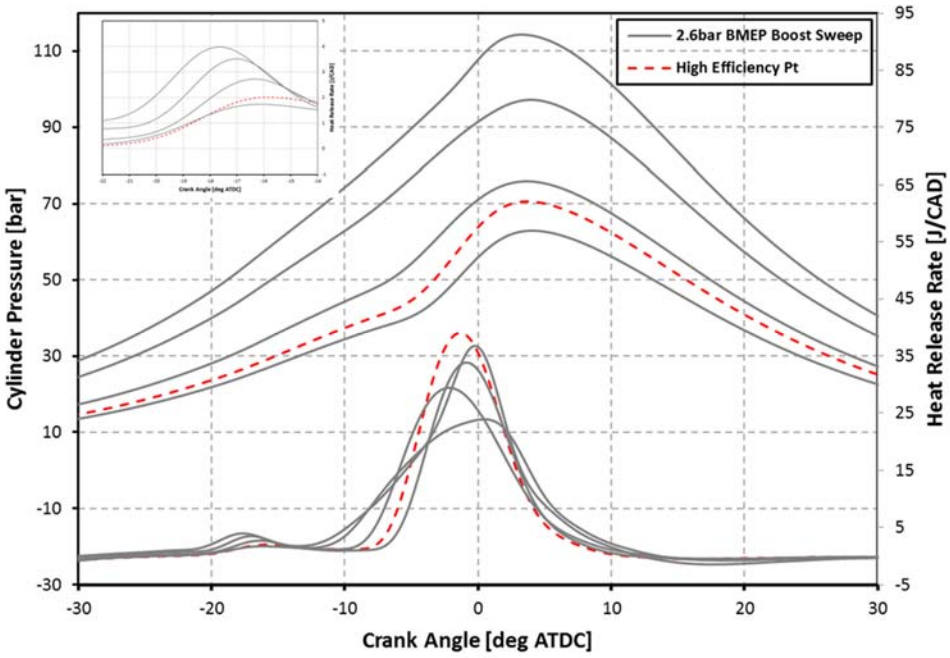

Figure 5-6 Cylinder Pressure [bar] and heat release rate [J/CAD] as a function of CAD for dieseline45 at 2.6bar BMEP, 1500 RPM and DI SOI timing of -40 dATDC

Table 5-1 Overview of performance and conditions for dieseline45 at 2.6bar BMEP, 1500 RPM and DI SOI timing of -40 dATDC

Intake Pressure [bar]	**RCCI/1.03**	**1.1**	**1.3**	**1.8**	**2.15**
Load BMEP [bar]	**2.6**				
Pedal Position [%]	14.3	15.1	15.7	18.7	21.5
DI Duration [ms]	0.631	0.597	0.584	0.454	0.349
PFI Duration [ms]	1.341	1.896	2.361	4.737	6.314
PFI Fraction [%]	16.5	25.1	29.8	54.2	65.2
Rail Pressure [bar]	500	500	500	495	500
Main SOI [deg. BTDC]	40	40	40	40	40
Intake Pressure [bar]	1.03	1.12	1.31	1.83	2.15
Intake Temp. [°C]	54	54	54	53	54
EGR [%]	0	0	0	0	0
MPRR [bar/deg.]	3.74	4.39	3.63	3.11	4.08
Peak Pressure [bar]	62.9	70.6	75.9	97.2	114.4
CA 50 [deg. ATDC]	-0.758	-1.179	-1.686	-1.119	-1.156
Comb Noise [dba]	80.4	81.6	77.7	74.3	80.3
BTE [%]	22.63	23.16	21.54	19.31	18.05
Comb. Eff. [%]	95.7	95.2	95.6	94.8	94.2

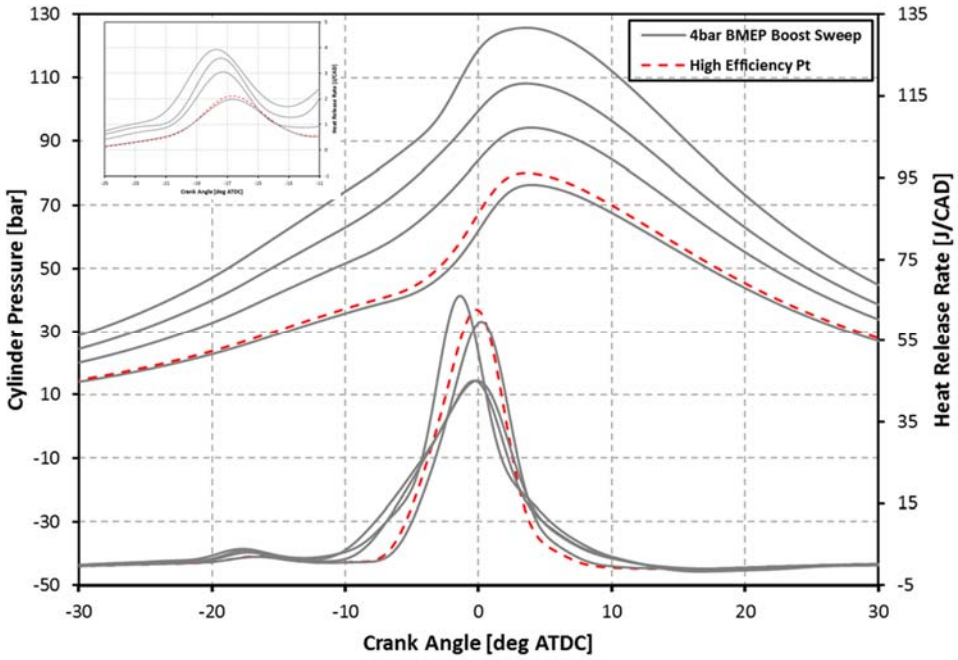

Figure 5-7 Cylinder Pressure [bar] and heat release rate [J/CAD] as a function of CAD for dieseline45 at 4bar BMEP, 1500 RPM and DI SOI timing of -40 dATDC

Table 5-2 Overview of performance and conditions for dieseline45 at 4bar BMEP, 1500 RPM and DI SOI timing of -40 dATDC

Intake Pressure [bar]	**RCCI/1.07**	**1.1**	**1.3**	**1.8**	**2.15**
Load BMEP [bar]	**4.0**				
Pedal Position [%]	18	18.7	20.2	22.2	25.5
DI Duration [ms]	0.524	0.523	0.458	0.427	0.294
PFI Duration [ms]	3.771	3.942	5.093	5.986	7.907
PFI Fraction [%]	43.5	44.9	55.6	61.6	74.6
Rail Pressure [bar]	510	505	500	500	495
Main SOI [deg. BTDC]	40	40	40	40	40
Intake Pressure [bar]	1.07	1.12	1.53	1.84	2.18
Intake Temp. [°C]	54	54	54	54	54
EGR [%]	0	0	0	0	0
MPRR [bar/deg.]	6.34	6.74	4.81	4.95	7.75
Peak Pressure [bar]	76.5	80.1	94.3	108.1	125.7
CA 50 [deg. ATDC]	-0.248	-0.573	-0.768	-1.156	-1.322
Comb Noise [dba]	86.8	87.1	81.4	81.9	87.6
BTE [%]	30.63	30.73	28.92	27.32	26.16
Comb. Eff. [%]	96.9	97.1	96.4	95.7	95.3

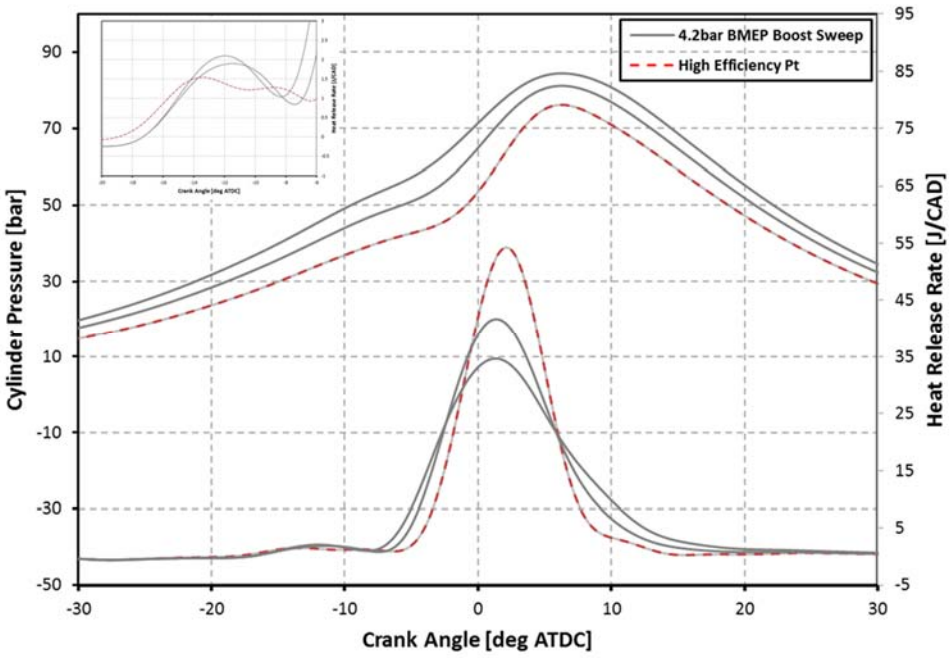

Figure 5-8 Cylinder Pressure [bar] and heat release rate [J/CAD] as a function of CAD for the dieseline45 RCCI case at 4.2bar BMEP, 2300 RPM and DI SOI timing of -40 dATDC

Table 5-3 Overview of performance and conditions for dieseline45 at 4.2bar BMEP, 2300 RPM and DI SOI timing of -40 dATDC

Intake Pressure [bar]	**RCCI/1.1**	**1.3**	**1.5**
Load BMEP [bar]	**4.2**		
Pedal Position [%]	29.6	30.2	31.2
DI Duration [ms]	0.545	0.537	0.501
PFI Duration [ms]	3.697	4.053	4.774
PFI Fraction [%]	46.5	49.3	56.1
Rail Pressure [bar]	501	500	500
Main SOI [deg. BTDC]	40	40	40
Intake Pressure [bar]	1.11	1.32	1.49
Intake Temp. [°C]	54	54	54
EGR [%]	0	0	0
MPRR [bar/deg.]	5.18	4.06	3.41
Peak Pressure [bar]	76.2	81.2	84.4
CA 50 [deg. ATDC]	2.207	2.04	2.371
Comb Noise [dba]	92.7	89.2	86.5
BTE [%]	31.99	30.82	30.07
Comb. Eff. [%]	96.4	94.8	93.4

5.2 Conclusions

The focus of this section of the study was to investigate the performance achieved by different boost levels in a multi-cylinder light-duty engine during steady-state RCCI operation using dieseline45. A comparison was made between an array of boost levels obtained by a newly installed intake set-up and previously reachable LTC/ RCCI levels of intake pressure using the stock turbocharger set-up. The tests were performed for a total of 3 test points at a DI SOI timings of -40 dATDC at previously determined CA50 values under otherwise matching operating conditions.

The three cases investigated are:

- 2.6 bar BMEP, 1,500 rev/min
- 4.0 bar BMEP, 1,500 rev/min
- 4.2 bar BMEP, 2,300 rev/min

All test cases showed acceptable levels of performance and expected trends.

It was shown that while high levels of boost decrease brake efficiencies due to increasing friction and pumping load losses, a small increase in boost can be beneficial. Improvements in brake thermal efficiency (BTE) were seen from the performance results for an intake pressure of 1.1 bar over the RCCI boost levels (1.03 bar and 1.07 bar). Note that, at the highest load point, the stock turbocharger was capable of reaching levels of 1.1 bar under RCCI operation.

BTE increased nominally by 1% at the 4.0 bar, 1,500 rev/min case up to 2.5% at the 2.6 bar, 1,500 rev/min case, resulting from an optimal balance between increased losses and improved combustion characteristics.

Combustion efficiencies and thus emission results for CO and HC were found to be increased with an increase in boost, while NOx emissions were reduced significantly even with only a small increase in boost. Note, the enhancement of the autoignition process and thus the advancement of

combustion phasing with an increase in boost required a significant increase in PFI fueling in order to match CA50 targets. Hence, the DI injection amounts were reduced and combustion temperatures are also expected to be reduced.

It was also observed that in general MPRR and combustion noise were reduced with an increase in boost and stayed under the self-imposed constraints of 10 bar/deg peak pressure rise rate and noise levels of 95 dB. Increasing boost pressure was shown to reduce peak heat release rate levels and widened the combustion duration.

Chapter 6 Comparing the Performance of Dieseline45 HCCI with RCCI Combustion Using Dieseline45

Experimental work is presented in this chapter, in which the performance of dieseline45 in a HCCI combustion regime is investigated. Following the work to determine optimal dieseline mixtures for RCCI operation, this study marks the next step towards the use of a pure single-fuel for RCCI combustion. In the first part, HCCI test results are compared to data obtained using both diesel and dieseline45, under a RCCI combustion strategy at a DI SOI timing of -40 dATDC, which provided the best overall BTE levels. This chapter also shows the results for pre-testing single-zone simulations that were carried out in order to determine feasibility. In the second part, the findings are further discussed and conclusions are drawn. Note that, additional material can be found in Appendix C.

6.1 Operating Conditions and Results

As mentioned above and also in more detail in chapter 3.6, two single-zone Cantera models were employed in connection in order to determine feasibility and achievability of HCCI combustion using Dieseline45 or any other dieseline blend.

Previously obtained performance results and maintained operating conditions for the reduced selection of test cases were used as input for intake valve closing (IVC) temperature and pressures as well as work output under matching efficiency and BMEP levels from the Cantera model. Table 6-1 and Table 6-2 show the conditions and the resulting outputs, respectively. In a second step the cycle simulation outputs were used within the HCCI simulation model. The results from Figure 6-1 show that dieseline45, very closely matches targeted CA50 locations for each of the three test cases (additional material in Appendix C). These results were then used in the engine to determine performance and emissions for HCCI operation using dieseline45.

Table 6-1 RCCI cycle simulation **i**nput conditions

Test case	**2.6 bar, 1500 RPM**	**4.0 bar, 1500 RPM**	**4.2 bar, 2300 RPM**
ULSD Fraction [%]	33.7	24.8	24.1
DI fuel [-]	n-heptane	n-heptane	n-heptane
Total PFI Fraction [%]	66.3	75.2	75.9
PFI fuel [-]	iso-octane	iso-octane	iso-octane
Fueling [g/inj]	0.013	0.01469	0.0149
Main SOI [deg. BTDC]	40	40	40
Injection Pressure DI [bar]	500	500	500
PFI SOI [deg. BTDC]	275	275	275
Injection Pressure PFI [bar]	2.75	2.75	2.75
Intake Pressure [bar]	1.115	1.115	1.112
Intake Temp. [°C]	54	54	54
Exhaust Pressure [bar]	1.266	1.261	1.238
Combustion Duration [CAD]	9.6	8.1	9.9
EGR [%]	0	0	0
BTE [%]	23.16	30.73	31.99

Table 6-2 Simulation outputs from RCCI cycle simulation

Test case	**2.6 bar, 1500 RPM**	**4.0 bar, 1500 RPM**	**4.2 bar, 2300 RPM**
IVC Temperature [°C]	404.8	393	400
IVC Pressure [bar]	1.382	1.376	1.384
Gross Work [J]	17.85	21.698	22.767
BTE [%]	22.48	30.2	31.45
BMEP [bar]	2.734	4.132	4.395

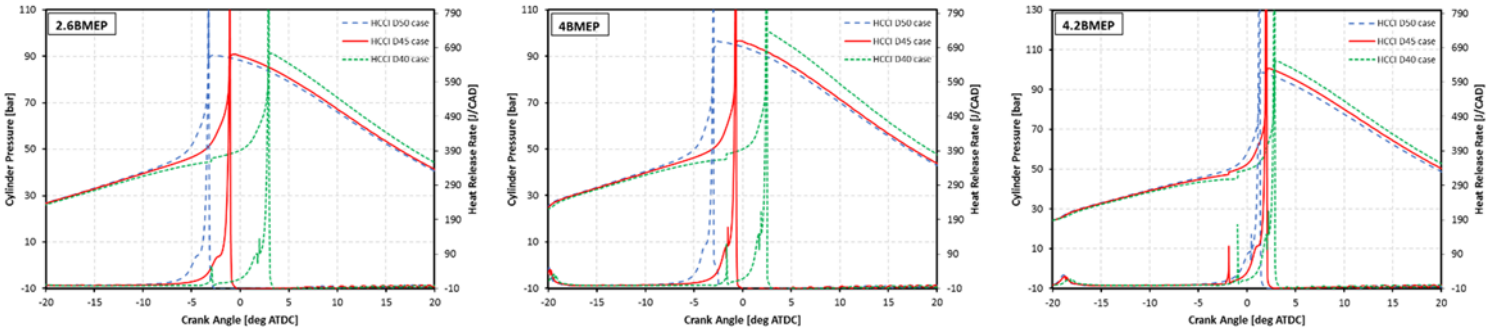

Figure 6-1 HCCI Simulation results for three test cases using different dieseline blends

The engine results show that in comparison to the RCCI combustion regime, HCCI is less efficient on a brake thermal basis [Figure 6-2]. This is due to the fact that, in order to reduce the MPRR to acceptable levels, the intake pressures had to be increased for all three cases, thus, increasing pumping work and friction work and as such increasing fueling rates to match load points. HCCI displays very aggressive combustion with high MPRR and high MHRR rates, that are significantly higher and at times more than double the values of diesel and dieseline RCCI [Figure 6-3 and 6-4]. Furthermore, the intake temperatures had to be raised to allow smoother and more stable combustion. This, in turn, further led to more violent combustion with high MHRR and peak HRR.

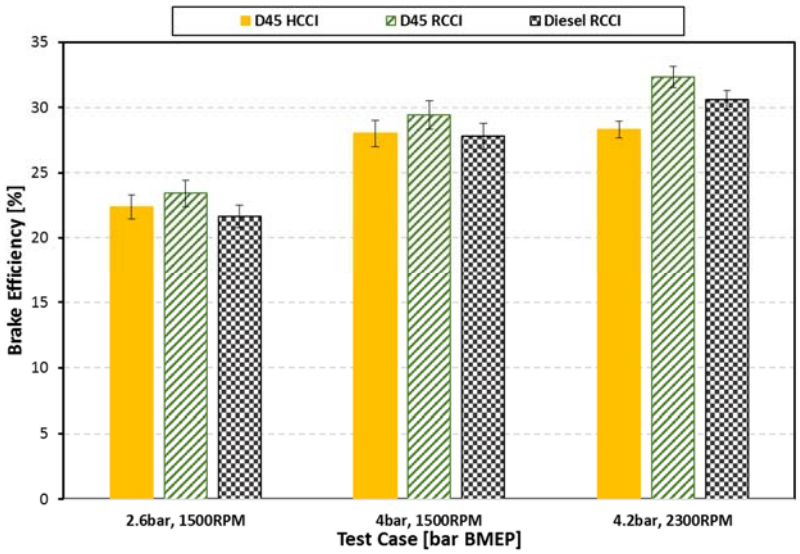

Figure 6-2 Brake efficiencies (%) for different combustion regimes as a function of operating points at the DI SOI timing of -40 dATDC

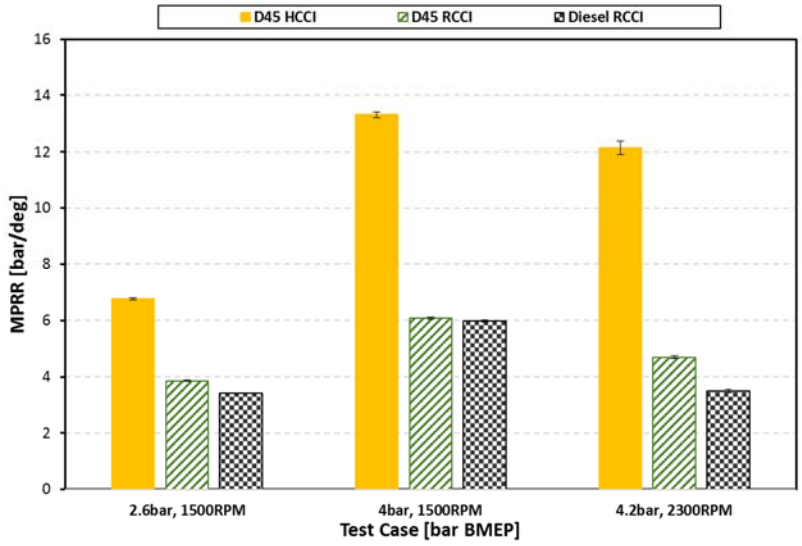

Figure 6-3 Maximum pressure rise rate [J/deg] for different combustion regimes as a function of operating points at the DI SOI timing of -40 dATDC

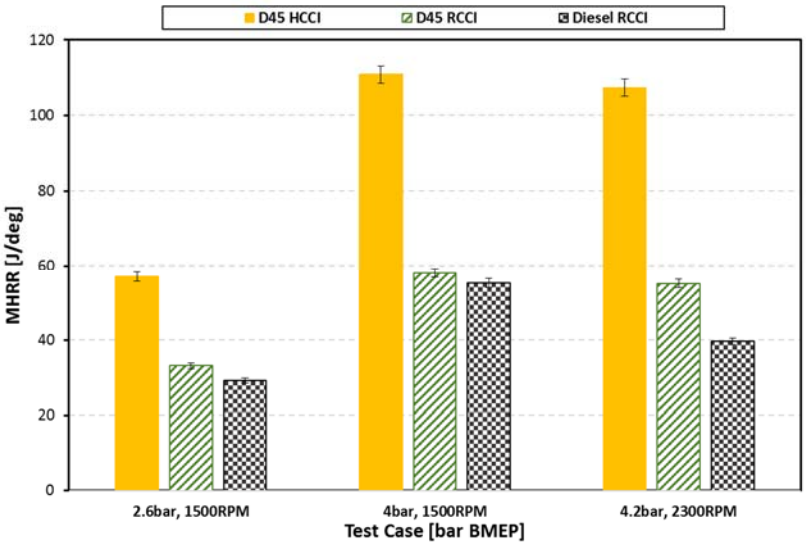

Figure 6-4 Maximum heat release rate [J/deg] for different combustion regimes as a function of operating points at the DI SOI timing of -40 dATDC

Nevertheless, due to the fully premixed combustion, the NOx emissions were very low, as expected [Figure 6-5]. However, the HC and CO emissions were almost twice the level for RCCI [Figure 6-6 and 6-7]. This increase is likely due to lower combustion temperatures stemming from the leaner mixtures especially for cases at 1,500 rev/min.

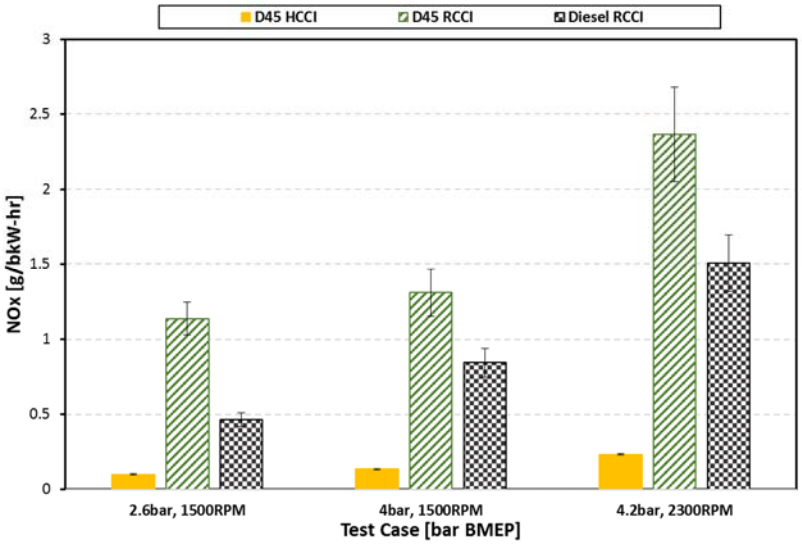

Figure 6-5 Nitric oxides emissions [g/bkW-hr] for different combustion regimes as a function of operating points at the DI SOI timing of -40 dATDC

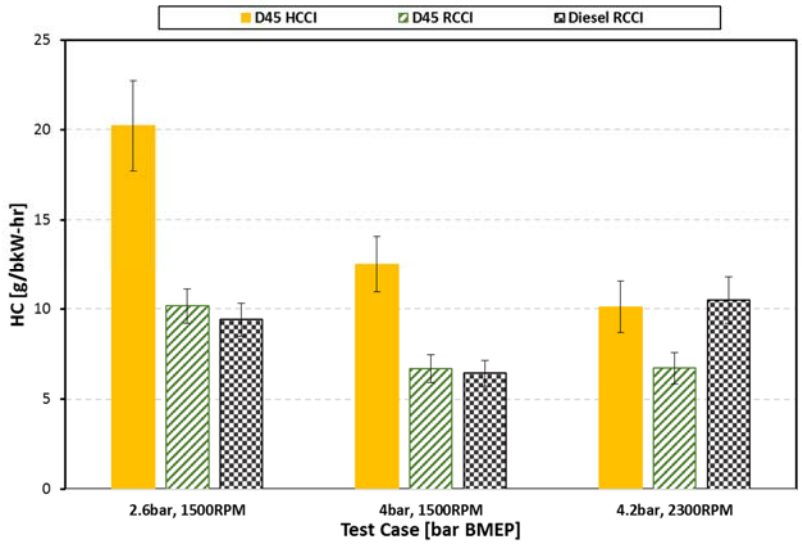

Figure 6-6 Hydrocarbon emissions [g/bkW-hr] for different combustion regimes as a function of operating points at the DI SOI timing of -40 dATDC

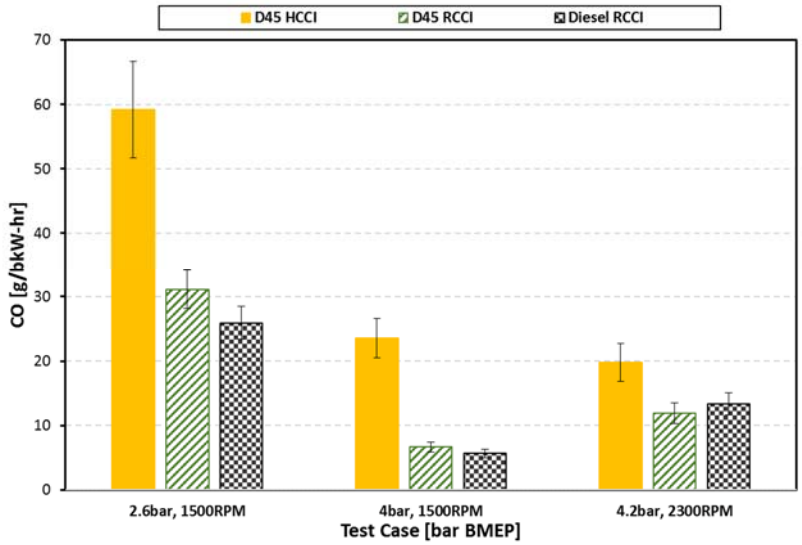

Figure 6-7 Carbon monoxide emissions [g/bkW-hr] for different combustion regimes as a function of operating points at the DI SOI timing of -40 dATDC

Pressure Traces

The pressure traces and the heat release rates including the LTHR traces during HCCI combustion are presented for each of the three test cases in Figure 6-8, 6-9 and 6-10. Note also that for comparison purposes, the diesel and dieseline RCCI cases are included. Furthermore, a table for each load point, displaying the performance results for the HCCI case and the two RCCI cases, is shown.

As mentioned previously, the intake pressures for the HCCI case are elevated and contribute to some extent to the increased peak pressure levels as well as to the LTHR, which is increased and advanced over the RCCI traces. In addition, the pressure traces display the typical rather abrupt on-set of combustion, where the pressure is almost constant for a short period of time in the TDC region before ignition takes place. Another observation can be made when looking at the HCCI HRR rates. As expected, they depict a very high peak and thus narrow distribution, falling in line with the very steep pressure traces that originate from simultaneous start of ignition throughout the cylinder. Along with elevated MPRR and MHRR, the noise levels are also

significantly increased over the RCCI cases, while combustion efficiencies are lower due to increased CO and HC emissions, as previously presented.

Note however, that CA50 values for dieseline45 HCCI closely match those of the RCCI cases and thus validate the finding from the simulation tools [Table 6-3, 6-4 and 6-5].

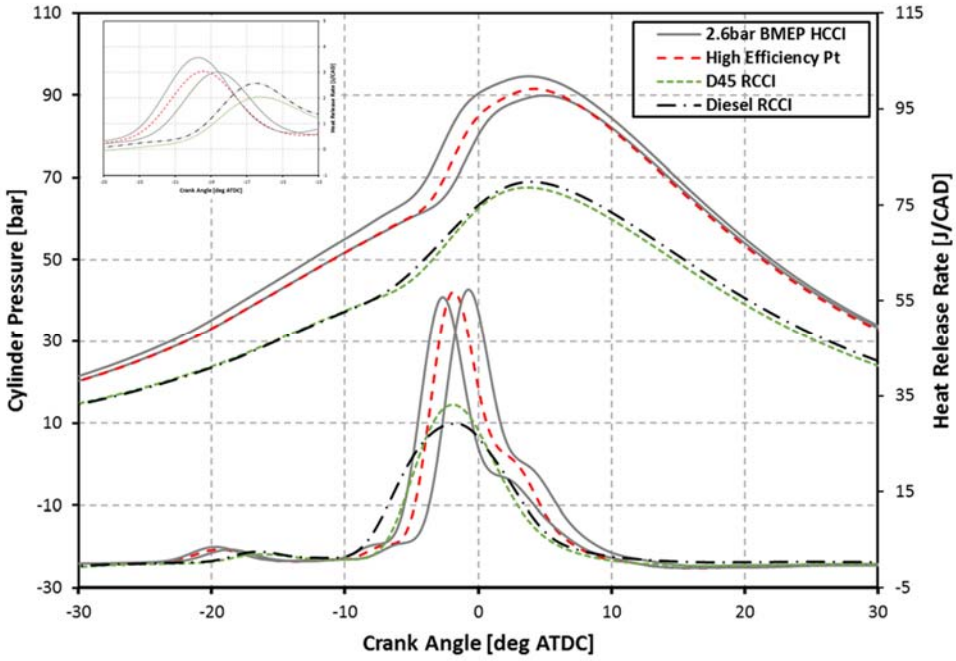

Figure 6-8 Cylinder Pressure [bar] and heat release rate [J/CAD] as a function of CAD for different combustion regimes at 2.6 bar BMEP, 1500 RPM and DI SOI timing of -40 dATDC

Table 6-3 Overview of performance and conditions for different combustion regimes at 2.6 bar BMEP, 1500 RPM and DI SOI timing of -40 dATDC

Fuel	**Dieseline45**		**Diesel**
Combustion Regime	**HCCI**	**RCCI**	**RCCI**
Pedal Position [%]	22.1	15.1	14.7
DI Duration [ms]	-	0.596	0.518
PFI Duration [ms]	7.084	1.733	2.763
PFI Fraction [%]	100	24.5	36.3
Rail Pressure [bar]	-	500	495
Main SOI [deg. BTDC]	-	40	40
Intake Pressure [bar]	1.50	1.11	1.12
Intake Temp. [°C]	65	54	54
EGR [%]	0	0	0
MPRR [bar/deg.]	6.77	3.86	3.42
CA 50 [deg. ATDC]	-1.203	-1.471	-1.529
Comb Noise [dba]	87.7	79.9	76.9
Phi [-]	0.311	0.342	0.391
BTE [%]	22.38	23.42	21.66
Comb. Eff. [%]	90.9	95.2	96.1

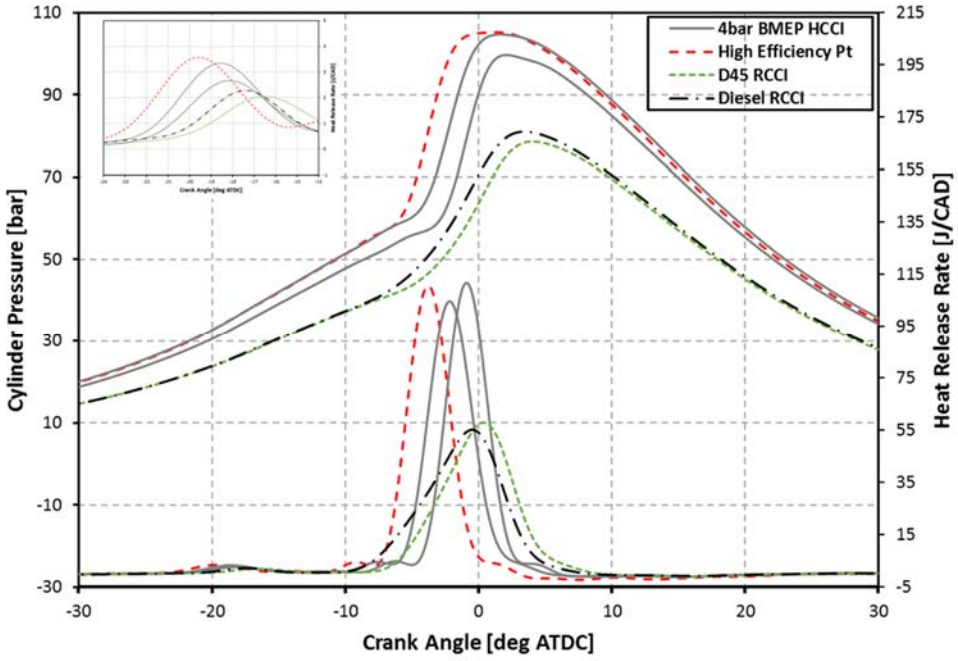

Figure 6-9 Cylinder Pressure [bar] and heat release rate [J/CAD] as a function of CAD for different combustion regimes at 4.0 bar BMEP, 1500 RPM and DI SOI timing of -40 dATDC

Table 6-4 Overview of performance and conditions for different combustion regimes at 4.0 bar BMEP, 1500 RPM and DI SOI timing of -40 dATDC

Fuel	**Dieseline45**		**Diesel**
Combustion Regime	**HCCI**	**RCCI**	**RCCI**
Pedal Position [%]	26.4	18.3	18.8
DI Duration [ms]	-	0.516	0.456
PFI Duration [ms]	8.438	3.983	4.769
PFI Fraction [%]	100	49.7	55.7
Rail Pressure [bar]	-	495	504
Main SOI [deg. BTDC]	-	40	40
Intake Pressure [bar]	1.49	1.11	1.12
Intake Temp. [°C]	65	55	55
EGR [%]	0	0	0
MPRR [bar/deg.]	13.31	6.09	5.99
CA 50 [deg. ATDC]	-3.843	-0.258	-1.151
Comb Noise [dba]	95.3	85.9	85.2
Phi [-]	0.378	0.401	0.462
BTE [%]	28.33	29.41	27.81
Comb. Eff. [%]	93.9	97.1	97.5

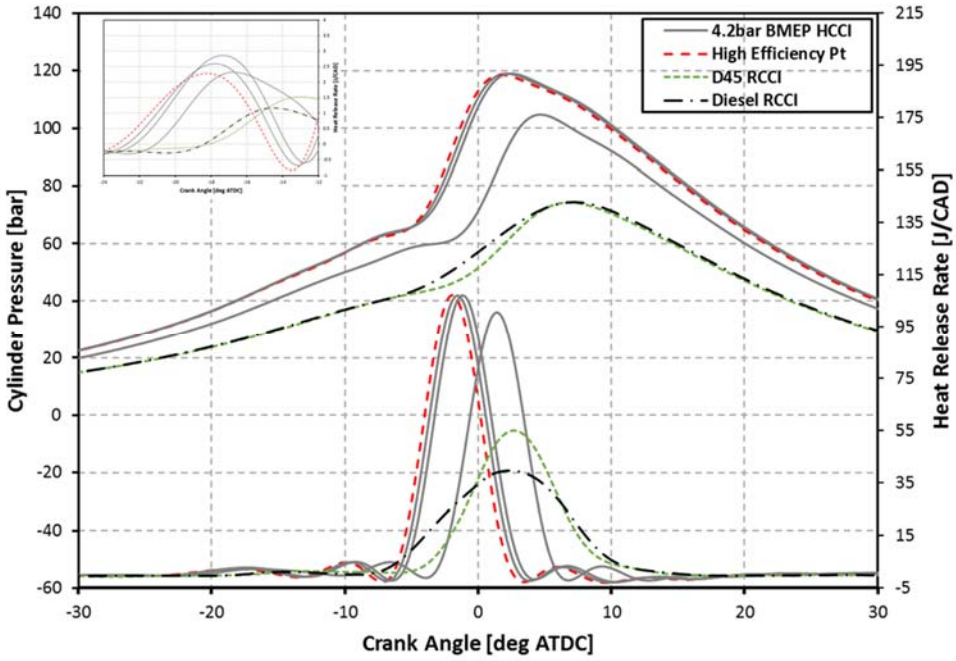

Figure 6-10 Cylinder Pressure [bar] and heat release rate [J/CAD] as a function of CAD for different combustion regimes at 4.2 bar BMEP, 2300 RPM and DI SOI timing of -40 dATDC

Table 6-5 Overview of performance and conditions for different combustion regimes at 4.2 bar BMEP, 2300 RPM and DI SOI timing of -40 dATDC

Fuel	**Dieseline45**		**Diesel**
Combustion Regime	**HCCI**	**RCCI**	**RCCI**
Pedal Position [%]	38.3	29.4	29.9
DI Duration [ms]	-	0.554	0.453
PFI Duration [ms]	9.211	3.656	4.954
PFI Fraction [%]	100	48.6	61.5
Rail Pressure [bar]	-	500	501
Main SOI [deg. BTDC]	-	40	40
Intake Pressure [bar]	1.65	1.11	1.11
Intake Temp. [°C]	65	55	55
EGR [%]	0	0	0
MPRR [bar/deg.]	12.15	4.69	3.49
CA 50 [deg. ATDC]	-2.018	2.709	2.306
Comb Noise [dba]	101.5	91.8	87.6
Phi [-]	0.481	0.422	0.438
BTE [%]	28.93	32.34	30.58
Comb. Eff. [%]	94.9	96.4	95.1

6.2 Conclusions

This section of the study focused on the investigation of performance for dieseline45 in a multi-cylinder light-duty engine during steady-state HCCI operation. HCCI results were compared to gasoline/diesel and gasoline/dieseline45 discussed in the previous chapters. The tests were performed for a total of 3 test points at a DI SOI timings of -40 dATDC and previously determined CA50 values were attempted to be matched.

The three cases investigated are:

- 2.6 bar BMEP, 1,500 rev/min
- 4.0 bar BMEP, 1,500 rev/min
- 4.2 bar BMEP, 2,300 rev/min

Prior to engine testing single-zone simulations were carried out to determine the feasibility and achievability. dieseline45 was found to be able to achieve target CA50 values under the existent conditions.

It was found that the intake temperature and intake pressure had to be raised significantly to achieve stable combustion. Thus, very early CA50 values were recorded for the high load HCCI cases, however combustion phasing was matched for the 2.6 bar case between the two strategies. The HCCI cases had an even bigger increase in MPRR due to increase in charge mass as well as enhancement of autoignition processes. Along with the high MPRR, high combustion noise levels above 95 dB were recorded due to the increased knocking tendency of HCCI.

Lower brake thermal efficiencies (BTE) were seen from the performance results of HCCI over the RCCI cases due to the required increased fueling rates. BTE decreased by 4.5% at the 2.6 bar, 1,500 rev/min case and by up to 10.5% at the 4.2 bar, 2,300 rev/min case.

Due to the increase in CO and HC emissions, combustion efficiencies for the HCCI cases were found to be increased, while NOx emissions were reduced significantly. This can partly be attributed to the increased boost, which provides a means of increasing fueling while maintaining a dilute charge to prevent NOx formation. The characteristics of HCCI combustion are capable of providing ultra-low NOx and particulate emissions.

Chapter 7 Performance of Single-Fuel RCCI Combustion Using Dieseline45

Following the investigation of dieseline45 HCCI, this chapter presents experimental work to investigate the performance of single-fuel RCCI operation at a DI SOI timing of -40 dATDC for the three test cases. Results for steady-state operation using dieseline45 for both the PFI and DI injected fuel, are shown and compared to gasoline/diesel and gasoline/dieseline45 cases. Although this approach is very similar to PFS combustion, the present work uses a very low octane number fuel. The previously explored operating conditions and individual CA50 targets were kept in place for this section. and additional material can be found in Appendix C.

7.1 Operating Conditions and Results

The ULSD levels of the previous RCCI tests reached levels of about 20% and were necessary because of the low reactivity of the EEE gasoline PFI fuel. The results from the previous chapter, where dieseline45 was proven to be feasible as a PFI fuel, this part of the study marks the final step of investigation for single-fuel RCCI operation.

In Figure 7-1, the single fuel approach shows improved brake thermal efficiencies over the diesel RCCI case for all three test points. In comparison to the dieseline45/gasoline RCCI case, the efficiency gains are rather significant for the low load case. With an increase in load this advantage is diminished and at the 4.2bar BMEP, 2300 RPM test point a slightly lower efficiency is recorded for the single-fuel RCCI case.

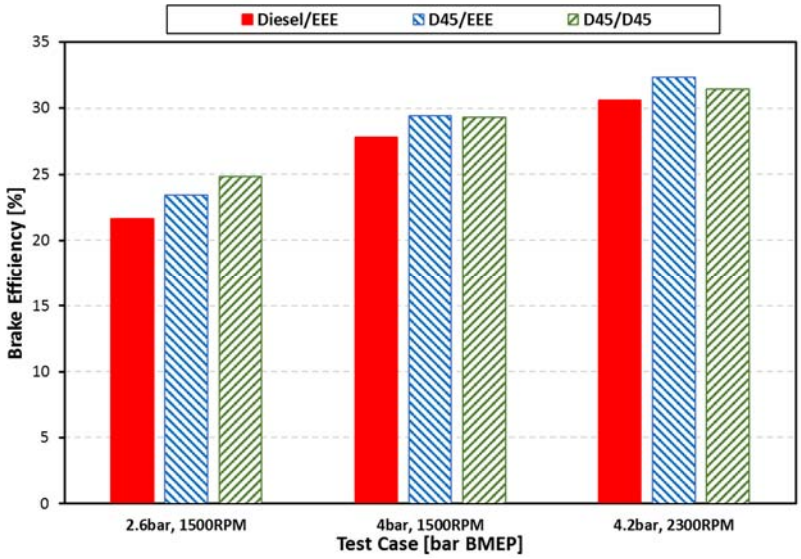

Figure 7-1 Brake efficiencies [%] for as a function of operating points at the DI SOI timing of -40 dATDC

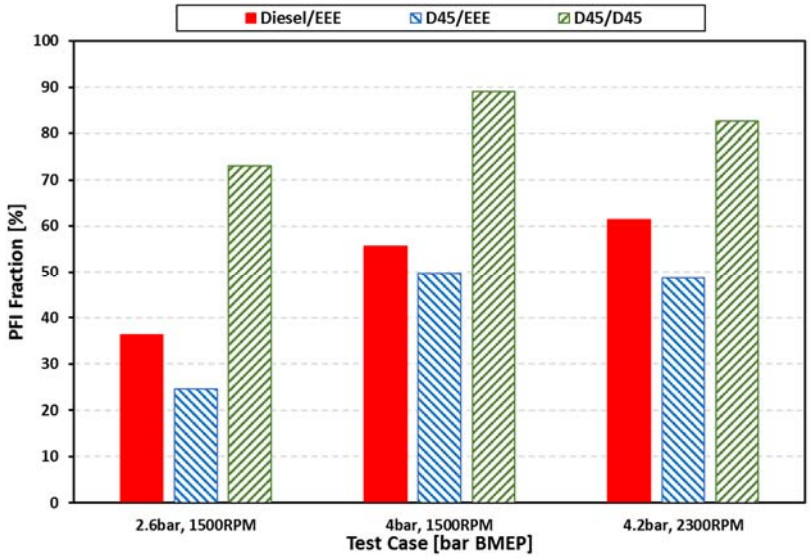

Figure 7-2 Maximum pressure rise rate [J/deg] for different combustion regimes as a function of operating points at the DI SOI timing of -40 dATDC

The increase in reactivity of the PFI fuel also allows for a much higher PFI fraction [Figure 7-2], and as result almost completely eliminates the NOx emissions [Figure 7-3]. This is due to the reduced DI injection durations and with that reduced extent of rich regions. In addition, the heat

transfer losses are reduced and therefore lower combustion temperatures can be expected. Note, that also the trends of increasing NOx with increasing load.

With a reduction in combustion temperatures, HC and CO emissions are increased above the levels for diesel/gasoline RCCI and dieseline45/gasoline RCCI [Figure 7-4 and 7-5], thus leading to reduced combustion efficiencies for all 3 test cases [Table 7-1].

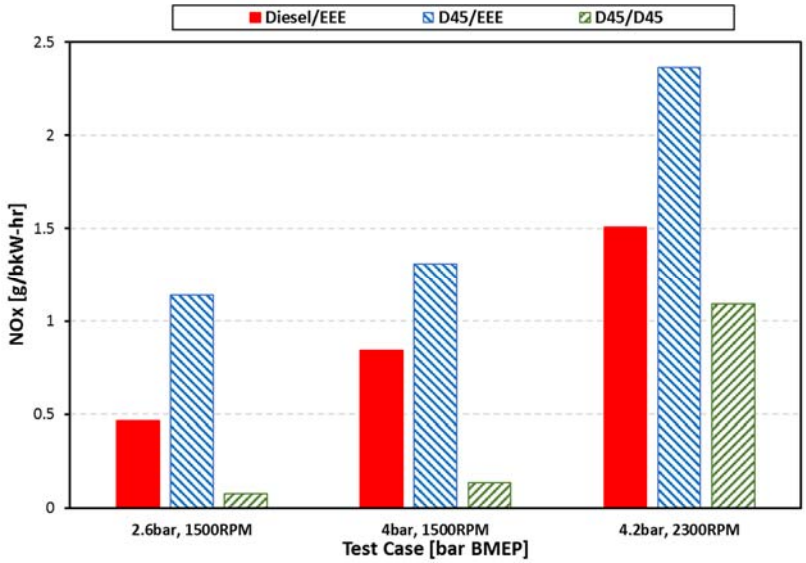

Figure 7-3 Nitric oxides emissions [g/bkW-hr] for different combustion regimes as a function of operating points at the DI SOI timing of -40 dATDC

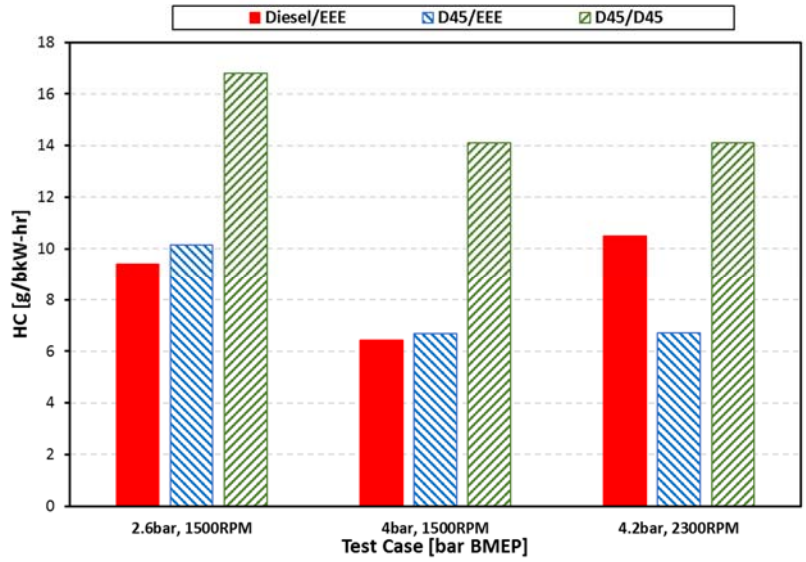

Figure 7-4 Hydrocarbon emissions [g/bkW-hr] for different combustion regimes as a function of operating points at the DI SOI timing of -40 dATDC

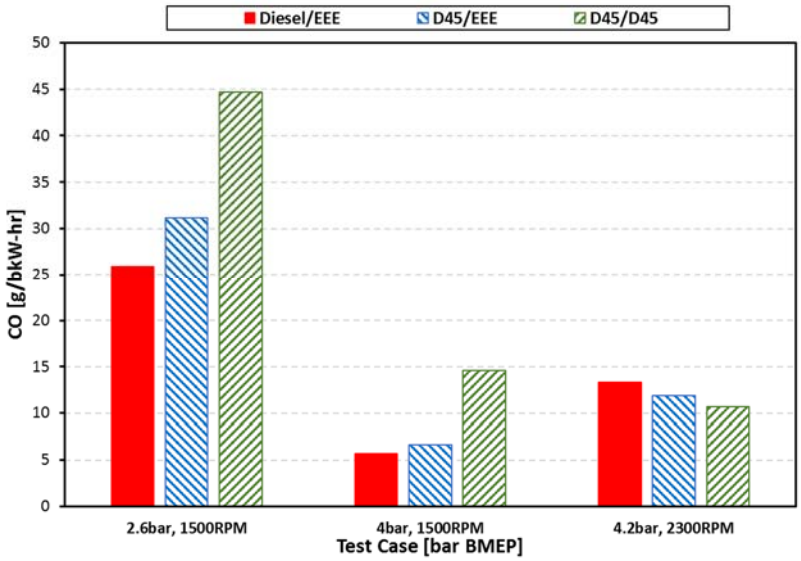

Figure 7-5 Carbon monoxide emissions [g/bkW-hr] for as a function of operating points at the DI SOI timing of -40 dATDC

Pressure Traces

At the low load point, the cylinder pressures for all three RCCI cases are identical with only small differences in the overall heat release rates and the LTHR trends [Figure 7-6]. At the higher load points, with further increased PFI fractions and thus a higher quantity of premixed fuel, the peak levels for the heat release rates for the single-fuel approach increase, and therefore the combustion duration is shortened. As a result, a more simultaneous onset of combustion throughout the combustion chamber is recorded and the MPRR are slightly increased as well [Figure 7-7 and 7-8].

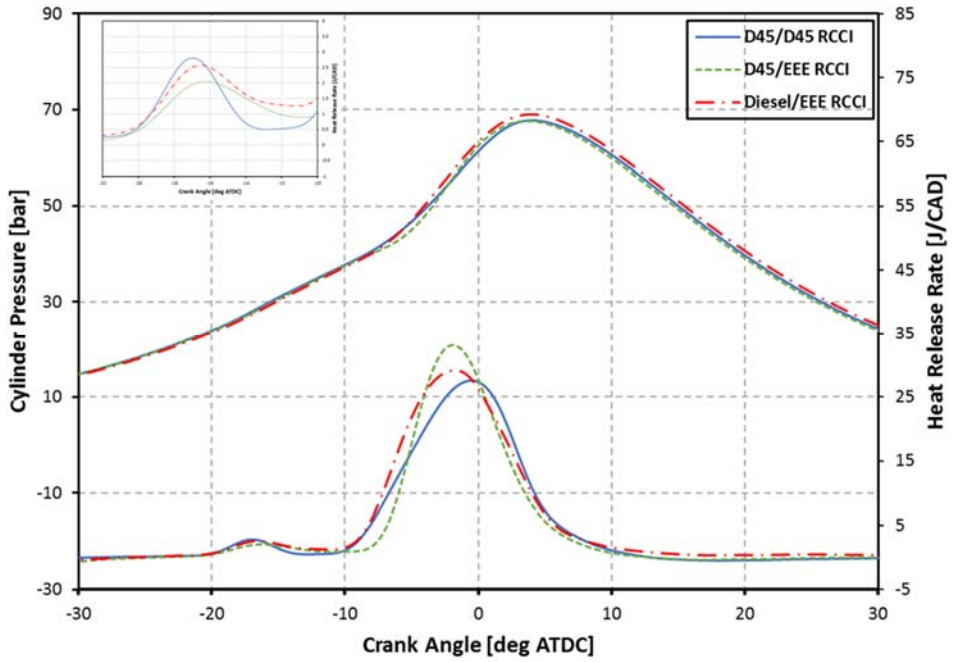

Figure 7-6 Cylinder Pressure [bar] and heat release rate [J/CAD] as a function of CAD for at 2.6 bar BMEP, 1500 RPM and DI SOI timing of -40 dATDC

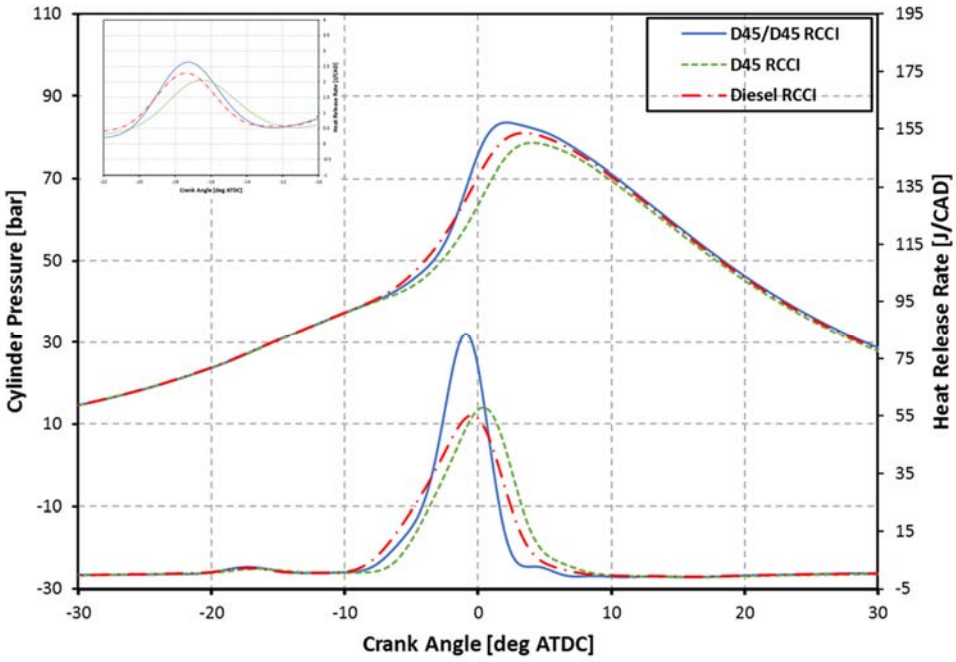

Figure 7-7 Cylinder Pressure [bar] and heat release rate [J/CAD] as a function of CAD for different combustion regimes at 4.0 bar BMEP, 1500 RPM and DI SOI timing of -40 dATDC

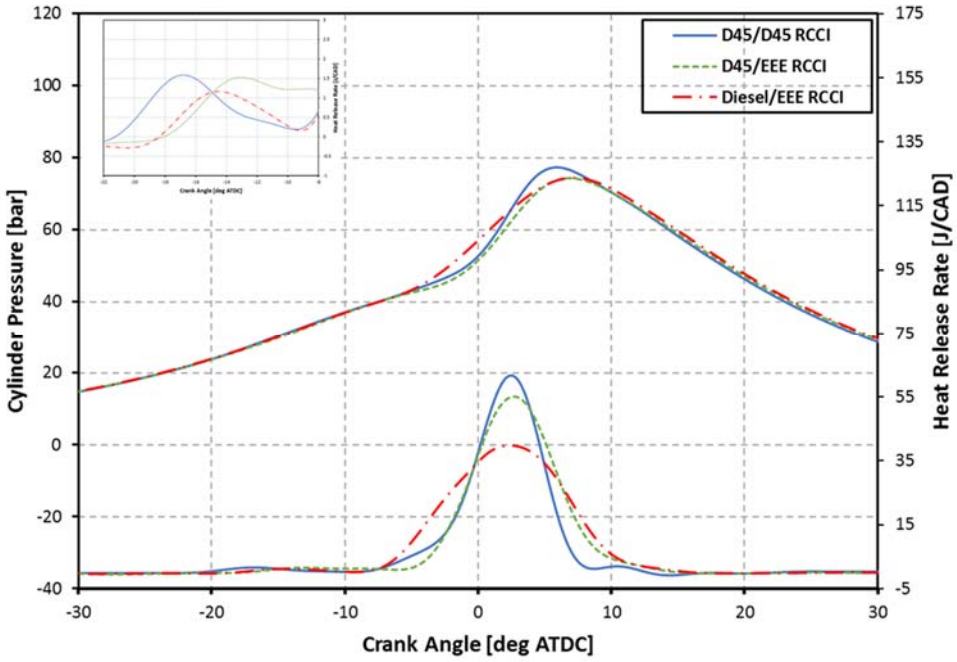

Figure 7-8 Cylinder Pressure [bar] and heat release rate [J/CAD] as a function of CAD for different combustion regimes at 4.2 bar BMEP, 2300 RPM and DI SOI timing of -40 dATDC

Table 7-1 lists the operating conditions and performance results for the single-fuel RCCI cases. Note that the operating conditions were matched along with the optimal CA50 values obtained previously. This highlights the substantial increase in PFI durations and PFI fractions, and the increased MPRR associated with single-fuel RCCI operation.

Table 7-1 Overview of performance and conditions for D45/D45 RCCI combustion at DI SOI timing of -40 dATDC

Dieseline45/Dieseline45			
BMEP Load [bar]	2.6	4.0	4.2
Speed [RPM]	1500	1500	2300
Pedal Position [%]	18.7	24.9	32.7
DI Duration [ms]	0.469	0.367	0.429
PFI Duration [ms]	4.259	6.984	6.351
PFI Fraction [%]	73.1	89.1	82.7
Rail Pressure [bar]	503	501	500
Main SOI [deg. BTDC]	40	40	40
Intake Pressure [bar]	1.1	1.1	1.1
Intake Temp. [°C]	55	55	55
EGR [%]	0	0	0
MPRR [bar/deg.]	3.08	9.63	5.91
CA 50 [deg. ATDC]	-1.105	-1.238	2.148
Comb Noise [dba]	76.6	92.5	94.9
Phi [-]	0.268	0.372	0.404
BTE [%]	24.83	29.33	31. 46
Comb. Eff. [%]	91.9	93.9	93.9

7.2 Conclusions

This section of the study focused on the evaluation of single-fuel RCCI or PFS operation in the multi-cylinder light-duty engine during steady-state conditions. A comparison was made between dieseline45 used as the PFI as well as the DI fuel, and gasoline/diesel and gasoline/dieseline45 RCCI operation. 3 test points at a DI SOI timings of -40 dATDC at previously determined CA50 values under otherwise matching operating conditions were performed.

The three cases investigated are:

- 2.6 bar BMEP, 1,500 rev/min
- 4.0 bar BMEP, 1,500 rev/min
- 4.2 bar BMEP, 2,300 rev/min

It was shown that it is possible to operate the MCE in RCCI mode using a single fuel at CA50 values matching the target CA50 values. Improvements in brake thermal efficiency (BTE) at the

low load points with lowered heat transfer losses were seen across the three test points from the performance results. BTE increased nominally by 6% at the 2.6 bar, 1,500 rev/min case over the gasoline/diesel and gasoline/dieseline45 cases, but at 4.0 bar, 1,500 rev/min slightly lower in comparison to gasoline/dieseline45, yet showed an increase over the gasoline/diesel case of up to 5.5%.

The use of higher reactive PFI fuel caused on advancement of combustion phasing and thus required a significant increase in PFI fueling in order to match CA50 targets. Hence, the DI injection durations were shortened and combustion temperatures are thus expected to be reduced.

However, emissions of CO and HC were increased for the single-fuel dieseline approach. A significant increase was recorded especially for HC. NOx emissions, on the other hand, were majorly decreased due to the shorter DI injection durations leading to a more dilute mixture.

It was also observed that in general MPRR and combustion noise were reduced for the single-fuel approach and stayed under the self-imposed constraints of 10 bar/deg peak pressure rise rate and noise levels of 95 dB. It should be pointed out that the pressure traces were identical for all the fuel combinations, while dieseline45/dieseline45 showed increased levels of HRR and shorter combustion durations.

Chapter 8 Performance of Transient RCCI Combustion Using Dieseline45

This chapter presents experimental work to examine the transient performance of dieseline45 as the high reactivity fuel for RCCI combustion in the light-duty MCE diesel engine at a DI SOI timing of -40 dATDC for fuel combination investigated in the previous chapter. The test conditions are presented and performance results of gasoline/dieseline45 and dieseline45/dieseline45 are shown and compared to results of gasoline/diesel RCCI combustion. Transient load steps were carried out in an upload and download scenario between 2.6 bar BMEP and 4 bar BMEP at a constant engine speed of 1,500 rev/min, and additional material is presented in Appendix D.

8.1 Operating Conditions and Results

In order to acquire comparable results for the 3 different fuel combinations under RCCI operation, the experimental conditions were matched as closely as possible. Figure 8-1, Figure 8-2 and Figure 8-3 show the run conditions during the step load change for the upload and download cases. All other relevant parameters, such as injection durations, total fueling, emissions, etc., are presented in the same format. Note also that all data is again presented as an ensemble average over a minimum of three complete data sets and all figures illustrate appropriate error calculations (95% CI).

The rail pressure was held constant at 500 bar for all 3 cases throughout the step change [Figure 8-1] in order to simplify calibration, but it showed small unexpected instabilities throughout the transient period, especially for the upload case. This, however, did not seem to affect the overall emissions and performance results. It should be noted again that adjustments had to be made to the common rail system for operation with gasoline/dieseline45 and dieseline45/dieseline45 in order to be able to pressurize the rail. The supply pressure was elevated

from 30 psi (200kPa) to approximately 45 psi (300kPa) to prevent the fuel from experiencing cavitation. This increased supply pressure was also employed for the gasoline/diesel case for consistency.

The temperature and pressure levels were matched between the cases and aligned with the previously obtained levels for steady-state operation. Variations in the intake pressure driven by the slow stock turbocharger response (seen in previous studies) could be avoided with the present customized intake system. All fuel combinations utilized a single DI injection strategy with a DI SOI timing of -40 dATDC

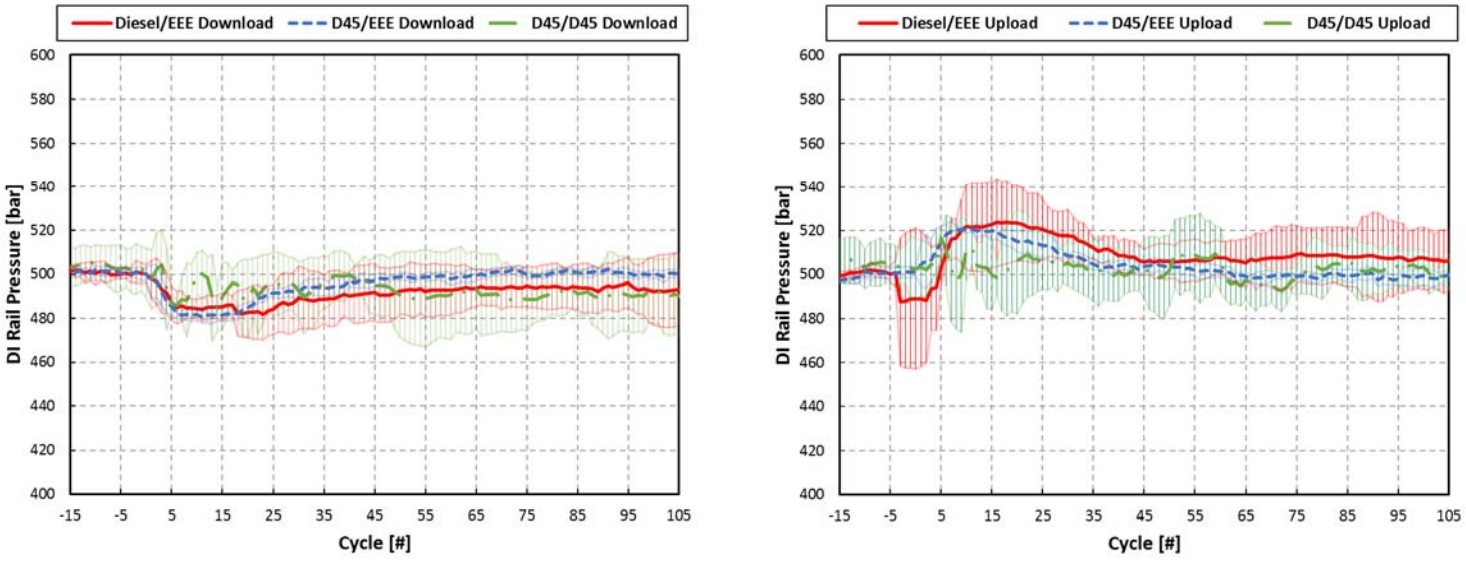

Figure 8-1 Rail pressure [bar] for the download and upload cases; 95% confidence interval is illustrated by the shaded area

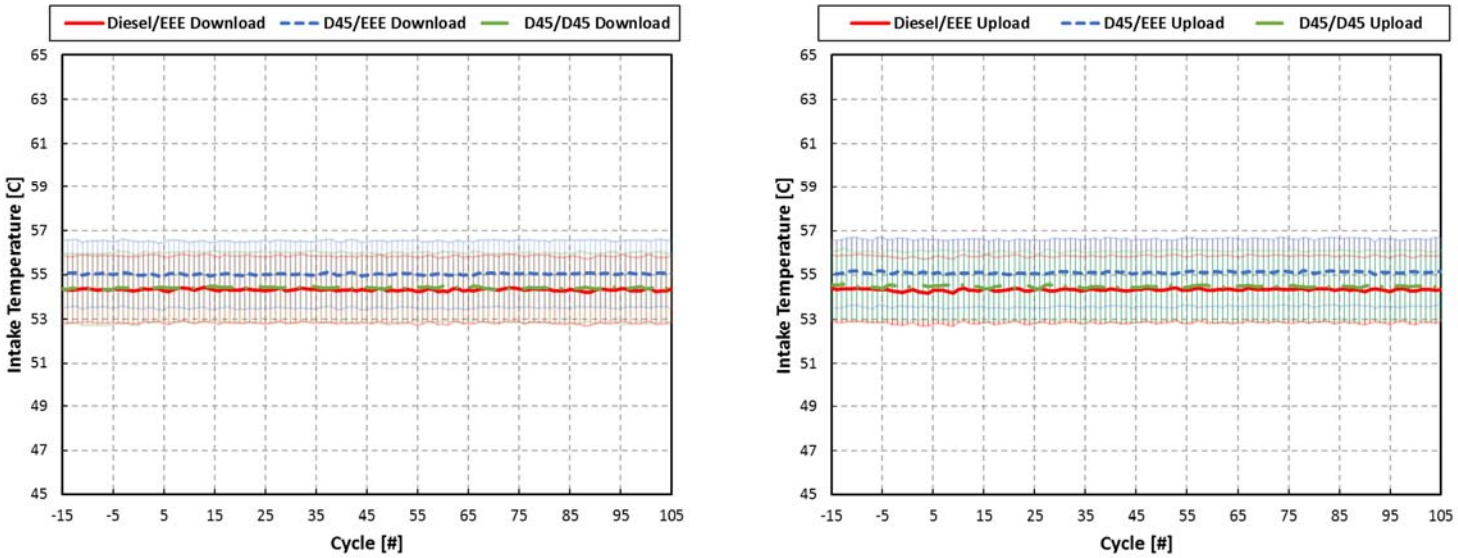

Figure 8-2 Intake manifold temperature [°C] for the download and upload cases; 95% confidence interval is illustrated by the shaded area

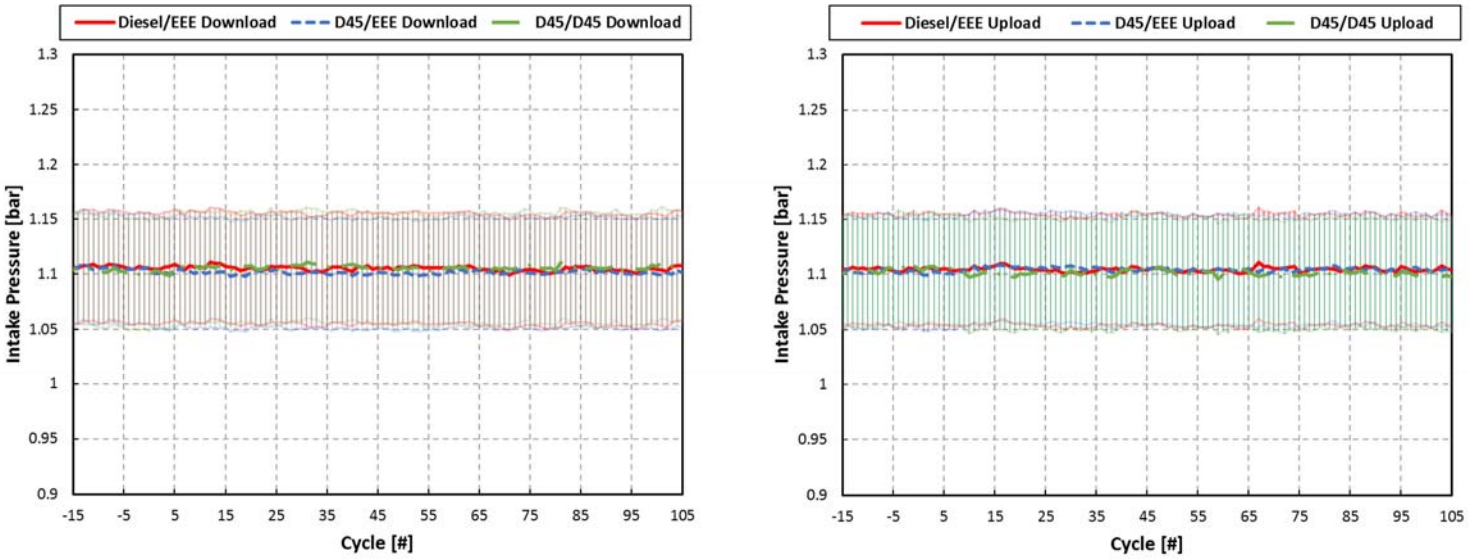

Figure 8-3 Intake manifold pressure [bar] for the download and upload cases; 95% confidence interval is illustrated by the shaded area

The engine was operated with a tip-in pedal command to achieve a transient load change from 2.6 to 4.0 bar BMEP at 1,500 rev/min following the steady-state calibration values of the 2D tables. Figure 8-4 shows the BMEP step change for both the upload and the download case as a function

of engine cycle number for the different fuel combination. Note, that for the upload and download case of the single-fuel approach, the load response is much slower, only reaching the targeted load point about 80 cycles after the other two cases. This can be related to the significantly higher PFI fraction and therefore increased wall wetting effects, as is known to influence port-injected SI engines. Work by Hanson [44] and Gross et al. [50] showed this phenomenon, and various control strategies have been developed [85, 86] to account for those interactions. However, as mentioned before, the current work did not employ the Drivven next-cycle controller or other advanced port-effect control strategies. Gasoline/dieseline45 on the other hand shows great alignment with the gasoline/diesel case, with both displaying a short and direct increase and decrease in load. This demonstrates the fueling effects also when matching air intake and fuel system responses.

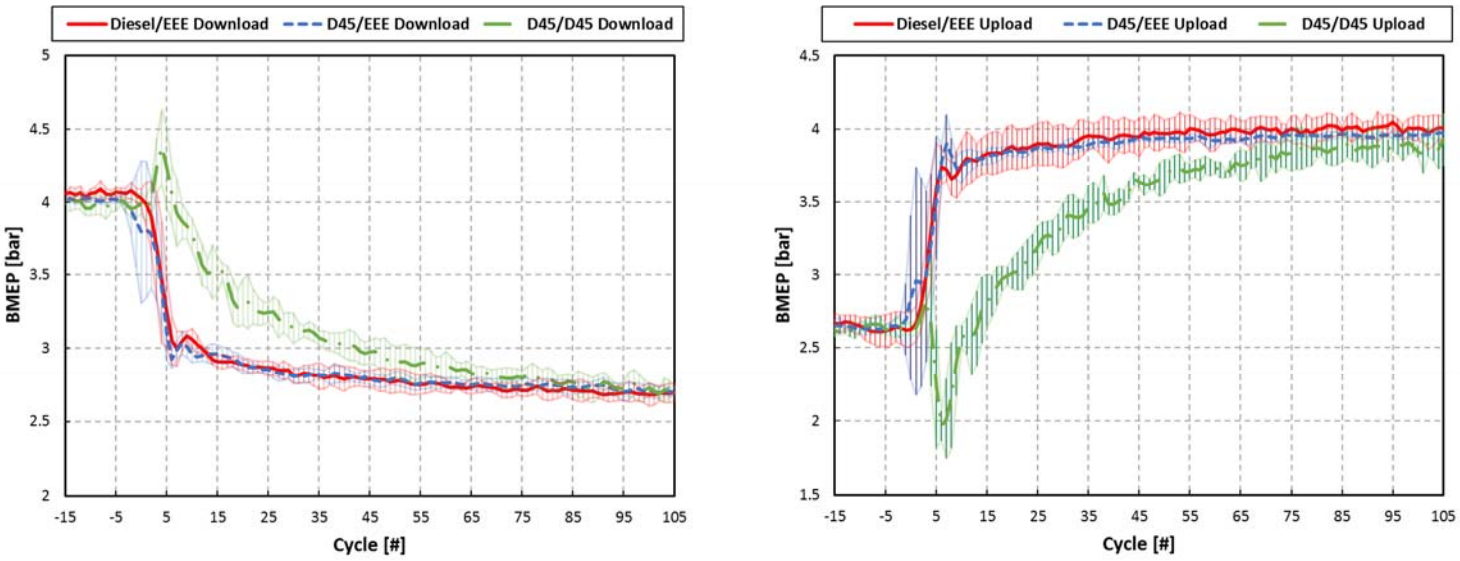

Figure 8-4 BMEP [bar] for the download and upload cases; 95% confidence interval is illustrated by the shaded area

Figure 8-5 compares the air-system performance. As discussed, the modified intake system set up allowed the drawbacks of the stock turbocharger to be overcome. The results were stable throughout the transient. Minor fluctuations can be seen for the MAF, which is likely to be caused

by the control mechanism of the proportional pressure valve. In general, the MAF values are highest for the dieseline45/dieseline45 case and lowest for the gasoline/dieseline45 case but without significant differences in comparison to the gasoline/diesel case.

The leaner equivalence ratios seen for the low load case of the download transient stem from the pedal command adjustments that were made during testing. A decreased value was commanded in order counteract fuel accumulation and thus allow faster response. The same strategy was applied for the upload case, but with less success.

Overall, stable combustion was maintained and transient air system effects were minimized. Hence, the mean values are stable and the associated confidence intervals are within acceptable levels.

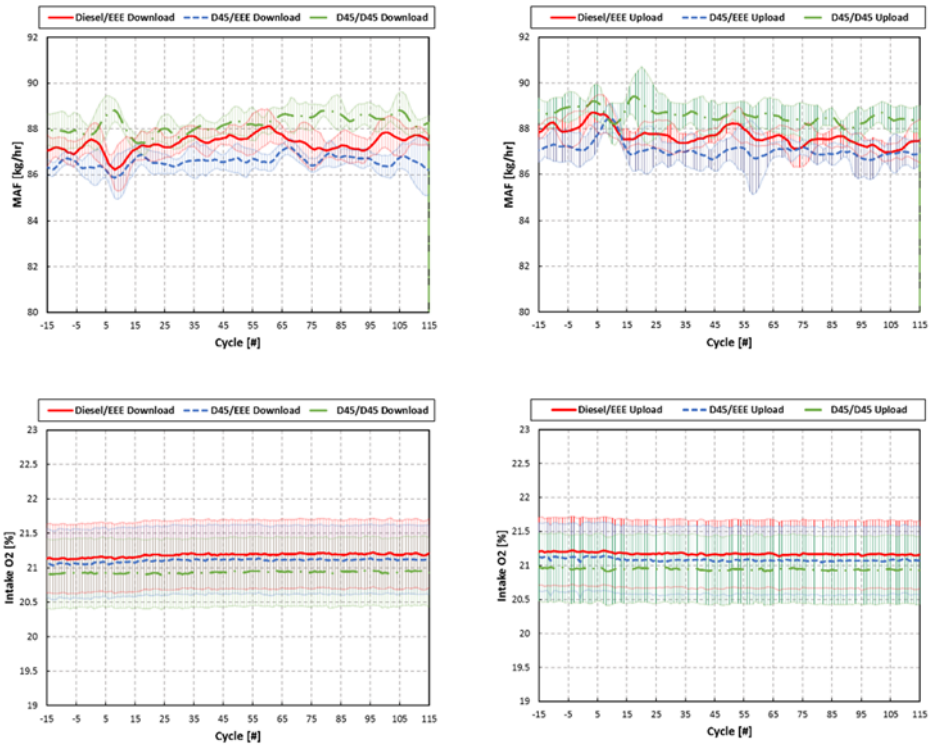

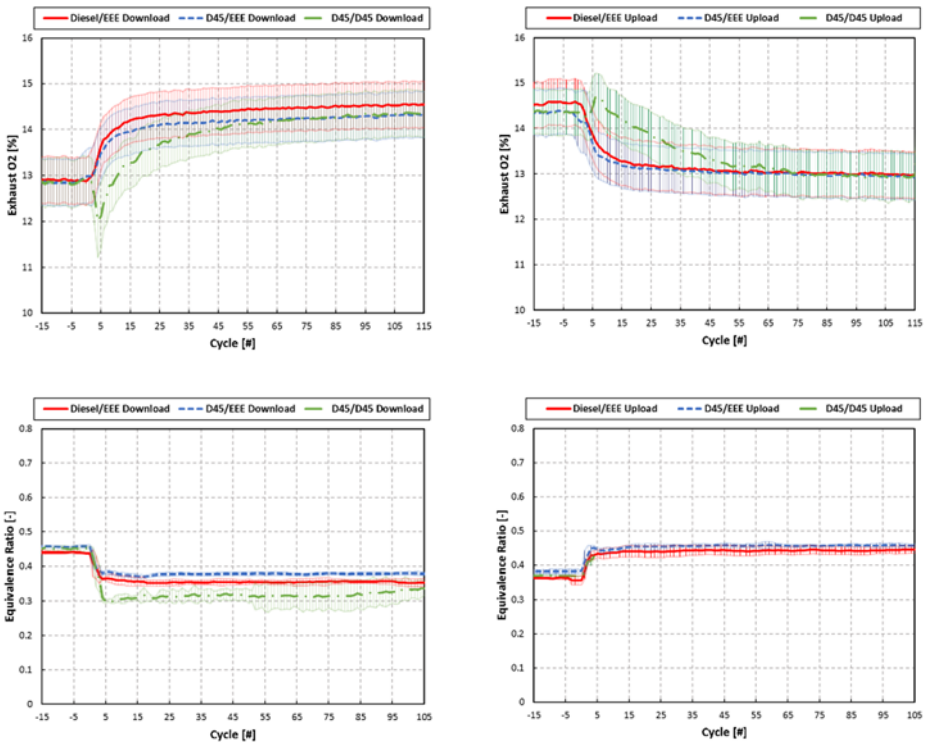

Figure 8-5 Air system response for the download and upload cases; 95% confidence interval is illustrated by the shaded area

Figure 8-6 shows the fueling commands of the down- and upload transient cases of all 3 fuel combinations. While the fueling of dieseline45/dieseline45 is reduced at the low load point for the download case due to the above explained adjustments, the use of dieseline45 as a DI fuel overall required slightly higher fueling rates during the transient tests. In order to match the CA50 values, and thereby compensate for the lower reactivity of the direct injected dieseline45, the main durations for gasoline/dieseline45 were increased, hence reducing the PFI duration and PFI fraction. The single-fuel case, on the other hand, allowed for increased PFI fractions due to the increased reactivity of the port-fuel injected dieseline45, thus reducing the DI injection durations below levels of gasoline/diesel RCCI. Increased confidence intervals for the upload case are recorded due to the aforementioned delay in load, which effects the torque-based table calibration and therefore the system commands.

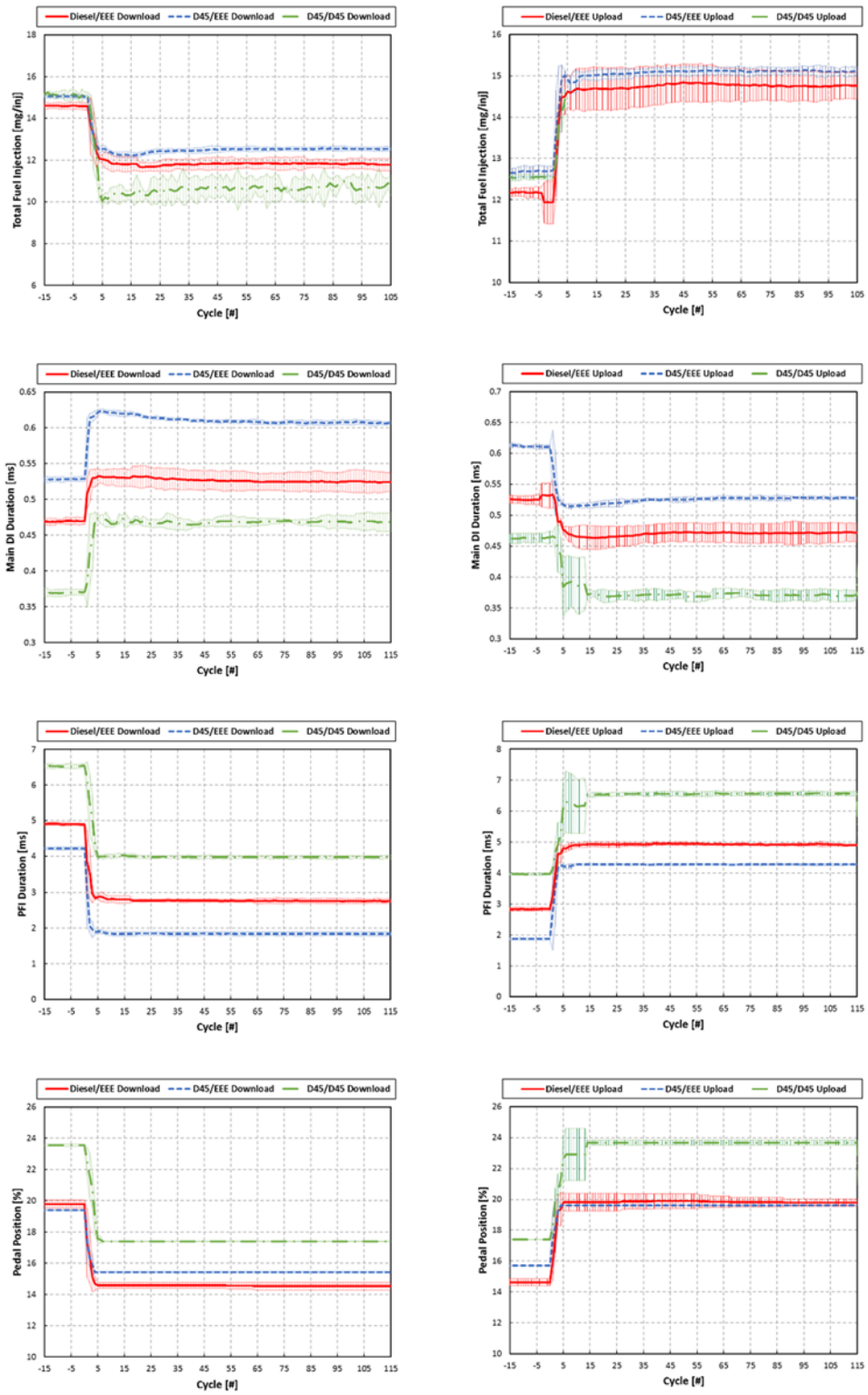

Figure 8-6 Fueling commands for the download and upload cases; 95% confidence interval is illustrated by the shaded area

Figure 8-7 compares the combustion performance of the three cases. As can be seen, the single-fuel approach displays a higher maximum pressure rise rate for the high load period, but still stays within the self-imposed limits. This is identical with the observations made for steady-state operation (see Chapter 7). Here, increased PFI fractions and thus a higher quantity of premixed fuel causes a simultaneous onset of combustion throughout the combustion chamber with increased peak heat release rate levels and a shortened combustion duration [Figure 7-7 and 7-8]. As a result, the MHRR and MPRR levels are increased as well. The same is true for the combustion noise levels, which are in direct relation to the MPRR and MHRR levels. As stated before, the CA50 timings were selected to match previously determined optimal CA50 values throughout the transient testing. However, all three fuel combinations showed a more or less pronounced response over the load change period. Dieseline45/dieseline45 depicts the highest overshoot of about 3CAD for the download case and about 5CAD for the upload case. In the download case, the targeted values are reached after about 90 cycles, while the upload case could not recover within the number of cycles recorded. This is most likely caused by cylinder wall temperature effects, that are not accounted for in steady-state calibration maps. Cylinder walls are cooler from running at low load, causing a delay in combustion due to slower kinetic reaction rates This is especially true for a kinetically controlled combustion strategy like RCCI. On the other hand, high cylinder wall temperatures from running at high load in combination with an increase in DI fuel amounts and hence increased stratification cause the combustion phasing to be advanced during the download phase.

Hanson [44] has also seen similar effects for non-EGR cases, where an additional reason for the slow response in combustion phasing can be found from the fact that further increased intake temperatures support a more reactive mixture, which consequently respond to the change in fueling quicker.

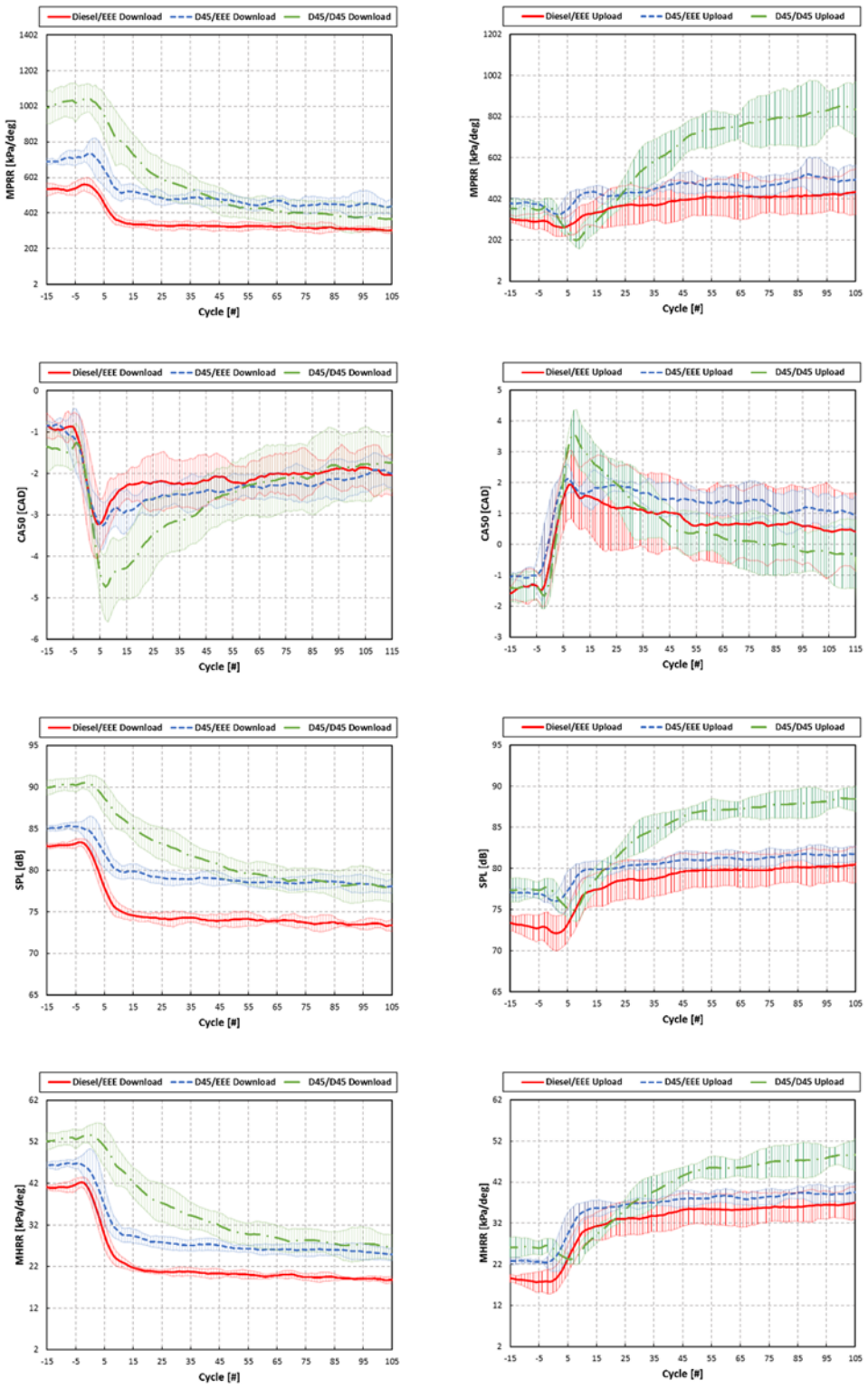

Figure 8-7 Combustion performance for the download and upload cases; 95% confidence interval is illustrated by the shaded area

Comparing the emission results in Figure 8-8, it can be seen that the transient results follow the trends found during steady-state operation, where HC was highest and NO was lowest for the single-fuel RCCI operation. The cause for the spike at the onset of the transient is thought to be connected to the cooler combustion chamber walls and port-fuel effects. The employment of a next-cycle controller could assist to react to variations quicker, but cannot entirely negate such spikes.

HC emissions are fairly constant across the load change for both the gasoline/diesel and the gasoline/dieseline45 case. The single-fuel case on the other hand shows an increase in HC with increasing load and vice-versa. The single-fuel HC emissions are increased, especially for the high load period, due to the high quantities of premixed fuel, hence increasing the charge equivalence ratio and reducing the amount of DI fuels. As a result, reduced combustion temperatures from the fewer rich regions can be expected. It is not entirely clear why responses to load changes are very minimal and that the overall trends for all three fuel combinations are opposite to those of steady-state results [Figure 7-4], one reason may again be due to cylinder wall temperature effects in combination with the injection adjustments for the different cases.

The NO emissions on the other hand follow the recorded steady-state trends. While the single-fuel approach shows low NO levels overall (only interrupted by the spike discussed earlier), the gasoline/diesel and gasoline/dieseline45 cases display higher NO levels from the increase in DI fraction. In addition, the difference between the high and low load periods for the gasoline/diesel and gasoline/dieseline45 are much higher compared to the dieseline45/dieseline45. While the difference in PFI fraction and thus PFI durations is similar for all fuel combinations [Figure 8-6], the cause for the larger difference between high and low load point is expected to be introduced by different conditions and processes in the cylinder, stemming from the increased DI fraction along with different charge mix conditions.

The soot opacity is not a concern for any of the fuel combinations, even though for dieseline45/dieseline45 a significant spike is recorded at the beginning of the transient, proving once more that the enrichment of the mixture from port injected fuel occurs. Other engine-out emissions were not recorded due to the transient nature of the tests.

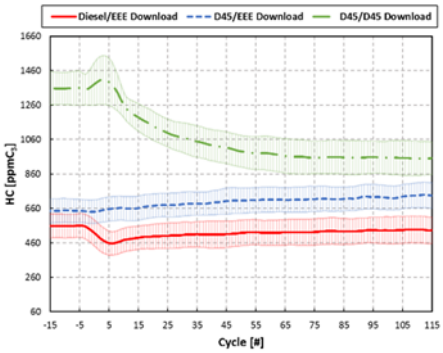

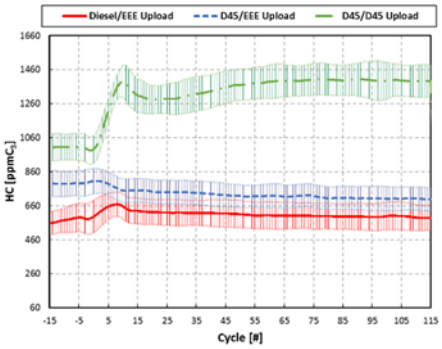

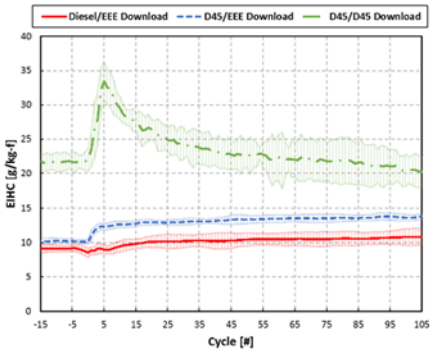

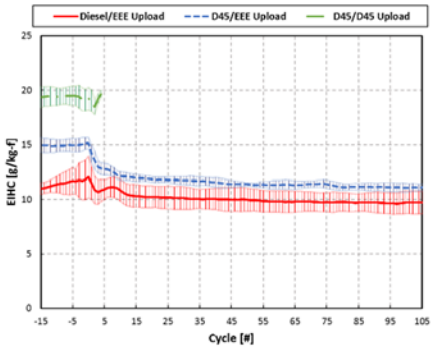

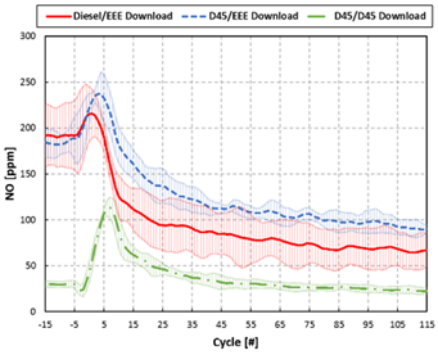

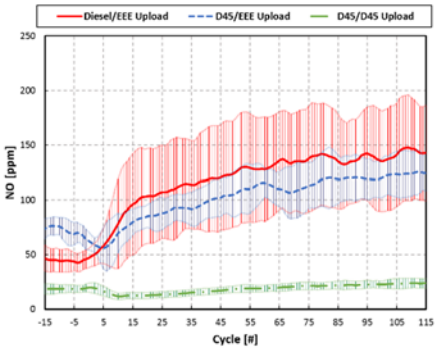

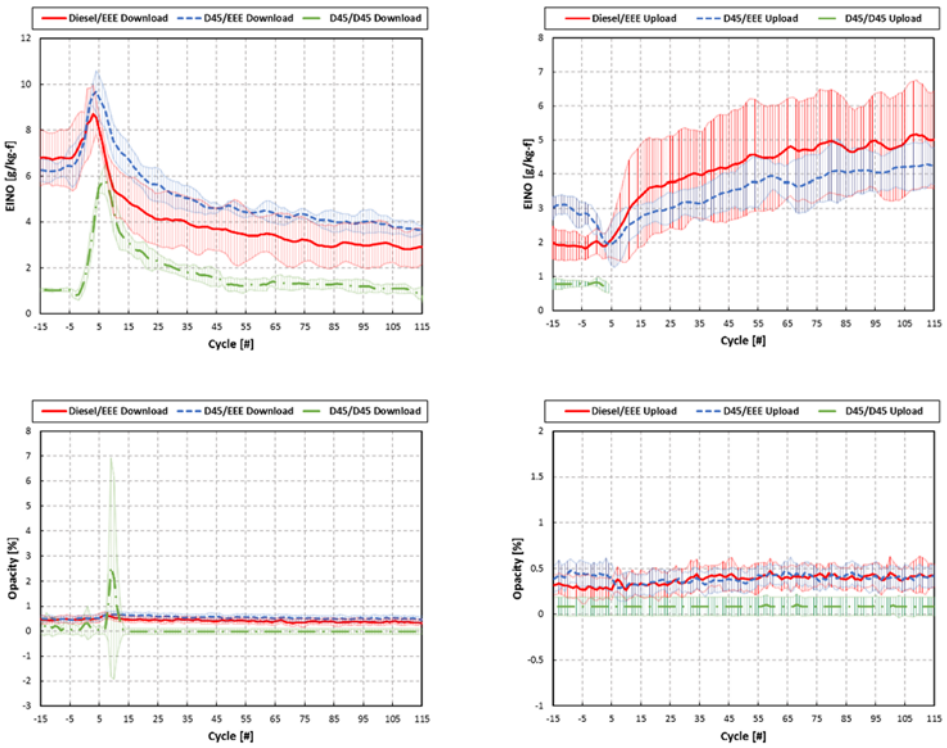

Figure 8-8 Emissions performance for the download and upload cases; 95% confidence interval is illustrated by the shaded area

8.2 Conclusions

This section of the study investigated the use of a dieseline45 as the high reactivity DI fuel, as well as a single-fuel approach using dieseline45 as both the port-fuel and DI injected fuel under transient RCCI operation. The tests were completed in the multi-cylinder light-duty engine equipped with the low CR piston and compared to gasoline/diesel RCCI combustion under matching intake conditions. The experiments were performed for a 2.6 to 4.0 bar BMEP upload and a 4.0 to 2.6 bar download transient. All 3 fuel combination cases used a DI SOI timing of -40 dATDC throughout the transient load change. For comparison, the rail pressure was matched for both cases along with closely matched combustion phasing. As a result, identical combustion characteristics for all fuel combination were achieved. The goal to closely match CA50 values led

to increased PFI quantities for the single-fuel approach with short DI injection durations due to the improved autoignition characteristics from the increased reactivity PFI fuel.

In conclusion, the capability to operate the engine in RCCI mode using dieseline45 over a transient load change without substantial issues was demonstrated. It was possible to conduct transient RCCI operation with a rather simple open-loop controller with acceptable results.

It was observed that the NO emissions of the gasoline/dieseline45 case were increased above the gasoline/diesel case. However, employing single-fuel operation led to a reduction in NO levels compared to diesel RCCI operation. In contrast, HC emissions were increased for both dieseline45 cases, especially at high load points for the dieseline45/dieseline45 case. Smoke opacity was not a factor for any of the fuel combinations as it was almost non-existent and constant throughout load changes. As shown earlier, the steady-state combustion efficiencies of dieseline45/dieseline45 showed reductions over the gasoline/diesel case, and this combination can be used for this transient.

The imposed noise and MPRR constraints were also met throughout the transient load changes. Differences in emissions and combustion performances due to variations in the thermodynamic boundary conditions and intake manifold runner wall wetting effects during the transient could be observed for all fuel combination, but were significantly enhanced for the single-fuel approach, having large amounts of port-injected increased reactivity fuel.

Chapter 9 Summary and Discussion

9.1 Performance and Emissions for Steady-State RCCI Combustion Using Dieseline

Chapter 4 studied the use of different dieseline blends as the high reactivity DI fuel for RCCI operation as a pathway to single-fuel RCCI. The tests were completed in the multi-cylinder light-duty engine equipped with an optimized, low CR piston as described above.

As with any kinetically controlled combustion strategy, the fuel properties play a major part in determining combustion performance and emissions. Therefore, a significant effort was made to investigate the range of fuels that can be utilized for RCCI with recent work also aiming towards a single-fuel RCCI approach, i.e., only small amounts of high reactivity additive fuels. This was mainly done by using small dosages of cetane improver to increase the reactivity of the DI fuel to a level allowing stable combustion. Motivated by those efforts, this section employed different blends of diesel and gasoline to achieve different reactivity DI fuels and thus assess the basic requirements, for a single-fuel approach.

From the results it can be seen that it was possible to achieve similar or even improved steady-state combustion and performance trends compared to gasoline/diesel RCCI over a complete range of CA50 values. All DI fuels also displayed similar CA50 values for their respective most efficient test points.

One of the major findings was that an optimum could be determined. Dieseline45 was selected out of a wide range of dieseline blends, since it outperformed all the other dieseline mixtures as well as the gasoline/diesel case under matched conditions. In addition, limitations were discovered for lower reactive fuels, such as dieseline20 and dieseline35. Both showing a limited ability to control CA50 and the operating load range. It was also found that NOx emissions are increased

with a decrease in diesel content and the corresponding decrease in reactivity. This caused changes in the emissions, with increased NOx from an increased DI fraction due to longer DI injections and slightly decreased HC from reduced PFI ratios.

In conclusion, additional questions have to be answered during future work regarding the special status of dieseline45. Why does it perform best? What are the important underlying characteristics? While assumptions can be made regarding the different vaporization properties of the different dieseline blends and the corresponding different levels of wall impingement, advanced CFD simulations would be helpful to determine in-cylinder processes.

9.2 Effects of Boost on Steady-State RCCI Combustion Using Dieseline45

In chapter 5 boosted RCCI operation was studied. Steady-state tests were completed with the multi-cylinder light-duty engine equipped with an optimized, low CR piston. In order to overcome the limitations of the stock turbocharger set-up, a custom intake system was implemented and used for this part of the study. Pressurized air was supplied directly into the intake, decoupling it completely from the turbocharger. As a result, the low exhaust enthalpies typically seen with LTC strategies were eliminated and pressures up to 2.15 bar were achievable. With the VGT mechanism kept in place, practiced turbocharger efficiencies were commanded manually and later by the use of 2D-torque-based tables.

From the results it can be seen for that appropriate boost pressure levels are beneficial to achieve improved performance for MCE RCCI combustion, consequently highlighting the drawbacks of a stock turbocharger set-up for RCCI/LTC operation, as described before by Hanson [43, 65] and Gross [50]. Nevertheless, future work needs to investigate and thus employ a more

advanced type boost system, such as a supercharger or twin-turbo set-up to overcome pressure fluctuations introduced by limitation of the proportional pressure control.

The limited load and speed range of the present study has to be considered when trying to draw a more detailed conclusion, i.e., whether non-linear effects of the VGT mechanism should be addressed for future investigations. The boost pressures were limited at the highest load due to the fully applied vane closure which resulted in unrealistic turbocharger efficiencies.

9.3 Comparing the Performance of Dieseline HCCI with RCCI Combustion Using Dieseline45

In chapter 6 HCCI operation using Diesline45 was studied as initial step towards a single-fuel RCCI approach (see Chapter 7). Steady-state tests were again completed with the multi-cylinder light-duty engine equipped with the low CR piston. From the results it can be seen that the intake conditions, i.e., intake temperature and pressure, had to be significantly increased over previously established conditions. The experiments matched well simulation results that gave guidelines to achieve stable combustion. Due to the devoted pressure and temperature autoignition was enhanced, and very early combustion phasing in comparison to RCCI cases was recorded for 2 of the 3 cases, while CA50 was matched closely for the low load point. This led to high levels of HRR and significantly increased MPRR levels. The results, showed the drawbacks and issues encountered with HCCI, while at the same time emphasizing the benefits of RCCI.

While this study did not make use of the EGR system, the addition of cooled EGR could be used in future investigations to retard combustion phasing and thus to prevent knocking and high MPRR.

RCCI and HCCI combustion gave good performance was achieved regardless, including ultra-low NOx and PM emissions, and have the potential for achieving high, well-controlled power levels.

9.4 Performance of Single-Fuel RCCI Combustion Using Dieseline45

In chapter 7 the use of dieseline45 as the high reactivity DI fuel as well as the low reactivity PFI fuel for RCCI operation or PFS was studied. The tests were completed in the multi-cylinder light-duty engine under steady-state operation. From the results it can be seen that it was possible to achieve improved combustion trends compared to gasoline/diesel RCCI. This is important, as it explores a method to achieve single-fuel RCCI combustion. As with other research in SCE and MCE using cetane improvers [46, 47, 49, 50], high peak efficiencies at different load points were seen. The low-octane fuel used in both injection systems further reduced NOx emissions along with requiring an increase of the port-injected fuel quantity. This method of operation can also be classified as a variation of the partial fuel stratification strategy (PFS). For this method the majority of the fuel is fully premixed and a small fraction is directly injected during the late part of the compression stroke. However, fuel octane ratings are usually higher for PFS and thus intake temperatures are far above intake temperatures used throughout this work. The single-fuel approach employed in this section, nevertheless, showed further improved NOx emissions while maintaining control over the combustion HRR and MPRR compared to an HCCI engine. In fact, while the pressure traces are more or less identical, the HRR is only slightly increased compared to dual-fuel RCCI operation.

In conclusion, future work needs to focus on reducing HC emissions, along with addressing high load efficiency limitations seen from this investigation. The implementation of EGR could

be one option as it has been shown to improve combustion efficiency and BTE levels. Specific calibration efforts, i.e., DI SOI timing, rail pressure and intake conditions, would also be the subject of future investigations.

9.5 Performance for Transient RCCI Combustion Using Dieseline45

In chapter 8 the use of dieseline45 as the high reactivity DI fuel for RCCI operation and in a single-fuel RCCI or PFS approach was studied. The tests were completed in the same multi-cylinder light-duty engine. The results show that it was possible to achieve similar transient combustion trends compared to gasoline/diesel RCCI. This is an important finding, as it further adds to the research efforts for RCCI and LTC in general.

With regards to previous MCE transient RCCI studies [44, 50], the present work also showed strong effects on emissions and combustion performance expected to be due to variations in the thermodynamic boundary conditions, i.e., combustion chamber wall temperatures. Furthermore, PFI fueling effects, i.e., intake wall wetting from fuel build-up well-known from SI engines and are documented in this work. Additional control mechanisms, such as model-based or feed-forward controls, will become inevitable for the adaption of RCCI in production engine.

Large improvements were seen by using present modified intake system, which eliminated poor turbocharger response and low intake pressure levels. However, more work needs to be done to investigate a more practical boost system, such as a supercharger or twin-turbo set-up to overcome pressure fluctuations caused by limitations of the proportional pressure control. In addition, the stock intake runner design should be investigated for transient RCCI operation. A design that avoids the dead-ended intake runner would mitigate cylinder-to-cylinder non-uniformity effects, especially when employing EGR, where the cylinder-to-cylinder balancing applied throughout this

work can only provide limited adjustments. This adjustment is also hampered by the inaccuracy of the BERU glow plug pressure transducers. Future work also needs to address HC issues, and a focus should be on the piston design. While the low ring-land height and flat-top design of the present study are certainly preferable and have proven their validity, questions still arise regarding the ideal compression ratio.

Finally, regarding at the single-fuel approach for a transient operation, the results are promising as improved performance over gasoline/diesel combustion was shown for matching operating conditions, including ultra-low NOx and PM combustion, and the ability to control HRR and MPRR.

References

[1] Wargo, J., Wargo, L., Alderman, N., and Brown, D. R., 2006, "The Harmful Effects of Vehicle Exhaust," Environment & Human Health, Inc., North Haven.
[2] Dec, J. E., 2009, "Advanced Compression-Ignition Engines - Understanding the In-Cylinder Processes," Proceedings of the Combustion Institute, 32,2, pp:2727-2742.
[3] Dec, J. E., 2009, "Advanced Compression-Ignition Engines - Understanding the In-Cylinder Processes," Proceedings of the Combustion Institute.
[4] Johnson, T. V., 2011, "Diesel Emissions in Review," SAE Technical Paper 2011-01-0304.
[5] Theis, J. R., Ura, J. A., Li, J. J., Surnilla, G. G., and Roth, J. M., 2003, "NOx Release Characteristics of Lean NOx Traps during Rich Purges," SAE Technical Paper 2003-01-1159.
[6] Heywood, J. B., 1988, Internal Combustion Engine Fundamentals, McGraw-Hill.
[7] Dec, J., "A conceptual Model of DI Diesel Combustion Based on Laser-Sheet Imaging," SAE Technical Paper 970873.
[8] Wagner, R., Curran, S., Dempsey, A., Sluder, S., Splitter, D., Szybist, J., and West, B., March 2014, "ORNL Advanced Combustion Research and Future Fuel Opportunities," Saudi Aramco Workshop "Future of Transport Fuels".
[9] Onishi, S., Jo, S. H., Shoda, K., Jo, P. D., and Kato, S., 1979, "Active Thermo-Atmosphere Combustion (ATAC) - A New Combustion Process For Internal Combustion Engines," SAE Technical Paper 790501.
[10] Gentili, R., Frigo, S., Tognotti, L., Hapert, P., and Lavy, J., "Experimental study of ATAC (Active Thermo-Atmosphere Combustion) in a Two-Stroke Gasoline Engine," SAE970363.
[11] Najt, P., and Foster, D., "Compression- Ignited Homogeneous Charge Combustion," SAE830264.
[12] Thring, R., "Homogeneous-Charge Compression-Ignition (HCCI) Engines," SAE892068.
[13] Gray, A. W., and Ryan, T. W., "Homogeneous Charge Compression Ignition (HCCI) of Diesel Fuel," SAE971676.
[14] Suzuki, H., Koike, N., and Odaka, M., "Combustion Control Method of Homogeneous Charger Diesel Engines," SAE980209.
[15] Olsson, J.-O., Tunestal, P., Johansson, B., Fiveland, S., Agama, J. R., and Assanis, D. N., 2002, "Compression Ratio Influence on Maximum Load of a Natural Gas-Fueled HCCI Engine," SAE Technical Paper 2002-01-0111.
[16] Christensen, M., Johansson, B., Amneus, P., and Mauss, F., 1998, "Supercharged Homogeneous Charge Compression Ignition," SAE Technical Paper 980787
[17] Olsson, J.-O., Tunestål, P., Haroldsson, G., and Johansson, B., 2001, "A Turbo-Charged Dual Fuel HCCI Engine," SAE Technical Paper 2001-01-1896, 2001, doi: 10.4271/2001-01-1896.
[18] Christensen, M., Hultquist, A., and Johansson, B., 1999, "Demonstrating the multi-fuel capability of a homogeneous charge compression ignition engine with variable compression ratio," SAE Technical Paper 1999-01-3679.
[19] Dec, J., Hwang, W., and Sjoberg, M., 2006, "An Investigation of Thermal Stratification in HCCI Engines Using Chemiluminescence Imaging," S. T. P. 2006-01-1518, ed.
[20] Dec, J., Sjoberg, M., and Hwang, W., 2009, "Ioslating the Effect of EGR on HCCI Heat-Release Rates and NOx emissions," SAE Int. J. Engines 2 (2), pp:58-70.

[21] Dec, J., Yang, Y., and Dronniou, N., 2011, "Boosted HCCI - Controlling Pressure-Rise Rates for Performance Improvements using Partial Fuel Stratification with Conventional Gasoline," SAE Technical Paper 2011-01-0897, doi:10.4271/2011-01-0897.
[22] Dec, J., and Yang, Y., 2010, "Boosted HCCI for High Power without Engine Knock and with Ultra-Low NOx Emissions - using Conventional Gasoline," SAE Technical Paper 2010-01-1086, doi:10.4271/2010-01-1086.
[23] Sjoberg, M., Dec, J., Babajimopoulos, A., and Assanis, D., 2004, "Comparing Enhanced Natural Thermal Stratification against Retarded Combustion Phasing for Smoothing of HCCI Heat-Release Rate," SAE Transactions, 113(3), pp.1557-1575, Paper 2004-01-2994.
[24] Sjoberg, M., and Dec, J., 2008, "Influence of Fuel Autoignition Reactivity on the High-Load Limits of HCCI Engines," SAE Int. J. of Engines 1(1), pp.39-58.
[25] Manente, V., Johansson, B., and Tunestal, P., 2010, "Influence of Inlet Pressure, EGR, Combustion Phasing, Speed and Pilot Ratio on High Load Gasoline Partially Premixed Combustion," SAE Technical Paper, 2010-01-1471, doi: 10.4271/2010-01-1471.
[26] Bessonette, P. W., Schleyer, C. H., Duffy, K. P., Hardy, W. L., and Liechty, M. P., 2007, "Effects of Fuel Property Changes on Heavy-Duty HCCI Combustion," (SAE Technical Paper 2007-01-0191, doi:10.4271/2007-01-0191).
[27] Kokjohn, S. L., Hanson, R. M., Splitter, D. A., and Reitz, R. D., 2009, "Experiments and Modeling of Dual Fuel HCCI and PCCI Combustion Using In-Cylinder Fuel Blending," (SAE Technical Paper 2009-01-2647, doi:10.4271/2009-01-2647).
[28] Splitter, D. A., Hanson, R. M., and Kokjohn, S. L., and Reitz, R. D., 2010, "Improving Engine Performance by Optimizing Fuel Reactivity with a Dual Fuel PCCI Strategy," THIESEL 2010 Conference on Thermo and Fluid Dynamic Processes in Diesel EnginesValencia, Spain.
[29] Inagaki, K., Fuyuto, T., Nishikawa, K., Nakakita, K., and Sakata, I., 2006, "Dual-Fuel PCI Combustion Controlled by In-Cylinder Stratification of Ignitability," (SAE Technical Paper 2006-01-0028, doi:10.4271/2006-01-0028).
[30] Kokjohn, S., Hanson, R., Splitter, D., Kaddatz, J., and Reitz, R., 2011, "Fuel Reactivity Controlled Compression Ignition (RCCI) Combustion in Light- and Heavy-Duty Engines," SAE Int. J. Engines 4(1):pp. 360-374, doi:10.4271/2011-01-0357.
[31] Hanson, R. M., Kokjohn, S. L., Splitter, D. A., and Reitz, R. D., 2010, "An Experimental Investigation of Fuel Reactivity Controlled PCCI Combustion in a Heavy-Duty Engine," (SAE Technical Paper 2010-01-0864, doi:10.4271/2010-01-0864).
[32] Kokjohn, S. L., 2012, "Reactivity Controlled Compression Ignition," PhD Dissertation, University of Wisconsin - Madison.
[33] Reitz, R. D., Kokjohn, S. L., Hanson, R. M., and Splitter, D. A., 2010, "Engine Combustion Control via Fuel Reactivity Stratification,"United States Patent US8616177.
[34] Splitter, D. A., Kokjohn, S. L., Rein, K., Hanson, R. M., Sanders, S., and Reitz, R. D., 2010, "An Optical Investigation of Ignition Processes in Fuel Reactivity Controlled PCCI Combustion," (SAE Technical Paper 2010-01-0345, doi:10.4271/2010-01-0345).
[35] Splitter, D. A., Wissink, M. L., DelVescovo, D., and Reitz, R. D., 2013, "RCCI Engine Operation Towards 60% Thermal Efficiency," SAE Technical Paper 2013-01-0279, doi:10.4271/2013-01-0279.
[36] Splitter, D. A., Wissink, M. L., Hendricks, T. L., Ghandi, J. B., and Reitz, R. D., 2012, "Comparison of RCCI, HCCI, and CDC Operation from Low to Full Load," THIESEL Conference on Thermo and Fluid Dynamic Processes in Diesel Engines, Valencia, Spain.

[37] Dempsey, A. B., Walker, N. R., Gingrich, E., and Reitz, R. D., 2014, "Comparison of Low Temperature Combustion Strategies for Advanced Compression Ignition Engines with a Focus on Controllability," Combustion Science and Technology, 186(2): pp.210-241.
[38] Reitz, R. D., and Duraisamy, G., 2015, "Review of high efficiency and clean reactivity controlled compression ignition (RCCI) combustion in internal combustion engines," Progress in Energy and Combustion Science, pp. pp. 12-71.
[39] Reitz, R. D., March 2016, "The Diesel Dilemma," MTZ, Springer, pp. pp 86-86.
[40] Kamimoto, T., and Bae, M., 1988, "High Combustion Temperature for the Reduction of Particulate in Diesel Engines," SAE Technical Paper, 880423, doi: 10.4271/880423.
[41] Splitter, D. A., Hanson, R. M., Kokjohn, S. L., and Reitz, R. D., 2011, "Reactivity Controlled Compression Ignition (RCCI) Heavy Duty Engine Operation at Mid and High Loads with Conventional and Alternative Fuels," SAE Technical Paper 2011-01-0363, doi:10.4271/2011-01-0363.
[42] Curran, S., Hanson, R., and Wagner, R., 2012, "Effect of E85 on RCCI Performance and Emissions on a Multi-Cylinder Light-Duty Diesel Engine," SAE Technical Paper, 2012-01-0376, doi:10.4271/2012-01-0376.
[43] Hanson, R., Curran, S., Wagner, R., and Reitz, R., 2013, "Effects of Biofuel Blends on RCCI Combustion in a Light-Duty, Multi-Cylinder Diesel Engine," SAE Int. J. Engines 6(1), doi:10.4271/2013-01-1653.
[44] Hanson, R. M., 2014, "Experimental Investigation of Transient RCCI Combustion in a Light Duty Diesel Engine," PhD Dissertation, University of Wisconsin - Madison.
[45] Dempsey, A. B., 2013, "Dual-Fuel Reacitivity Controlled Compression Ignition (RCCI) with Alternative Fuels," PhD Dissertation, University of Wisconsin - Madison.
[46] Splitter, D. A., Reitz, R. D., and Hanson, R. M., 2010, "High Efficiency, Low Emissions RCCI Combustion by Use of a Fuel Additive," SAE Int. J. Fuels Lubr. 3(2):742-756, doi:10.4271/2010-01-2167.
[47] Hanson, R. M., Kokjohn, S. L., Splitter, D. A., and Reitz, R. D., 2011, "Fuel Effects on Reactivity Controlled Compression Ignition (RCCI) Combustion at Low Load," SAE Int. J. Engines 4(1):394-411, doi:10.4271/2011-01-0361.
[48] Kaddatz, J. R., Andrie, M., Kokjohn, S. L., and Reitz, R. D., 2012, "Light-Duty Reactivity Controlled Compression Ignition Combustion Using a Cetane Improver," SAE Technical Paper 2012-01-1110, doi:10.4271/2012-01-1110.
[49] Dempsey, A., 2015, "Characterization of Reactivity Controlled Compression Ignition (RCCI) using Premixed Gasoline and Direct-Injected Gasoline with a Cetane Improver on a Multi-Cylinder Engine " SAE Technical Paper 2015-01-0855, doi:10.4271/2015-01-0855.
[50] Gross, C. W., and Reitz, R. D., 2015, ""Single-Fuel" RCCI Operation With Customized Pistons in a Light-Duty Multi-Cylinder Engine," ASME Internal Combustion Engine Division Fall Conference Houston, Texas; ICEF2015-1051.
[51] Olsson, J., Tunestal, P., Haraldsson, G., and Johansson, B., 2001, "A Turbo Charged Dual Fuel HCCI Engine," SAE Technical Paper 2001-01-1896, doi:10.4271/2001-01-1896.
[52] Dahl, D., and Denbratt, I., 2011, "HCCI/SCCI Load Limits and Stoichiometric Operation in a Multi-Cylinder Naturally Aspirated Spark Ignition Engine Operated on Gasoline and E85," Int. J. of Engine Research, 12, pp.58-68, doi:10.1177/14680874JER392450.
[53] Curran, S., Prikhodko, V., Cho, K., Sluder, C. S., Parks, J., Wagner, R., Kokjohn, S., and Reitz, R., 2010, "In-Cylinder Fuel Blending of Gasoline/Diesel for Improved Efficiency and Lowest Possible Emissions on a Multi-Cylinder Light-Duty Diesel Engine," SAE Technical Paper 2010-01-2206, doi:10.4271/2010-01-2206.

[54] Curran, S., Hanson, R., and Wagner, R., 2012, "Reactivity Controlled Compression Ignition Combustion on a Multi-Cylinder Light-Duty Diesel Engine," Int. J. of Engine Research 1468087412442324, doi:10.1177/1468087412442324.
[55] Dempsey, A., 2015, "Characterization of Reactivity Controlled Compression Ignition (RCCI) using Premixed Gasoline and Direct-Injected Gasoline with a Cetane Improver on a Multi-Cylinder Engine " SAE Technical Paper 2015-01-xxxx, doi:10.4271/2015-01-xxxx.
[56] CFR, C. o. F. R., 2012, part:86, pp.543-620, "Title 40: Protection of Environment," http://www.gpo.gov.ezproxy.library.wisc.edu/fdsys/pkg/CFR-2012-title40-vol20/pdf/CFR-2012-title40-vol20.pdf.
[57] DieselNet, accessed Nov. 2014, "Emission Test Cycles," https://www-dieselnet-com.ezproxy.library.wisc.edu/standards/cycles/.
[58] Swain, D., Jackson, C., Lindhjem, C., and Hoffman, G., 1998, "A Method for Comparing Transient NOx Emissions With Weighted Steady State Test Results," SAE Technical Paper 980408, doi:10.4271/980408.
[59] Samulski, M., and Jackson, C., 1998, "Effects of Steady-State and Transient Operation on Exhaust Emissions from Nonroad and Highway Diesel Engines," SAE Technical Paper 982044, doi:10.4271/982044.
[60] Eastwood, P., Tufail, K., Winstanley, T., Darlington, A., Karagiorgis, S., Hardalupas, Y., and Taylor, A. M., 2010, "Estimation of Deviations in NO and Soot Emissions Between Steady-State and EUDC Transient Operation of a Common-Rail Diesel Engine," SAE Int. J. Engines 2(2):pp. 648-659, doi:10.4271/2009-24-0147.
[61] Lindgren, A., Larsson, G., and Hansson, P. A., 2010, "Evaluation of Factors influencing Emissions from Tractors and Construction Equipment during Realistic Work Operation using Diesel Fuel and Bio-Diesel as Substitute," Biosystems Engineering, 107, pp.123-130.
[62] Glewen, W., Heuwetter, D., Foster, D., Andrie, M., and Krieger, R., 2012, "Analysis of Deviation from Steady-State Performance During Transient Operation of a Light-Duty Diesel Engine," SAE Int. J. Engines 5(3), doi:10.4271/2012-01-1067.
[63] Hagena, J. R., Filipi, Z. S., and Assanis, D. N., 2006, "Transient Diesel Emissions: Analysis of Engine Operation During Tip-in," SAE Technical Paper 2006-01-1151, doi:10.4271/2006-01-1151.
[64] Glewen, W., 2012, "Experimental Investigation of Transient Operation and Low Temperature Combustion in a Light-Duty Diesel Engine," PhD Thesis, University of Wisconsin - Madison.
[65] Hanson, R., and Reitz, R., 2013, "Transient RCCI Operation in a Light-Duty Multi-Cylinder Engine," SAE Int. J. Engines 6(3):pp. 1694-1705, doi:10.4271/2013-24-0050.
[66] Babbit, G. R., 1999, "Transient Engine Test System for Hardware-in-the-Loop Powertrain Development," PhD Dissertation, University of Wisconsin - Madison.
[67] Feist, M., 2001, "Implementation of a Transient Hydrostatic Engine Dynamometer," M.S. Thesis, University of Wisconsin - Madison.
[68] Lahti, J. L., and Moskwa, J. J., 2002, "A Transient Hydrostatic Dynamometer for Testing Single-Cylinder Prototypes of Multi-Cylinder Engines," SAE Technical Paper 2002-01-0616, doi:10.4271/2002-01-0616.
[69] Burton, J. L., 2008, "Investigation of Transient Emissions and Mixed Mode Combustion for a Light-Duty Diesel Engine," MS. Thesis, University of Wisconsin - Madison.
[70] Ltd., C., 2001, "fNOx400 Fast Response Nitric Oxide Measurement System."
[71] Schurov, S., Collings, N., Hands, T., and Peckham, M. e. a., 1998, "Fast Response NO/HC Measurements in the Cylinder and Exhaust Port of a DI Diesel Engine," SAE Technical Paper 980788, doi:10.4271/980788.

[72] Lapuerta, M., Martos, F. J., and Cardenas, M. D., 2005, "Determination of Light Extinction Efficiency of Diesel Soot from Smoke Opacity Measurements," Measurement Science and Technology 16, pp.2048-2055.
[73] AVL, 2001, "Smoke Measurement," AVL LIST GmbH.
[74] Williams, D. R., 2008, "Transient Effect of Speed and Load on Low Temperature Diesel Combustion," M.S. Thesis, University of Wisconsin - Madison.
[75] Kokjohn, S., 2016, "Personal Communication."
[76] DelVescovo, D., 2016, "The Effects of Fuel Stratification and Heat Release Shaping in Reactivity Controlled Compression Ignition (RCCI) Combustion," PhD Dissertation, University of Wisconsin - Madison.
[77] Wang, H., Yao, M., and Reitz, R. D., 2013, "Development of a Reduced Primary Reference Fuel (PRF) Mechanism for IC Engine Combustion Simulations," Energy & Fuels, 27,(27), pp. pp. 7843-7853.
[78] Splitter, D. A., Wissink, M., Kokjohn, S. L., and Reitz, R., 2012, "Effect of Compression Ratio and Piston Geometry on RCCI Load Limits and Efficiency," SAE Technical Paper 2012-01-0383, doi:10.4271/2012-01-0383.
[79] Hanson, R., Curran, S., Wagner, R., Kokjohn, S., Splitter, D., and Reitz, R., 2012, "Piston Bowl Optimization for RCCI Combustion in a Light-Duty Multi-Cylinder Engine," SAE Int. J. Engines 5(2):pp. 286-299, doi: 10.4271/2012-01-0380.
[80] Dempsey, A., Curran, S., Wagner, R., and Kokjohn, S., 2012, "Effect of Piston Bowl Geometry on Dual-Fuel Reactivity Controlled Compression (RCCI) in a Light-Duty Engine Operated with Gasoline/Diesel and Methanol/Diesel," SAE Int. J. Engines, 6(1): pp.78–100, doi:10.4271/2013-01-0264
[81] Diesels, 2013, "Diesels Difference Engine: Born Again," The Economist; Babbage Science and Technology.
[82] Hitomi, M., Nakai, E., Terazawa, Y., Takamatsu, H., and Shimo, D., 2013, "Realization of a concept for ultra-low compression ratio of 14.0," Japan Society of Mechanical Engineers Awards.
[83] Sluder, C., and Wagner, R., 2006, "An Estimate of Diesel High-Efficiency Clean Combustion Impacts on FTP-75 Aftertreatment Requirements," SAE Technical Paper 2006-01-3311, doi:10.4271/2006-01-3311.
[84] Kenney, T., Gardner, T., Low, S., Eckstrom, J., and al., e., 2001, "Overall Results: Phase I AdHoc Diesel Fuel Test Program," (SAE Technical Paper 2001-01-0151, doi:10.4271/2001-01-0151).
[85] Shan, X., Burl, J., Jankovic, M., and Cooper, S., 2008, "Transient Fuel X-Tau Parameter Estimation Using Short Time Fourier Transform," SAE Technical Paper 2008-01-1305, doi:10.4271/2008-01-1305.
[86] Osburn, A., and Franchek, M., 2004, "Transient Air/Fuel Ratio Controller Identification Using Repetitive Control," J. of Dynamic Systems, Measurement and Control, 126, pp.781-789.

Chapter 10 Appendices

10.1 Appendix A: Supplementary material

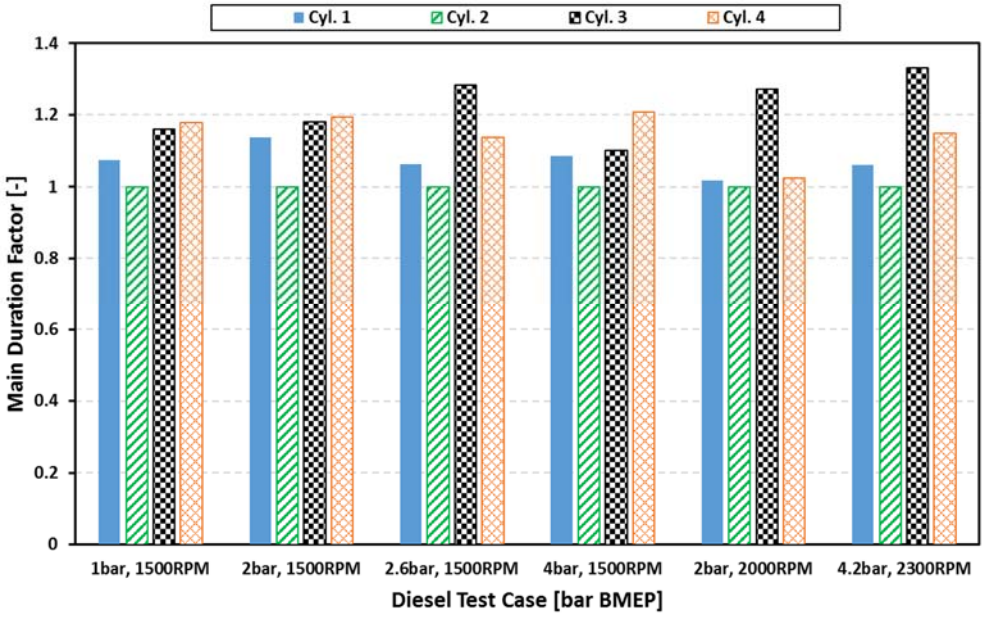

Figure 10-1 Main Duration adjustment for each cylinder at all load points for Diesel RCCI

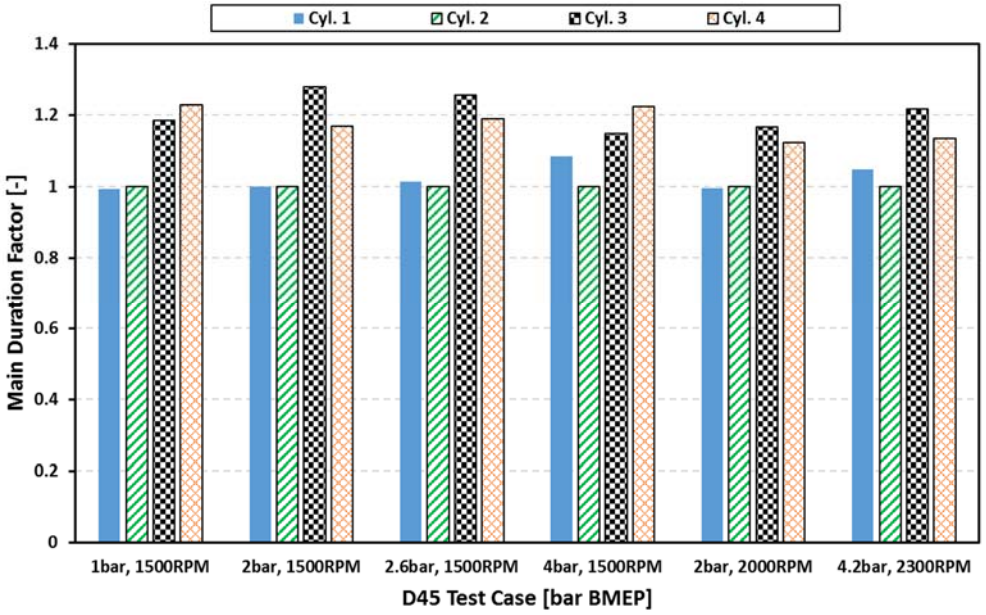

Figure 10-2 Main Duration adjustment for each cylinder at all load points for D45 RCCI

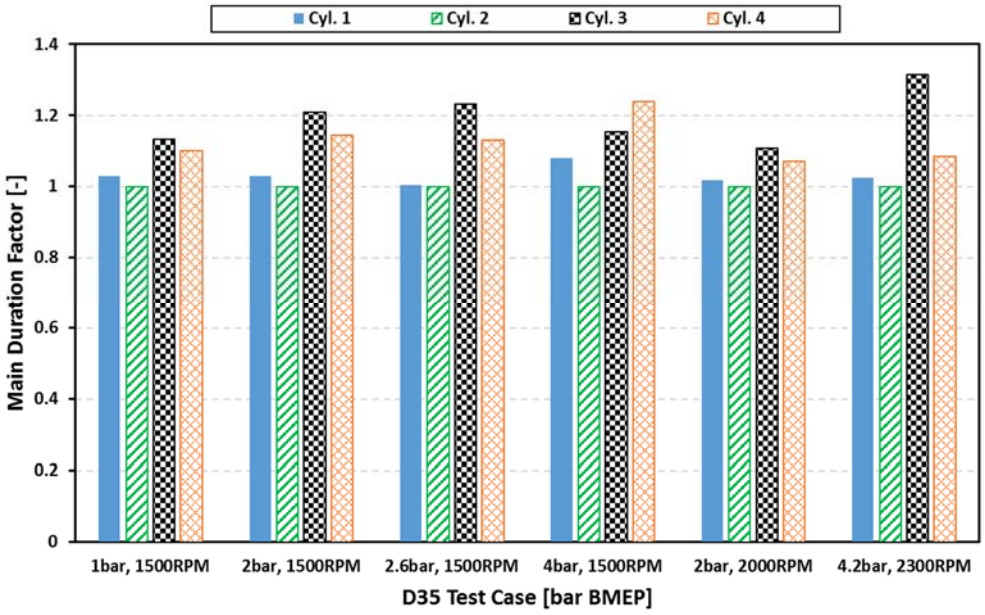

Figure 10-3 Main Duration adjustment for each cylinder at all load points for D35 RCCI

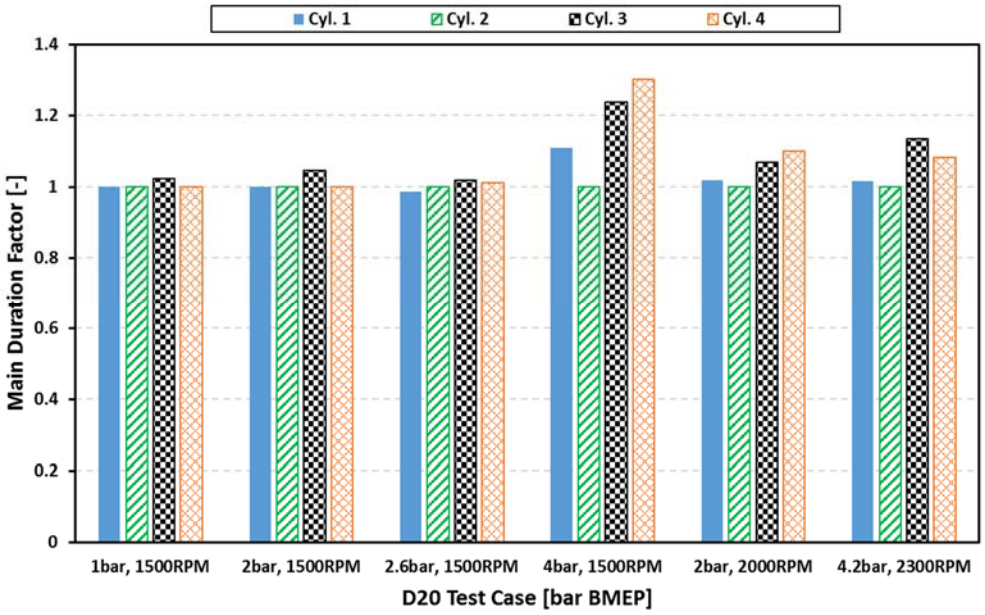

Figure 10-4 Main Duration adjustment for each cylinder at all load points for D20 RCCI

10.1 Appendix B: Steady-State RCCI Results for Fuel Comparison

10.1.1 1.0 bar BMEP, 1,500 rev/min

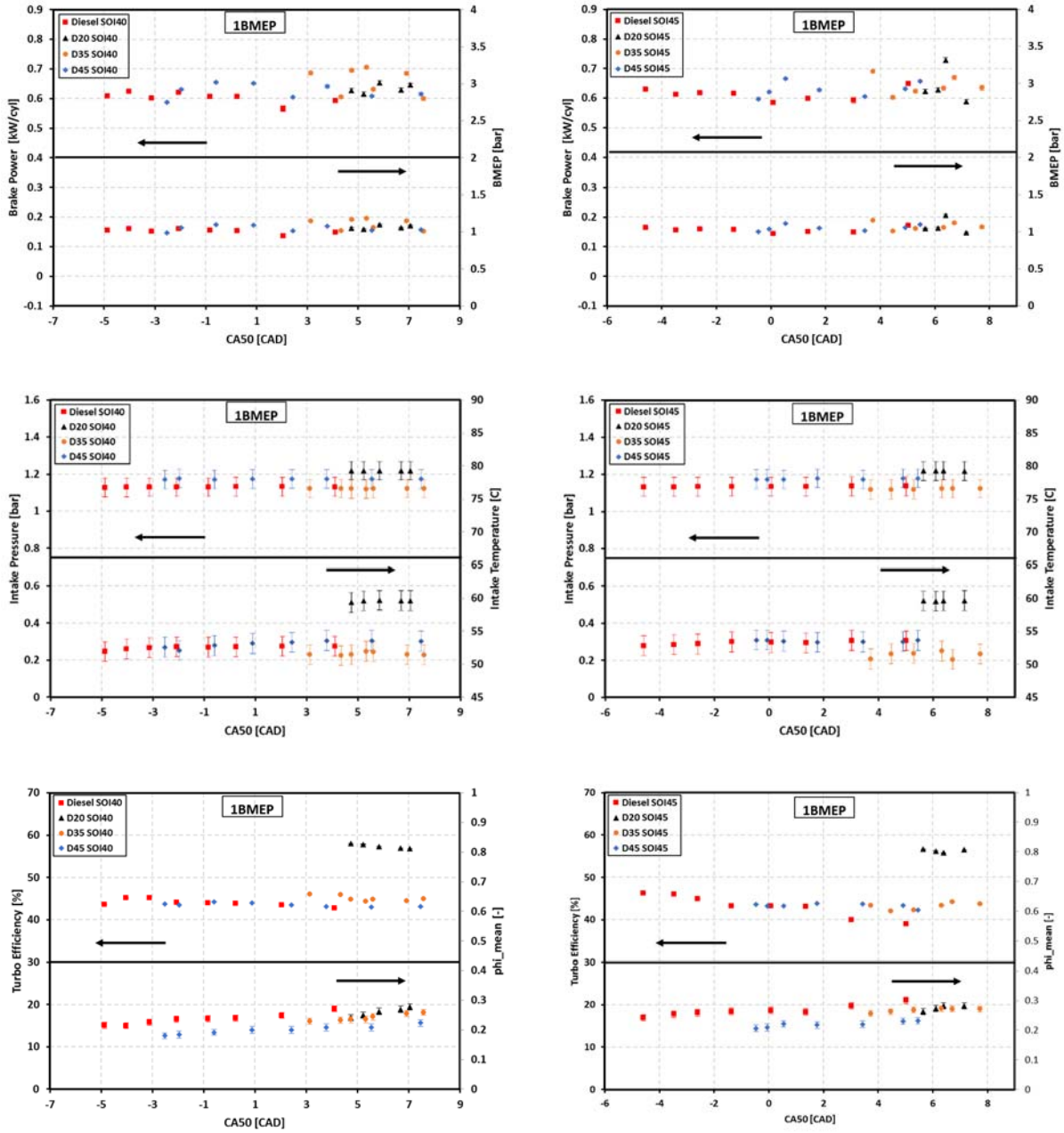

Figure 10-5 Operating Conditions as a function of the combustion phasing (CA50) at the DI SOI timing of -40 and -45 dATDC

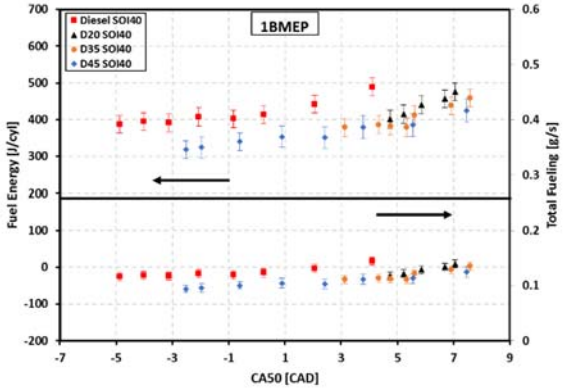
1BMEP
Diesel SOI40
D20 SOI40
D35 SOI40
D45 SOI40
Fuel Energy [J/cyl]
Total Fueling [g/s]
CA50 [CAD]

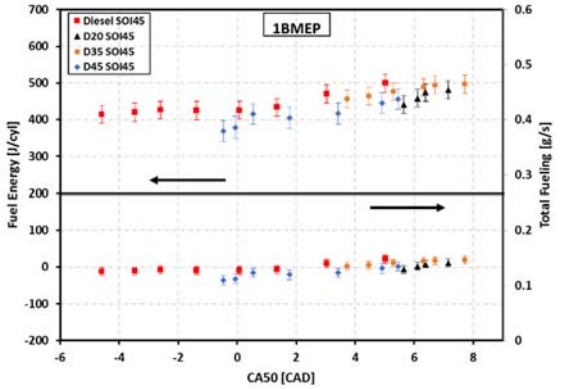
1BMEP
Diesel SOI45
D20 SOI45
D35 SOI45
D45 SOI45
Fuel Energy [J/cyl]
Total Fueling [g/s]
CA50 [CAD]

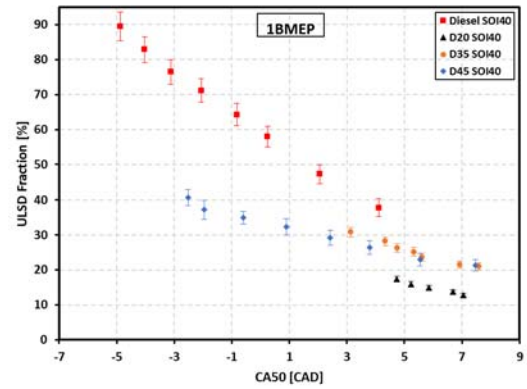
1BMEP
Diesel SOI40
D20 SOI40
D35 SOI40
D45 SOI40
ULSD Fraction [%]
CA50 [CAD]

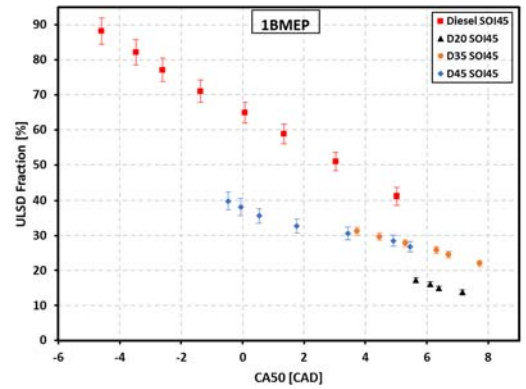
1BMEP
Diesel SOI45
D20 SOI45
D35 SOI45
D45 SOI45
ULSD Fraction [%]
CA50 [CAD]

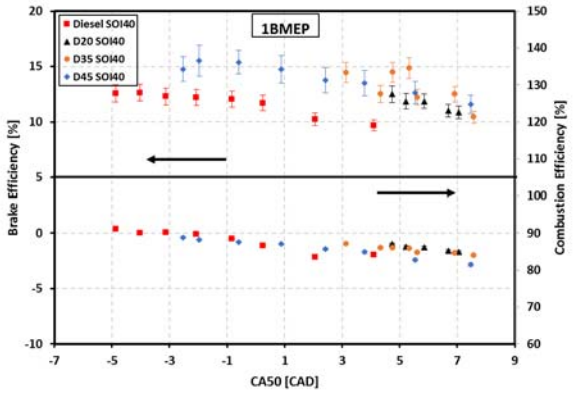
1BMEP
Diesel SOI40
D20 SOI40
D35 SOI40
D45 SOI40
Brake Efficiency [%]
Combustion Efficiency [%]
CA50 [CAD]

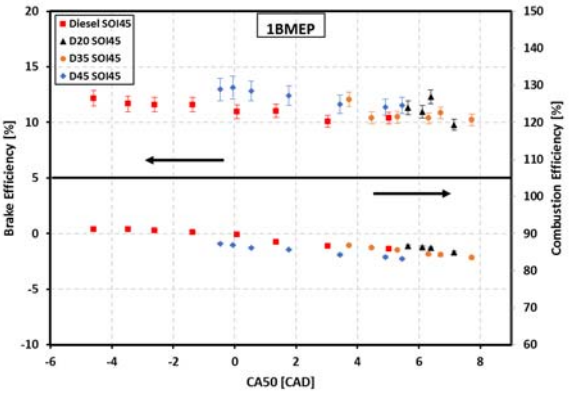
1BMEP
Diesel SOI45
D20 SOI45
D35 SOI45
D45 SOI45
Brake Efficiency [%]
Combustion Efficiency [%]
CA50 [CAD]

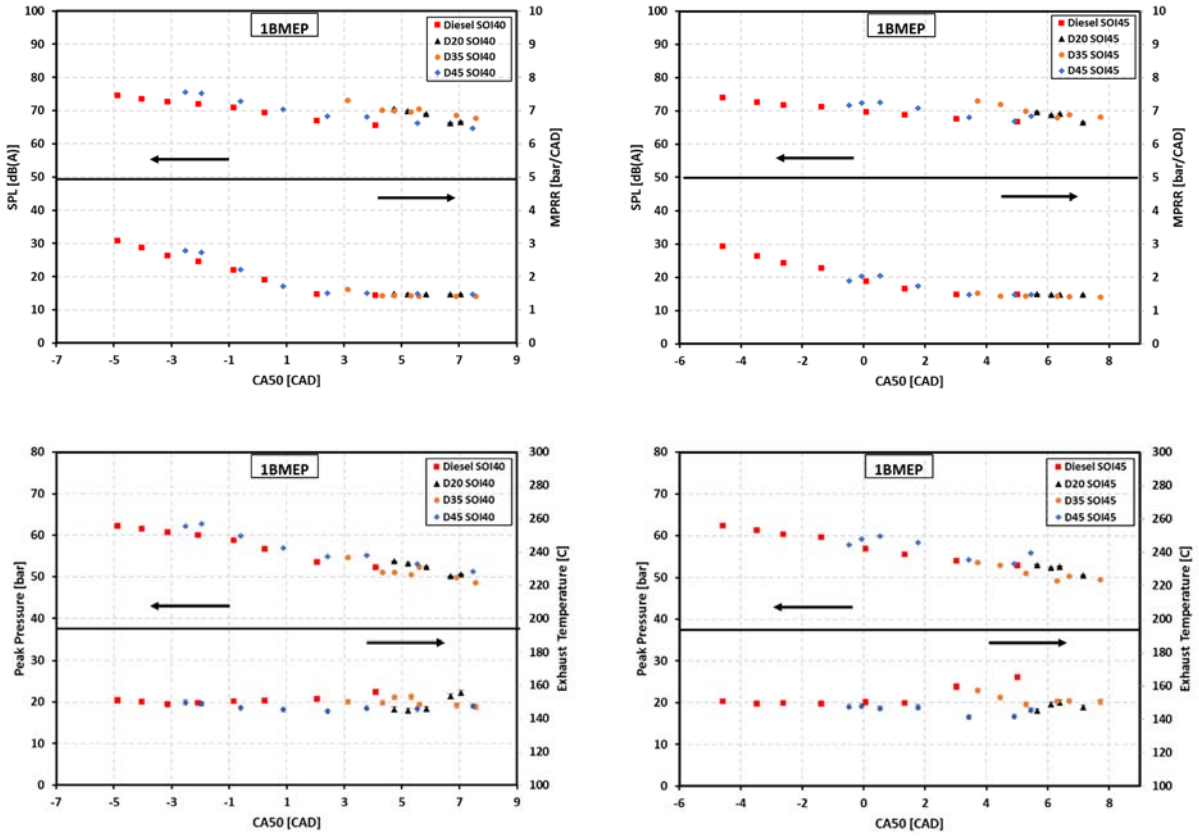

Figure 10-6 Performance results as a function of the combustion phasing (CA50) at the DI SOI timing of -40 and -45 dATDC

Table 10-1 1.0 bar BMEP Operating Conditions for best brake efficiency cases of each DI fuel at SOI -40 ATDC

Fuel	**Diesel**	**D45**	**D35**	**D20**
Pedal Position [%]	10.6	12.9	15	15.9
DI Duration [ms]	0.548	0.587	0.587	0.632
PFI Duration [ms]	1.104	1.192	1.551	0.919
PFI Fraction [%]	17.1	17.3	28	12.8
Rail Pressure [bar]	501	495	502	502
Main SOI [deg. BTDC]	40	40	40	40
Intake Pressure [bar]	1.13	1.17	1.12	1.22
Intake Temp. [°C]	52	52	52	59
EGR [%]	0	0	0	0
MPRR [bar/deg.]	2.86	2.72	1.41	1.48
CA 50 [deg. ATDC]	-4.027	-1.963	5.329	4.739
Comb Noise [dba]	73.5	75.1	69.4	70.6
Phi [-]	0.214	0.188	0.235	0.241

BTE [%]	12.64	15.55	14.8	12.5
Comb. Eff. [%]	90.1	88.3	85.8	87.1

Table 10-2 1.0 bar BMEP Operating Conditions for best brake efficiency cases of each DI fuel at SOI -45 ATDC

Fuel	**Diesel**	**D45**	**D35**	**D20**
Pedal Position [%]	9.7	13.5	15.1	17.8
DI Duration [ms]	0.580	0.596	0.649	0.629
PFI Duration [ms]	0.976	0.929	0.847	1.579
PFI Fraction [%]	11.8	15.3	10.7	25.5
Rail Pressure [bar]	485	495	500	500
Main SOI [deg. BTDC]	45	45	45	45
Intake Pressure [bar]	1.13	1.17	1.12	1.22
Intake Temp. [°C]	53	54	51	60
EGR [%]	0	0	0	0
MPRR [bar/deg.]	2.94	2.04	1.52	1.482
CA 50 [deg. ATDC]	-4.587	-0.429	3.727	6.389
Comb Noise [dba]	73.9	72.4	72.8	69
Phi [-]	0.243	0.209	0.257	0.282
BTE [%]	12.17	13.13	12.07	12.29
Comb. Eff. [%]	91.1	86.9	86.7	86.1

Pressure traces

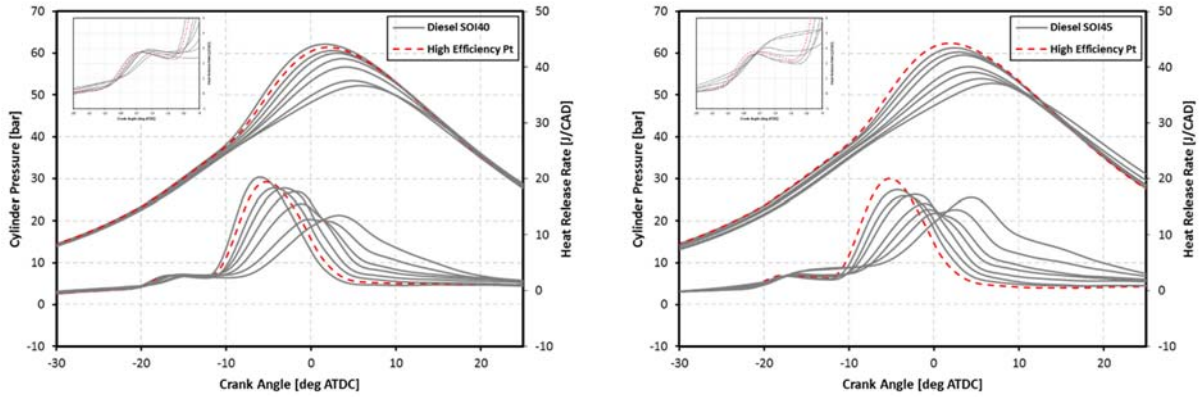

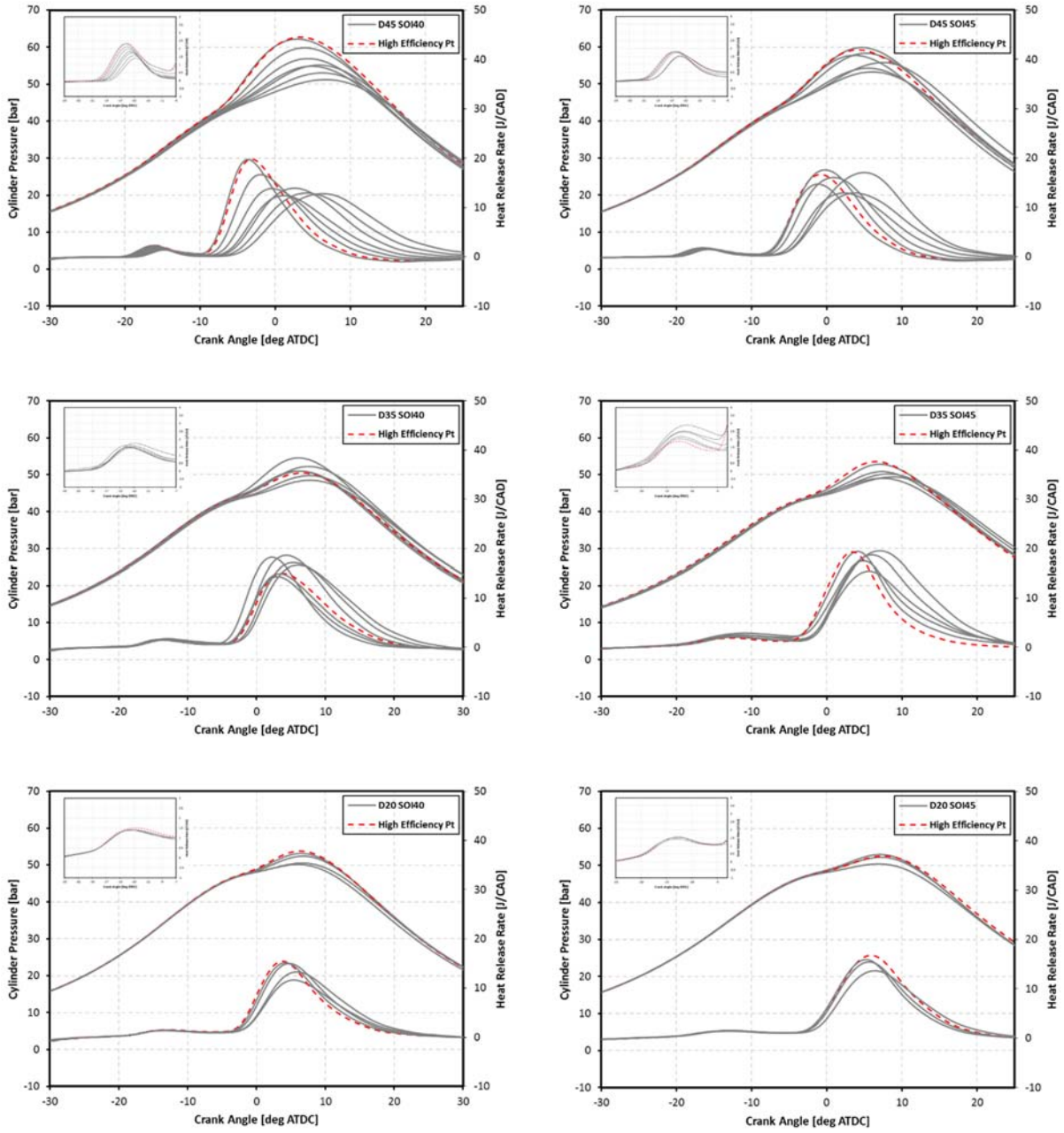

Figure 10-7 Cylinder Pressure [bar] and heat release rate [J/CAD] as a function of CAD at the DI SOI timing of -40 and -45 dATDC

Emissions results

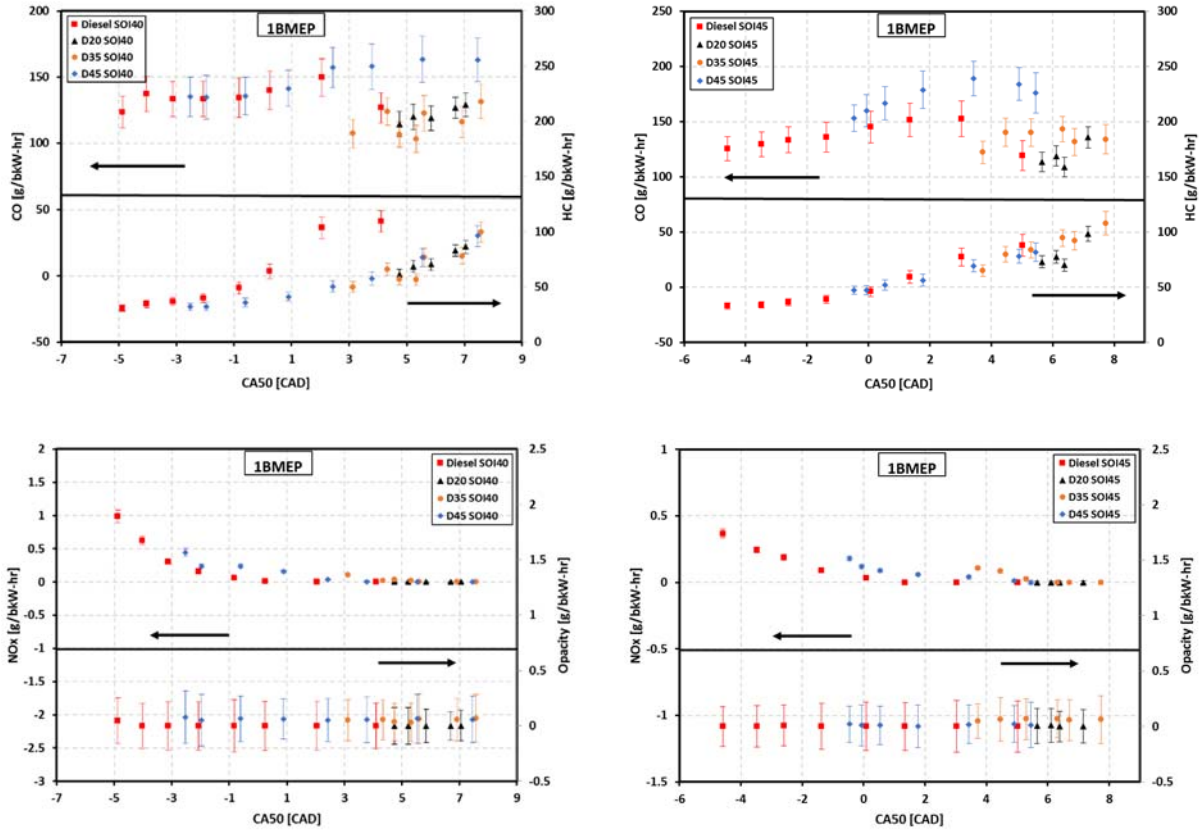

Figure 10-8 Engine-out emissions [g/bkW-hr] as a function of the combustion phasing (CA50) at the DI SOI timing of -40 and -45 dATDC

10.1.2 2.0 bar BMEP, 1,500 rev/min

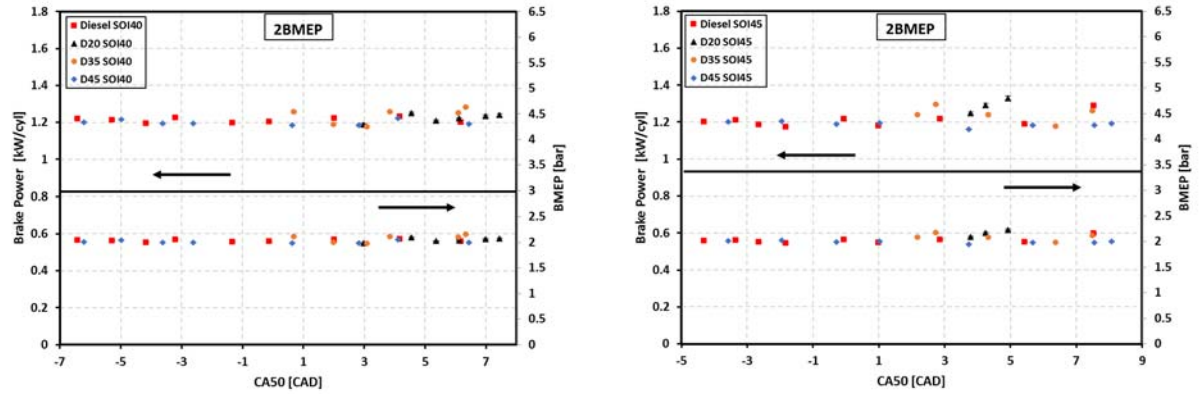

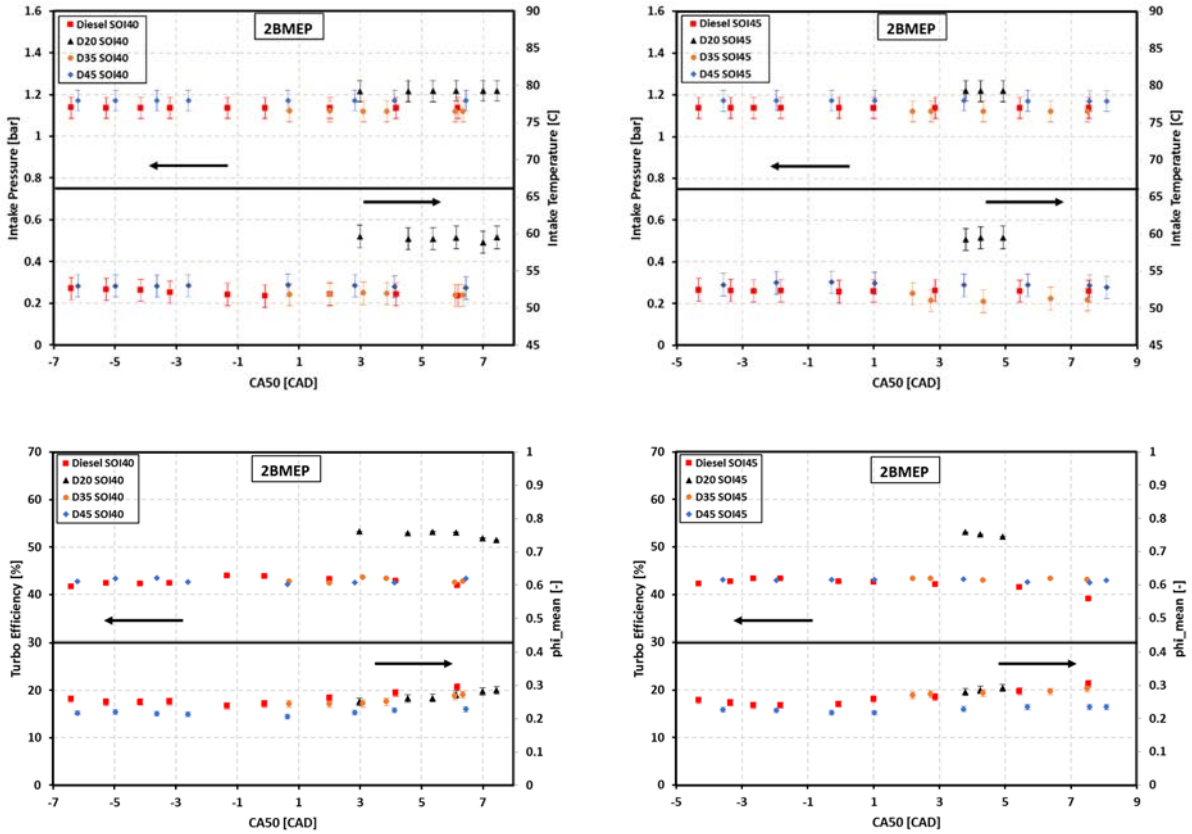

Figure 10-9 Operating Conditions as a function of the combustion phasing (CA50) at the DI SOI timing of -40 and -45 dATDC

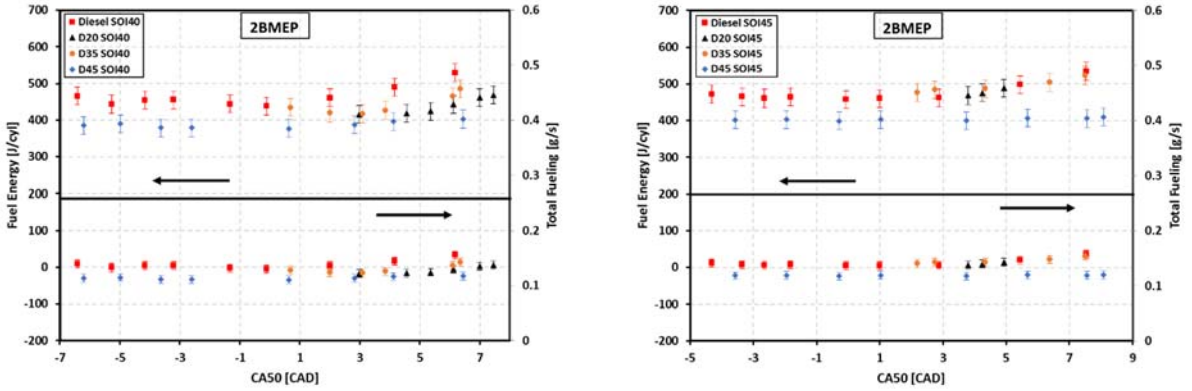

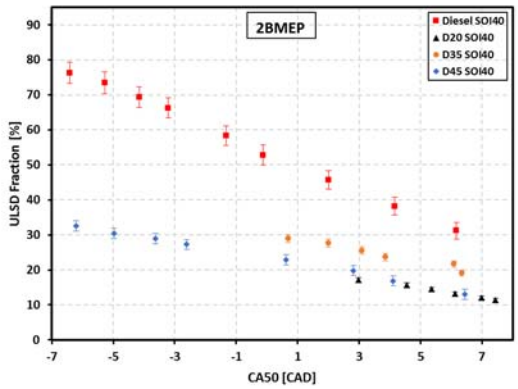
2BMEP
Diesel SOI40
D20 SOI40
D35 SOI40
D45 SOI40
ULSD Fraction [%]
CA50 [CAD]

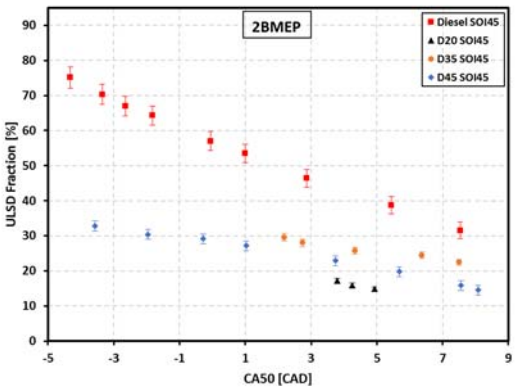
2BMEP
Diesel SOI45
D20 SOI45
D35 SOI45
D45 SOI45
ULSD Fraction [%]
CA50 [CAD]

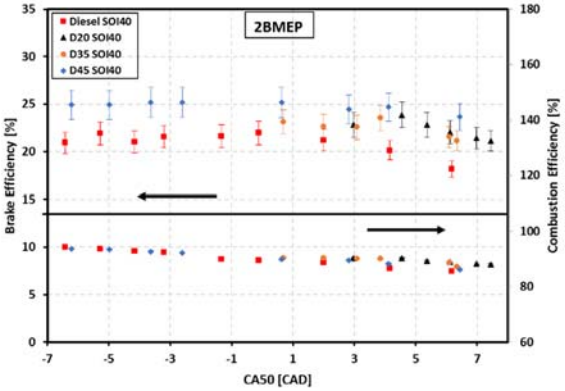
2BMEP
Diesel SOI40
D20 SOI40
D35 SOI40
D45 SOI40
Brake Efficiency [%]
Combustion Efficiency [%]
CA50 [CAD]

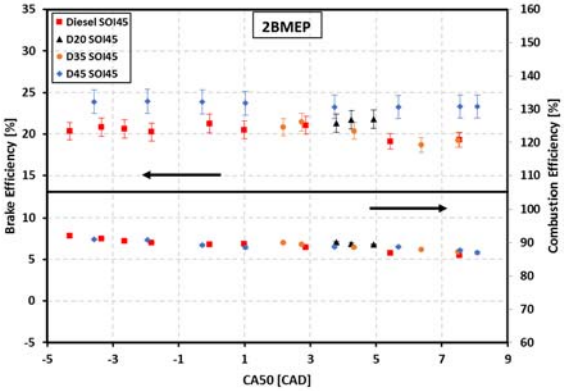
2BMEP
Diesel SOI45
D20 SOI45
D35 SOI45
D45 SOI45
Brake Efficiency [%]
Combustion Efficiency [%]
CA50 [CAD]

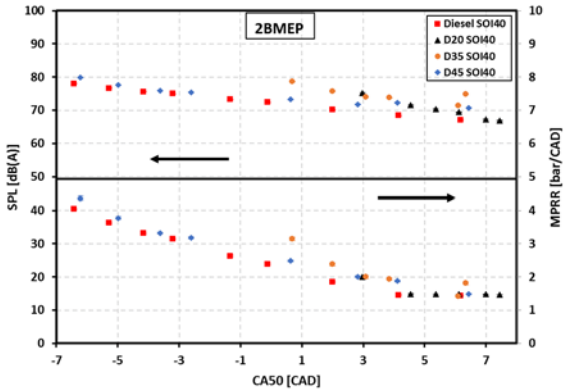
2BMEP
Diesel SOI40
D20 SOI40
D35 SOI40
D45 SOI40
SPL [dB(A)]
MPRR [bar/CAD]
CA50 [CAD]

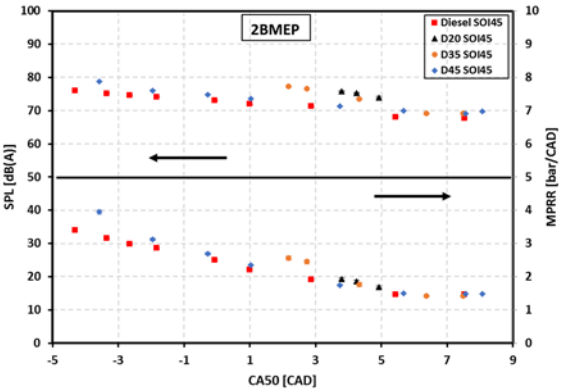
2BMEP
Diesel SOI45
D20 SOI45
D35 SOI45
D45 SOI45
SPL [dB(A)]
MPRR [bar/CAD]
CA50 [CAD]

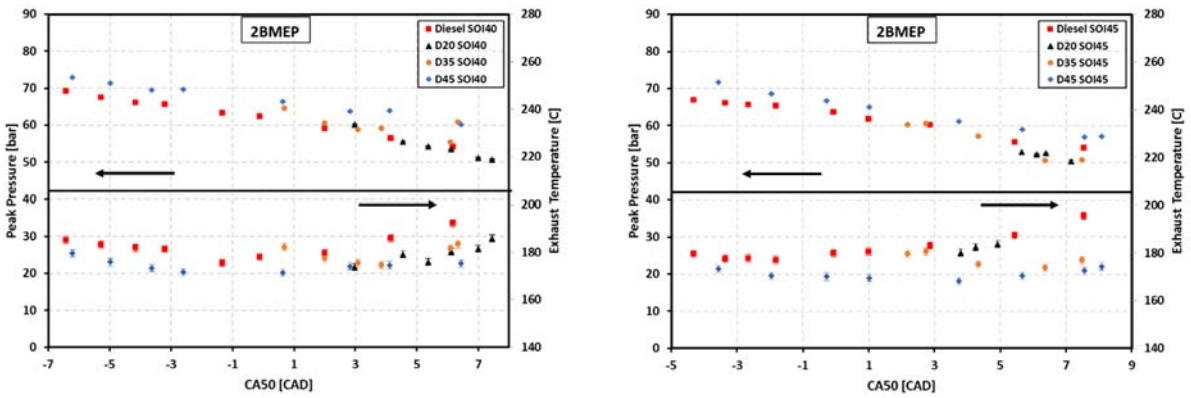

Figure 10-10 Performance results as a function of the combustion phasing (CA50) at the DI SOI timing of -40 and -45 dATDC

Table 10-3 2.0 bar BMEP Operating Conditions for best brake efficiency cases of each DI fuel at SOI -40 ATDC

Fuel	**Diesel**	**D45**	**D35**	**D20**
Pedal Position [%]	12.5	15.5	16.3	17.4
DI Duration [ms]	0.506	0.535	0.576	0.677
PFI Duration [ms]	1.976	1.968	1.845	1.271
PFI Fraction [%]	47.2	39.5	32.3	21.6
Rail Pressure [bar]	495	505	503	495
Main SOI [deg. BTDC]	40	40	40	40
Intake Pressure [bar]	1.14	1.17	1.12	1.22
Intake Temp. [°C]	52	53	52	59
EGR [%]	0	0	0	0
MPRR [bar/deg.]	2.39	3.18	1.94	1.49
CA 50 [deg. ATDC]	-0.177	-2.612	3.855	4.551
Comb Noise [dba]	72.4	75.4	73.7	71.6
Phi [-]	0.244	0.223	0.251	0.262
BTE [%]	21.98	25.12	23.56	23.88
Comb. Eff. [%]	89.6	92.2	90.1	90.3

Table 10-4 2.0 bar BMEP Operating Conditions for best brake efficiency cases of each DI fuel at SOI -45 ATDC

Fuel	**Diesel**	**D45**	**D35**	**D20**
Pedal Position [%]	12.8	16	17.1	19..2
DI Duration [ms]	0.541	0.566	0.648	0.645
PFI Duration [ms]	1.875	1.701	1.347	1.675
PFI Fraction [%]	57.0	32.5	20.0	25.8
Rail Pressure [bar]	495	510	490	500
Main SOI [deg. BTDC]	45	45	45	45
Intake Pressure [bar]	1.14	1.17	1.12	1.22
Intake Temp. [°C]	52	53	51	60
EGR [%]	0	0	0	0
MPRR [bar/deg.]	2.49	3.12	2.44	1.69
CA 50 [deg. ATDC]	-0.262	-1.958	2.739	4.926
Comb Noise [dba]	73.0	76.0	76.6	73.9
Phi [-]	0.244	0.224	0.274	0.292
BTE [%]	21.27	23.94	21.42	21.79
Comb. Eff. [%]	89.5	90.8	89.5	89.4

Pressure traces

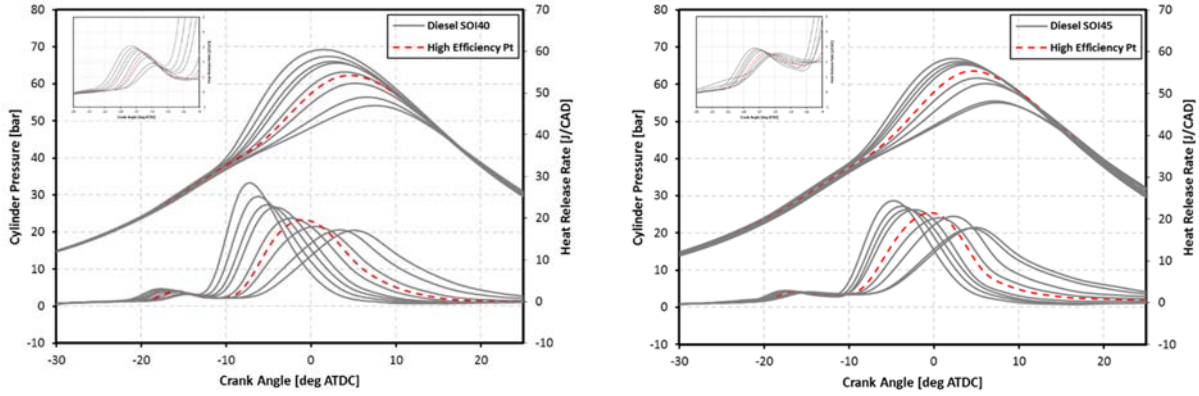

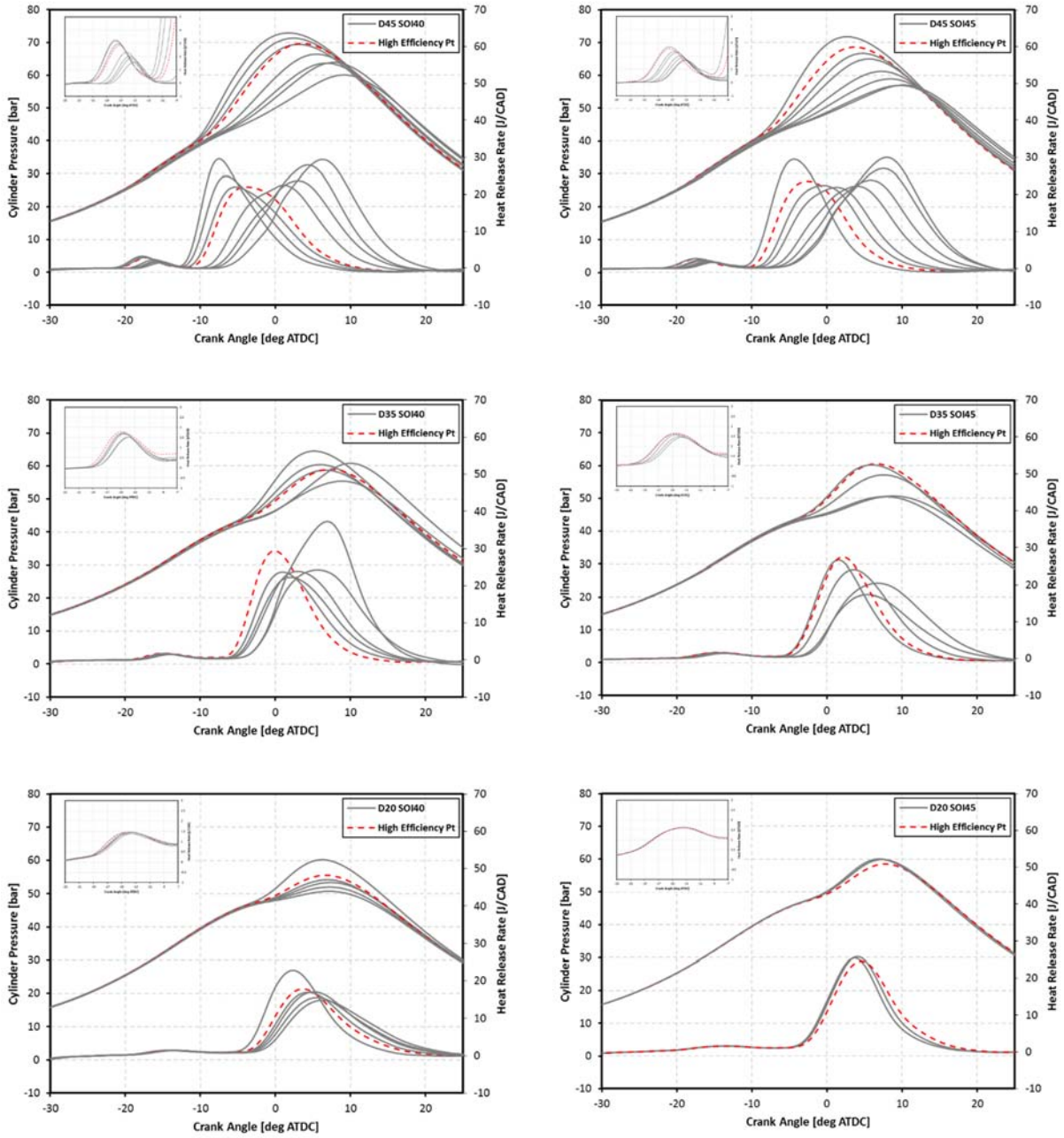

Figure 10-11 Cylinder Pressure [bar] and heat release rate [J/CAD] as a function of CAD at the DI SOI timing of -40 and -45 dATDC

Emissions results

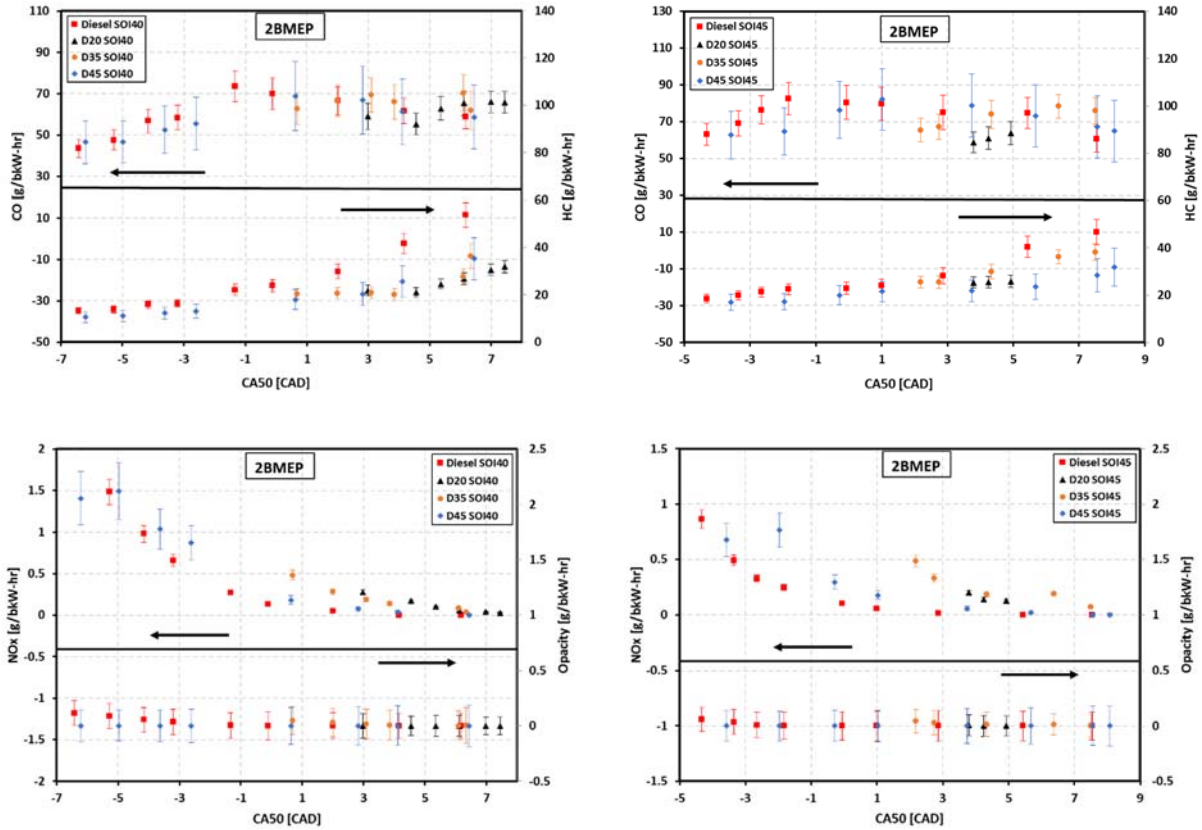

Figure 10-12 Engine-out emissions [g/bkW-hr] as a function of the combustion phasing (CA50) at the DI SOI timing of -40 and -45 dATDC

10.1.3 2.0 bar BMEP, 2,000 rev/min

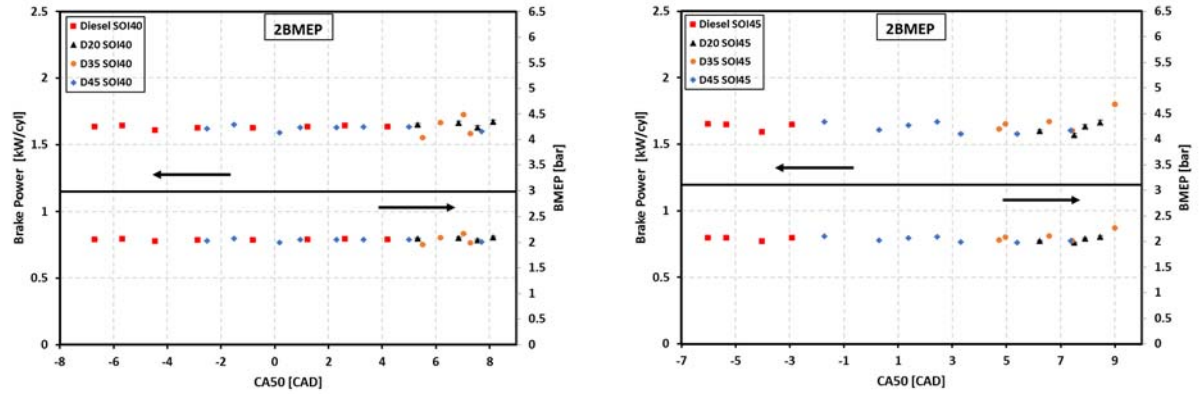

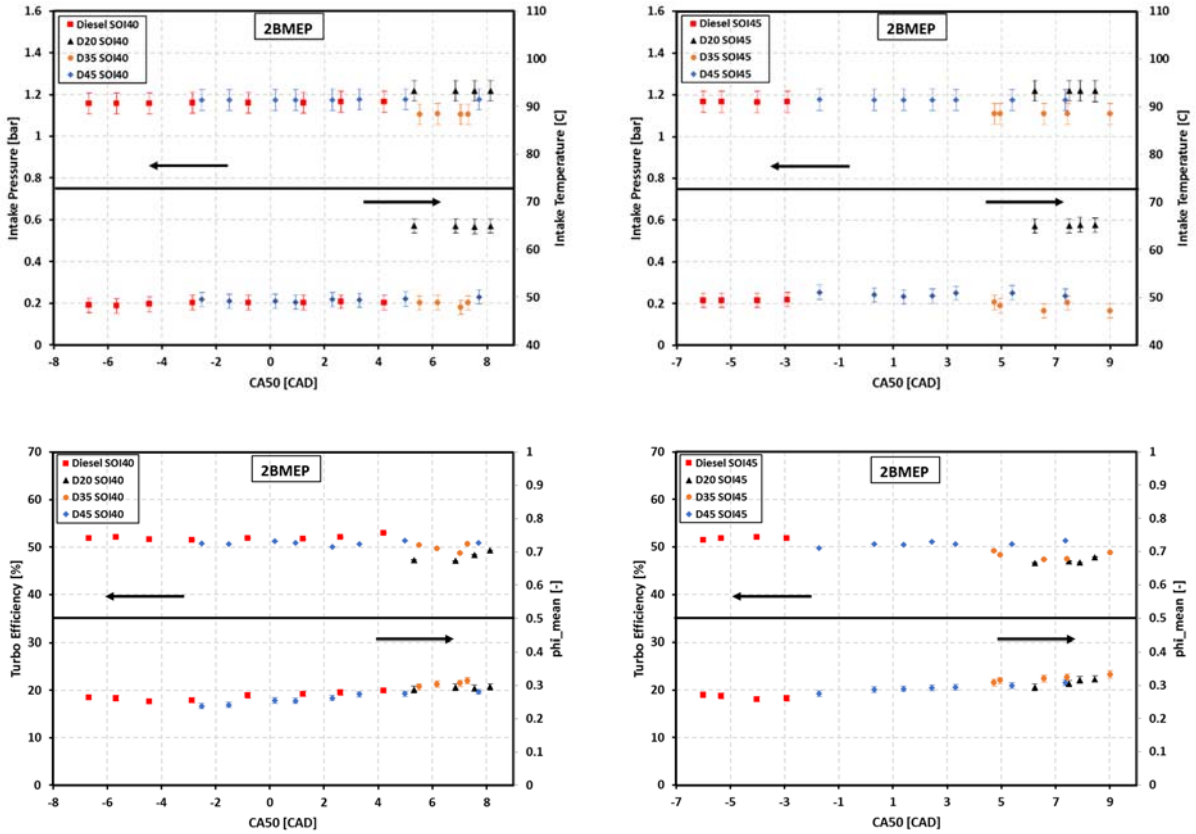

Figure 10-13 Operating Conditions as a function of the combustion phasing (CA50) at the DI SOI timing of -40 and -45 dATDC

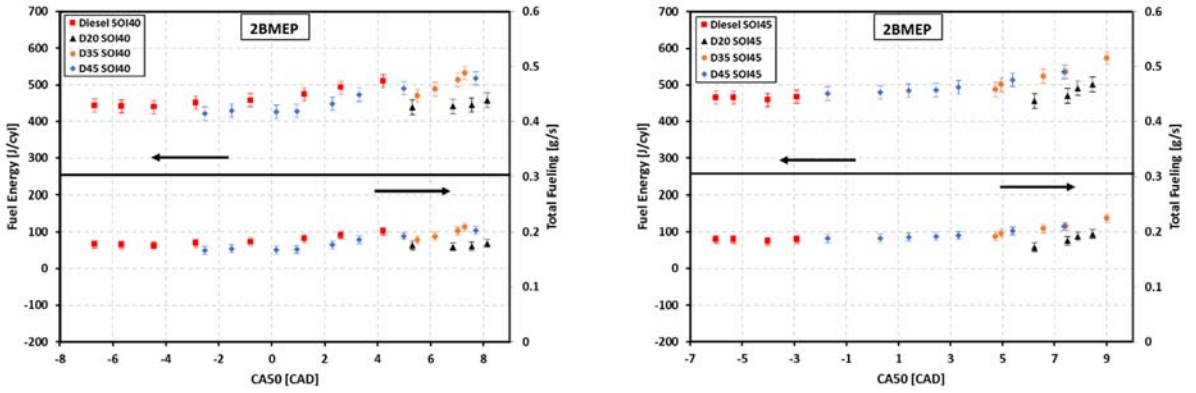

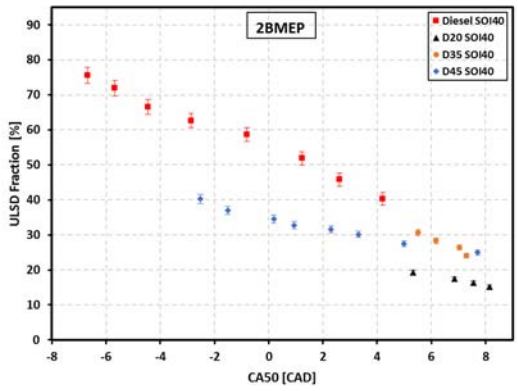
2BMEP
Diesel SOI40
D20 SOI40
D35 SOI40
D45 SOI40
ULSD Fraction [%]
CA50 [CAD]

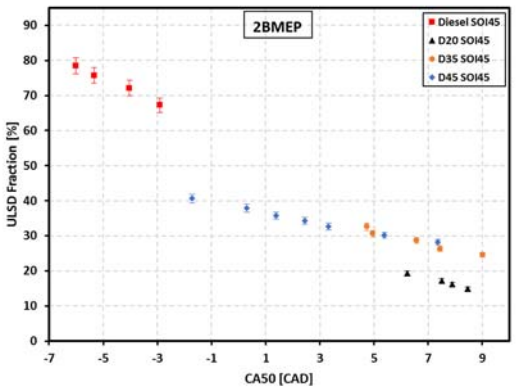
2BMEP
Diesel SOI45
D20 SOI45
D35 SOI45
D45 SOI45
ULSD Fraction [%]
CA50 [CAD]

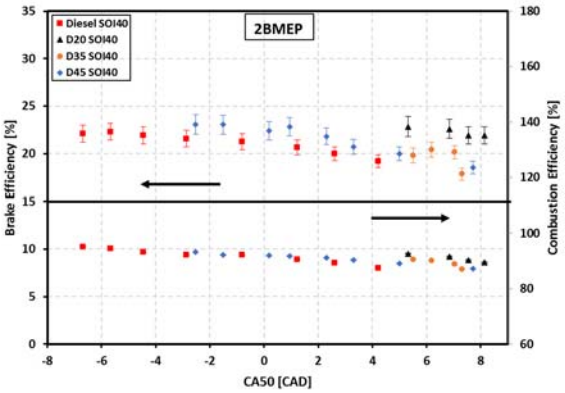
2BMEP
Diesel SOI40
D20 SOI40
D35 SOI40
D45 SOI40
Brake Efficiency [%]
Combustion Efficiency [%]
CA50 [CAD]

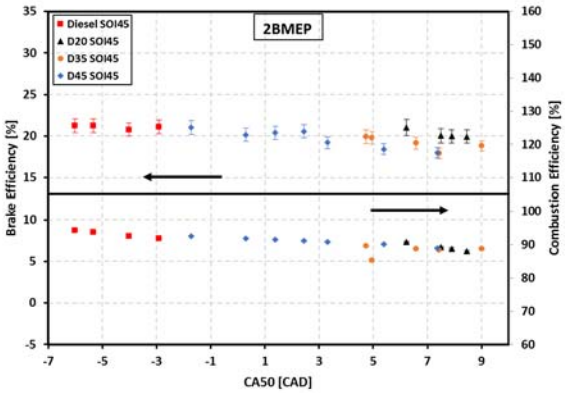
2BMEP
Diesel SOI45
D20 SOI45
D35 SOI45
D45 SOI45
Brake Efficiency [%]
Combustion Efficiency [%]
CA50 [CAD]

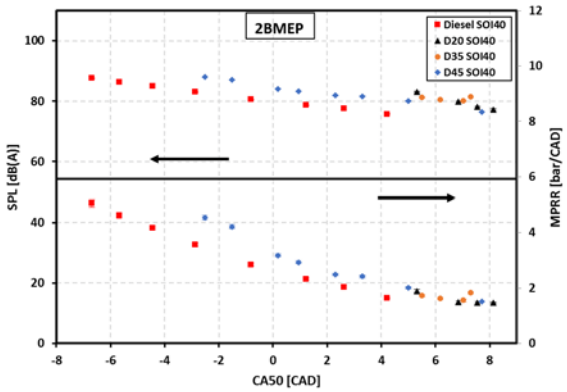
2BMEP
Diesel SOI40
D20 SOI40
D35 SOI40
D45 SOI40
SPL [dB(A)]
MPRR [bar/CAD]
CA50 [CAD]

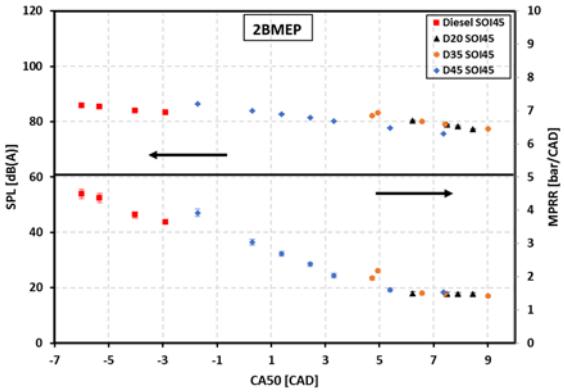
2BMEP
Diesel SOI45
D20 SOI45
D35 SOI45
D45 SOI45
SPL [dB(A)]
MPRR [bar/CAD]
CA50 [CAD]

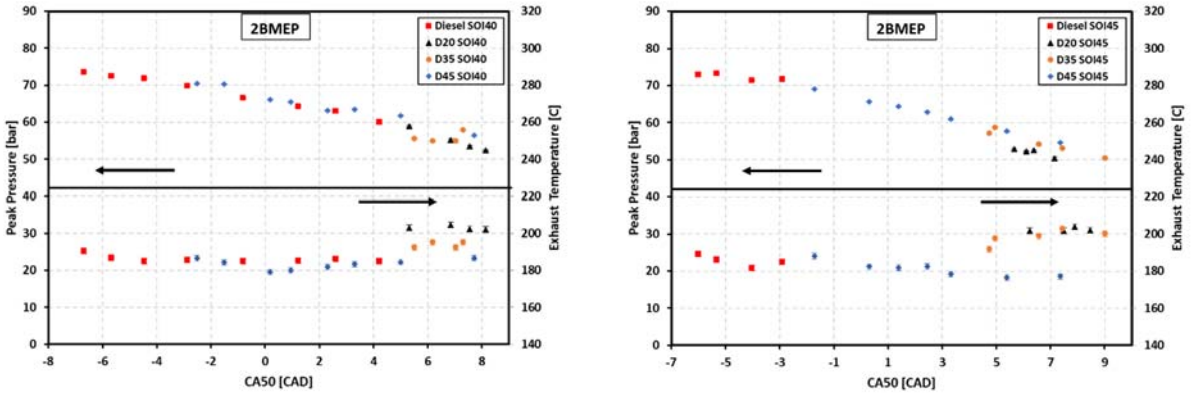

Figure 10-14 Performance results as a function of the combustion phasing (CA50) at the DI SOI timing of -40 and -45 dATDC

Table 10-5 2.0 bar BMEP Operating Conditions for best brake efficiency cases of each DI fuel at SOI -40 ATDC

Fuel	**Diesel**	**D45**	**D35**	**D20**
Pedal Position [%]	21.2	20.9	24.5	24.6
DI Duration [ms]	0.543	0.563	0.628	0.685
PFI Duration [ms]	2.198	1.056	1.231	0.642
PFI Fraction [%]	28.1	17.74	19.2	7
Rail Pressure [bar]	500	500	501	503
Main SOI [deg. BTDC]	40	40	40	40
Intake Pressure [bar]	1.15	1.17	1.11	1.22
Intake Temp. [°C]	49	50	50	65
EGR [%]	0	0	0	0
MPRR [bar/deg.]	4.62	4.22	1.61	1.89
CA 50 [deg. ATDC]	-5.678	-1.514	6.181	5.319
Comb Noise [dba]	86.4	87.1	80.5	83.1
Phi [-]	0.262	0.251	0.304	0.288
BTE [%]	22.31	23.06	20.42	23.62
Comb. Eff. [%]	94.6	92.2	90.1	92.7

Table 10-6 2.0 bar BMEP Operating Conditions for best brake efficiency cases of each DI fuel at SOI -45 ATDC

Fuel	**Diesel**	**D45**	**D35**	**D20**
Pedal Position [%]	21.6	20.3	23.1	25.7
DI Duration [ms]	0.588	0.622	0.677	0.703
PFI Duration [ms]	1.833	0.778	0.678	0.681
PFI Fraction [%]	21.5	10	7	5
Rail Pressure [bar]	495	500	505	500
Main SOI [deg. BTDC]	45	45	45	45
Intake Pressure [bar]	1.17	1.18	1.11	1.22
Intake Temp. [°C]	50	51	49	65
EGR [%]	0	0	0	0
MPRR [bar/deg.]	4.49	3.92	1.94	1.50
CA 50 [deg. ATDC]	-6.007	-1.720	4.736	6.231
Comb Noise [dba]	85.9	86.4	82.1	80.4
Phi [-]	0.271	0.275	0.308	0.294
BTE [%]	21.25	21.03	19.90	21.04
Comb. Eff. [%]	94.3	92.6	89.7	90.8

Pressure traces

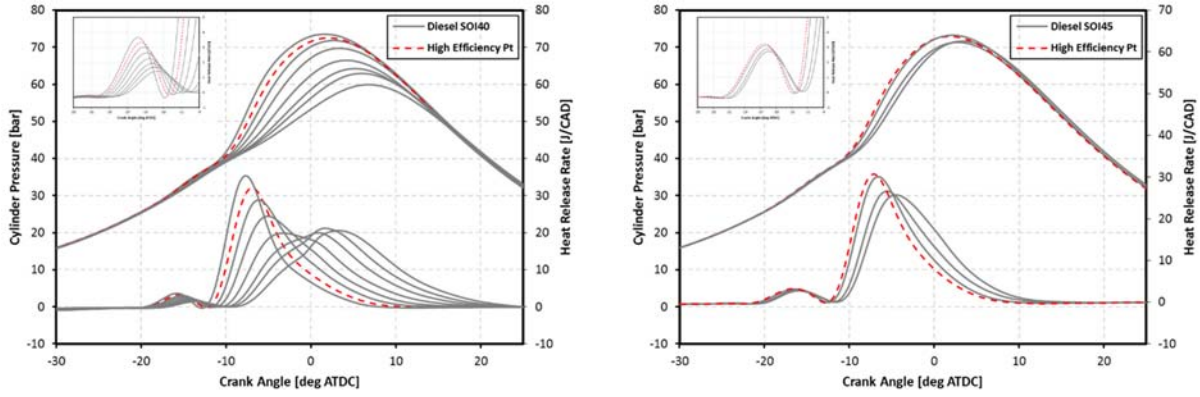

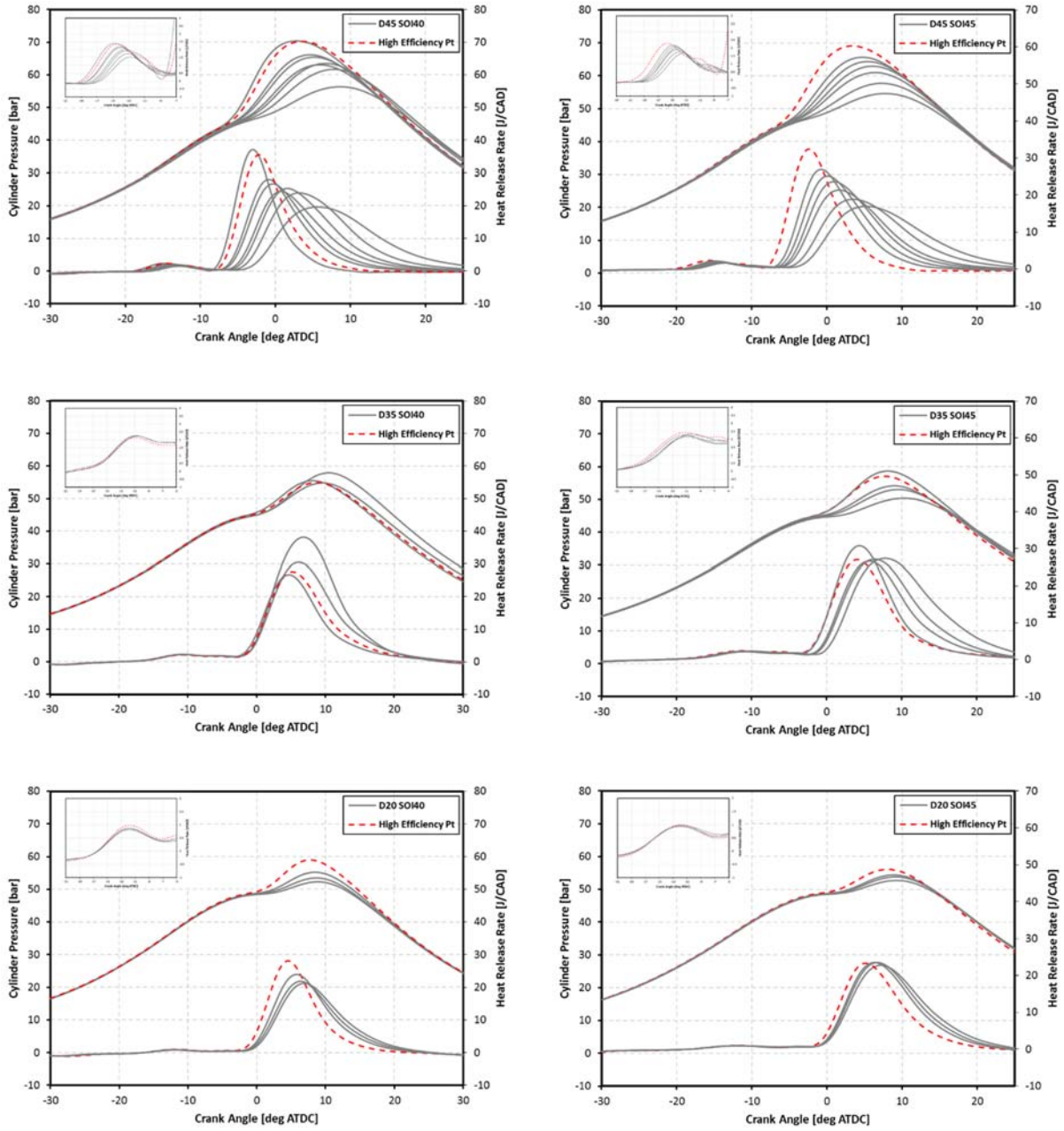

Figure 10-15 Cylinder Pressure [bar] and heat release rate [J/CAD] as a function of CAD at the DI SOI timing of -40 and -45 dATDC

Emissions results

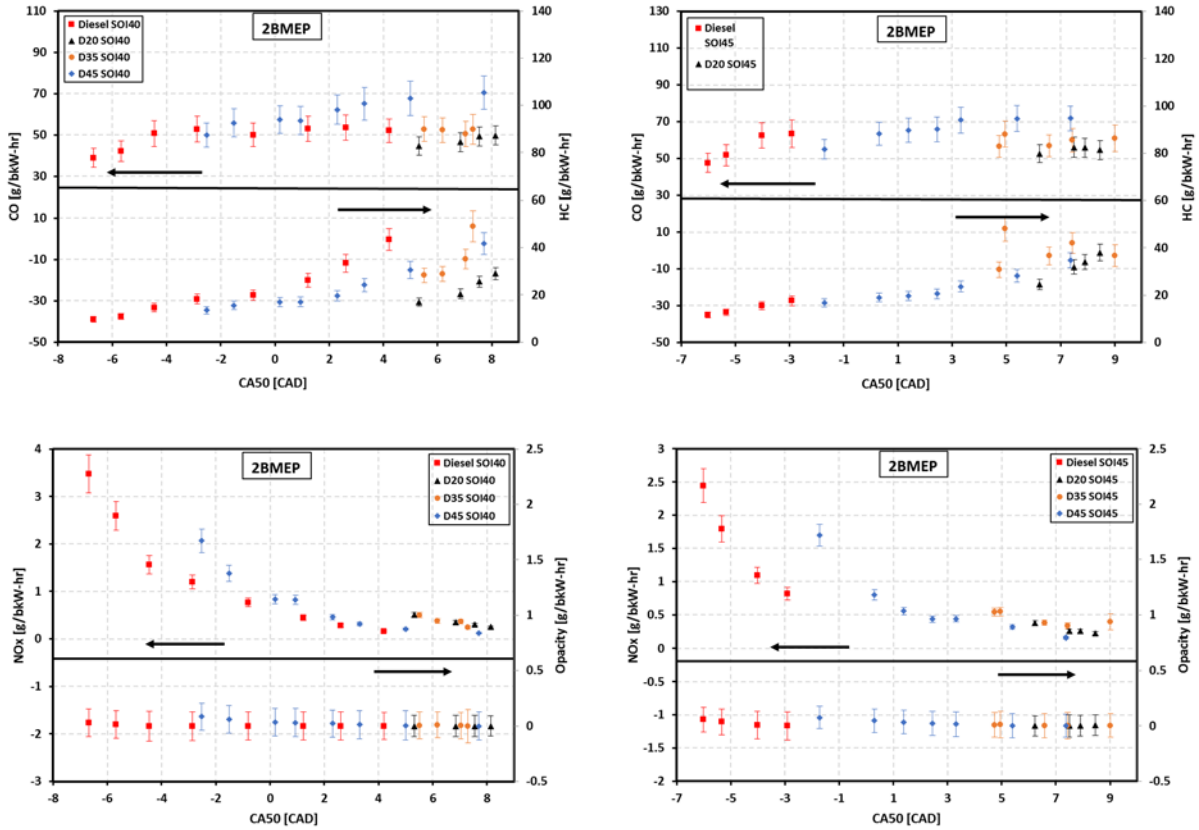

Figure 10-16 Engine-out emissions [g/bkW-hr] as a function of the combustion phasing (CA50) at the DI SOI timing of -40 and -45 dATDC

10.1.4 2.6 bar BMEP, 1,500 rev/min

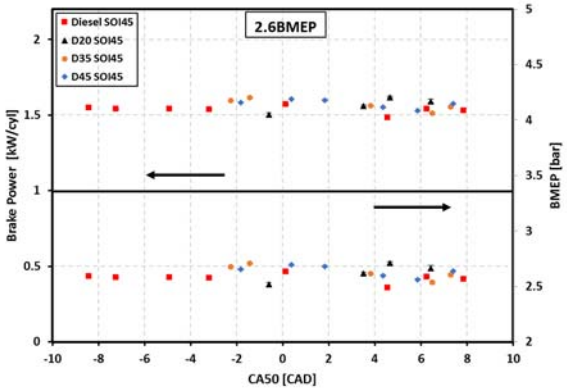

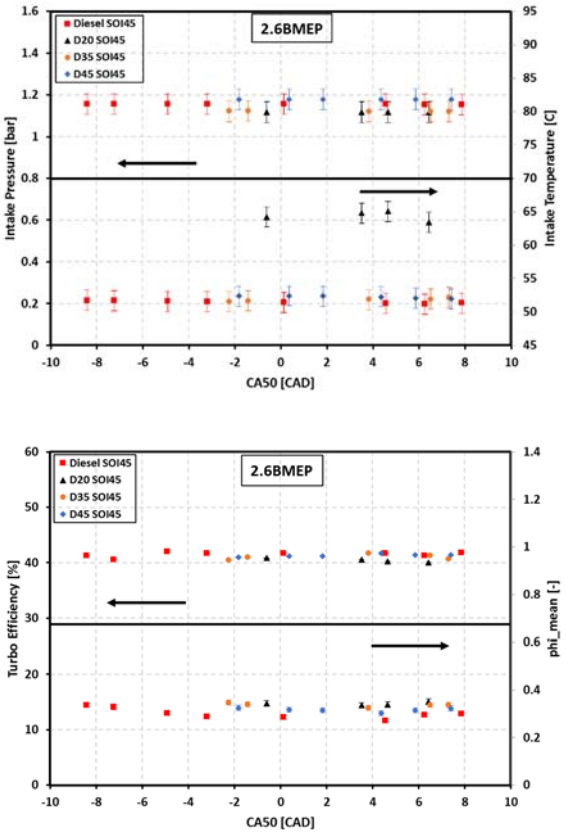

Figure 10-17 Operating Conditions as a function of the combustion phasing (CA50) at the DI SOI timing of -45 dATDC

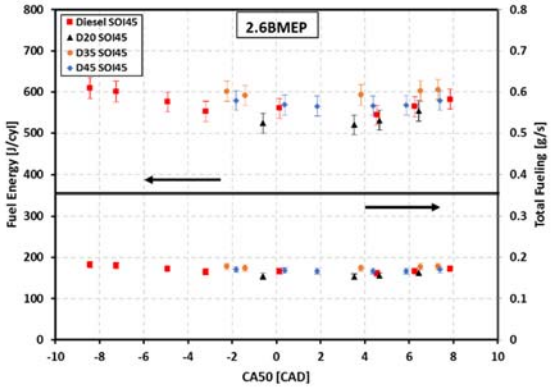

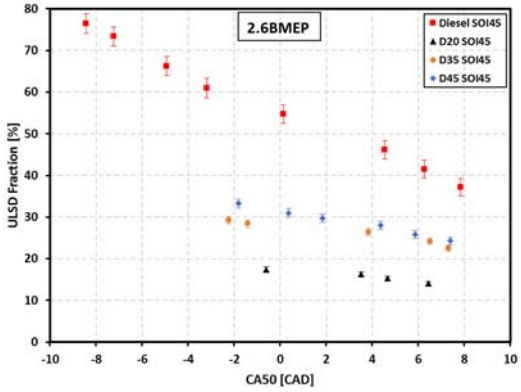
2.6BMEP
Diesel SOI45
D20 SOI45
D35 SOI45
D45 SOI45
ULSD Fraction [%]
CA50 [CAD]

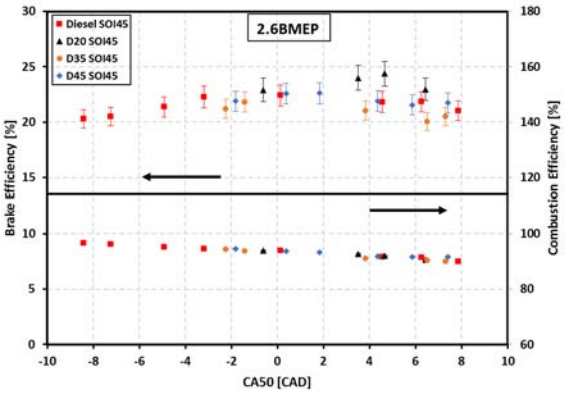
2.6BMEP
Diesel SOI45
D20 SOI45
D35 SOI45
D45 SOI45
Brake Efficiency [%]
Combustion Efficiency [%]
CA50 [CAD]

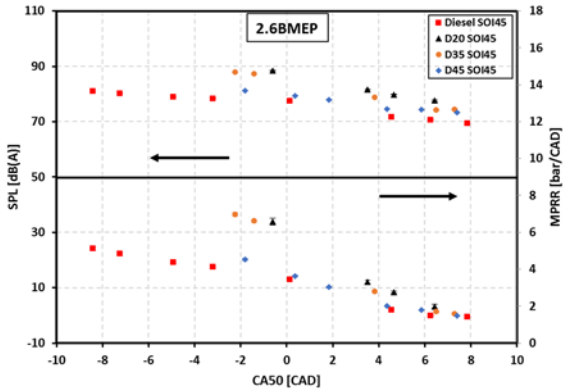
2.6BMEP
Diesel SOI45
D20 SOI45
D35 SOI45
D45 SOI45
SPL [dB(A)]
MPRR [bar/CAD]
CA50 [CAD]

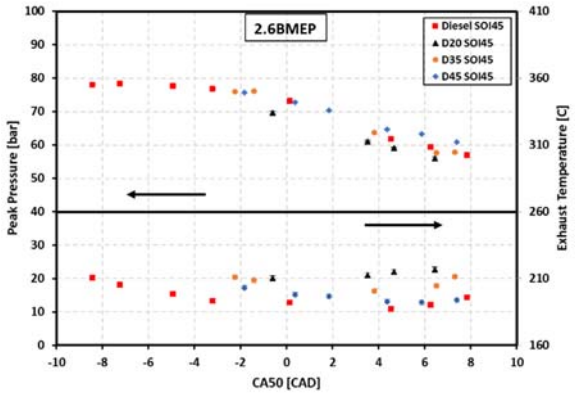

Figure 10-18 Performance results as a function of the combustion phasing (CA50) at the DI SOI timing of -45 dATDC

Table 10-7 2.6 bar BMEP Operating Conditions for best brake efficiency cases of each DI fuel at SOI -45 ATDC

Fuel	**Diesel**	**D45**	**D35**	**D20**
Pedal Position [%]	17	17.4	18.9	18.7
DI Duration [ms]	0.493	0.540	0643	0.658
PFI Duration [ms]	3.147	2.517	1.551	1.638
PFI Fraction [%]	45.2	34.0	18.8	23.7
Rail Pressure [bar]	500	505	500	495
Main SOI [deg. BTDC]	45	45	45	45
Intake Pressure [bar]	1.16	1.18	1.12	1.12
Intake Temp. [°C]	51	52	52	65
EGR [%]	0	0	0	0
MPRR [bar/deg.]	3.45	3.03	6.60	2.76
CA 50 [deg. ATDC]	-0.051	1.836	-1.415	4.657
Comb Noise [dba]	77.4	77.9	87.1	79.8
Phi [-]	0.286	0.314	0.339	0.339
BTE [%]	22.40	22.61	21.82	24.37
Comb. Eff. [%]	93.9	93.3	93.7	92.1

Pressure traces

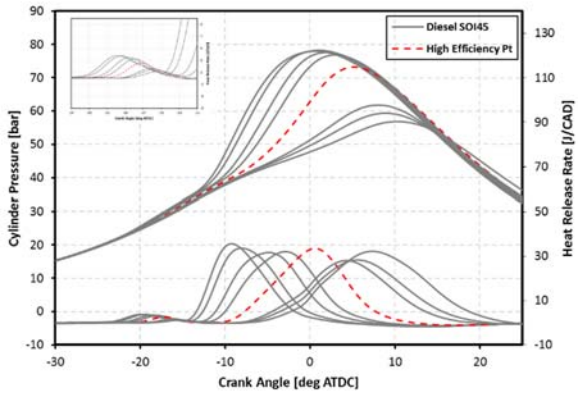

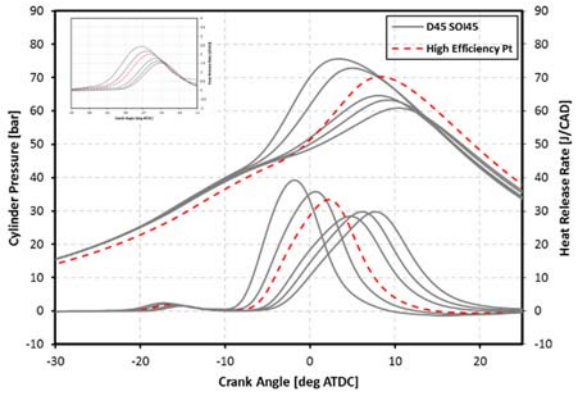

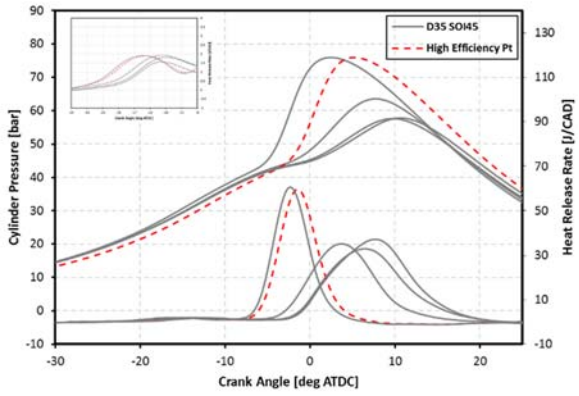

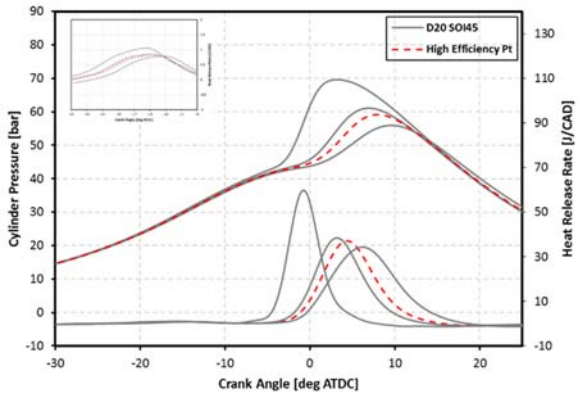

Figure 10-19 Cylinder Pressure [bar] and heat release rate [J/CAD] as a function of CAD at the DI SOI timing of -45 dATDC

Emissions results

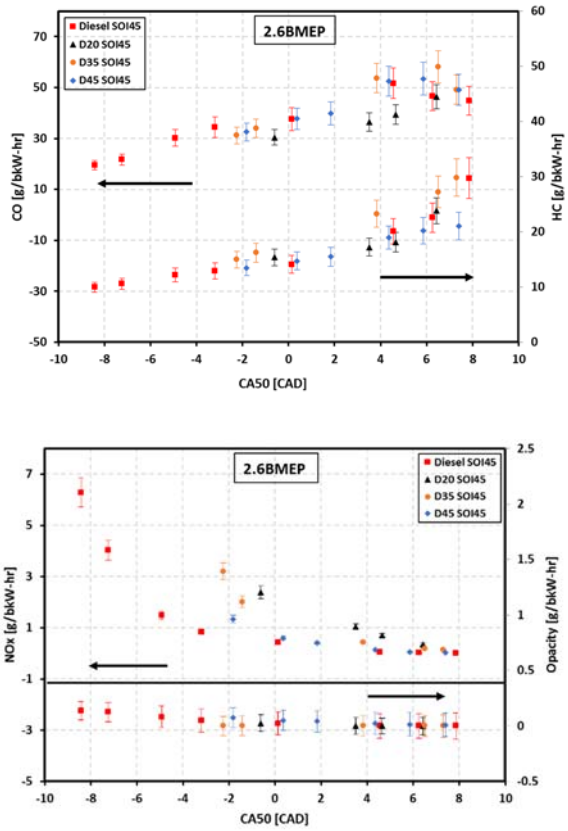

Figure 10-20 Engine-out emissions [g/bkW-hr] as a function of the combustion phasing (CA50) at the DI SOI timing of -45 dATDC

10.1.5 4.0 bar BMEP, 1,500 rev/min

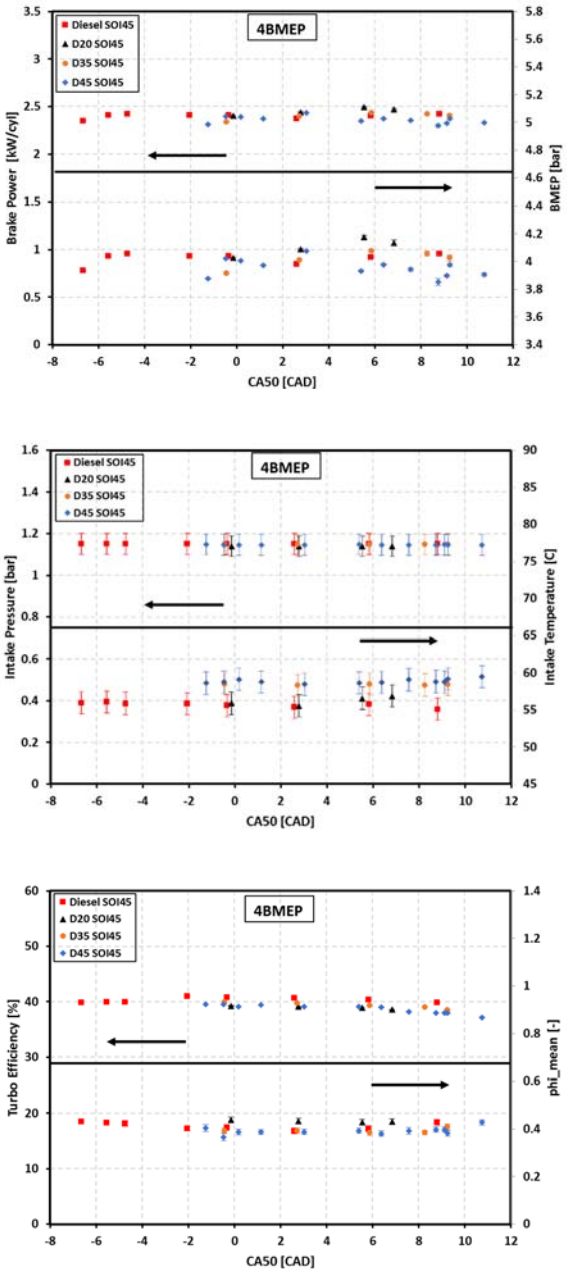

Figure 10-21 Operating Conditions as a function of the combustion phasing (CA50) at the DI SOI timing of -45 dATDC

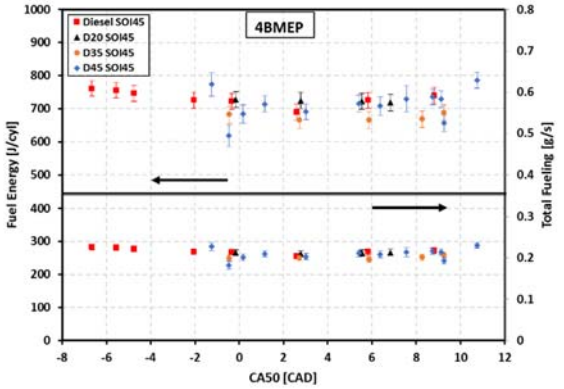
4BMEP
Diesel SOI45
D20 SOI45
D35 SOI45
D45 SOI45
Fuel Energy [J/cyl]
Total Fueling [g/s]
CA50 [CAD]

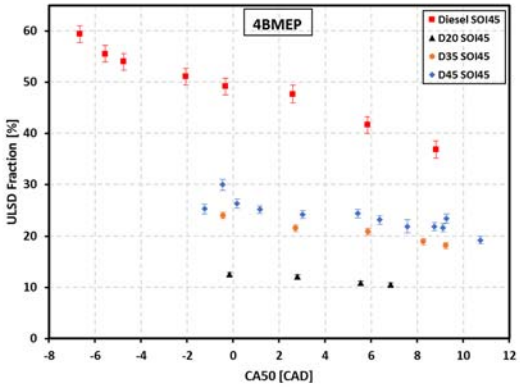
4BMEP
Diesel SOI45
D20 SOI45
D35 SOI45
D45 SOI45
ULSD Fraction [%]
CA50 [CAD]

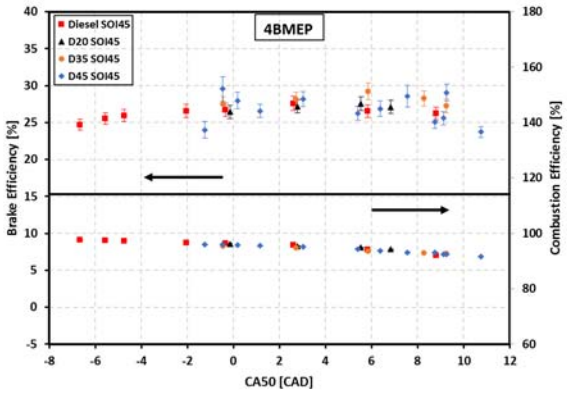
4BMEP
Diesel SOI45
D20 SOI45
D35 SOI45
D45 SOI45
Brake Efficiency [%]
Combustion Efficiency [%]
CA50 [CAD]

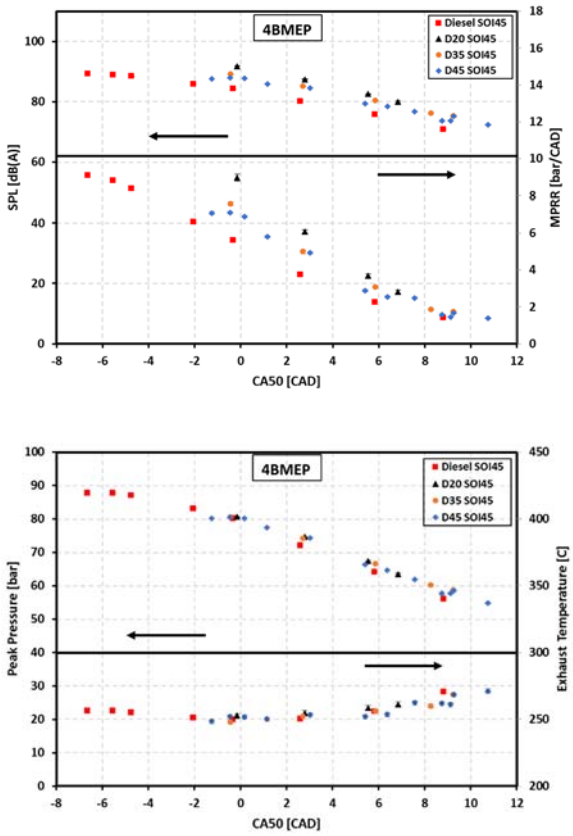

Figure 10-22 Performance results as a function of the combustion phasing (CA50) at the DI SOI timing of -45 dATDC

Table 10-8 4.0 bar BMEP Operating Conditions for best brake efficiency cases of each DI fuel at SOI -45 ATDC

Fuel	**Diesel**	**D45**	**D35**	**D20**
Pedal Position [%]	18.7	18.4	18.4	17.4
DI Duration [ms]	0.519	0.601	0.584	0.634
PFI Duration [ms]	4.523	3.617	3.833	3.105
PFI Fraction [%]	52.3	43.5	53.6	45.7
Rail Pressure [bar]	490	505	505	505
Main SOI [deg. BTDC]	45	45	45	45
Intake Pressure [bar]	1.15	1.15	1.15	1.14
Intake Temp. [°C]	55	58	58	57
EGR [%]	0	0	0	0
MPRR [bar/deg.]	3.74	7.11	3.07	3.69
CA 50 [deg. ATDC]	2.597	-0.461	5.867	5.543
Comb Noise [dba]	80.1	87.9	80.3	82.6
Phi [-]	0.391	0.367	0.386	0.428
BTE [%]	27.57	29.55	29.19	27.53
Comb. Eff. [%]	95.7	96.0	93.6	94.9

Pressure traces

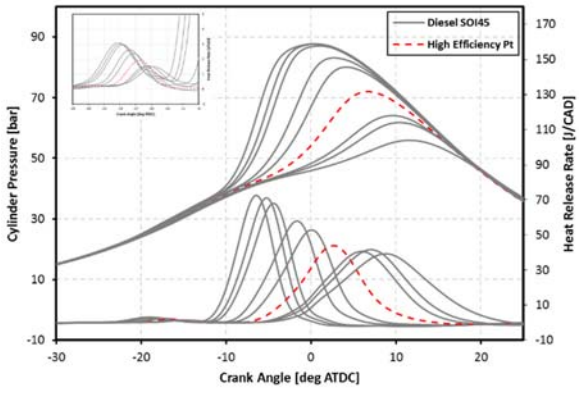

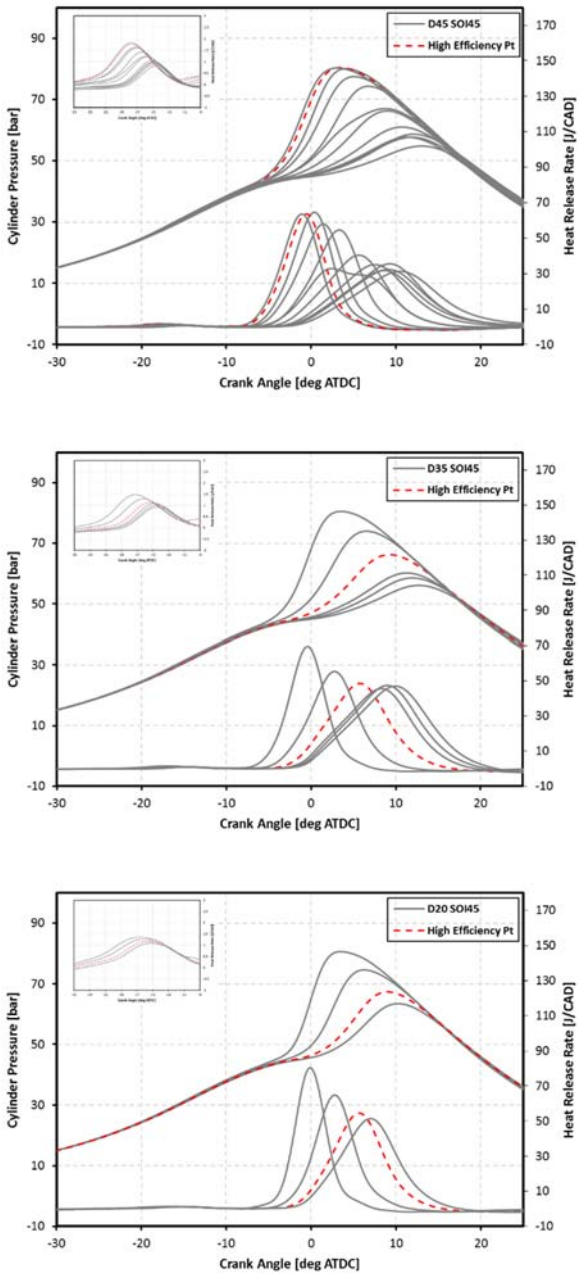

Figure 10-23 Cylinder Pressure [bar] and heat release rate [J/CAD] as a function of CAD at the DI SOI timing of -45 dATDC

Emissions results

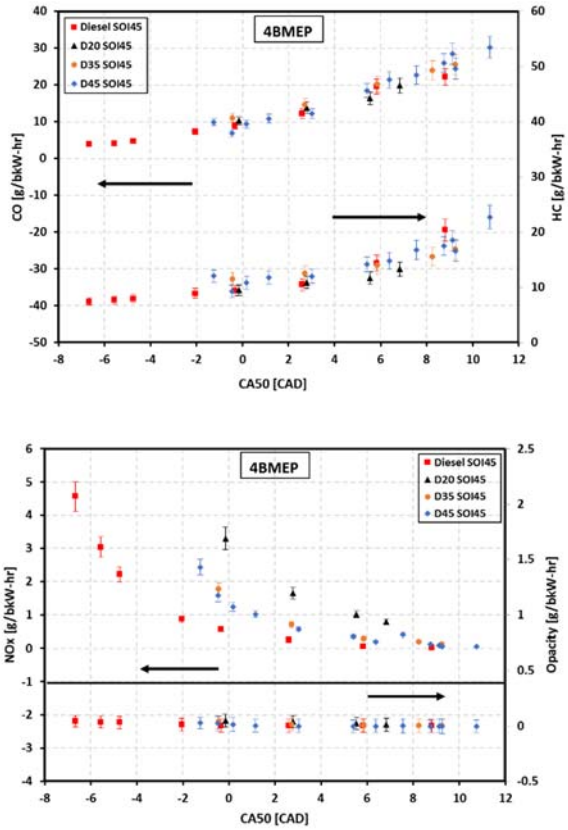

Figure 10-24 Engine-out emissions [g/bkW-hr] as a function of the combustion phasing (CA50) at the DI SOI timing of -45 dATDC

10.1.6 4.2 bar BMEP, 2,300 rev/min

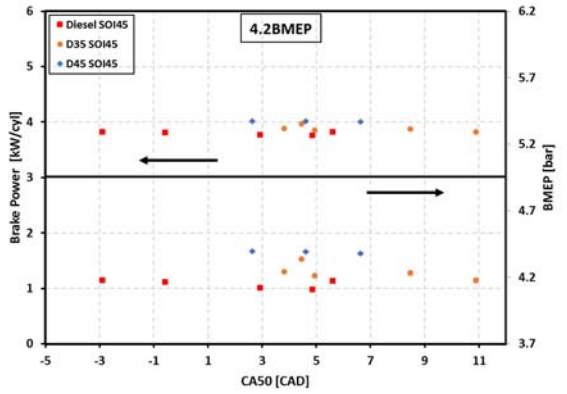

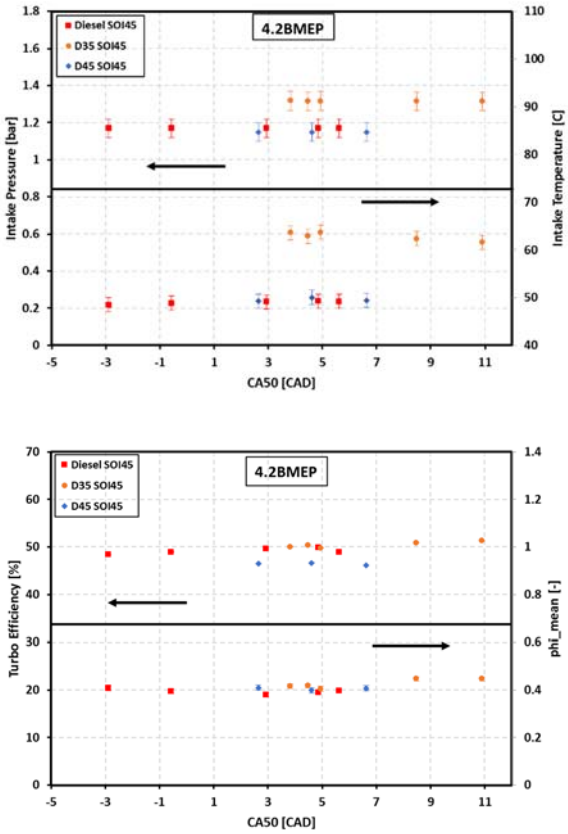

Figure 10-25 Operating Conditions as a function of the combustion phasing (CA50) at the DI SOI timing of -45 dATDC

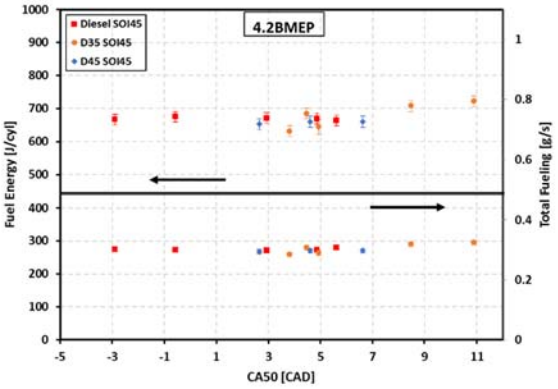

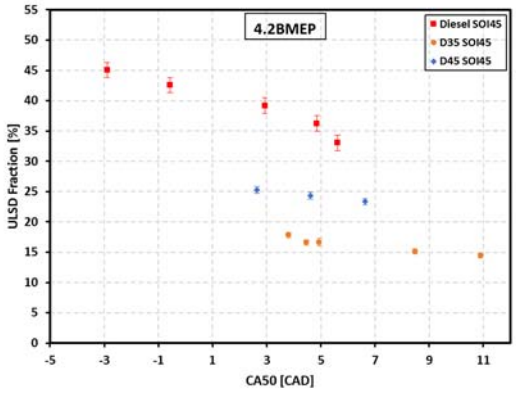
4.2BMEP
Diesel SOI45
D35 SOI45
D45 SOI45
ULSD Fraction [%]
CA50 [CAD]

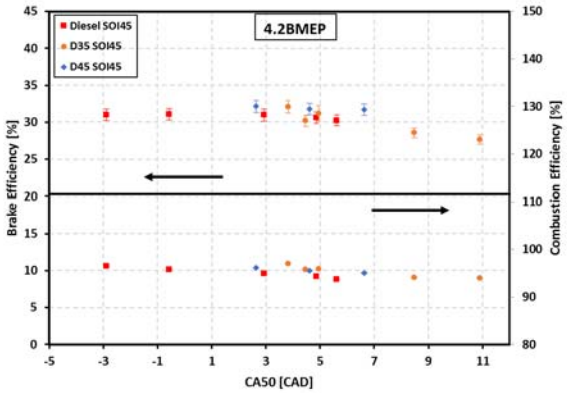
4.2BMEP
Diesel SOI45
D35 SOI45
D45 SOI45
Brake Efficiency [%]
Combustion Efficiency [%]
CA50 [CAD]

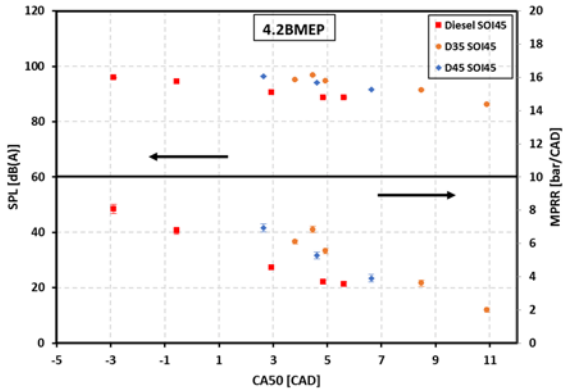
4.2BMEP
Diesel SOI45
D35 SOI45
D45 SOI45
SPL [dB(A)]
MPRR [bar/CAD]
CA50 [CAD]

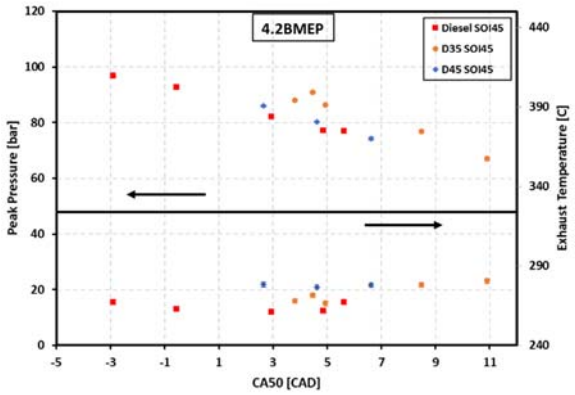

Figure 10-26 Performance results as a function of the combustion phasing (CA50) at the DI SOI timing of -45 dATDC

Table 10-9 4.2 bar BMEP Operating Conditions for best brake efficiency cases of each DI fuel at SOI -45 ATDC

Fuel	**Diesel**	**D45**	**D35**
Pedal Position [%]	32.9	32.4	32.7
DI Duration [ms]	0.499	0.585	0.531
PFI Duration [ms]	4.451	3.623	3.963
PFI Fraction [%]	57.4	43.9	49.1
Rail Pressure [bar]	500	500	500
Main SOI [deg. BTDC]	45	45	45
Intake Pressure [bar]	1.17	1.15	1.32
Intake Temp. [°C]	48	49	64
EGR [%]	0	0	0
MPRR [bar/deg.]	6.77	6.93	6.09
CA 50 [deg. ATDC]	-0.570	2.641	3.819
Comb Noise [dba]	94.5	96.4	95.0
Phi [-]	0.395	0.409	0.416
BTE [%]	31.09	32.15	32.08
Comb. Eff. [%]	95.8	96.2	96.9

Pressure traces

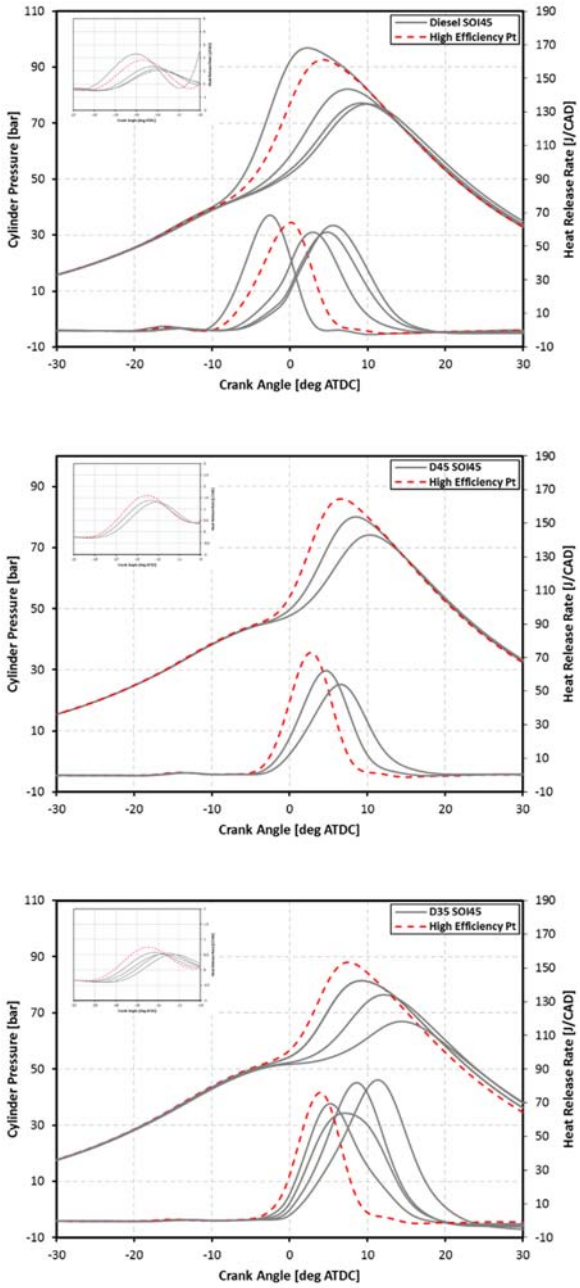

Figure 10-27 Cylinder Pressure [bar] and heat release rate [J/CAD] as a function of CAD at the DI SOI timing of -45 dATDC

Emissions results

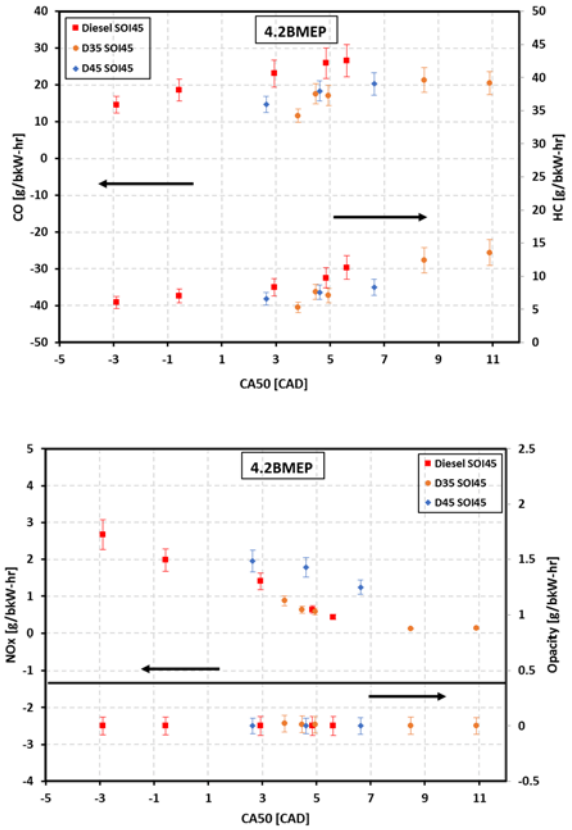

Figure 10-28 Engine-out emissions [g/bkW-hr] as a function of the combustion phasing (CA50) at the DI SOI timing of -45 dATDC

10.1.7 Investigation of higher-% Dieseline DI mixtures

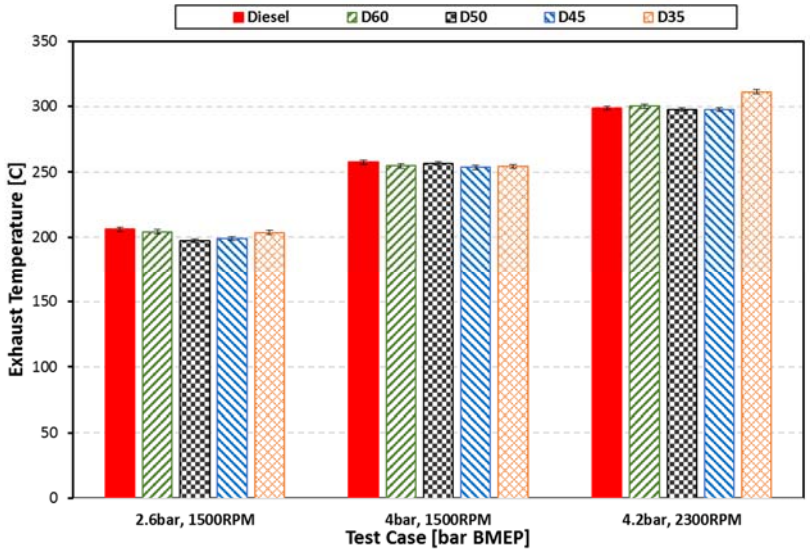

Figure 10-29 Exhaust temperatures [°C] for different DI fuels as a function of operating points at the DI SOI timing of -40 dATDC

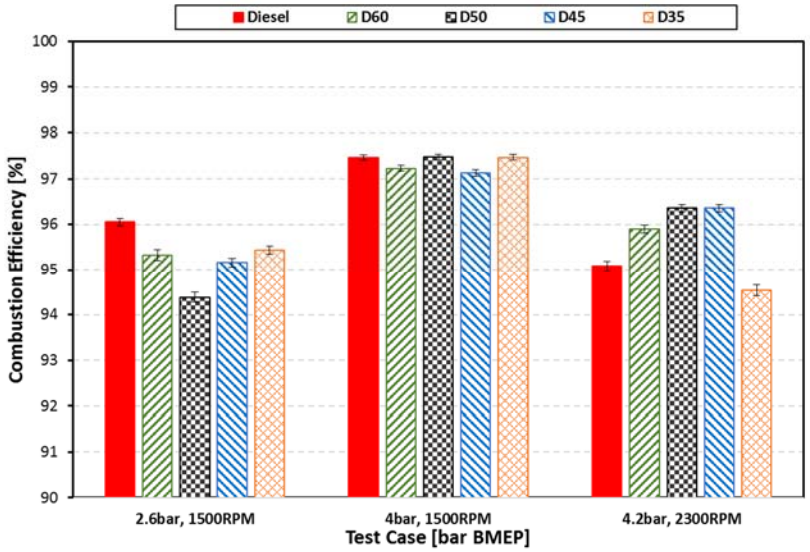

Figure 10-30 Combustion efficiency[%] for different DI fuels as a function of operating points at the DI SOI timing of -40 dATDC

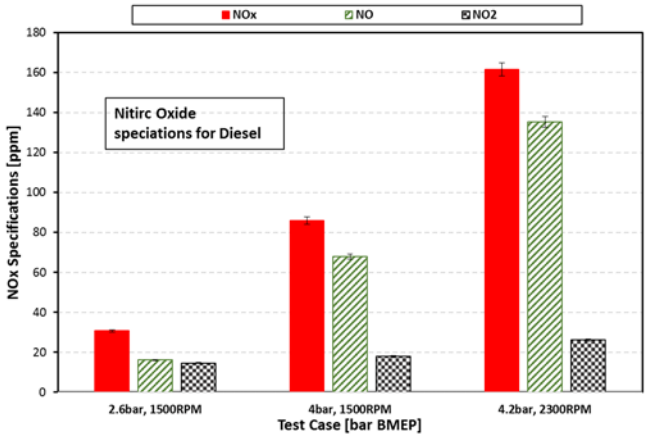

Figure 10-31 NOx specifications [ppm] for diesel as a function of operating points at the DI SOI timing of -40 dATDC

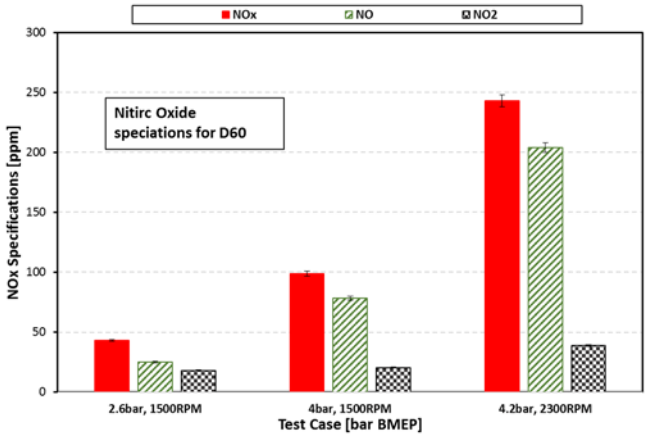

Figure 10-32 NOx specifications [ppm] for D60 as a function of operating points at the DI SOI timing of -40 dATDC

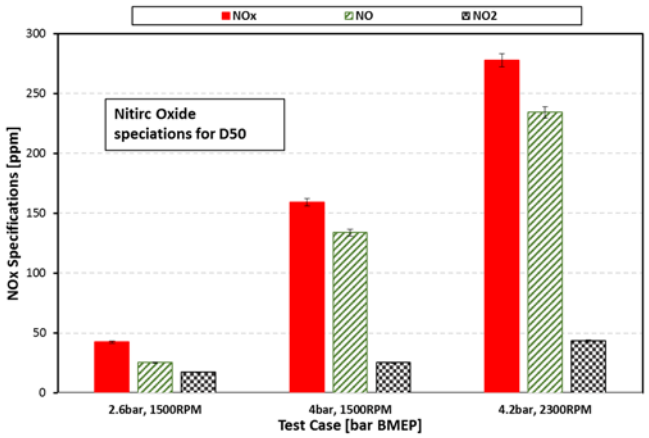

Figure 10-33 NOx specifications [ppm] for D50 as a function of operating points at the DI SOI timing of -40 dATDC

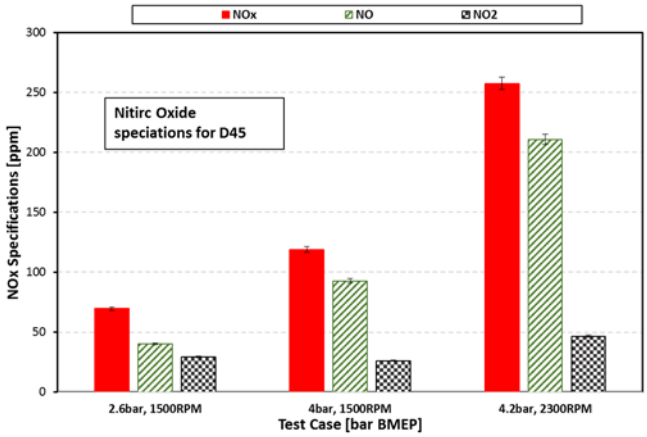

Figure 10-34 NOx specifications [ppm] for D45 as a function of operating points at the DI SOI timing of -40 dATDC

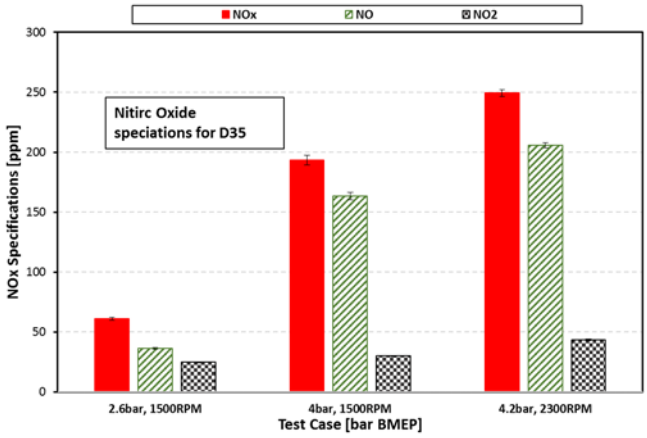

Figure 10-35 NOx specifications [ppm] for D35 as a function of operating points at the DI SOI timing of -40 dATDC

10.2 Appendix C: Steady-State Results for Boost Sweep, HCCI and Single-Fuel Dieseline45 Investigation

10.2.1 Effects of Boost on Steady-state RCCI Combustion Using Dieseline45

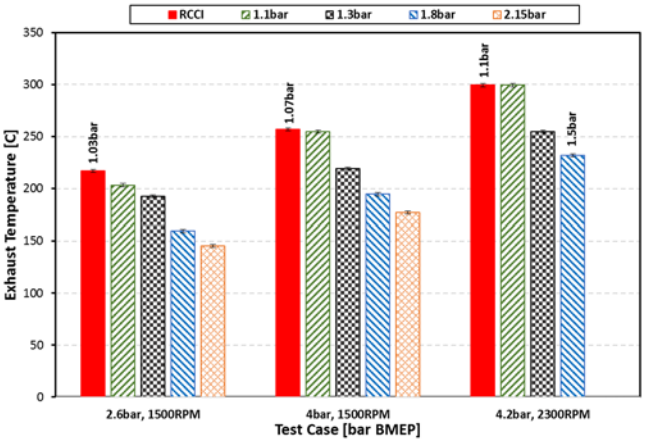

Figure 10-36 Exhaust temperatures [°C] for D45 at different boost levels as a function of operating points at the DI SOI timing of -40 dATDC

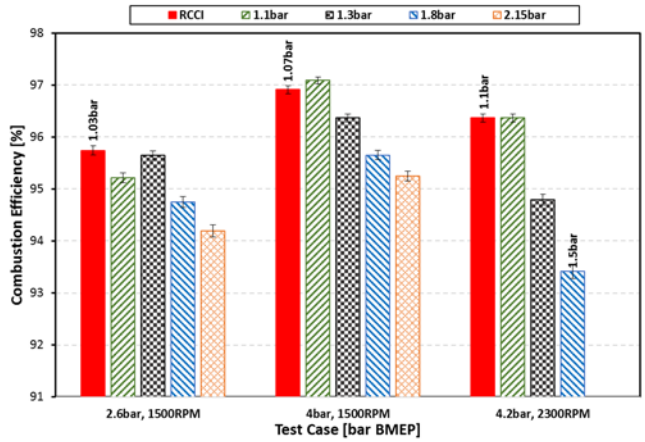

Figure 10-37 Combustion efficiency [%] for D45 at different boost levels as a function of operating points at the DI SOI timing of -40 dATDC

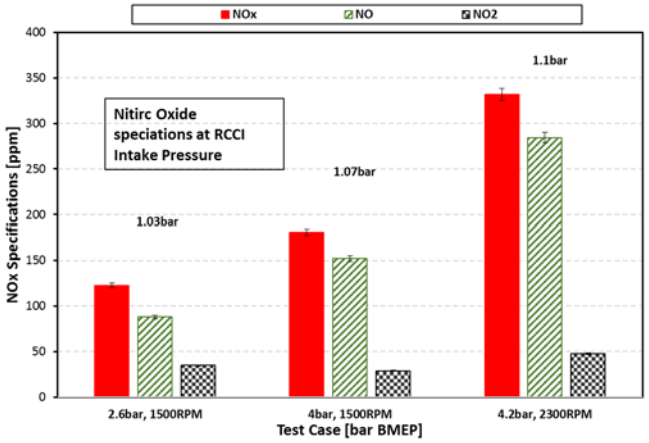

Figure 10-38 NOx specifications [ppm] for RCCI boost levels as a function of operating points at the DI SOI timing of -40 dATDC

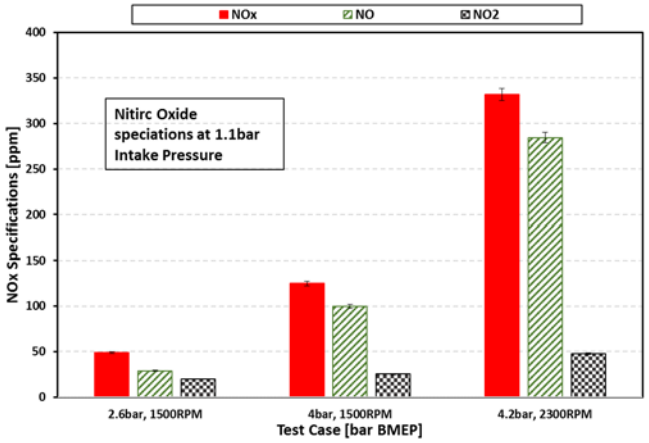

Figure 10-39 NOx specifications [ppm] for 1.1 bar boost level as a function of operating points at the DI SOI timing of -40 dATDC

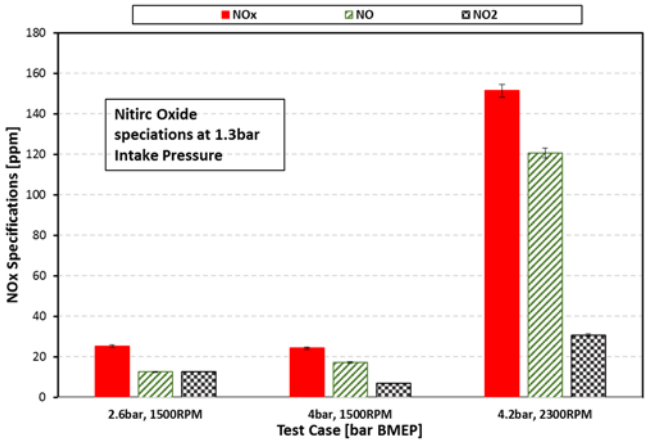

Figure 10-40 NOx specifications [ppm] for 1.3 bar boost level as a function of operating points at the DI SOI timing of -40 dATDC

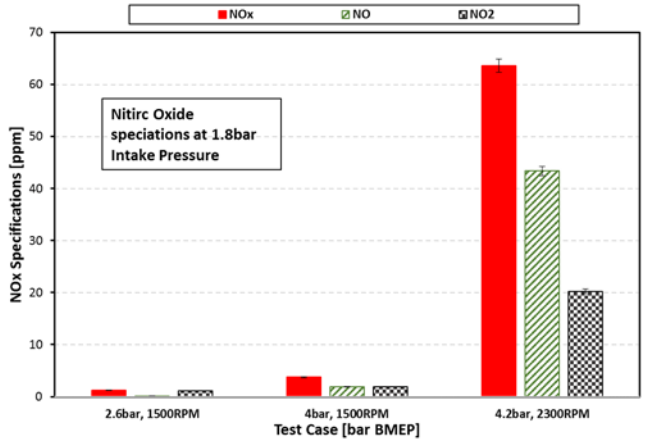

Figure 10-41 NOx specifications [ppm] for 1.8 bar boost level as a function of operating points at the DI SOI timing of -40 dATDC

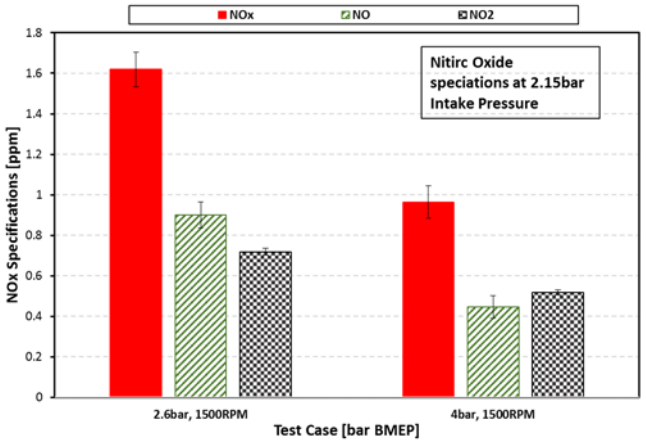

Figure 10-42 NOx specifications [ppm] for 2.15 bar boost level as a function of operating points at the DI SOI timing of -40 dATDC

10.2.2 Comparing the Performance of Dieseline HCCI with RCCI Combustion Using Dieseline45

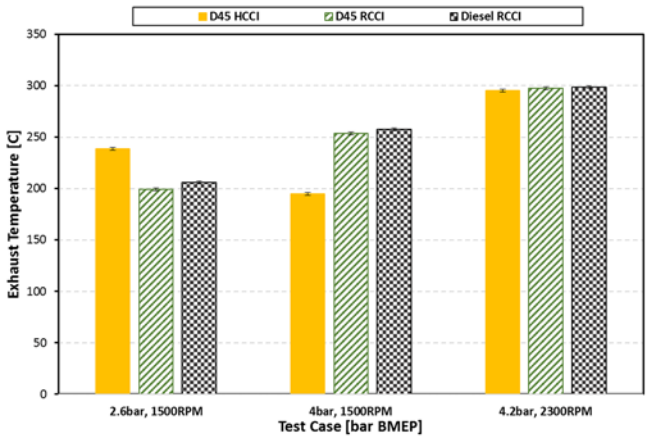

Figure 10-43 Exhaust temperatures [°C] for different combustion modes as a function of operating points at the DI SOI timing of -40 dATDC

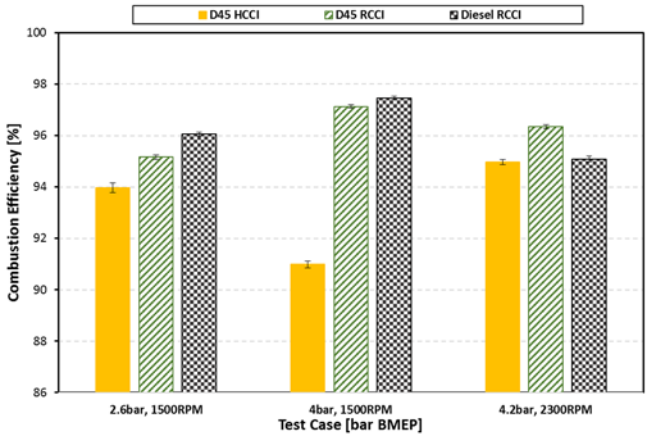

Figure 10-44 Combustion efficiency [%] for different combustion modes as a function of operating points at the DI SOI timing of -40 dATDC

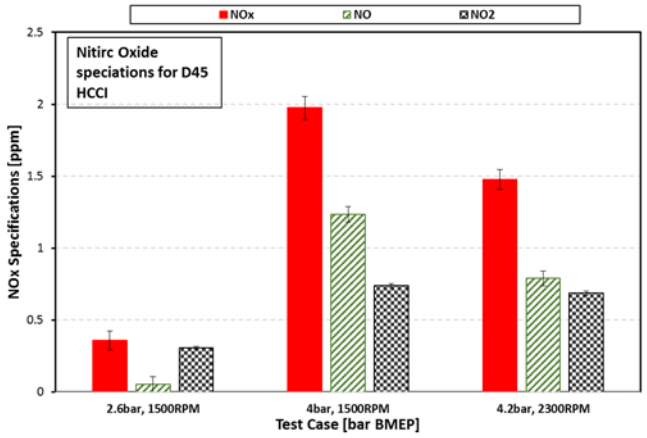

Figure 10-45 NOx specifications [ppm] for D45 HCCI as a function of operating points at the DI SOI timing of -40 dATDC

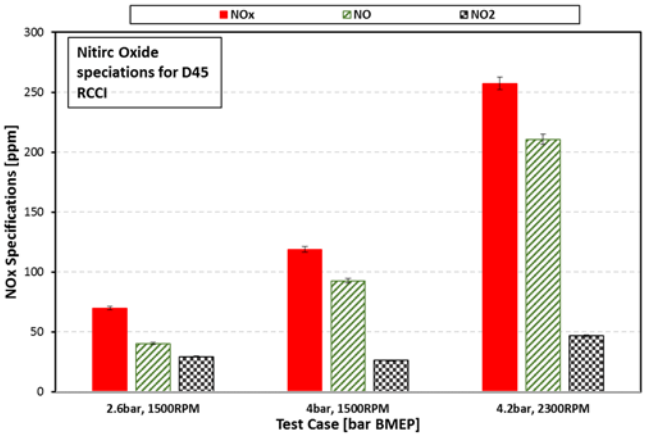

Figure 10-46 NOx specifications [ppm] for D45 RCCI as a function of operating points at the DI SOI timing of -40 dATDC

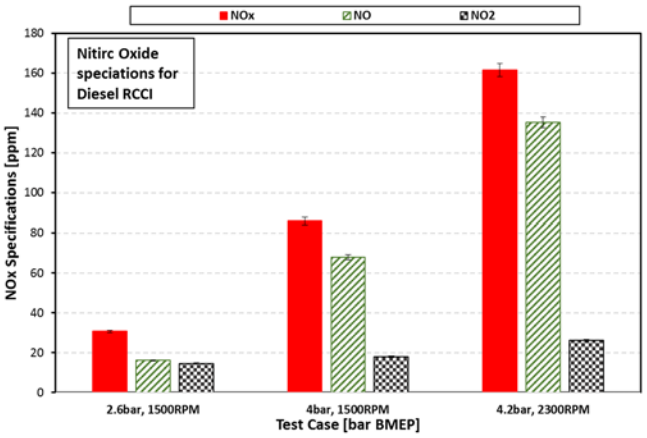

Figure 10-47 NOx specifications [ppm] for diesel RCCI as a function of operating points at the DI SOI timing of -40 dATDC

10.2.3 Performance of single-fuel RCCI Combustion Using Dieseline45

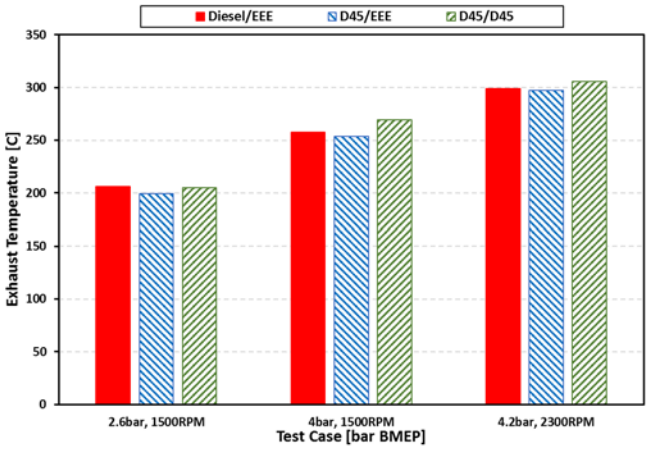

Figure 10-48 Exhaust temperatures [°C] for different fuel combinations as a function of operating points at the DI SOI timing of -40 dATDC

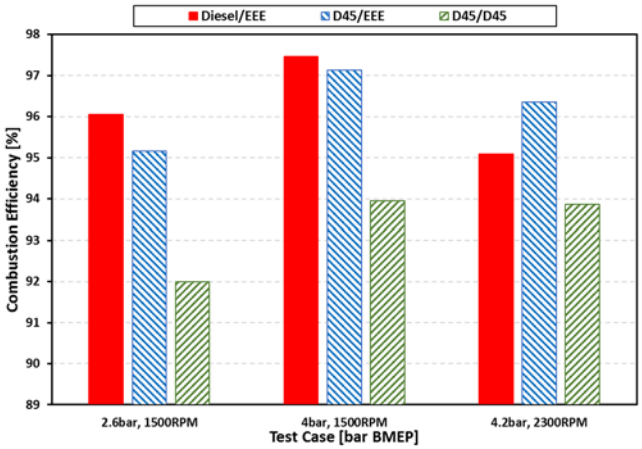

Figure 10-49 Combustion efficiency [%] for different fuel combinations as a function of operating points at the DI SOI timing of -40 dATDC

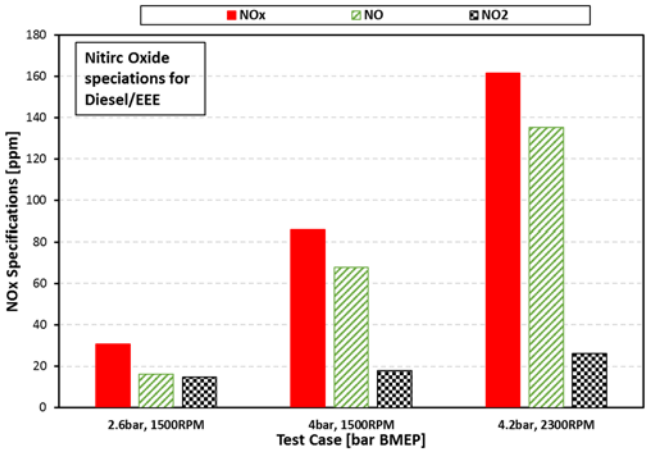

Figure 10-50 NOx specifications [ppm] for diesel/EEE as a function of operating points at the DI SOI timing of -40 dATDC

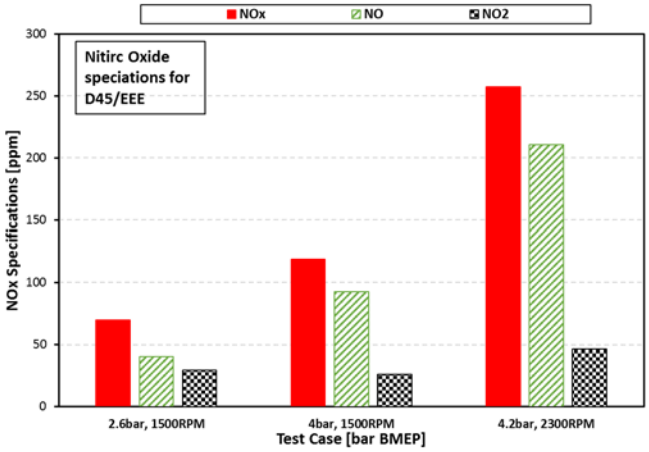

Figure 10-51 NOx specifications [ppm] for D45/EEE as a function of operating points at the DI SOI timing of -40 dATDC

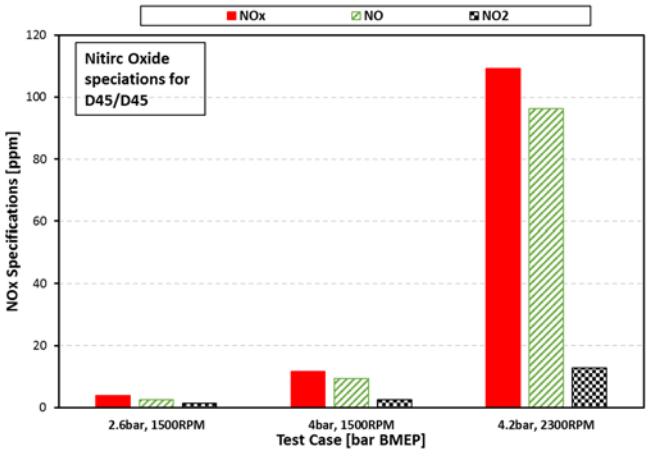

Figure 10-52 NOx specifications [ppm] for D45/D45 as a function of operating points at the DI SOI timing of -40 dATDC